CRANFIELD UNIVERSITY

J. W. WATSON

Investigation of Cyclist and Pedestrian Impacts with Motor Vehicles using Experimentation and Simulation

School of Applied Science

PhD

CRANFIELD UNIVERSITY

SCHOOL OF APPLIED SCIENCES

PhD

Academic Year 2009-2010

J.W.WATSON

Investigation of Cyclist and Pedestrian Impacts with Motor Vehicles using Experimentation and Simulation

Supervisor: Prof P. Irving

February 2010

ABSTRACT

Physical tests were performed with a bicycle and a dummy in a controlled laboratory environment to reproduce cyclist accidents. The kinematics of 13 sled tests were used to identify the cyclist head impact location, understand the interaction between the cyclist and bicycle and to validate a mathematical model.

The finite element software code LS-DYNA was used to simulate 70 cyclist and pedestrian accidents with motor vehicles with four different vehicle shapes which supplemented the physical testing. The study has shown that when cyclists and pedestrians were struck by any of the vehicles their whole body kinematics can be distinguished into two phases, initially a rotation followed by a sliding action. The Sports Utility Vehicle (SUV) vehicle produced more of a rotation action rather than sliding, whereas the other vehicles produced a combination of the two.

The current pedestrian legislation does not cover all head impact locations for cyclists and therefore needs to be extended to encompass the windscreen and A-Pillar regions of the vehicles. The wrap around distance (WAD) for all the vehicles, apart from the SUV, should be extended to encompass a larger region. For the SUV the current WAD region is adequate in protecting cyclists and pedestrians and does not need to change. The predicted head impactor angle for cyclists is 40 degrees which is lower than the current legislative value of 65 degrees and the predicted pedestrian head impact angle is higher at a value of 80 degrees for the MPV, SM and LFC. For the SUV the proposed impactor angle increased to 100 degrees for cyclists and pedestrians.

This research has demonstrated significant differences in terms of input variables and outcomes between cyclist and pedestrian accidents involving vehicles. It has used mathematical models to obtain injury data from a human mathematical model and physical testing to replicate real world cyclist accident scenarios. Recommendations have been proposed for future legislative testing techniques for cyclists, based on existing pedestrian legislation. These recommendations to alter legislation will improve vehicle design and make future vehicles more cyclist-friendly.

Acknowledgements

I would like to express my gratitude to my supervisors Prof. Tony Pickett and more recently Prof. Phil Irving for their guidance in the co-ordination of the research in a methodical approach.

I am also grateful to members of Cranfield Impact Centre, including Roger Hardy who initially inspired me to undertake the work, Robin Butler, Clive Shaw and Tony Scott for help in conducting the physical tests and Ralph McAuliffe for photography.

I would also like to acknowledge the 6th Framework European project APROSYS – Advanced PROtective SYStems, who sponsored part of the research in conjunction with Cranfield Impact Centre.

This thesis is dedicated to Mr Charles Sawyer (1940-2009) who was a fellow cyclist and a constant inspiration to improve cyclist safety.

CONTENTS

Table of Figures

Abbreviations

Advanced PROtective SYStems	APROSYS
Analysis of Variance	ANOVA
Centre of Gravity	CG
Cranfield Impact Centre	CIC
Diffuse Axonal Injury	DAI
European Commission	EC
European Experimental Vehicle Committee	EEVC
EUROpean New Car Assessment programme	EuroNCAP
Finite Element	FE
General Technical Regulations	GTR
Head Injury Criteria	HIC
Killed or Seriously Injured	KSI
Large Family Car	LFC
Millisecond	msec
Multi-Purpose Vehicle	MPV
Physical Testing	PT
Sports Utility Vehicle	SUV
Struck Leg Back	SLB
Struck Leg Down	SLD
Struck Leg Forward	SLF
Struck Leg Up	SLU
Super Mini	SM
Virtual Testing	VT
Working Group 10/17	WG10/17
Wrap Around Distance	WAD

Chapter 1 Introduction

1.1 Introduction

There are 100,000 people killed on the roads of Europe every year. In addition, over a million further people suffer injuries as a result of vehicle accidents involving all forms of transport modes. Of those killed on European roads, 2000 of them are cyclists and 7000 are pedestrians, while several hundred thousand are injured (European Commission, Directorate-General for Energy and Transport, 2008). Measures have been introduced with varying success, to reduce the number of in-car casualties with the use of seatbelts having a significant effect when they were introduced in the 1970's (Nahum and Melvin, 1993). By restraining vehicle passengers, the loads being exerted on them were reduced, thereby preventing them from striking vehicle interior components such as steering wheels or even being ejected from vehicles. Nowadays devices such as airbags, crumple zones around the vehicle and seatbelts that change their characteristics during a collision are common. Cyclists' collisions are of a different nature to vehicle occupants as there is no device to alter their kinematics and are likely to receive a direct force from their interaction with the vehicle. As there is limited scope to reduce cyclist injuries by changing the design of the bicycle; this research has focused on changing vehicle design.

Figure 1-1: Example of Cyclist Accident (FunnyPictures.net.au, 2009)

In the majority of cases cyclists and pedestrians are struck by the front of a passenger car and this was recognised by the European Experimental Vehicle Committee (EEVC) in 1982. Working Group 10 of the EEVC was formed in 1987 and they devised a set of testing methods to assess pedestrian protection for passenger cars. Initially, the use of a manikin or test dummy to represent a living person was considered, which was similar to the approach used for vehicle occupants. However, this was deemed to be unsuitable as there are a wide range of pedestrian accident scenarios and there was an issue with reproducing the accidents with any repeatability. The pedestrian test methods involved firing a series of impactors, which represented specific human body parts such as the head and lower legs onto the front of a vehicle. Measurement devices attached to the impactors recorded the deceleration or load levels during the impact with the vehicle front and these were assessed against pre-determined criteria. If the load or acceleration levels were too high the vehicle was considered not to be pedestrian friendly and would fail to meet the standards necessary to pass the legislation. If vehicles do not pass the legislation they cannot be introduced into the market and therefore manufacturers address safety testing legislation seriously.

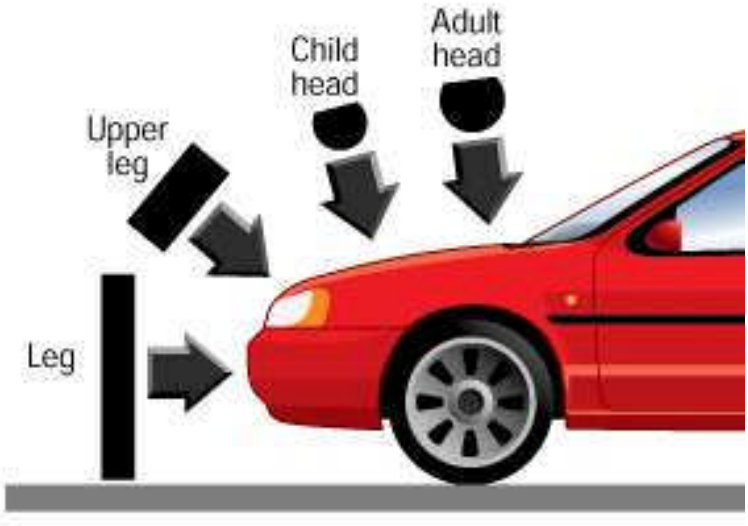

Figure 1-2: Pedestrian Impactors (European New Car Assessment Programme, 2009)

Pedestrian legislation has taken nearly 30 years to implement and is currently being further discussed among the majority stakeholders such as vehicle manufacturers', lobbying groups, researchers and governments across Europe. Although the legislation has been introduced there is debate as to the authenticity of the tests and their replication of real world pedestrian accidents. This has focused the vehicle manufacturers on designing vehicles with regard to pedestrians who come into contact outside a vehicle, as well as the occupants within the vehicle. A phase 1 series of legislative physical tests was implemented in 2005 for new designs and a second phase 2 is planned for 2010, (but is still under discussion) which will cover all vehicle models available on the market.

The emphasis with legislation to date has focused on pedestrian accidents with cyclists. They have not had any specific legislation targeted to prevent and reduce fatalities or injuries and very few researchers have considered in detail the differences between cyclist and pedestrian accidents. It is an assumption that the introduction of pedestrian legislation will also aid cyclists, as both groups generally come into contact with the front of the vehicle. The majority of the research to date has focused on pedestrian accident types, despite cyclists accounting for a significant number of fatalities and casualties.

There are fundamental differences between the two user groups in terms of their kinematics and injuries sustained. Cyclists strike the vehicle in a different orientation and contact different parts of the vehicle which have different levels of stiffness. This research focuses on understanding the nature of cyclists' accidents and how measures to reduce and minimise their impact can be incorporated into existing legislation.

1.2 Cycling Transport Mode

Cycling is a popular mode of transport associated with commuting, sport and leisure activities. The bicycle has been in existence for over 100 years, but has had to share the roads with other forms of transport. When two different transport modes such as cyclists and vehicles interact, especially at road junctions, accidents are more prevalent than on straight roads.

Cyclists, along with pedestrians are known as vulnerable road users as they do not have the protection of a structure around them and do not have passive safety features with their bicycles such as airbags or seatbelts to improve their chances of surviving an accident. Cyclist and driver road sense is not always able to anticipate the severe consequences of collisions. In research conducted in Finland of car to bicycle accidents, 37% of the collisions studied showed that drivers and cyclists are not always able to react or were unaware of an imminent collision, (Räsänen and Summala, 1998). In these collision types, the possibility to reduce the cyclist's injuries could be realised by changing the design of the vehicle or the bicycle (Singh et al., 2007). Further injury reduction techniques may be obtained by the use of protective equipment by the cyclist or the collision could be avoided in the first instance (Rodgers, 1995).

To reduce the number of accidents, various road safety measures have been implemented over the years, such as improvements to driver behaviour, road layouts and vehicle designs. Legislation has also been introduced to prevent loss of life or serious injury by ensuring that vehicle manufacturers meet certain vehicle safety standards. This legislation has reduced the total road traffic fatalities in the last 30 years, but there is potential to reduce the number further and governments have set targets for this.

1.3 Cyclist and Pedestrian Road Usage

In the UK in 1952, 11% of passenger kilometres were undertaken by cyclists and 58% was by motor vehicles. More recently in 2006, the percentage for cyclists had dropped to 1% and motor vehicle passenger kilometres had increased to 85% (Department for Transport, 2007). In 1952, cyclists formed a greater proportion of road users and held greater authority and respect on the roads. The majority of people had ridden a bicycle at some time in their lives on the roads, had developed the skills to cycle efficiently and were aware of the associated dangers. Nowadays, with cyclists on roads being in the minority many car drivers are unaware of the distance required to overtake cyclists safely and cannot anticipate their movements as they lack the experience of performing the tasks themselves as cyclists. Inevitably

collisions occur with the lack of driver vision being a common cause. Räsänen (1998) claimed that if a cyclist with a driving licence, cycled through a known accident site they would be involved in a different type of accident compared to a driver without any cyclist experience.

To understand the nature of cyclist accidents, fatality and injury rates provide an indication of the likelihood of being killed on the roads. Poland had 603 cycling fatalities in 2007, which was the highest number of all EU states. The UK, had 152 fatalities in 2007 and The Netherlands had 188 (European Commission, Directorate-General for Energy and Transport, 2008). To fully understand the risk associated with cycling compared with other forms of transport, fatalities should be analysed with either journeys completed, kilometres travelled or passenger hours.

In developing countries, where cycling is a more common form of transport, the number of fatal accidents are a greater proportion of total accidents (Jacobsen, 2003). With the need for a more environmentally friendly form of transport, cycling is likely to become a more important transport choice for individuals, ahead of the motor vehicle. Understanding the nature and cause of bicycle related injuries has been of interest to a wide range of organisations including government and manufacturing organisations and will continue to be.

1.4 Differences between Cyclists and Pedestrians

Research focussing on pedestrian safety over the last 30 years has provided a significant resource and background to the cyclist safety issue, but the assumption that cyclists are similar to pedestrians is not always valid. Similarities do exist between the two road users, such as the exposure of limbs to direct contact with the vehicle and impact speeds are similar but cyclists have a higher centre of gravity compared to pedestrians due to their positioning on the bicycle and their feet are not in contact with the ground on impact. A cyclist will also be travelling at a greater velocity compared to a pedestrian. This has consequences for their impact conditions with the vehicle as shown by Watson et al. (2009). To date, the cyclist has been conveniently labelled under the vulnerable road user category and legislation that has

been targeted at protecting pedestrians, has also been labelled as contributing to protecting cyclists as well. The legislation is in the form of an EC directive whose title refers to "pedestrians and other vulnerable road users before and in the event of a collision with a motor vehicle". The document mentions vulnerable road users, but concentrates on pedestrian protection only and no reference is made to cyclists (European Parliament and Council, 2003). To understand if cyclists can be grouped with pedestrians, further research work is needed to quantify their similarities and/or differences. The EC 6th Framework Integrated Project APROSYS (Advanced Protective SYStems) addressed these differences and supports this research.

1.5 Objectives of Research

The specific objectives of this research are to:

- Establish the significant differences in terms of input variables and outcomes between cyclist and pedestrian accidents involving vehicles.
- Use simulation models and physical testing to replicate real world cyclist accident scenarios.
- To analyse the injury data from a human mathematical model of a cyclist.
- Recommend future legislative testing techniques for cyclists, based on existing pedestrian legislation.

In this thesis, physical tests were performed with a bicycle and a dummy in a controlled laboratory environment. The computer modelling was performed using the finite element LS-DYNA software code with four different vehicle shapes in over seventy different accident scenarios. The use of finite element modelling techniques has been widely used to predict injury results from road traffic accidents, but has not been used to predict specific cyclist injury mechanisms such as knee shear and bending moments, (Hardy et al., 2009). Human body modelling has the advantage of being able to predict real world injuries instead of dummy indices. By using the two complementary methodologies of testing and modelling, the differences in outcomes of pedestrian and cyclist accidents with motor vehicles were derived.

The implications of these differences, in terms of future legislation for motor vehicle design for pedestrians were also considered. Recommendations for future cyclist legislation are laid out in detail.

1.6 Hypothesis of Research

The premise of this research is that cyclists and pedestrians have different impact kinematics when struck by vehicles. These differences have not been previously measured in a quantitative manner. Therefore to make a distinction between them, this research using finite element modelling and physical testing has been conducted.

1.7 Thesis Layout

Chapter 2 contains a review of current literature in the field of cyclist injuries in road traffic accidents and their comparison with other forms of transport. Accident statistics are reviewed for cyclists in various countries worldwide. Current finite element modelling and testing techniques for cyclist and pedestrian accidents are also referenced.

Chapter 3 describes the methods used to analyse cyclists' accidents. Physical testing and Mathematical modelling were the two methods chosen. Statistical techniques were also used to analyse the results obtained from the mathematical simulations. The STATISTICA software program was used to extract trends for all simulations.

The simulation and physical test results are reported in Chapter 4 for Phase 1 of the results. These were looking at a variety of accident scenarios and provided an indication as to the important variables in cyclists' accidents. The physical tests performed were used to provide data for the mathematical models and a validation procedure for the models.

Chapter 5 describes the Phase 2 simulations and tests performed with pedestrian and cyclist models which were designed to investigate the effect of changing vehicle speed and geometry. Cyclists' injuries and trajectories are compared with pedestrian results.

Discussions from the two phases and consequences for vehicle design are described in Chapter 6, along with ANOVA analysis. Specific cyclist injuries are discussed and the effects of changing vehicle shape and speed of the vehicle on cyclists injuries. Chapter 7 discusses the effect on current pedestrian legislation if cyclists were to be taken into account.

Chapter 8 contains the conclusions from the research and Chapter 9 covers recommendations for further work.

Chapter 2 Literature Review

2.1 Cyclist Accident Data

2.1.1 UK Cyclist Fatality Accident Data

Of the 2000 cyclists killed on European roads in 2007, 136 of them occurred in the UK (UK Department for Transport, 2008). In addition to the cyclist fatalities, pedestrian fatalities accounted for 646 deaths and 1,432 vehicle users were killed in the UK. A cost benefit analysis study showed that the cost of one human fatality was £1.3 million, (Roy et al., 2009); therefore reducing the number of cyclist fatalities by just 10 would save a potential £13 million. This figure was calculated to include the repair costs of vehicles, the effects of traffic congestion, insurance and medical costs.

For the basis of this road accident data, a fatality is a human casualty who has sustained injuries, which caused death less than 30 days after the accident. Confirmed suicides are excluded and a fatal accident is when at least one person was killed.

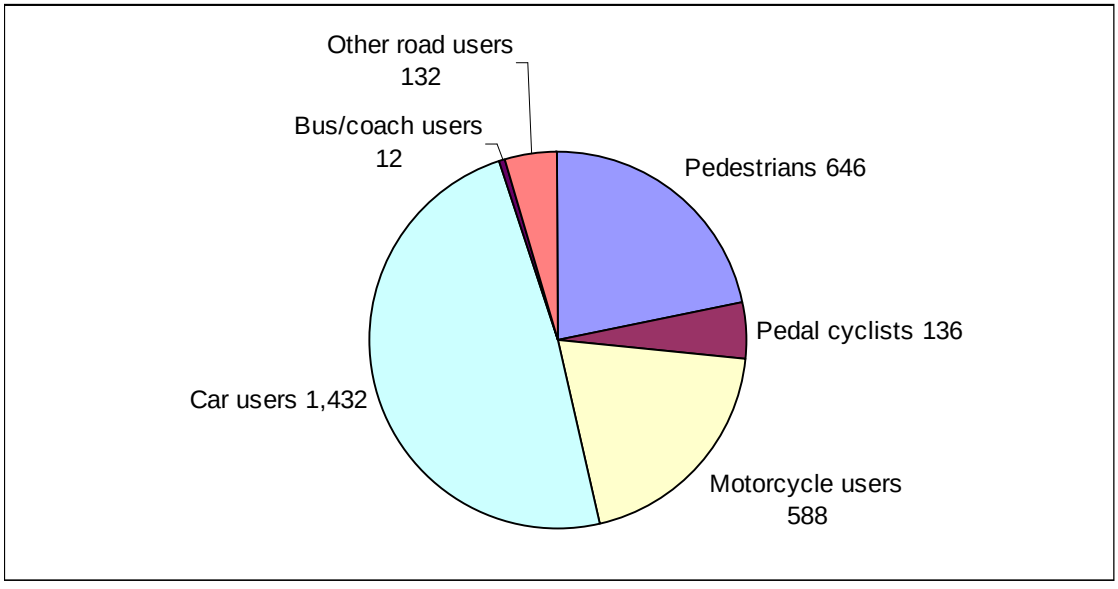

Figure 2-1: Fatalities by Road User Type 2007 (UK Department for Transport, 2008)

The UK road traffic accident statistics show that there was a general trend for a reduction in pedal cyclist fatalities, from a high point in 1984 when nearly 350 cyclists were killed. The number of fatalities has remained at a consistent level since 2000 with no major changes (Figure 2-2).

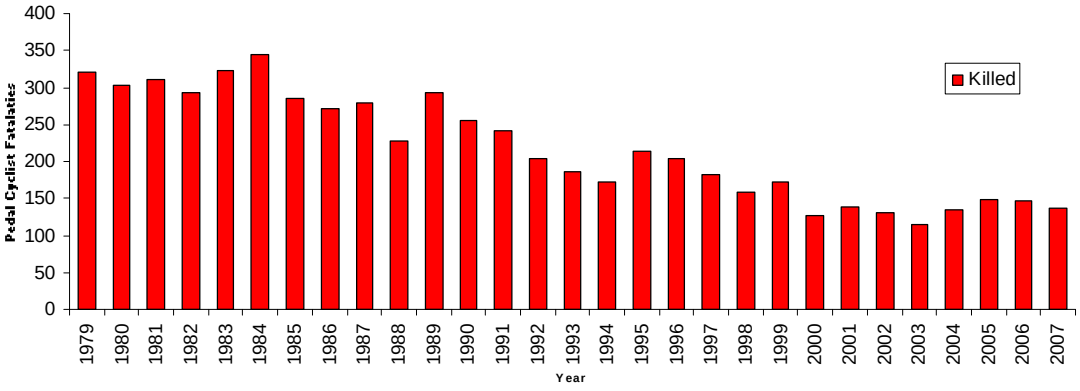

Figure 2-2: Pedal Cycle Fatalities 1979- 2007 (UK Department for Transport, 2008)

However, comparing the exact number of fatalities does not convey the true risk or vulnerability of cycling unless they are compared per hour of exposure, per kilometre travelled and per journeys completed. In the UK, cyclist and pedestrian fatality rates are very similar when assessed against the number of kilometres travelled (UK Department for Transport, 2008), Figure 2-2. As cyclists travel at different speeds to pedestrians an improved measure of cyclist fatality risk is to consider hours of exposure when a cyclist or pedestrian is undertaking their activity. A cyclist is two and a half times more likely to be killed per hour when compared with a pedestrian. Motorcyclists, pedestrians and cyclists are the three groups of users that have greater fatality rates than the car. Travel by air, sea, railways, coach and vans are all safer. Motorcycling is by far the most dangerous form of transport.

Table 2-1 assumes that the car has a risk of 1 and the other modes of transport are shown relative to the car. The air transport refers to all types of air travel, large public and small private.

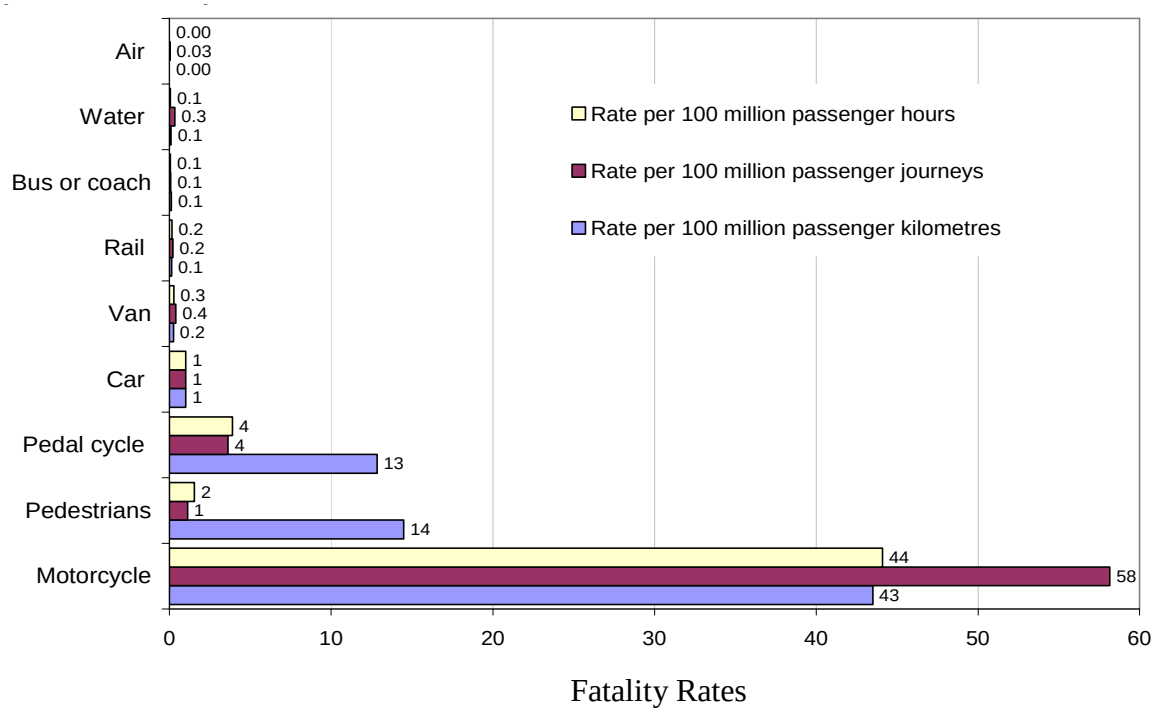

Table 2-1: Fatality rates per 100 million passenger kilometres, journeys and hours in UK 2006, Relative to the Car = 1, (UK Department for Transport, 2008)

The rate of cyclists killed per number of journeys completed is higher than pedestrians. Therefore, if cyclists complete longer journeys, every time that they use the roads they are more likely to be involved in a fatal accident. Pedestrians can complete numerous smaller journeys before they are likely to be involved in a fatal accident. The statistics from completed journeys and hours exposed to traffic are more indicative of the risks for vulnerable road users.

This data can be analysed in an alternative way by looking at the time spent on the road before you have a risk of one in a million of being killed. A pedal cyclist has to be exposed for 2 hours and 40 minutes, whereas an air passenger has to be exposed for 4,300 hours of travel time. Air travel is an extremely safe mode of transport considering the distances that are covered, the hours travelled and the number of journeys completed. Motorcycling is the most dangerous mode of transport as the exposure time needed is only 14 minutes to have a risk of one in a million of being killed.

2.1.2 UK Casualty Rates for Other Road Transport Modes

Although fatalities make up a small proportion of the total number of cyclist casualties (Figure 2-3), the risk values from fatal cyclist accidents are higher, if killed and seriously injured values are combined. A cyclist is four times more likely to be killed or seriously injured in an accident compared to a pedestrian, but if all casualties are considered the difference increases to six times (Table 2-2). In comparison to car accidents, cyclists and pedestrians are at a greater risk of injury in all six categories highlighted in Table 2-2.

			All values rate per million
Mode	Passenger Kilometres	Passenger Journeys	Passenger Hours
Killed and Seriously Injured			
Car	2.2	29	87
Van	0.6	14	31
Motorcycle	120	2100	4700
Pedal cyclist	53	200	640
Pedestrians	37	38	160
Bus or Coach	0.9	8	19
All Casualties			
Car	26	350	1000
Van	6.8	150	320
Motorcycle	420	7500	17000
Pedal cyclist	350	1300	4300
Pedestrians	160	170	700
Bus or Coach	16	140	340

Table 2-2: Road Passenger Casualty Rates by Mode of Travel in 2006 (UK Department for Transport, 2008)**.**

2.1.3 UK Cyclist Casualty Rates

When cyclist casualties are compared over the last 28 years the number of fatalities was a small proportion. The largest proportion is the slightly injured category. The ratio of killed/serious injured to slight casualties has remained at a constant level, even if the total number of casualties has reduced to 16,195 in 2007 (Figure 2-3).

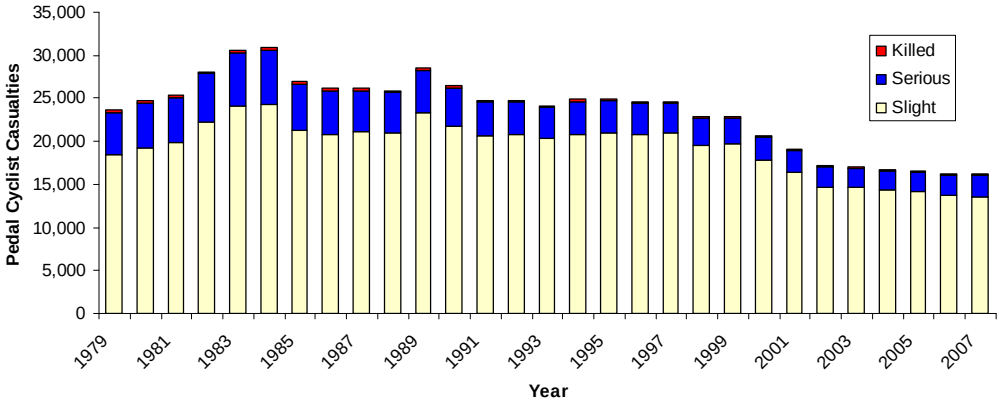

Figure 2-3: Pedal Cycle Casualties 1979 – 2007 (UK Department for Transport, 2008)

2.1.4 Gender and Age of Cyclist Fatalities

According to the UK STATS19 database, which is a record of road traffic accidents collected by the UK Police, cyclists aged between the ages of 11 to 15 form the greatest numbers of cyclist casualties. Children are more likely to be involved in cycling accidents due to their inexperience in road conditions and the popularity of cycling at that age. After the age of 30 there is a steady decline of casualties and the proportion of male to female casualties' ratio is consistent at 80:20 and this disparity is also highlighted in Figure 2-4.

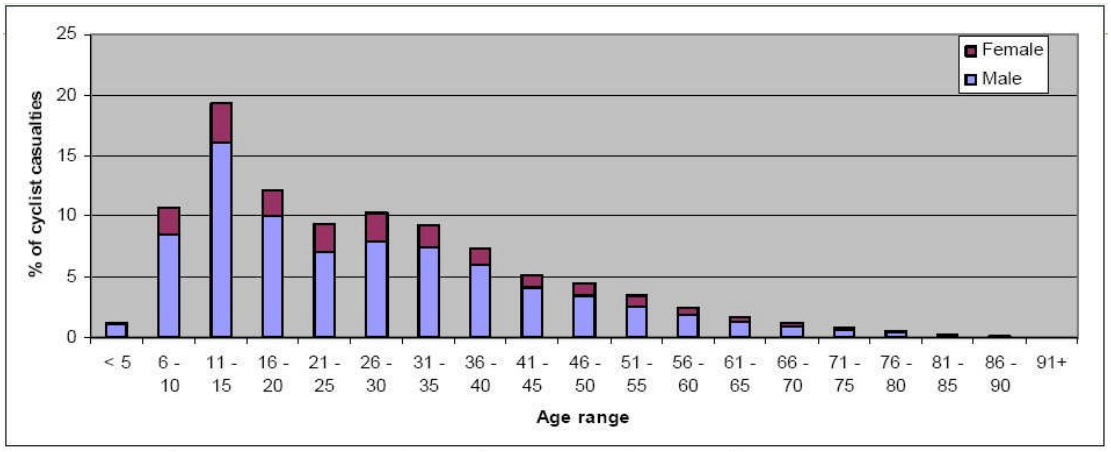

Figure 2-4: Age and Gender of Cyclists from UK Fatals Database (Carter, 2005)

2.1.5 UK Transport Accident Data Trends

As an overall trend, the number of fatalities in all road traffic accidents on UK roads has been falling over the last 26 years (Table 2-3). Cyclist fatalities have mirrored these trends with the rate falling from 345 in 1984, to 136 in 2007. However, between 2003 and 2006 the number of pedal cyclist fatalities increased. This change in trend may be just a statistical fluctuation or it may be attributable to the increasing number of cyclists on the roads. Over the next few years the number may rise further due to the cost of motoring forcing drivers to switch to a more environmental means of transport such as cycling. If the cycling usage rate continues to increase, the check that would prove that cycling is a less dangerous transport mode, would be to analyse the fatality rate per journeys covered, as in Table 2-1, instead of analysing the total number of cycling fatalities, as previously shown in Figure 2-1.

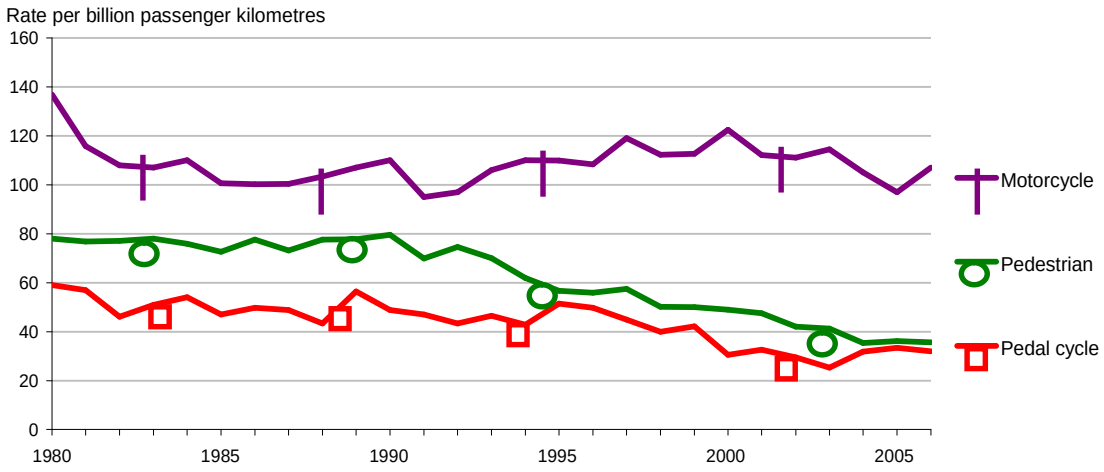

Table 2-3: Passenger fatality Rates, Motor cycles, pedestrians and pedal cycles: 1980 to 2006 (UK Department for Transport, 2008)

2.1.6 European Accident Data

In other European countries the accident data varies between member states. In The Netherlands 20.1 % of fatalities are cyclists due to their high cycling participation rates (European Commission, Directorate-General for Energy and Transport, 2008). In comparison, Greece which although has only a slightly lower total number of fatalities but a lower percentage (1.5 %) of them are cyclists. With EU statistics the methodology of collecting data is different amongst the police and accident units that process data; however the percentage of cyclist fatalities compared to total road fatalities would not differ significantly with the exception of Spain (Carter, 2005). The proportion of fatalities in Spain was 4.7% compared with 0.7% for the UK. This was attributed to more elderly people who cycled in Spain and that they were more frequently involved in fatal accidents.

In Sweden, the ratio of men to women fatalities was 53:47, which is more equal compared to the UK and Spain where a greater proportion of men are being killed in cycling accidents. This is attributed to the greater number of men in the UK choosing cycling as a mode of transport.

	UK	Sweden	Germany	Spain
Proportion of fatalities	0.7%	1.4%	0.8%	4.7%
Proportion of seriously injured	13.4%	17.2%	19.8%	24.8%
Most frequently injured age group	11 - 15	11 - 15	10 – 15	15 - 20
Proportion of child casualties	31%	18%	19%	14.5%[8]
Male:female ratio	80:20	53:47	61:39	89:11

Figure 2-5: Proportion of Cyclist Fatalities and Seriously Injured, Age Groups and Male/Female Ratio (Carter, 2005)

2.1.7 China Accident Data

In China, bicycles are the most common mode of transportation. The total number of cyclists' accidents in 2007 was 4939, slightly lower than the number of pedestrian accidents (5407) and the fatality rate for cyclists is far below pedestrians (957 compared with 1954). Therefore, you are more likely to die if involved in a pedestrian accident, compared with involvement in a cyclist accident. However, the injury rate per accident is higher for cyclists than pedestrians. This implies that cyclists are more likely to be injured in an accident, but are less likely to be involved in a fatal one (China Automotive Information Net, 2008).

Type	Number of Traffic Accidents (case)	Number of Deaths (person)	Number of Injuries (person)
Total	327209	81649	380442
Serious Accidents	71289	81649	42602
Extraordinarily Serious Accidents	1469	5713	4508
Vehicles	309261	77696	363428
Motor Vehicles	213666	56089	243122
Motorcycles	83008	17403	106989
Bicycles	4939	957	4680
Ped and Passengers	5407	1954	3994

Table 2-4: Chinese Accident Statistics (China Automotive Information Net, 2008)

Vehicle ownership per population is considerably higher in Europe compared with China which gives an indication of the density of motor vehicles and their integration with vulnerable road users such as cyclists. In Europe there are 300 cars per 1,000 of the population whereas in China there are only 40 cars per 1000, (Green Car Congress, 2010). This figure is likely to grow considerably in China, but it has a long way to catch up with Europe. From 1991-2001, the overall length of road constructed within China only increased by 30 per cent while total road passenger volume and road cargo volume went up by 120 per cent and 46 per cent respectively. Therefore, Chinese roads are becoming more congested, but they are also of a lower quality than European roads, (Shanghai Star, 2004).

Accident analysis from Japan was considered for pedestrians and cyclists against different vehicle shapes, which is unique amongst any literature published. The data from Japan showed similar trends as China with Maki et al. (2003) stating that "bicyclists were less likely to sustain a fatal head injury than pedestrians" (Figure 2-6). The data also showed that cyclists suffered a greater number of fatal head injuries (3.5 per 1000 accidents) with SUV's and minivans. In comparison, pedestrians suffered 18 fatal head injuries per 1000 accidents. The vehicle shape which produced the least number of cyclist fatal head injuries was the sports and speciality vehicle (Under 1 per 1000 accidents). An important result from the accident data was that the head was the injury region most severely injured in fatal accidents accountable for the most significant injury mechanism in 64% of pedestrian and 72% for cyclist accidents. These figures have been derived from large databases of over 6,500 accidents which add credence to the figures. Of these fatal head injuries approximately 12 occurred for every 1000 pedestrian accidents. In comparison only 1 to 3 occurred for every 1000 bicycle accidents, which was much lower. Therefore, according to Maki et al. (2003) you are more likely to receive a fatal head injury if you are involved in a pedestrian accident instead of a cyclist accident. These figures are in conflict with the UK data where the risk of being a casualty is greater for a cyclist, rather than a pedestrian.

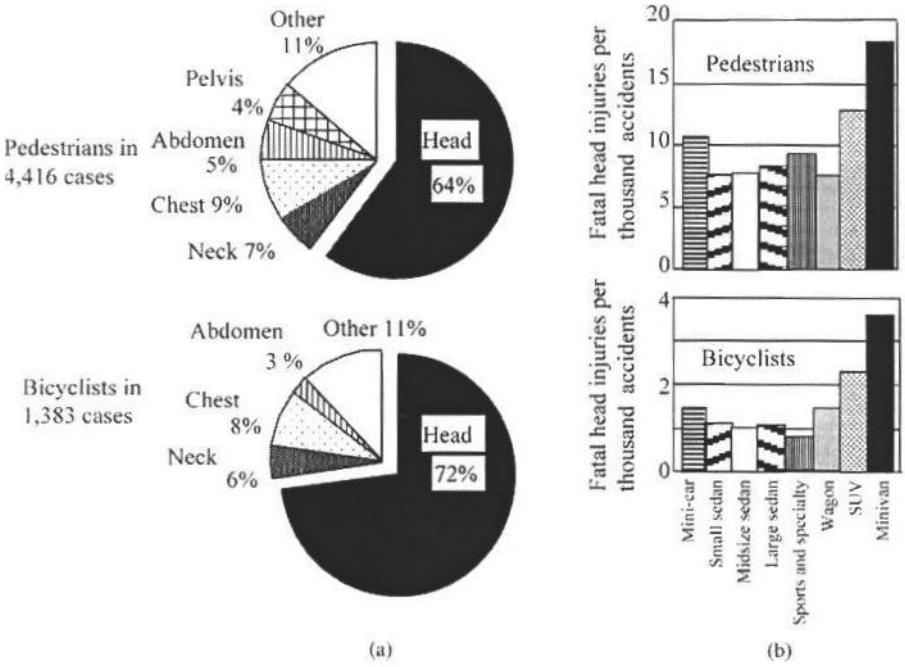

Figure 2-6: Breakdown of Fatal Injury Regions and Distribution of Fatal Head Injuries and Serious Injuries by Vehicle Type (Maki et al., 2003)

2.1.8 UK Government Strategy

To address the issue of road accident casualties, in 2000, the Government published a safety strategy entitled 'Tomorrow's Roads Safer for Everyone.' By 2010, the aim was to achieve the following outcomes, compared with the average for 1994-98:

• A 40% reduction in the number of people killed or seriously injured (KSI) in road accidents;

• A 50% reduction in the number of children KSI (children are defined as being those aged under 16);

• A 10% reduction in the slight casualty rate, expressed as the number of people slightly injured per 100 million vehicle kilometres

Compared with the 1994-98 average baseline, in 2007

• The number of people KSI was under 31,000, 36 per cent below the baseline.

• The number of children KSI was 55 per cent below the baseline.

• The slight casualty rate was 32 per cent below the baseline for all accidents.

• In this period the traffic has risen by an estimated 16 per cent.

Therefore the greatest reduction in casualties has been with children, whereas the number of adults killed or seriously injured has not been sufficient enough to reach the target. At this stage the Government should be able to meet the targets if the current reductions continue at the same rate. The accident statistics from pedal cyclists show that although the numbers of fatalities and serious injuries are reducing and contributing to the targets, the drop in car driver casualties is greater and therefore affecting the reduction in the targets by a greater proportion.

2.1.9 Passive and Active Safety Approaches

The method of addressing the 2010 problem has been tackled with two approaches, 'passive' or 'active' safety. A passive safety approach involves the use of seatbelts, airbags and vehicle design to protect the occupant or vulnerable road user once the accident has happened. The alternative active approach is to try and stop the accident occurring in the first instance by braking the car automatically, using Anti-Lock Braking Systems (ABS) or firing the airbag before the accident has occurred. For cyclists the passive safety approach would offer more opportunities for injuries to be reduced following changes in the design of vehicles. Implementing those changes to vehicles are more likely if legislation is in place to test vehicles at the impact locations where cyclists are likely to strike vehicles. Vehicle manufacturers need a legislative framework to design protection systems for all types of vulnerable road users, not just pedestrians which are currently in place.

Various studies have been performed to date to address the issue of pedestrian and cyclist fatalities and serious injuries. In most cases physical tests and/or mathematical models have been used to address pedestrian accidents. However, there has not been any work explicitly directed towards cyclist accidents using a human mathematical model in combination with physical tests.

2.2 Crash Safety Legislation for Motor Vehicles

2.2.1 Crash Tests, Dummies and Cadavers

The reconstruction of vehicle crashes has been performed for over 50 years and the understanding of the nature and causes of vehicle crashes has led to a considerable amount of work on the crash performance of vehicle structures. A controlled collapse of the vehicle structure benefits the occupants by limiting the acceleration peaks that cause injury to them. Ralph Nader published his book 'Unsafe at Any Speed' in 1965, which exposed the automotive industry of not taking the safety of occupants seriously enough, (Nader, 1965). Nader campaigned for safety features to be standard on vehicles and the acceptance that changes to the vehicle can make a difference to the survivability of a crash. Up to 1965, the blame for fatalities and injuries from crashes had been attributed to driver error, but Nader challenged that attitude. Initially, in a number of court cases automotive companies were reluctant to reveal the engineering details of their vehicle designs and preferred to settle out-of-court if they were challenged. Subsequently, companies did start to take safety seriously as the public became more aware of the dangers associated with being involved in a crash.

The tolerance of the human body to withstand vehicle impacts has also been researched extensively. Volunteer tests were initially used, but as the need to investigate higher speeds the risk of permanent injury increased to an acceptable level and alternative methods were needed. Colonel John B. Stapp was an early pioneer in volunteer testing. He strapped himself to a sled and was propelled at speeds which nowadays would be deemed to be too dangerous (Peters and Peters, 2002). The tests performed by volunteers did produce useful information regarding human tolerance limits and further attempts to replace the humans with animals was not considered appropriate or accurate enough.

As an alternative cadavers (or parts of) were used to replace volunteers in crash tests, (Kerrigan et al., 2005). They were used to establish human injury tolerance limits for occupants and pedestrians in crash scenarios, but their use has been limited as there are only a small number of establishments in the world that can use them and there are ethical issues with their use, (Nahum and Melvin, 1993). They have the advantage

of providing test data on real human tissue, but most available cadavers are elderly which limits their applicability. During a road traffic collision the human reacts to the impending collision by tensioning muscles or trying to avoid the collision just before an impact. A cadaver cannot perform these actions, but then neither can a dummy, and even computer models are limited in their capabilities to simulate these pre-impact motions. The usage of child cadavers is even further limited as their usage is deemed ethically unacceptable by society.

The next alternative to cadavers was the use of crash test dummies as replacement drivers or passengers of vehicles in frontal and side impact tests. Dummies do not have the complexities of a human but they do have the capability to assess the performance of a vehicle by providing repeatable data, which allows engineers to compare different vehicle structures in crash tests. The bio-fidelic properties or ability to replicate human injuries is constantly being debated but their use in the crash testing environment is now considered to be permanent. A physical crash test dummy is positioned in various seating positions within a vehicle with an extensive array of recording equipment to capture the severity of a specific accident. In these controlled tests a barrier consisting of aluminium honeycomb is propelled into the side of the vehicle or the vehicle itself is propelled into a rigid wall. The vehicles are destroyed in the tests and the severity of tests deems them unsuitable for human volunteers to be used. The Hybrid III dummy is the most commonly used dummy; it was developed by General Motors and represents a 50^{th} percentile (average) person, (Backaitis and Mertz, 1994). The European Commission (EC) is the legislative body that enforces these tests and makes them mandatory for all vehicles on the roads.

A drawback of using dummies is their inability to capture the same kinematics and injuries observed in real world crashes from humans. They are made stiffer than a human, especially in the spine region, so that they can be used repeatedly. They are constantly being developed for different sized occupants, including children and have been used outside the automotive sector for military applications such as understanding fighter pilot ejection and blast testing. The dummies do have

advantages that vehicles can be assessed against a measure that gives consistent results and the performance of vehicles can be evaluated under laboratory conditions.

Initially, the use of a test dummy to replace a living person was considered for future pedestrian legislation, which was similar to the approach used already for vehicle occupants. However, this was unsuitable as there are a wide range of pedestrian accident scenarios to be considered and there was an issue with reproducing these accidents with any repeatability.

2.2.2 Pedestrian Impactor Testing Methodology

In the majority of cases, cyclists and pedestrians are struck by the front of a motor vehicle and this was recognised by the European Experimental Vehicle Committee (EEVC) in 1982. Working Group 10 (WG10), of the EEVC was formed in 1987 and they devised a set of testing methods to assess pedestrian protection for passenger cars. A follow on group, WG17, was formed and continued to investigate the pedestrian impactors. From these working groups, a set of impactors with the geometry of pedestrian body parts were devised and were the basis of future legislation.

Instead of using a full pedestrian dummy an alternative approach was devised of splitting the human body into the components that were more likely to come into contact with the vehicle during an accident. These components were similar in construction to the dummy models with their inherent stiffness and the ability to capture the real world accidents.

The pedestrian impactor methodology involved firing a series of impactors, which represented specific human body parts such as the head and lower legs onto the front of a vehicle, (

Figure 1-2). Measurement devices attached to the impactors recorded the deceleration or load levels during the impact with the vehicle front and these were assessed against pre-determined criteria. If the load or acceleration levels were too high the vehicle was considered not to be ‘pedestrian friendly’ and would fail to meet the standards

necessary to pass the legislation. A phase 1 series of legislative physical tests was implemented in 2005 for new designs and a second phase 2, although still being discussed, is planned for 2010 which will cover all vehicle models available on the market (Figure 2-7 and Figure 2-8).

The legislation is a high priority for manufacturers because if vehicles do not pass they are unable to be introduced into the market place. Further issues have arisen regarding their validity to replace a full dummy test, in particular if the impactors strike the same regions of the vehicle that a dummy or human would strike. For the pedestrian tests the wrap around distance (WAD) concept, was used to calculate the regions of impact, but an alternative method may be more appropriate. In addition, the bio-fidelic nature of the impactors is being discussed which is the same ongoing debate as is the case for the dummies used in interior vehicle tests.

When test devices are used such as the pedestrian lower legform they are designed to be used under specific loading conditions such as the leg standing upright. However, in reality a pedestrian's leg is not always positioned in a straightened stance at the time of vehicle impact and a cyclist's leg is likely to be raised off the ground. As such the legislative pedestrian leg impactor is not the most appropriate tool to assess cyclist injuries.

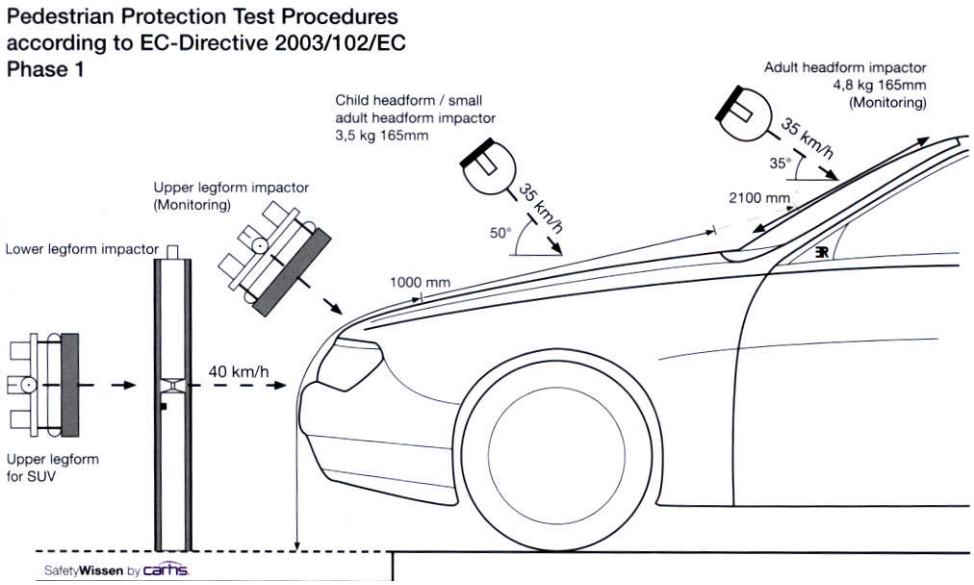

Figure 2-7: Phase 1 Pedestrian Protection Legislation from October 2005 (Carhs Training, 2008)

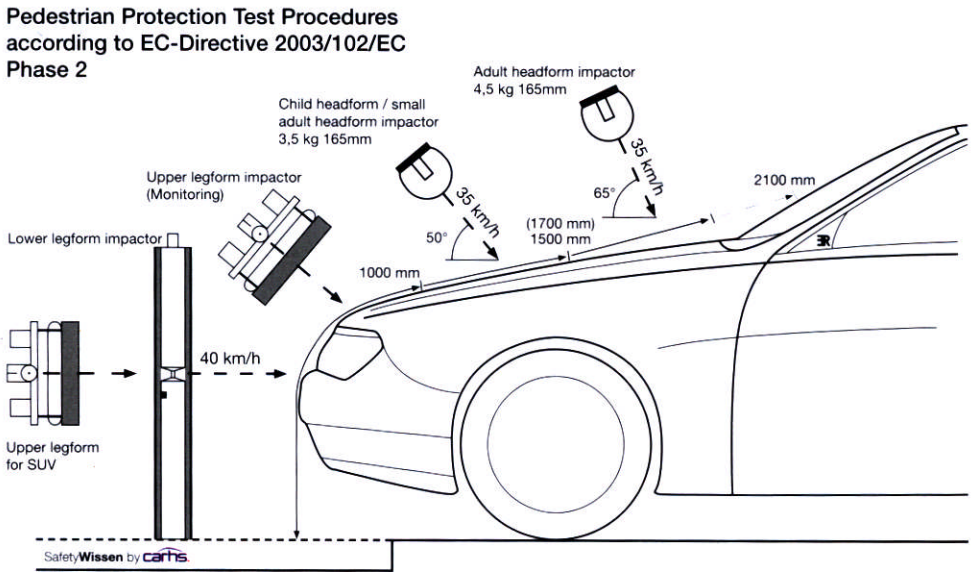

Figure 2-8: Phase 2 Pedestrian Protection Legislation from September 2010 (Carhs Training, 2008)

For all vehicle safety requirements including pedestrian impactor tests and vehicle crash tests for occupants, manufacturers address the safety tests seriously as they influence sales and the marketability of their vehicles. There is now focus among

vehicle manufacturers to design vehicles with respect to pedestrians who come into contact outside of the vehicle, as well as the occupants within the vehicle.

Although pedestrian legislation has taken nearly 30 years to implement it is still currently being discussed among the majority stakeholders such as vehicle manufacturers, lobbying groups, researchers and governments across Europe. There is debate as to the authenticity of the tests and their replication of real world pedestrian accidents.

2.2.3 Development of Pedestrian Tests

The introduction of the legislation has focused the vehicle manufacturers into changing the front end geometry to be more compliant or pedestrian friendly. From the original approach of EEVC working group 17 (European Parliament and Council, 2003) the test details have changed significantly as the car industry have claimed that the introduction of day-time running lights and brake assist have mitigated the need for the legislation. A key difference between Phase 1 and 2 of the legislation is the lack of impact testing on the windscreen of the vehicle. It was deemed that pedestrian impacts would more likely to occur on the bonnet and any impacts on the windscreen would result in low injury values. The tests are targeted towards protection of vulnerable road users, and in that category pedestrians, cyclists and wheelchair users are grouped together. No specific reference is made to cyclists within the legislation as it is dominated by the issue of pedestrian impacts with vehicles. A benefit of the legislation is the effect forced on vehicle manufacturers to adapt their designs to pass the tests, but there is scope for them to be further adapted to cover cyclist impacts as well.

2.2.4 EuroNCAP

Alongside the European legislation, EuroNCAP exist as a consumer body to improve vehicle safety. They have been performing tests with the WG17 impactors since 2001, but their criteria are slightly different from the EC. They do include a windscreen head impactor test up to a WAD of 2100mm, but this test is not always

implemented. Their head impact speeds are also higher than WG17, 40 km/hr, instead of the 35 km/hr.

2.3 Differences in Injury Mechanisms Between Motor Vehicles Occupants and Cyclists/Pedestrians in Impacts

There is also a fundamentally different approach to understanding the effect of a collision on a pedestrian, as compared to a vehicle occupant. A pedestrian or cyclist receives a direct impact with a vehicle in a collision, and the vehicle transfers its energy into the cyclist by direct loading from the front-end of the vehicle to the cyclist. When a vehicle occupant is involved in an accident the driver or passenger experiences forces and because of having inertia is projected in the direction of travel even if after the vehicle has come to a stop. Restraint systems such as seatbelts and airbags work effectively to prevent the occupants from being propelled within the vehicle interior, but do not protect against the damage caused by the inertia of internal human organs such as the heart or lungs and how they interact with the rib cage.

To balance the safety needs of road users, a vehicle manufacturer needs to design the vehicle structure with the required structural integrity to withstand and keep the occupant within a survival space, but at the same time it needs to be compliant for impacts with pedestrians and cyclists. It is this conflicting demand of the structure, which is one of the greatest challenges for designers.

2.3.1 Differences in Crashes between Pedestrians and Cyclists

The emphasis with legislation to date has focused on pedestrian accidents instead of cyclist accidents. They do not have any specific legislation targeted towards preventing or reducing cyclist fatalities and injuries. Very few researchers have considered in detail the differences between cyclists and pedestrian accidents. It is an assumption that the introduction of pedestrian legislation will also aid cyclists, as they generally come into contact with the front of the vehicle. The majority of the research has focused on pedestrian accident types, despite cyclists accounting for a large number of fatalities and casualties.

There are fundamental differences between the two user groups in terms of their kinematics and injuries sustained. Cyclists strike the vehicle in a different orientation and make contact with different parts of the vehicle which have different levels of stiffness. This research focuses on understanding the nature of cyclists' accidents and how they can be incorporated into existing legislation.

2.4 Future Accident Data Trends

Jacobsen (2003) stated that "A motorist is less likely to collide with a person walking and bicycling if more people walk or bicycle. Policies that increase the numbers of people walking and bicycling appears to be an effective route to improving the safety of people walking and bicycling". This data was obtained from the UK, Denmark, The Netherlands and the USA. This experience was also witnessed in the city of York in the UK. A Cyclists Touring Club (CTC) survey found that when 12 % of people cycle to work there were 10 serious injuries per 10,000 cycle commuters, (Webster, 2008). In comparison across the whole of Britain only 2.8% of the population cycle to work and of those there were 32 injuries per 10,000 cycle commuters.

In 2008 there has been an increase in bicycle sales in response to an increase in fuel prices and the economic climate. It is cheaper to cycle and with the roads becoming more congested the bicycle can be a quicker form of transport as the number of vehicles on the roads increases. This is more relevant for inner cities, which also have the factor of congestion charging increasing the cost of driving a vehicle. The SUV vehicle shape was highlighted by Depreitere (2004) as a vehicle type that is increasing in use and would cause an increasing number of pedestrian injuries due to its front-end shape and the increase in use may subside if the cost of motoring continues to increase. As a consequence this may also affect cyclist injuries.

For the bicycle to be perceived as a safe form of transport, more cycling journeys need to be undertaken to increase the visibility of cyclists and make car owners more aware of their specific needs. More cycle lanes, improved education for children and better road junction design for cyclists where most accidents happen, will make a significant difference. An increase in cycle journeys taken may well increase the

number of cyclist casualties, but the percentage of casualties to the total number of journeys could decrease.

2.5 Cyclist Head Injuries

2.5.1 Introduction to Head Injuries

There is a consensus among pedestrian and cyclist accident research that the head is the most important region of the body to protect during an impact (Maki et al., 2003; Mills, 2008). It is the cause of the majority of fatal accidents, but the injury mechanisms of the head are not always understood. This review of head anatomy and common injuries highlights the vulnerability of the head in cyclist accident impacts and the importance of obtaining accurate impact conditions.

2.5.2 Head Injury Statistics

Maki et al. (2003) described the head as the most important body region to be considered in Japanese accidents. In 64 % of pedestrian cases head injury was the cause of fatality, but for cyclists the percentage was 72%. Different vehicle types were also examined including the mini-Van and SUV vehicle types which produced the greatest number of fatal head injuries. A pedestrian was also four times more likely to receive a fatal head injury per 1000 accidents, indicating that cycling was a safer form of transport when compared with walking, (Figure 2-6).

Otte (1989) identified that below 30 km/hr no serious head injuries were observed for cyclists. More specifically, head injuries were not associated with fracture below 30 km/hr and it is the combination with bone fracture that causes the most serious injury of the brain. These injuries are realised when cyclists strike the bonnet, windscreen and A-Pillar areas. Otte also commented that 73 % of collisions were between the front of the vehicle and the cyclist. Therefore, in the simulation task the cyclist has been positioned in a side on orientation with the front of the vehicle. The data from Otte was recorded in the German Federal Republic in 1987.

Mills (2008) commented that cyclist head impacts were vulnerable to trauma when struck from the side and a shoulder contact prior to head impact reduced the head

impact velocity. The influence of the shoulder in collisions with the bonnet was a result observed in the simulations performed and reported in Chapters 4 and 5. Accurate representation of the shoulder mechanism would ensure that a realistic head velocity was obtained from the simulations. In addition, two thirds of head injuries could be prevented by the wearing of cycle helmets, (Richter et al., 2007).

2.5.3 Head Anatomy and Injury Mechanisms

Willinger et al. (1994) described the head anatomy as, "the brain occupies the top half of the skull; it is subdivided in the midline into two cerebral hemispheres, separated by the falx cerebri (a membrane between hemispheres), a vertical tough membrane hanging from the skull. The cerebral hemispheres are joined at their lower portions by the corpus callosum, in which masses of nerve fibres connect the right and left halves of the brain. The brain and the skull are separated by three membranes which are continuous over the brain surface and by the cerebrospinal fluid. Blood vessels (including the bridging veins) which supply the brain pierce the membranes and run between brain and skull", (Figure 2-9).

The brain sits on top of the cerebellum which is 'posterior to the brain stem' (Tortora and Grabowski, 2000) which in turn is connected to the spinal cord. 'The falx cerebri separates the two hemispheres of the cerebrum and the falx cerebelli separates the two hemispheres of the cerebellum' (Tortora and Grabowski, 2000). The cerebrum and cerebelli are further separated by the tentorium cerebelli.

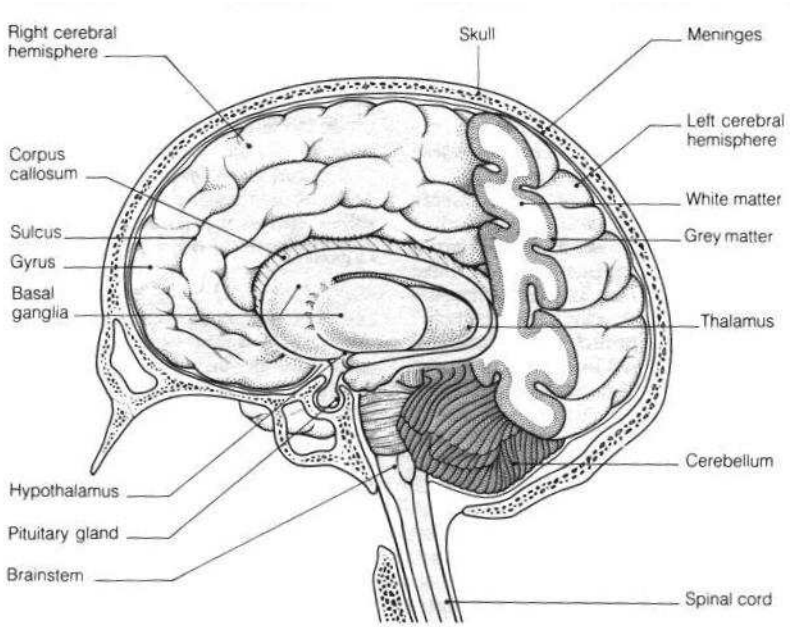

Figure 2-9: Brain Anatomy (Tortora and Grabowski, 2000)

Bandak and Eppinger (1994) noted that 'brain injuries occur due to rapid momentum changes resulting from direct contact forces to the head or from non-contact forces transmitted through the neck as a result of velocity difference between the head and the rest of the body(Bandak and Eppinger, 1994). This is precisely what happens when a head strikes the bonnet or windscreen of a vehicle". Bandak and Eppinger (1994) also commented that damage can be to the neuronal (nerve tissue), vascular (blood vessels) or cytoskeletal (the brains matrix material) structures. A common mode of damage to the nerves is Diffuse Axonal Injury (DAI) and can be "observed in more than 50 % of all head injuries".

2.5.3.1 Head Injury Criterion (HIC)

The Head Injury Criterion (HIC) was developed on the basis of direct impact with the skull in a forward direction against a rigid plate. It was based on linear acceleration of the head over a defined time period and was originally used for interior head injury assessment under the FMVSS201 legislation. In 1965, the Wayne State Curves were developed for assessing fore head impacts onto a hard surface such as a steering wheel (Peters and Peters, 2002). The curve shows that if the duration of impact is low

(5-10 ms) the acceleration level needed to cause injury increases, (80-250g). HIC is now accepted and used in a multitude of situations where the head is damaged, even when the head does not come into direct contact with an object (Jiroušek and Jíra, 2005). There is also not a rotational acceleration component, only a linear acceleration component in the calculation; therefore the de-coupling of the brain from the skull which is the cause of DAI injury is not covered by HIC (Willinger et al., 1994). There is further evidence from Eppinger et al. (1999) that the HIC was unsuitable for an assessment of brain injury without head contact. In cyclist head impacts with the bonnet and windscreen, the brain generally experiences a linear and rotational acceleration pulse.

2.5.3.2 Importance of Head Impact Conditions with Vehicle

Up to the time the head strikes the vehicle, a number of other injury mechanisms are capable of resulting in severe injury for a cyclist, for example, only knee ligament damage is described in section 2.6. The emphasis in this research is for the injuries and kinematics of the cyclists up-to head contact. The head contacts with the bonnet have been modelled and the simulations have been allowed to continue beyond the head striking the bonnet or windscreen. However, the bonnet and windscreen models have been included for indicative purposes and therefore any head injury assessments are dependent on validated accurate material modelling of the vehicle structure. To have calculated an accurate HIC value, a detailed model would have been required of the bonnet and under-bonnet components to map the different regions and their localised stiffnesses.

The kinematics leading up-to head contact, the head strike just before impact and the angle at which the head strikes the vehicle are three main variables that have been analysed. These three parameters were compared with the impact conditions stipulated in current and future pedestrian legislation without directly looking at head injuries. Comprehensive research on head injuries following impacts with the bonnet are addressed by (Willinger et al., 1994) (Verschueren et al., 2007) and (Horgan and Gilchrist, 2003).

2.6 Cyclist Lower Limb Injuries

2.6.1 Lower Limb Injury Statistics

Examining the Japanese accident statistics from Maki et al. (2003), the leg region accounted for the highest percentage of serious injury regions for pedestrians and cyclists, 49% of pedestrian and 43% of cyclists. Other body regions which contributed to a serious injury were the head 21%, arm 13% and chest 10% (Figure 2-10). From the serious leg injuries an average of 20 to 40 occurred for every 1000 accidents. The SUV accounted for the highest accident rate.

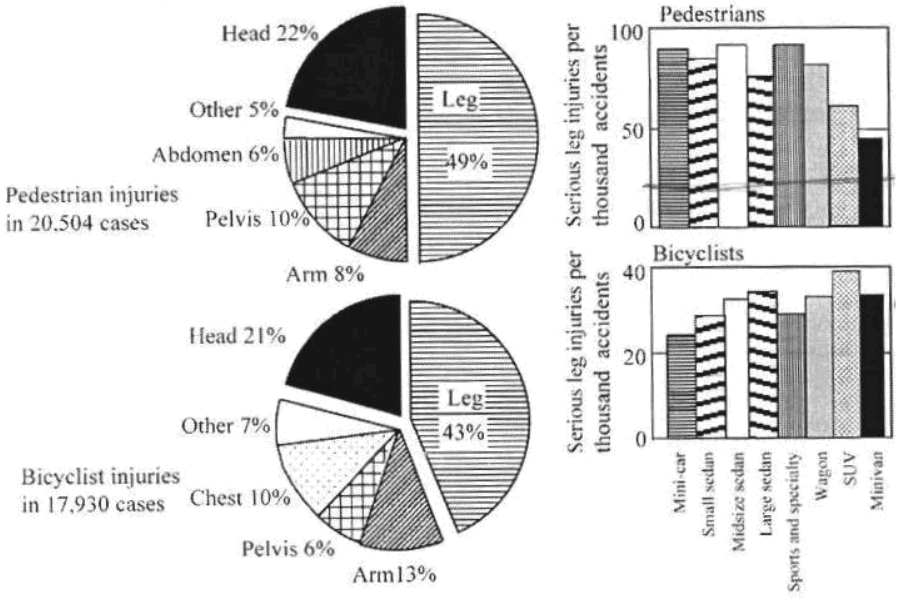

Figure 2-10: Breakdown of Serious Injury Regions and Distribution of Serious Leg Injuries by Vehicle Type (Maki et al., 2003)

2.6.2 Lower Limb Anatomy

Lower limb injuries are not life threatening injuries but they can involve long term recovery costs and incur long term disability. As a cost to society it is possible that a lower leg injury can be greater than a head injury if the injury needs intensive care over 20 or 30 years. The knee joint is particularly prone to damage due to its likelihood to be directly loaded in a cyclist side-on collision. Bermond et al. (1993) described the knee joint anatomy as, “The femur or thigh bone is connected at the

knee joint to the tibia and fibula. The patella or knee cap sits at the front of the knee joint. The condyles of the femur and tibia bones are semi-spherical balls that are fixed into the knee joint. They are part of a ball and socket like joint that provides articulation for the knee. The condyles are covered with cartilage which allows free movement of the joint."

"The bones of the knee joint are connected together by ligaments, with the medial lateral ligament and lateral collateral ligaments being positioned on the outside of the knee joint. Inside the knee joint the anterior and posterior cruciate ligaments are crossed over each other and are continually stressed," (Bermond et al., 1993).

2.6.3 Bone Injury Mechanisms

Levine (1986) described lower limb injuries in particular bone fractures which "are likely to be displaced or un-displaced. An un-displaced fracture is when a bone has not changed in its profile, but cracks have appeared on its surface that may have reached to the core of the bone. A displaced fracture is when part or parts of the bone are no longer in their original anatomical position and will need re-alignment. Fractures can occur at different locations along the bone length with some fractures puncturing the skin surface, these are known as 'open fracture'. There is a classification range of bone fractures determined by their location and severity called the Salter and Harris epiphyseal injury classification (Levine, 1986)". The epiphyseal is the area of the bone where growth takes place and is situated by the knee joint. Manoli (1986) described fractures to femurs and in particular tibias which are common in pedestrian accidents. At the top of the tibia there is less soft tissue to protect the bone and an open type fracture is common. The nerves in this region can also be damaged.

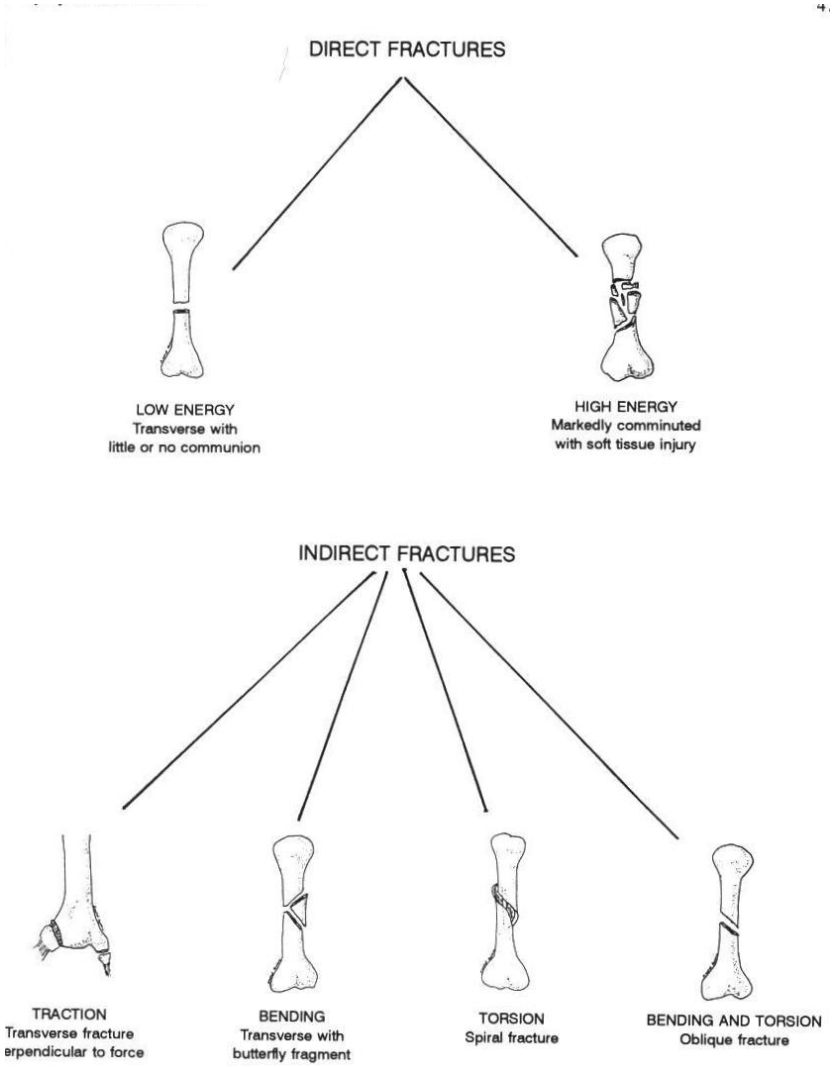

Figure 2-11: Types of Bone Fracture (Nahum and Melvin, 1993)

2.6.4 Knee Injury Criteria

Knee ligament injuries are due to a consequence of bending and/or shear force being directly applied to the knee joint or via loading of the femur and/or tibia. The medial and lateral ligaments can tear completely or suffer partial tearing, (Figure 2-12). The anterior cruciate ligament is also 'commonly associated' with injury to the knee in pedestrian accidents.

Arnoux et al. (2005) identified how hard it was to measure the failure level for the knee ligaments. Hence why an FE model was used to estimate strain levels. It was

difficult to isolate pure shear or bending at the knee joint as there are a number of ligaments working in tandem. 16 degrees and 15 mm were cited by Arnoux as failure criteria of the knee joint.

Kajzer et al. (1993) performed tests which showed the medial collateral ligament ruptures at 123 N m, even though these tests were performed at only 20 km/hr. In a latter paper Kajzer performed tests at 40 km/hr on cadavers and obtained shear values of 2.6 kN at a displacement of 16-28 mm. The bending moment was also greater than the 20 km/hr tests with a value of 331 N m. In these tests the author comments that the tests were performed in the purest possible shear or the purest possible bending, which mirrors a similar comment from Arnoux that it is difficult to obtain data that is 100% pure in bending or shear.

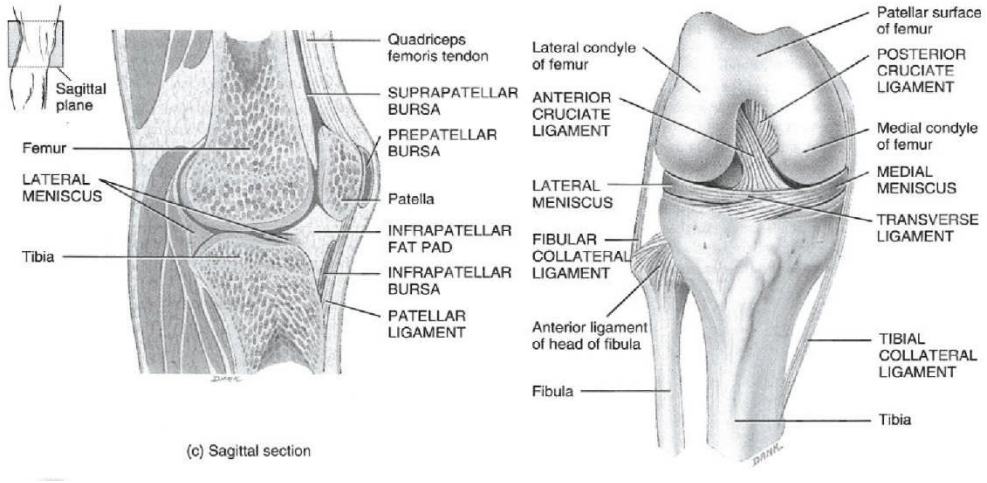

Figure 2-12: Knee Ligaments Anatomy (Tortora and Grabowski, 2000)

In a later paper by Kerrigan (2003) the failure bending moment of the knee was determined to be 134 N m from cadaver testing where the influence of the femur and tibia had been isolated in the tests. The influence of axial loading was not fully investigated and the number of tests was not suitable to generate data that was statistically significant. A general comment with all knee impact cadaver research was that every researcher had performed the tests with a slightly different testing technique. The method of holding the bones and recording the data varied considerably; therefore, it was very difficult to choose definitive knee joint properties.

The shear force and bending moment properties of the knee are intrinsically linked together as they affect one another and their peak values occur at similar times during impacts with a vehicle. Early simulations in testing the Humanoid Model (Howard et al., 1998), showed shear capability of up-to 10 mm had a significant effect on the bending moment reached in the knee joint. Modelling the knee joint as a hinge joint without shear capability would hamper the accuracy of the moment results.

2.6.5 Injury direction

Maki et al. (2003) highlighted that 66% of fatalities occur when the cyclist is struck from the side, which is more likely to occur at road traffic junctions. Huijbers and Janssen (1988) also stated that "the collision in which the bicycle is hit laterally by the front of a car occurs relatively often and causes relatively severe injuries".

2.6.6 Secondary Impacts

Throw distances can be calculated but a large margin of tolerance should be applied to any curves derived, as there is a lack of data from specific accident details such as braking or road surfaces (Mills, 2006). This research did not concentrate on the throw distance of bicyclists after they had struck the vehicle due to the difficulty and variability in predicting injuries. It was also considered that injuries obtained through the primary strike with the vehicle were likely to be the severest. Any subsequent or secondary injuries with the ground or other vehicle would be unable to be quantified objectively and their severity is likely to be less than the primary impact with the vehicle, (Huijbers and Janssen, 1988). Otte (1989) commented that the 'The throwing distances of cyclists are similar to those of pedestrians', but they are also difficult to predict as is shown in the data scatter of Figure 2-13. Mukherjee et al. (2006) also commented that the variation "in the point of contact causes significant changes" to the throwing distance.

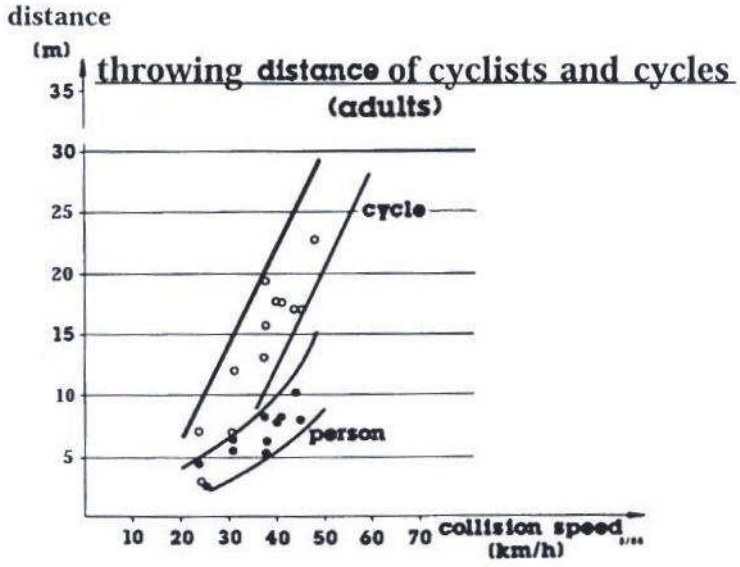

Figure 2-13: Throwing Distance of Cyclist V Impact Speed (Otte, 1989)

2.7 Pedestrian and Cyclist Computer Modelling

2.7.1 Introduction

The approaches which have been used by previous researchers to investigate cyclist crashes are:

- Analysis of accident data to identify injury patterns and causes.
- Physical impact testing of full scale cadavers with real vehicles.
- Cadaver testing performed on the lower limb anatomy only.
- Reconstruction of cyclist accidents using dummies and vehicle mock-ups in a controlled laboratory environment.
- Development of computer simulation models of cyclists to predict injury values and to identify significant variables.

2.7.2 Mathematical Modelling

The finite element (FE) modelling technique has been applied to many different engineering problems, but extensively it has been used to analyse collapsing structures and in particular vehicle impacts. The method involves splitting a structure

into discretized elements with their own particular properties. The initial development of the technique started in the middle to late 1950's by Courant (1943) and the National Aeronautics and Space Administration (NASA) instigated the development of the software code NASTRAN in 1965. The elements which constitute a FE model can be made into three, four or eight sided elements and at each corner of the elements a node is positioned. The four noded element is sometimes referred to as a shell or quad and an eight nodded element is labelled a solid or cube. When a series of shells or solids are connected together they form a mesh and nodes are shared between adjacent elements. The nodes of the element are used as the mathematical means of loading the elements by external forces. The material properties of a shell or solid element can be defined to enable the response of a material to be calculated when external work is applied. If the mesh is designed with a fine mesh the calculations involved are more intense, but the accuracy of the response generally increases. With the increase of computer power over the last 20 years, the use of high performance computers to use the FE technique has become more widespread.

For a complex structure such as a motor vehicle with a large number of different materials, the FE mesh needs to be further divided into different properties. A group of elements with the same material properties are grouped into a part and have their individual collapse properties defined. For a motor vehicle there is a need to model the linear and non-linear behaviour of materials when they are involved in impacts and vehicle manufacturers have been using FE modelling for over 20 years.

Typical crash events last up to 70 ms for a side crash and for 70-100 ms for a frontal crash. To calculate the gradual response of the structure as it undergoes deformation a calculation at each stage needs to be determined. Each time this occurs a timestep is taken by the model until the event has finished. A normal timestep may be $1x10^{-6}$ or 1 micro second. If a model of a vehicle consisted of 1 million elements there are a large number of calculations performed to reach 70 ms which makes the use of high performance computers a necessity. This technique is known as explicit finite element modelling and software codes such as PAMCRASH, RADIOSS and LS-DYNA have been used over the last 30 years to model impacts with vehicles and vulnerable road

users. LS-DYNA originated from work performed by Hallquist at the Lawrence Livermore National Laboratory in 1976 and since then the code has been updated regularly (Hallquist, 1976; Livermore Software Technology Corporation, 2007).

A method to reduce the number of calculations and subsequently reduce the computer or Central Processing Unit (CPU) time is to convert a proportion of the elements into rigid elements where no calculations are necessary. This is the technique favoured by the MADYMO software code.

With all FE modelling the accuracy of the model is determined by the skill of the analyst to input reliable data and the adoption of a modelling method which is appropriate. The interpretations of the responses from the model also need to be analysed and checked rather than taken as 100% accurate as an FE model will only be as accurate as the data that is being used to construct it. To build confidence in an FE model a series of validation steps are normally undertaken to show how accurate the model is against a controlled impact event, where the input and output variables are known. These events are not always a full crash event and may be an impact involving only a sub-set of components. The FE model is most useful when it can predict the results of impacts which have not previously been physically conducted and show the change in deformation.

2.7.3 Software Codes

A number of pedestrian and cycling models to date have utilised the MADYMO software code (Janssen and Wismans, 1985; Ishikawa et al., 1994; Yang and Lovsund, 1997); (Maki et al., 2003; Serre et al., 2007).

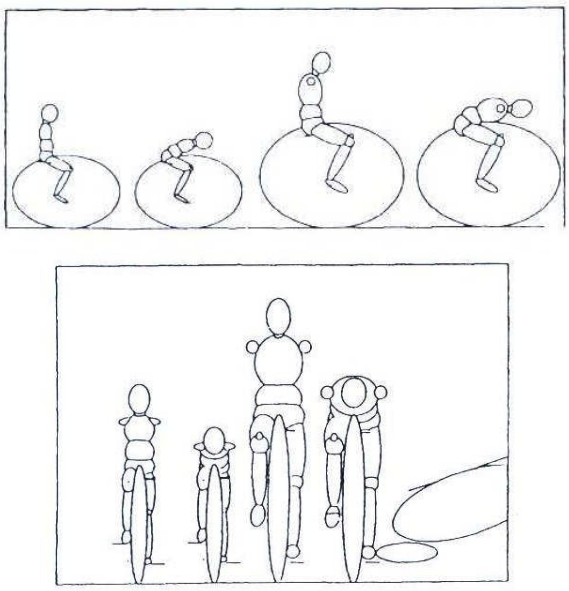

Figure 2-14: Frontal and Lateral Views of Cyclist Models. (Huijbers and Janssen, 1988)

The software code is suitable for running multiple models as it simplifies structures into a series of ellipsoids, connected by joints with the appropriate mass and inertia properties. The dummy and vehicle were modelled with ellipsoids which are approximations to their exact geometry and their stiffness values were modelled as single force V deflection load curves. The simplification of the cyclist and vehicle and the shorter run-time does provide the MADYMO approach with an advantage over the FE approach. Although to achieve more accurate results including accurate kinematics and specific injuries, the FE approach is more suitable.

LS-DYNA is an explicit 3D non-linear finite element code developed by Livermore Software Technology Corp (LSTC). It has been extensively used in crash simulations to model vehicle impacts such as coach rollovers and airbag inflations (Hardy et al., 2000). The FE approach allowed the input of material data based on experimental tests such as EuroNCAP pedestrian data which was performed in Chapter 5. The capability of LS-DYNA to deal with large deformations of structures, interactions between different material types and complex geometry enabled the interaction between the cyclist and the vehicle to be closely simulated. The code was chosen due

to the author's background knowledge of the code and the pre and post processing software that was available.

2.7.4 Finite Element Human Modelling

The principles and techniques used for pedestrian modelling are described in this review as they are very relevant to cycling modelling. With the addition of the bicycle and a change in stance from pedestrian to cycling, the two scenarios can be considered to be very similar.

To assess the injury indices of cyclists using a FE model, the use of a dummy or human like model has been used by different authors (Yasuki, 2006; Nagasaka et al., 2003). There has been a tendency in the last 10 years to veer towards using human like FE models as they would appear to represent more bio-fidelic properties and a dummy is not capable of reproducing injury mechanisms. As a first step to generate a human FE model Cranfield Impact Centre was involved in a programme of work to develop a model for use in pedestrian accidents. The model was titled the 'Humanoid Model' and was the first of its kind to reconstruct real world pedestrian accidents (Howard et al., 1998).

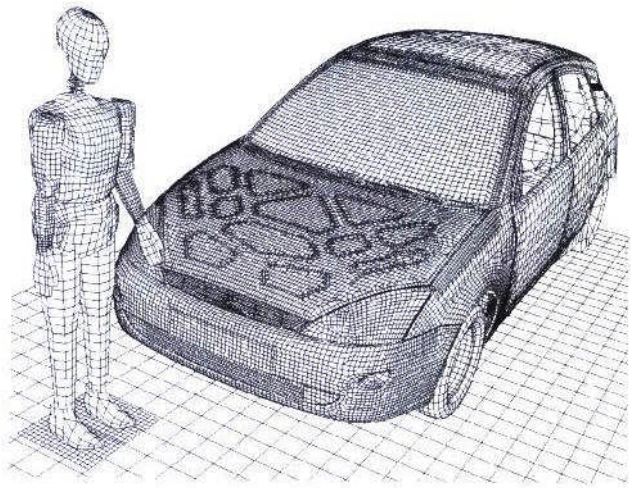

Figure 2-15: Humanoid Pedestrian Model (Howard, 2002)

The Humanoid Model was a simpler version of other human models and has been superseded by more complex models such as Serre et al. (2007) and Cardot et al. (2006). The basis of constructing the Humanoid Model was to simplify the injury mechanisms for a pedestrian, avoid extensive CPU times and to generate a model that could be adapted for a range of pedestrian sizes. This research has used the Humanoid Model by adapting the pedestrian stance into a cyclist stance that has been based on literature and has been validated in a number of real world accident scenarios, (Howard et al., 1998; Howard et al., 2000).

2.7.4.1 In-Depth Knee Modelling

Cardot et al. (2006) coupled a dummy with detailed leg details and a rigid upper body with flexibility centred on a number of joints in a cycling model. The paper extended from previous work carried out by INRETS in Marseille, France. The Lower Limb Model for Safety (LLMS) was used to model ligaments in the knee joint and bones of the lower limb with intense detail. Individual ligaments were analysed using the LLMS model, in particular the lateral collateral ligament and the anterior cruciate ligament being the ‘most strained ligaments’.

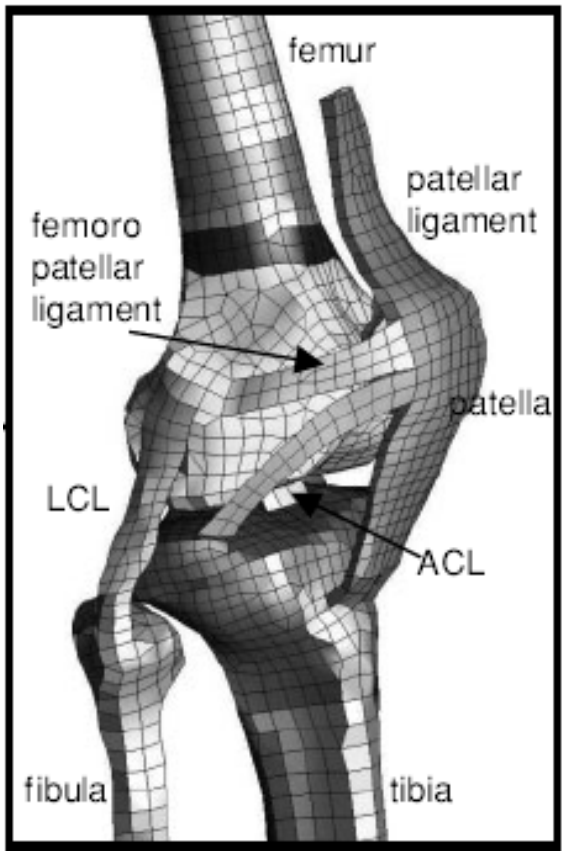

Figure 2-16: Lower Limb Model for Safety (LLMS) Knee Model Showing Knee Ligaments and Bones (Cardot et al., 2006)

When compared to experimental tests performed by Cardot, where no ligament damage was observed, the injury threshold values were considered to be not appropriate for a cyclist as the leg was bent at the knee. If the leg was not straightened the lateral ligaments were not in tension, hence their loading would not be so severe when compared with a pedestrian type accident, where the legs are more upright. The comment is also made by Cardot that the comparison was made with one physical test which is not enough to fully capture the variability in ligament damage for a cyclist.

Schuster et al. (2000) developed a FE model of a human leg which was able to model failure mechanisms in the knee such as ligament damage and menisci injury. This level of detail was essential when evaluating specific accident reconstruction cases. For the Humanoid Model the level of knee injury was represented by a translational spring for shear behaviour and a rotational spring for bending behaviour. This

modelling approach provided the necessary indicators of leg injury for cyclist scenarios.

2.7.4.2 Bicycle Models

Bicycles have been modelled and stressed by (Bolourchi, 1986) and (Soden et al., 1986), using the finite element method to enhance the design of bicycle frames. They did not address the crash performance in any accident scenarios or the kinematics of the cyclist. Eilert-Petersson (1997) also used the FE method to analyse bicycle frames, but used beam elements rather than shell elements to model stresses and strains within the frame. This technique would use less CPU time, but would not be able to fully replicate precise failure mechanisms of frame tubing or joints.

Huijbers and Janssen (1988) in the 1980s used one ellipsoid shape in the MADYMO software code to replicate the whole bicycle, but the large bicycle wheels gave the look of a 'penny farthing' bicycle rather than a modern bike. The stiffness of the bicycle was accounted for by a single stiffness value which was a gross simplification.

Maki (2000) concentrated efforts towards the wheel as it was considered important in rear and frontal impacts. Tests were performed and a wheel FE model was validated with the test results. The bicycle used was a 26 inch with no top tube. Singh et al. (2007) also used MADYMO to simulate bicycles but no information was presented regarding the bicycle model outputs.

The attempts to date have not developed an FE bicycle model capable of predicting failure site and loads in a crash environment. The finite element approach allows the failure mechanisms and locations to be modelled accurately during the initial stages of the impact sequence. This research has performed physical tests on actual bicycles to provide a unique source of data which allowed a more validated model to be created. The developed FE model of the bicycle allowed the contribution of the bicycle in accidents and the effect on cyclist injuries to be evaluated.

2.7.5 Cyclist Modelling

One of the first attempts to reconstruct bicycle accidents using a mathematical technique was performed by Huijbers and Janssen (1988). This work was a continuation of early work by Janssen (1985). In the earlier work experiments were performed with cadavers and dummies on bicycles to obtain kinematics and injuries.

One of the principle conclusions from Huijbers and Janssen (1988) was that vehicle shape had a considerable influence on the relative head impact velocity of the cyclist, although for child impacts the shape did not have such a significant effect. The head impact acceleration was also increased when the vehicle front was low compared to a high vehicle front, such as a SUV. On the hypothesis presented in this paper it was considered important that various different vehicle fronts were chosen to be investigated in the simulations and experimental work.

In a number of papers by Maki and co-workers simulations have been performed based on accident statistics from Japan, (Maki et al., 2003; Maki et al., 2000; Maki and Kajzer, 2001). The author has considered lateral bicycle impacts in addition to frontal and rear crash scenarios. A unique feature of this series of papers was the different techniques used to address cyclist accidents including modelling, accident reconstruction and statistical analysis of accidents.

Bellogi et al. (2005) performed LS-DYNA simulations of vehicle impacts to cyclists in a number of different orientations. The cyclist was aligned with the vehicle in different scenarios. The resulting head impact location was varied from hitting the windscreen at the base or missing the vehicle completely when the bicycle was struck on its rear wheel. A morphing technique tool was used to generate a vehicle profile that optimised the HIC results from the simulations, although some of the HIC results were considerably high in the region of 21000. In normal crash tests the 1000 value is considered to be the pass/fail criteria and therefore such a high value is well in excess. By introducing the morphing technique the HIC value was only reduced to 17800, but the peak acceleration was reduced from 900g to 550g. Therefore indicating that peak acceleration of the head is not necessarily the most effective method of assessing

head injury. This large value of 17800 is a very unrealistic value and it is likely that an incorrect assessment has been performed. Although no access to the FE model was available it may be that the HIC has been calculated using an un-representative vehicle bonnet resulting in an overly stiff contact in the FE model. Bellogi et al. (2005) also used HIC when the head was striking the vehicle on its side. This head strike angle is typical for cyclist head impacts onto the bonnet, but was not intended for the use of HIC in these circumstances. Many authors such as Verschueren et al. (2007) have addressed the issue of HIC measurements for head impacts which are not in a frontal head orientation. Sideways collisions were considered to give a higher HIC value, but Verschueren et al. (2007) also addressed rotational velocity and acceleration and the need for an accurate vehicle speed to calculate accurate values.

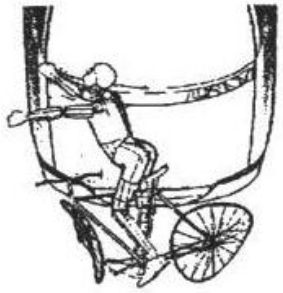

Figure 2-17: Cyclist Simulation in LS-DYNA (Bellogi et al., 2005)

McLundie (2007) developed a model of a bicycle in conjunction with tests which are described in Chapter 4 of this research. The objectives behind the Humanoid Model were developed by Hardy et al. (2000) and subsequently changed from a pedestrian to cyclist model before being used by McLundie. A number of simulations were performed but no specific conclusions as to the features of cyclist injuries or kinematics were formulated by McLundie. A comparison with motorcycle legislation highlighted different impact conditions which may be suitable for a cyclist legislative test. However, motorcyclists do not have the same type of accidents as cyclists, their combined mass is greater and their impact orientations are different.

2.8 Physical Testing

Reconstructions of pedestrian accidents with Post Mortem Human Subjects (PMHS) have been performed by Kerrigan et al. (2005) and Masson et al. (2005) with the aim of reconstructing road traffic accidents, but have not analysed kinematics and/or injuries to understand the trends or the effects of varying vehicle heights or cyclist stances.

As an alternative to physical testing, Haight (1990), conducted reconstructions of specific accidents on the road. Although this work was very important in highlighting the capabilities and accuracy of modelling, the work did not make any predictions for vehicle design. The simulations may have been used for a legal application; therefore they would have needed to be accurate and precise in their input data and therefore validated for only one scenario.

Janssen and Wismans (1987) also performed tests with cadavers, but the tests were done over 20 years ago and vehicle shapes and stiffness have changed considerably since then. SUVs are more prominent and vehicle stiffnesses have increased due to other crash safety legislation introduced for frontal impact protection for vehicle occupants.

2.8.1 Cyclist Accident Reconstruction

Currently there have been very few attempts to re-create bicycle accidents in the laboratory. In most cases, pedestrian rather than cyclist reconstructions have been performed with cadavers and dummy models. Cyclist reconstructions have also been performed with stuntmen (Werner et al., 2001). These have been concentrated on frontal impacts and involved the cyclist being projected onto safety matting. The investigation work by Werner et al. (2001) was intended to look into suspension systems of bicycles and their effect on crash kinematics. The stuntman rode into a rigid barrier locked the brakes and was projected over the handlebars. Werner et al. (2001) claims that the stuntman did not tense his muscles in anticipation of the impending accident. This was intended to capture the real life accident trajectories of

someone involved in a cyclist collision. For a frontal collision, it is more likely that a cyclist will react before the accident occurs. In the case of a side impact collision, there is very little that a cyclist can do as the impact is likely to occur at a road junction and as has been described previously, vehicle drivers and cyclists do not know of the impending accident. Werner (2001) also described a very limited amount of MADYMO modelling of cyclists and did not link the testing to the simulation, nor was there any definite conclusions declared.

2.9 Vehicle Design

In a UK Parliamentary Advisory Committee for Transport Safety (PACTS) report, (Neilson, 1999), the purpose of a soft vehicle front was emphasised and how it improved safety for the vulnerable road user under two counts. A softer vehicle front spreads the load over a wider area and reduced the initial peaks that would produce a fracture in a bone or serious soft tissue injuries. The structure also prevented "excessive loadings from building up as the relative speed between the pedestrian and the vehicle front reduces to zero". A hazard also identified was contact with the external rear view mirrors, but they can be made to deform on impact to reduce their hazardous nature, as well as windscreen wiper motors and linkages. Although Neilson (1999) referred to vulnerable road users, the papers main focus was on pedestrians but could be extended to cyclists.

Neilson (1999) also commented, with a similar view to Räsänen and Summala (1998) that as drivers do not see cyclists and pedestrians before they are struck, their impact speeds are high. 'The frontal stiffness of vehicles tends to vary greatly across the width of the vehicle and many areas are currently too stiff.' An alternative approach to use airbags could be a solution to more extreme impacts, venting and compartments within the air bag would be essential to prevent bottoming out. Avoidance braking systems may work for vehicles, but could not be implemented on coaches as they could cause multiple injuries to the passengers instead.

A number of authors have commented that vehicle shape was the most influential factor in pedestrian accidents in addition to Huijbers and Janssen (1988). Howard and

Watson (2000) commented that vehicle brake dive was an important consideration in pedestrian simulations results, as it caused the greatest difference in kinematics, in particular at higher velocity impacts of 40km/hr.

Roudsari et al. (2004) investigated light truck vehicles (LTVs) in the United States of America (US) and identified that, 'vehicle type strongly influences risk of severe injury and death to pedestrian. This may be due in part to the front end design of the vehicle. Hence, vehicle front end design, especially for LTVs, should be considered in future motor vehicle safety standards.' Maki et al. (2003) also highlighted that SUV's were not involved in pedestrian accidents as much as cyclist accidents. This would imply that there may be a different injury mechanism taking place between cyclists and pedestrians when struck by a SUV. Maki suggests that the leading bonnet edge was a contributory factor.

2.10 Summary

Current real world accident analyses of cyclist accidents and injuries have been extensively documented, but injury causation mechanisms have not been fully addressed. To evaluate and understand the nature of cyclist accidents, the use of physical dummy testing and human body modelling has been used, although not always in conjunction with one another. In some instances, they have been used to reconstruct specific accidents and understand the injury mechanisms for those scenarios only (Serre et al., 2007). Different vehicle shapes have been addressed to indicate the importance of geometry as a contributing factor for pedestrian and cyclist injuries (van Hassel et al., 2007). Human body modelling work to date has been limited in the area of head impact conditions, knee injury values and their relationship to cycling stance.

This research brings together a novel approach of physical testing and human body modelling to assess a greater range of accident scenarios that has not been considered before. Cyclist knee injuries and head impact conditions with motor vehicles will be assessed and their differences with pedestrians have not previously been studied for

four vehicle types. Recommendations for the improvement of cyclist impact conditions by extending current pedestrian legislation have also not been considered.

Chapter 3 Methodology of Physical Testing and Modelling Bicycle Accidents

3.1 Advantages of Physical Testing and Modelling

Two approaches were used in this research to investigate cyclist accidents, physical testing and mathematical modelling. Two important considerations were taken into account when determining which methodology to use,

- Accuracy and robustness of results
- Time and costs to conduct methodology

Static and dynamic tests were conducted at Cranfield Impact Centre, (CIC). The static tests were conducted on a rigid platform T-Bed and the dynamic tests were conducted on a pendulum impactor and a sled rig.

The mathematical modelling was conducted on a desktop computer and offered the capability to simulate a multitude of bicycle accidents by altering variables, such as vehicle speed, cyclist stance or vehicle shape. The physical testing did not allow for these alterations and by analysing virtual human models rather than dummy models a more accurate representation of real world accidents was conducted. Greater emphasis was placed on the modelling rather than the physical testing approach.

3.1.1 Limitations of Physical Testing and Mathematical Modelling

The inability to use a physical vehicle with the appropriate stiffness and geometry was a limitation of the physical testing. A new vehicle would have been needed for every test completed, as the impact with the cyclist would have caused irreparable damage. The CIC test rig was not capable of delivering a velocity above 15 m/s and the test dummy was not able to measure the same quantity of injury data with which the mathematical model could deliver.

The use of physical testing added confidence to the modelling approach, by providing a laboratory controlled impact for defined scenarios which were used in the validation

of the model. A limited number of physical tests were repeated for a number of stances, but it would have been preferred if more tests had been performed to identify the full range of test scatter.

3.2 Phase 1 and Phase 2 Testing and Modelling Methodologies

Two series of physical testing and mathematical modelling were conducted during this research, Phase 1 and Phase 2. Static and dynamic testing was conducted at the start of the project in addition to an initial modelling activity and these activities were grouped under Phase 1. Developing on from Phase 1, a second series of activities were undertaken which involved physical testing and modelling, but with greater emphasis on modelling different vehicle shapes, Phase 2.

A number of different vehicle types were analysed during both phases of the research. In Phase 1, a large family car (LFC) was solely used, whereas all four vehicle types were used in Phase 2.

		Vehicle Types	Type of User	Number of Tests and Simulations
Phase 1	Testing	LFC	Cyclists and Pedestrians	4
	Simulations	LFC	Cyclists and Pedestrians	22
Phase 2	Testing	LFC, SUV	Cyclists Only	9
	Simulations	LFC, SUV, MPV, SM	Cyclists and Pedestrians	36

Table 3-1: Phase 1 and 2 Physical Testing and Modelling Specification

Physical testing provided the opportunity to recreate cyclist accidents in a laboratory, in a controlled environment. Conditions such as impact velocity and orientation of the cyclist were pre-determined, allowing the opportunity to assess accurately the repeatability of outcomes. Performing physical testing in a laboratory was very labour intensive as several persons were needed to operate the dynamic sled, cameras and

instrumentation. When repeat tests were performed without major changes to the set-up, approximately five sled tests were able to be performed within one day.

3.3 Physical Testing Methodology - Static and Dynamic Tests

3.3.1 Static Tests

The Phase 1 static tests were performed on bicycle frames and wheels using the CIC test facilities. The bicycles were attached to a T-Bed platform by various attachment points including the seat post, handlebars and front forks. The bicycles were inverted for a number of tests to allow the connections to be made for the hydraulic actuator that provided the loading input. Additional steel brackets were welded onto the bike to provide the attachment point for the hydraulic actuator to the bicycle via a rose-joint connection. For a number of tests a hydraulic ram was used to load the wheels whilst the seat post and handlebars were rigidly attached to the T-Bed.

3.3.2 Bicycles used in Physical Tests

A variety of bicycles were used for the static and dynamic testing. These were obtained from Mr Bill McLundie, from Jaguar, who also used them for his research. Adult, junior and young child bicycles were used (Figure 3-1 and Figure 3-2). These bicycles were considered to be typical of those used for adults, in terms of material and geometry. No data was possible to identify those bicycles that had been involved in accidents. The adults bicycle main tubes were constructed from aluminium and the two smaller bikes had steel frames.

Figure 3-1: Adult Bicycle

Figure 3-2: Junior and Young Child Bicycles

3.3.3 Dynamic Sled Testing

To complement the static testing, a series of dynamic sled tests were conducted in Phase 1 and Phase 2. In Phase 1, dynamic tests were conducted on the CIC pendulum rig, with the impactor striking the wheel, with the handlebars and seat rigidly attached to the ground. Acceleration results were recorded from the pendulum and after the tests a visual inspection of the frame deformation at key failure locations was recorded. A number of these test results were reported by McLundie (2007).

3.3.4 Dummy used in Dynamic Sled Testing

The reconstruction of the kinematics of a cyclist was obtained from the use of a crash test dummy representing an adult male. Dummies have been used extensively in automotive crash testing for the last 30 years and have proved to be the most accurate method of obtaining data from laboratory controlled crash tests. A ‘Sierra Stan’ dummy was used for the sled impacts, which was developed by the Sierra Engineering Company under a contract with the United States Air Force in 1967.

As human subjects were not used, a dummy was the best possible approach to obtain the kinematics of a cyclist and the dummy would have the capability to be placed in an identical position for each test. No injury indices were taken from the dummy due to a lack of instrumentation; therefore the main results to be extracted from the dummy were the head trajectory path, the head impact location and the response of

the vehicle. The dummy used was the most accurate one available for the research as there are no specific dummies currently designed or built for cyclist impacts with vehicles. The alternative option of using a EuroSID or Hybrid III dummy would not have provided any vast improvement in kinematic results. However, these dummies would have provided an option of greater instrumentation of the dummy's head, chest and pelvis.

In setting up the cyclist on the bicycle, the dummy was lifted into place and supported by a crane when the feet were placed on the pedals. This was a difficult manoeuvre as the dummy's pelvis was not suited to being seated on a bicycle saddle and the feet did not stay on the pedals whilst other parts of the dummy were being manipulated into place. To keep the dummy in a stable position on the bicycle, the feet had to be strapped with tape to the pedals and the hands to the handlebars to keep them in position before the tests took place. The tape was broken immediately on contact and therefore did not affect the kinematics of the dummy.

Up to the point of impact the dummy was further supported onto the bicycle by a rope attached to an eye bolt which was screwed into the head of the dummy. In the 1st phase of experiments the rope was held by a person after it had been passed through a number of pulleys. This was necessary as it was difficult to support the weight of the dummy without affecting the initial position of the cyclist. As the vehicle approached the cyclist the rope was released prior to impact and the dummy was struck without any tension in the supporting rope. It was not possible to replicate any reaction or tendency to steer the bicycle away from the impending impact or provide any applied motion to the cyclist. For the Phase 2 tests an automated drop release mechanism was used, which provided a more accurate release rate.

3.3.5 High Speed Film

The sled tests were filmed with high speed cameras from various angles to capture the kinematics of the cyclist as it was propelled onto the bonnet. Detailed shots of how the legs interacted with the bumper were also obtained. To be able to capture the kinematics of the dummy during the impact with the vehicle, the camera was set at

1000 frames per second, which is the standard rate used in many sled testing applications, Appendix J.

3.3.6 Sled Vehicle Mock-Up Construction

The vehicle mock-up that was used to replicate the front-end of a vehicle was constructed of wooden panels mounted onto a steel framework. Two strips of foam on the front of the mock-up represented the bumper and grill (Figure 3-3). The wooden panels and foam strips allowed a degree of flexibility in the bumper and grill areas which did not exert a damaging effect on the dummy. The mock-up could be used for repeated tests and was able to be easily mounted onto the sled platform. Identical test conditions were maintained for each test by replacing the foam, when it was damaged by the impact with the bicycle and dummy.

Two vehicle heights were chosen for the test to represent a large family car (LFC) and a sports utility vehicle (SUV). The SUV had the same angled geometry as the LFC but was 250mm higher. The dimensions of the vehicles were taken from a study which investigated vehicle profiles from the APROSYS project (Carter, 2005).

The vehicle was rigidly attached to the sled trolley and the cyclist was mounted on a wooden support to allow the vehicle to make contact with the cyclist before the sled made contact with the support. The wooden support was also positioned to give a level ground reference with respect to the vehicle mounted on the trolley.

Figure 3-3: LFC and SUV Mock-Up Vehicle Construction

3.3.7 Sequence of Sled Testing

The mock-up vehicle struck the cyclist mounted on the platform and initiated the kinematics of the cyclist. The platform, supporting the cyclist, was subsequently not further involved in the impact as the wheels of the cycle were lifted off the platform by the upwards lift of the vehicle to the cyclist. Later on in the testing sequence the platform was struck directly from the sled trolley, but at this stage the kinematics of the cyclist were initiated and the trolley interaction with the wooden support did not affect the kinematics of the cyclist. A rope was used to support the cyclist just before contact and it was important to release at the appropriate moment to avoid the potential for the cyclist to fall to one side before impact. Tests were invalid if the rope was released too early, and the cyclist fell or the cyclist was suspended for too long and effectively was 'hung', whilst the mock-up struck the cycle underneath. The sequence of the test is shown in Figure 3-4.

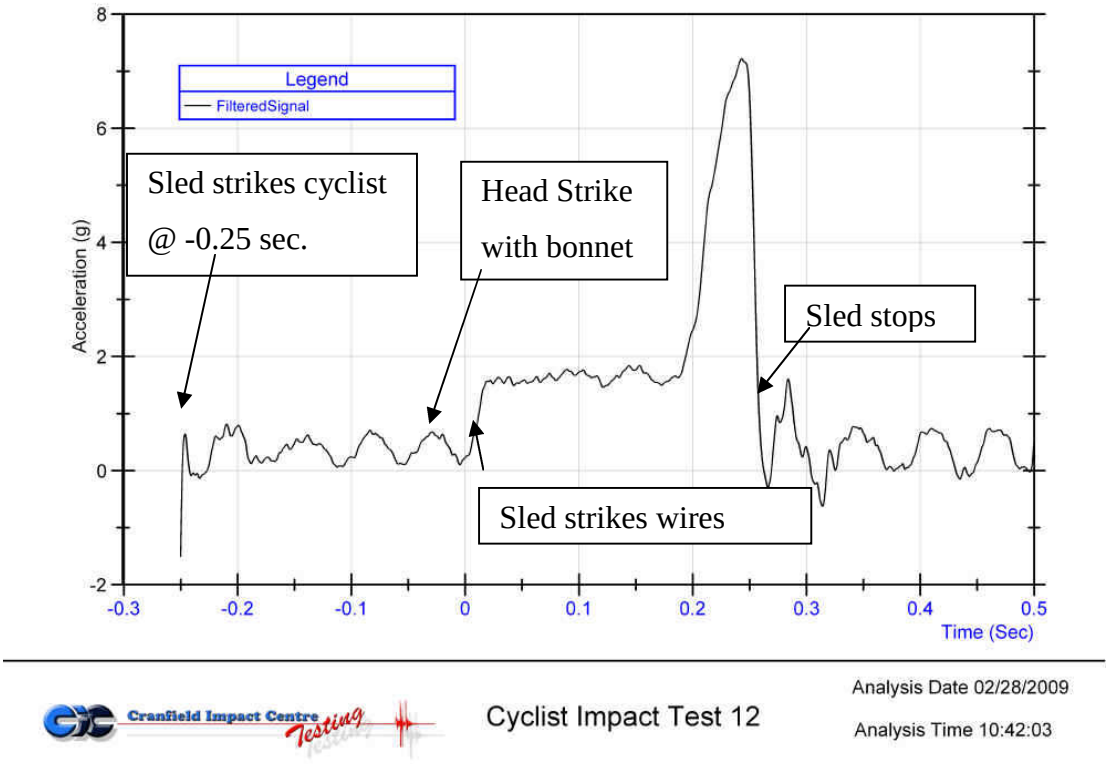

Figure 3-4: Acceleration V Time Signal of Trolley - Test 12, SUV

If the rope had been held for too long the force in striking the dummy would have pulled the rope out of the operator's hands and it would be released anyway. The high speed images showed that the cyclist did not fall to either side and the feet were kept on the pedals in the majority of cases prior to first impact.

3.3.8 Wire Break System

After impact with the cyclist, the trolley was decelerated by a wire break system mounted on the floor of the track. The wire break system is designed to provide a measured deceleration pulse to the trolley by the bending of a specific number of wires. The wires were arranged to slow the trolley with an approximate 1.5g deceleration for a period of 0.5 seconds followed by an increased deceleration when the trolley was fully stopped. The 1g pulse replicated a vehicle slowing down under emergency braking conditions.

3.3.9 Data Acquisition

The acceleration signal was recorded by an accelerometer mounted on the front of the sled platform, but not in direct contact with the impact. After a test was completed, the signal was transmitted wirelessly back to the control cabin in the CIC sled area using TDAS software. The raw acceleration signal was then filtered using the CFC 60 SAE J211 standard, using the National Instruments software programme, DIADEM.

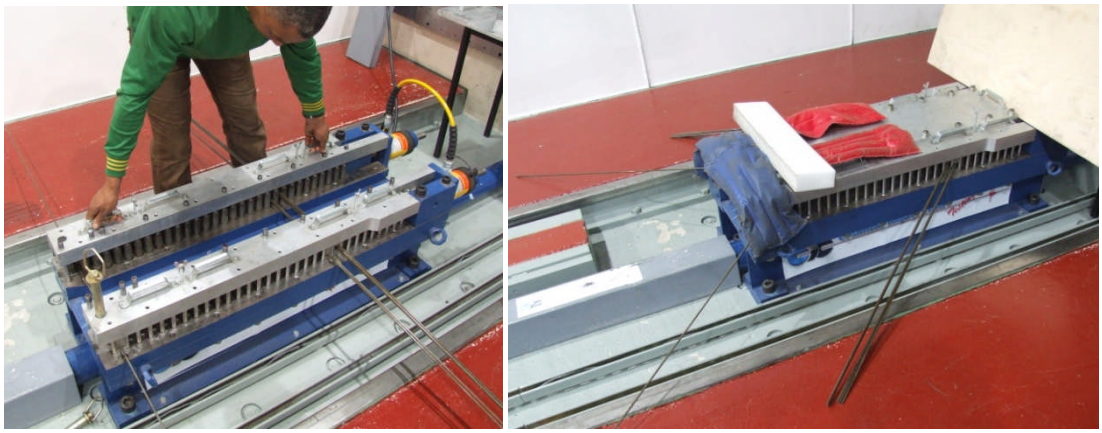

Figure 3-5: CIC Sled Wire Break System – In Assembly and Pre-Test

3.4 Mathematical Modelling Methodology

To complement the physical testing approach, a series of FE mathematical models were set-up and conducted using the LS-DYNA software code. Background to the modelling approach was explained in Section 2.7.2 (Mathematical Modelling) and examples of using FE software for cyclist modelling in Section 2.7.3 (Software Codes). The mathematical modelling part of this research was studied in greater depth than the physical testing, because complex scenarios and more detailed injuries could be analysed using this methodology.

In the earlier Phase 1 simulations (Chapter 4), a number of different bicycle scenarios based on a cyclist being struck from the side were modelled. The objective of these was to understand which scenarios had the most effect on injury results for cyclists and pedestrians impacts with vehicles. In the Phase 2 simulations (Chapter 5), the scenarios were fixed in a lateral orientation and more detailed modelling was performed with specific vehicle shapes.

The mathematical modelling activity was performed at the Cranfield Impact Centre using a dual core, 3.6 GHz Personal Computer.

3.4.1 Bicycle Model

An FE model of a bicycle frame was developed using the dimensions from an adult aluminium bicycle frame and are shown in Adult Bike Dimensions. The main bicycle tube geometry which formed a general triangle shape was modelled as individual tubes which were jointed together with localised rigid bodies. The elastic and plastic failure capability of the tubing was modelled, allowing the tubes to bend and show permanent deformation when impacted. It was assumed that the joints did not become detached by separation from the tubing and the region immediately surrounding the joints had the capability to deform. It was deemed necessary to model plastic deformation to replicate results observed in the dynamic tests.

The FE model consisted of a number of different types of elements, including flat four-sided rectangles which are commonly referred to as shells. These shells have

four nodes positioned at each corner and are used to model the elastic and plastic deformations of metal. The tubes of the bicycle frame were modelled with shell elements and configured into a circular section and the properties used for the shell elements are shown in Table 3-2. The material properties were obtained from (MatWeb, 2009).

Material	Density	Young's Modulus	Poisson's Ratio	Yield Stress
	Tonne/mm^3	N/mm^2		N/mm^2
Aluminium	4.82E-9	72000.0	0.33	290.0

Table 3-2: Aluminium Frame Properties

The wheels were modelled by representing the steel spokes as beam elements and the rubber tyres as elastic shell elements. McLundie (2007) previously had used spring elements, but these were considered too unstable to represent the wheel.

Figure 3-6: Finite Element Model of Adult Bicycle

Pedals and cranks were modelled with shell elements and were included to allow the cyclist's feet to sit on the pedals. The cranks had the ability to turn through 360 degrees by a cylindrical joint modelled at the bottom bracket, which allowed for the cranks to be rotated during the impact event. For different cyclist settings the feet had the ability to be located onto the pedals and oriented to any desired position. When various feet orientations were chosen such as struck leg-up the feet were positioned first and the legs were then adjusted to adopt a realistic cycling stance. The joint orientations of the legs were rotated and translated according to the pre-determined bio-fidelic stiffness's included in the model. There were also limits included in the joints to prevent the leg joints from rotating beyond their bio-fidelic range.

Figure 3-7: Detailed View off Pedals and Crank

The steering column was included to replicate the movement of the handlebars and upper body kinematics when they were struck by the vehicle. A cylindrical joint was used with a pivot location at the top and bottom of the steering column to keep the forks attached, but to allow the front forks to rotate.

3.4.2 Hand Connection To the Handlebars

The hand to handlebar connection was initially modelled by a small development sub-model and then later transferred to the full model. The sub-model used a minimal amount of CPU time and allowed the concept of releasing the hands from the handlebars to be perfected before transferring to the full model. The grip of the cyclist played an important role in determining when the hand released from the handlebar during the simulations. If the grip of the cyclist was weak, then the hands became detached from the handlebars at an early stage of the simulation. If they were too tightly squeezed onto the handlebars the upper torso and arms were kept longer in their original alignment than was to be expected during a crash sequence. Once the hands became detached, the upper torso and arms were free to move in any orientation.

The geometry of the hands, fingers and compression of the soft tissue were not modelled in detail as it was considered too complex a modelling task and no extra insight would have been gained. Instead, a spring element was used to represent the hand to handlebar connection. The designated force and displacement level was obtained from Incel (2002), and the spring element was extended to simulate the release of the hand from the handlebars with the two springs programmed to work independently. The displacement level was set at 10 mm, with an 860 N force level. For a typical simulation, the right hand released early at approximately 30 ms, whilst the left hand did not release for every simulation. If one hand stayed connected to the handlebars due to the force level not being reached, the subsequent upper torso and arm kinematics were heavily influenced. At higher speeds of 15 m/s this affect was not seen, because the forces involved in the collision were higher and the hands released at an early stage (10-20 ms).

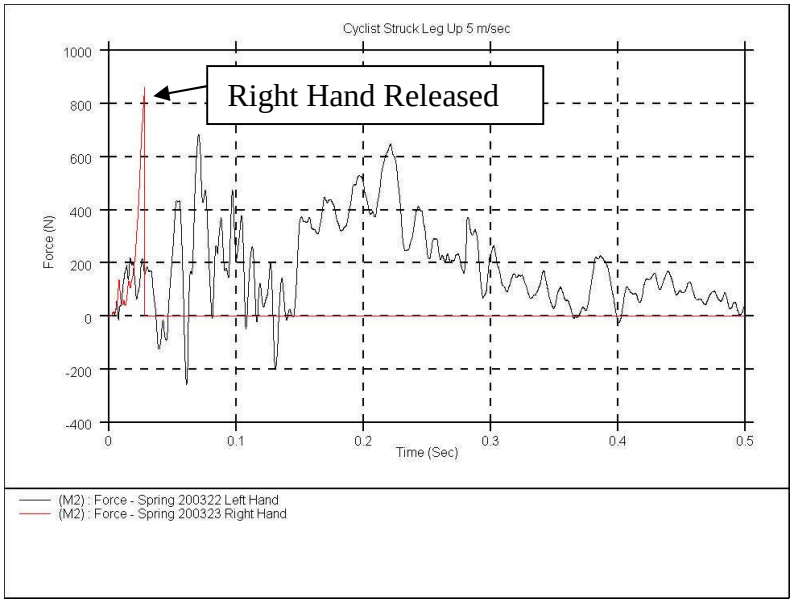

Figure 3-8: Hand Grip Force versus Time for Left (connected) and Right Hand (released at 0.03 s)

3.4.3 Vehicle Models

The Large Family Car (LFC) model was developed to be used for the cyclist and pedestrian simulations. The model was based on Ford vehicle geometry from a previous research project conducted by CIC (Figure 3-9). To allow the front of the vehicle to deform when contacting the cyclist it was necessary to model the vehicle front with a flexible capability. The bumper was connected to a translational spring and damper, which in turn was connected to the centre of gravity of the vehicle. Although the bumper was modelled using a rigid un-deformable material, the spring allowed the bumper to compress under impact with a pre-defined bumper-like characteristic. The bonnet and windscreen were modelled as deformable solid elements positioned in a rigid shell element box. The implementation of deformable properties for the vehicle front was vital in representing real world injuries of the pedestrian or cyclist. The kinematics could be replicated with a rigid but geometrically correct representation of the vehicle.

The SUV, MPV and SM vehicle shapes were also based on geometry from current vehicles (Carter, 2005), but their defined contact definitions with the Humanoid and

bicycle were different. Further details of their construction are reported in Hardy et al. (2007).

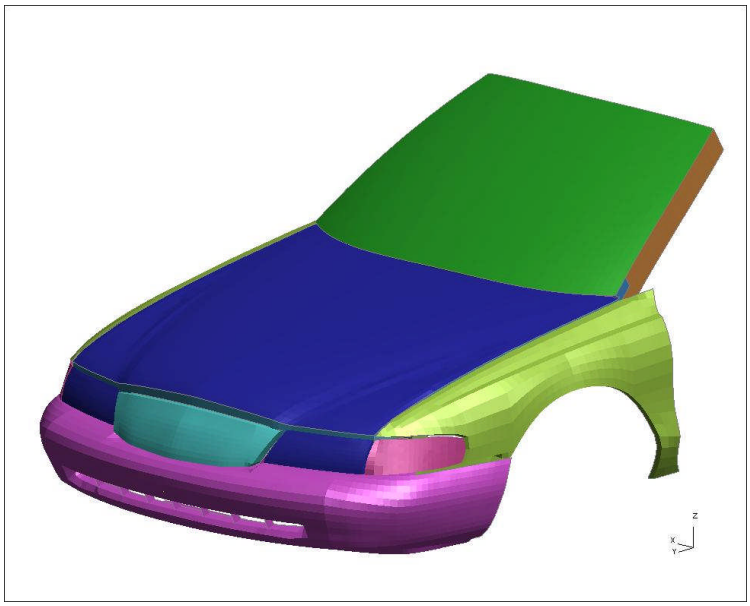

Figure 3-9: Large Family Car (LFC) Vehicle Model

3.4.4 Humanoid Cyclist Model

The FE cyclist model originated from a pedestrian finite element model developed by the author and Roger Hardy whilst working for Cranfield Impact Centre and the Ford Forchungszentrum Aachen FFA (Howard et al., 1998). It was named the 'Humanoid' model as it reproduced human, instead of dummy-like properties. The author was responsible for the construction and development of the finite element model, whilst Hardy was responsible for management of the project and sourcing relevant literature. Permission to use the Humanoid Model was obtained for this research.

The objective of the first Humanoid Model was to enable an assessment of real world pedestrian accidents, as opposed to using the pedestrian impactors. Human injury mechanisms could be assessed and the influence of different vehicle shape and impact speeds. By utilising the Humanoid Model it was possible to predict injury mechanism without having to build expensive prototype designs that would only be able to be used in a single physical crash test, Figure 3-10.

Figure 3-10: Humanoid and Bicycle Model Combined.

The initial Humanoid Model was compiled based on the features of finite element models of the HYBRID III and EUROSID dummies. Further developments were made to improve the bio-fidelic properties of the Humanoid by updating properties from literature. The driving forces for changing the initial model were the dominant pedestrian injuries identified from real world accidents. The ability to model those injury mechanisms effectively changed, as updates of the FE software were obtained.

Emphasis was centred on the legs of the Humanoid as they were the first parts which were struck by the vehicle and they influenced the subsequent kinematics. Instead of progressing to a complex design with every bone, muscle and tissue represented, a simpler approach was adopted. The knee ligaments were initially represented by spring elements and then beam elements to encapsulate the shear and bending capabilities of the knee joint and a graph of their force V deflection characteristics are shown in Figure 3-11 and Figure 3-12. In a later model adapted for this research they were represented by a single discrete beam element. In comparison with Kajzer et al.

(1997), the knee failure criteria has been specified at more conservative values of 110 N m of bending moment with 11.4 degrees of rotation, and 2.6 kN of shear force with 10 mm of deflection.

An important aspect of the knee joint was the turning point in the graph at a bending moment of 114 N m and a shear force of 2.6 kN. If the load applied to the knee reached these levels the knee was considered to have reached its maximum load carrying capability and subsequently the slope of the bending moment load curve changed to 10% of its original slope. The 10% figure was chosen so that the knee kept its integrity after reaching its maximum load carrying capability and did not adversely influence the kinematics of the rest of the impact event. The curves are also mirrored about the (0, 0) point, as the properties of the knee were considered to be equal no matter which direction they were struck.

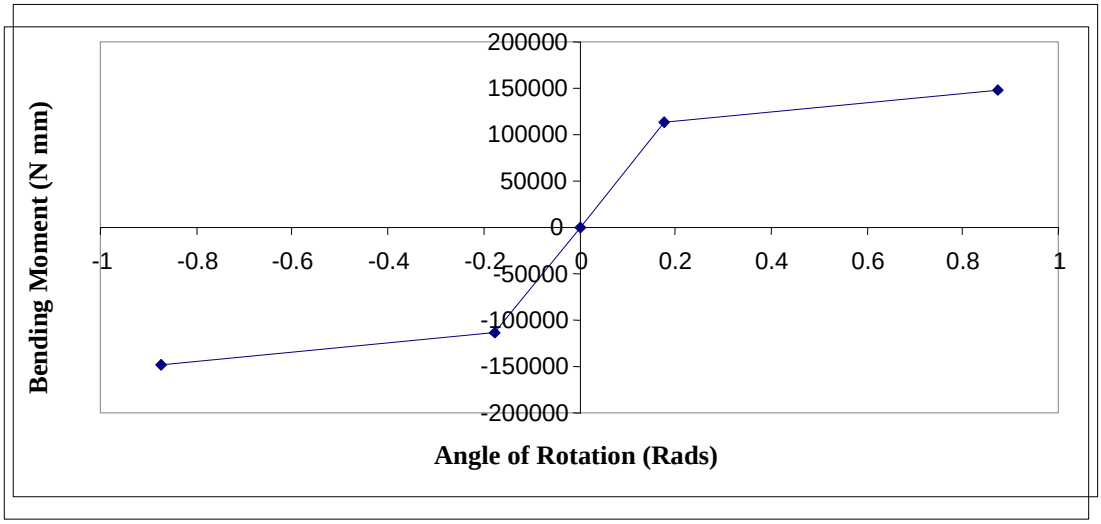

Figure 3-11: Bending Moment Properties for Knees

The knee shear force curve increased its stiffness after the load limit had been reached because the knee joint would not be able to withstand any further deflection after the 2.6 kN level had been reached. Instead, the knee joint would effectively 'lock' and then start to rotate according to the bending moment curve. Although the shear displacement was relatively small (10 mm), it had a significant effect on the performance of the knee during the impact event with a vehicle.

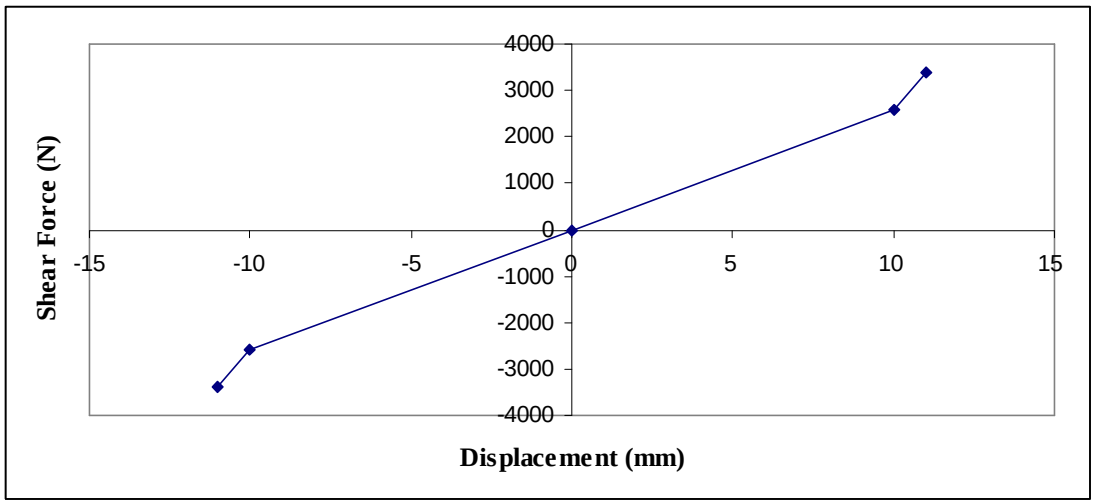

Figure 3-12: Shear Force Properties for Knee

The neck was changed significantly from the initial EUROSID neck model to a more complex construction. Individual vertebrae were included with 6 degrees of freedom between each of the cervical vertebrae and data was obtained from the literature of cadaver tests to validate the motion of the neck in the forward and lateral orientations (van der Horst et al., 1997).

The femur and tibia leg bones were represented by beam elements, with the capability to fracture at a number of pre-determined locations along their length with solid elements included around the beams to represent the flesh and muscle tissue in a similar manner to Arnoux et al. (2002b) and Yasuki (2006).

The Humanoid was developed for the regions that were most likely to receive injuries in pedestrian accidents. Those impact regions were fortunately very similar to cyclists. The details of the upper legs were extended into the crotch of the Humanoid as the hip region of the pedestrian frequently came into direct contact with the vehicle front, in particular for SUV vehicles. The arms, hands and torso regions were not fully developed into precise human geometry or properties.

The programme of work that generated the original Humanoid Model also generated a range of Humanoid sizes to represent children and adults. A scaling programme was devised to change the geometry and properties of the Humanoid to match the users

request for a specific individual. This feature was more suited to specific accident reconstructions rather than a broad analysis of pedestrians and cyclists.

3.4.5 Validation of Humanoid

The Humanoid dummy was validated for use in pedestrian impact scenarios by using results obtained from cadavers and human volunteer tests to compare its performance (Howard et al., 2000). Staged pedestrian cadaver tests performed by Ishikawa et al. (1993) with two vehicle shapes were used. Impact speeds were chosen for the validation to cover a varied range of impact conditions and the 50^{th} percentile Humanoid was used in the scenarios as it closely matched the height of the cadavers used in the cadaver experiments.

The validation was conducted on three levels, body segment trajectories, head resultant velocity and head accelerations. The trajectory of the cadavers was obtained from target markers positioned on the head, pelvis, knee and foot and the comparisons between Humanoid and cadaver trajectories showed excellent agreement for both scenarios. The head struck the bonnet for both simulations within a 100 mm range and the head velocity was within 1 m/s of the cadaver result, but the head accelerations were not in close agreement. This was due to the dependency of contact stiffness in the models being accurately defined and the model was not fully capable of defining the localised deformations of the bonnet.

To improve the Humanoid further, a more deformable FE model with better localised articulation of the torso in particular, would allow the cyclist/pedestrian to wrap around the vehicle in a more bio-fidelic manner. The Humanoid torso had fixed articulation by two rotational joints at the top and bottom of the lumbar spine, whereas in a human the lumbar spine can provide greater flexibility all along its length. Overall, it was concluded that the Humanoid Model was capable of showing excellent validation for pedestrian trajectories and predicting injuries up-to 39 km/hr. It was also highly suitable to be used for cyclist simulations, where the impact conditions are of a similar nature.

3.5 Test Scatter and Stochastic Modelling

Previous work by Otte (1989) had highlighted the dangers of relying on pedestrian testing with full dummy models. There was a sensitive nature to the physical testing method, with lots of variables which were beyond control, including the sled velocity and orientation of the dummy. A large range of variance in the test results was produced even for tests which were intended to be identical in set-up. Therefore, to accurately capture that variance, for a specific set of impact conditions, a high number of sled tests, beyond the scope of this thesis would be needed. A large number of different variables were analysed by the modelling approach, but they would not be able to be fully replicated by the 14 full-scale physical tests performed in this research. Instead, the mathematical modelling was used to define a wider range of cyclist injury results, under a greater number of loading conditions in comparison to the physical testing.

Stochastics refers to the random nature of the results which can be obtained from physical tests, from apparently identical initial conditions. The results from the tests are referred to as output variables and it was important to identify the controlling variables to obtain an accurate scatter of the test results.

An input variable, such as the test velocity, was not always achieved at the pre-determined value and as a result, an unintentional change in the input conditions was applied to the cyclist during the sled test. The velocity measured had a further variance of 1-2 percent in the speed measuring device, which was determined by the repeated use of the sled against a calibrated speed measuring device. Environmental conditions such as temperature and humidity varied in the sled building and have an effect on the accuracy of the speed measuring device and sled propulsion system. The velocity was recorded within the last metre before impact when the sled was in a non-propelled mode and effectively ‘coasting’.

Physical tests would not deliver the same repeated kinematics and head impact location on the bonnet due to the vagaries associated with physical testing. However, the modelling was not able to capture the sensitivity of the physical tests, as the

output of the models was only determined by the input parameters. To compare one simulation with one physical test would not be a fully justified technique; however from the tests performed an indication of the likelihood of head impacts locations can be determined, rather than a specific location.

3.5.1 Validation of Mathematical Models using Physical Tests

The important advantage of performing physical tests in Phase 1 was to provide data which would validate the FE model developed in this research. Validation of the FE model was an integral part in justifying the research methodology and justifying the conclusions determined from the FE modelling. The validation of the model used a comparison of the deceleration outputs from the results of the FE modelling and the physical tests conducted. The validation technique compared the performance of the FE model under a number of different impact conditions and categorised the range of use of the model.

The data obtained from the dynamic tests on the complete bicycle was acceleration v time, which was recorded from an accelerometer and the comparison with the FE model is shown in 4.1 (Validation of the FE Bicycle Model).

3.5.2 Results available from the Humanoid Model

An advantage of using a mathematical model was the capability to extract data from numerous potential injury locations of the cyclist/pedestrian. Data was plotted against time values for the simulation and converted into the necessary units using the T-HIS software package. Acceleration data was filtered using the frequency classes specified in Table 3-3, in accordance with the SAE J211 filter procedures (SAE, March 1995).

	Units	Filtering
Tibia	g (ms^{-2})	CFC180
Knee Shear	N	N/A
Knee Bending Moment	Nm	N/A
Pelvis Acceleration	g (ms^{-2})	CFC60
Chest Acceleration	g (ms^{-2})	CFC60
Head Acceleration	g (ms^{-2})	CFC60
Trajectories	mm	N/A
Head Impact Angle	degrees	N/A
Head Impact Velocity	m/s	N/A
Vehicle Velocity	m/s	N/A

Table 3-3: Units of Measured Results from Humanoid Model and Filtering Class

When analysing the output graphs from each simulation, the maximum, minimum and the specific time value of peaks were recorded. All peaks were checked to see if they occurred during the impact phase of the simulation and a detailed spreadsheet was created in Microsoft EXCEL. A shortened version of the data was subsequently moved to STATISTICA for further analysis.

3.5.3 Automatic LS-DYNA Reporting

In the first phase of simulations the software package REPORTER, was used to capture the results from LS-DYNA simulations in an automated process. The software was developed from Ove Arup a UK based supplier and was designed to be used with LS-DYNA simulation results. When analysing multiple simulations with a large number of data points, REPORTER can be used to capture output in a presentation style immediately after the simulation has finished. A script is programmed to gather specific data from the output files of a simulation and to automatically generate a PowerPoint or an EXCEL file of results.

This process was applied to the first phase results; however when a checking procedure was carried out on the data a number of errors were found which made the software inaccurate and therefore unsuitable. For example, when a simulation

terminated with an error due to a contact becoming unstable towards the end of the run time, the beam that represented the knee received an irregular impulse and the knee result increased rapidly to an unrealistic value. The REPORTER package would use this value as being the maximum bending moment of the beam, even though it occurred in a time period that was beyond the perceived time of injuries received from the cyclist to vehicle impact event. The peak was clearly erroneous and therefore was corrected with the maximum data that occurred at an earlier time. To prevent errors of this nature, all curves were generated manually and checked individually and the REPORTER programme was not used in the 2nd phase of simulations.

3.6 Statistical Techniques to Analyse Results

To enable an effective way of investigating significant differences/effects from the large quantity of modelling data generated by the simulations, two statistical approaches were adopted; Linear Regression and Analysis of Variance (ANOVA). Descriptive statistical techniques were also used for the head trajectories of the cyclist and pedestrian. The use of these techniques is explained using sample data from the first phase of simulations and the implementation of these techniques is included in Chapter 6.

3.6.1 Scatterplots and Correlation Coefficients

As a first approximation to understanding the relationship between the variables or outputs from the models, X versus Y scatter plots were drawn. They were useful to show all the data points to detect if there were any outliers or rogue points and if the effect of one variable on a corresponding variable could be identified. For example, the knee shear influenced the corresponding knee bending moment and by plotting the two variables together the relationship between the two variables was determined. In Figure 3-13, a scatter plot of the data showed the individual data points with the axes representing the two knee variables. An attempt was made to fit a linear regression model to the data, using the least squares fit technique. A correlation coefficient of 0.406 was obtained from the linear regression model.

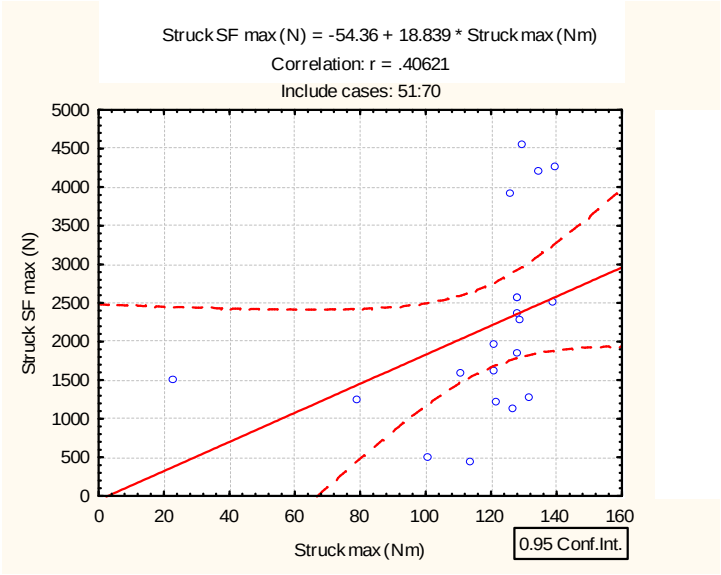

Figure 3-13: Scatter Plot of Struck Knee Max Bending Moment Versus Struck Knee Max Shear Force – Phase 1 Simulations

3.6.2 Linear Regression Model

The method of least squares fit is a technique which was applied to the data output from the computer models to fit a linear regression model. The aim of the method is to extract predictions from a data set and to reduce the influence of errors which may have been obtained during the mathematical modelling or physical tests.

Regression analysis is a technique to show 'how strongly related a pair of variables are via a measure of correlation;…it can also actually measure the extent of the effect that a change in the independent variable has on the dependent variable' (Rose and Sullivan, 1996). The general aim is to simplify and summarize complex information in order to ascertain the underlying patterns in the data. For the analysis the cyclist/pedestrian injuries are independent variables and the car type, cyclist or pedestrian, and vehicle speed are dependent or categorical variables.

3.6.3 ANOVA – Analysis of Variance

The standard deviation is the square root of the variance and is more commonly used to describe the dispersion as the number is smaller. For the struck knee bending

moment the mean was 192 N m and the variance of 19600 was used to calculate a standard deviation of 140, (Figure 3-14). The mean value with a +1 and – 1 standard deviation value was plotted, centred on the mean value of 192 N m.

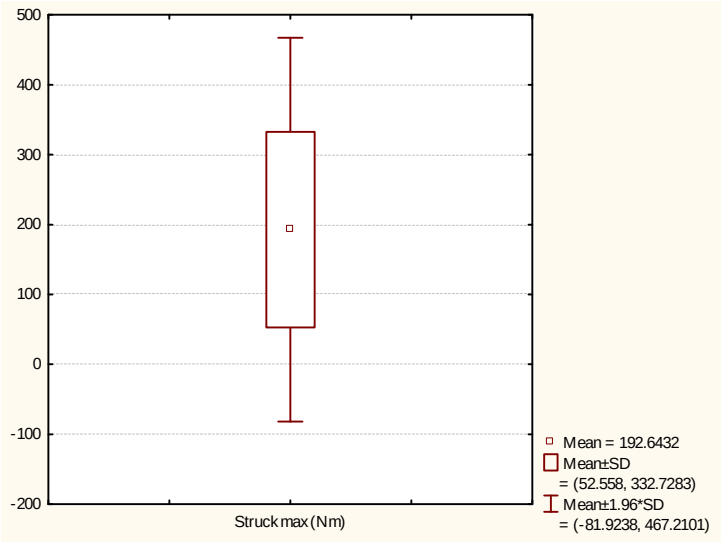

Variable	Descriptive Statistics (041208) Include cases: 1:36,47:50,52:54,59,65,67				
	Valid N	Mean	Minimum	Maximum	Std.Dev.
Struck max (Nm)	46	192.6432	69.05473	717.0000	140.0852

Figure 3-14: Statistical Data (including Standard Deviation) of Struck Knee Bending Moments

The corresponding data can be sub-divided into pedestrian and cyclist categories to identify differences between groups. In this case, the pedestrian group has a higher bending moment mean (254 N m) than the cyclist group (138 N m).

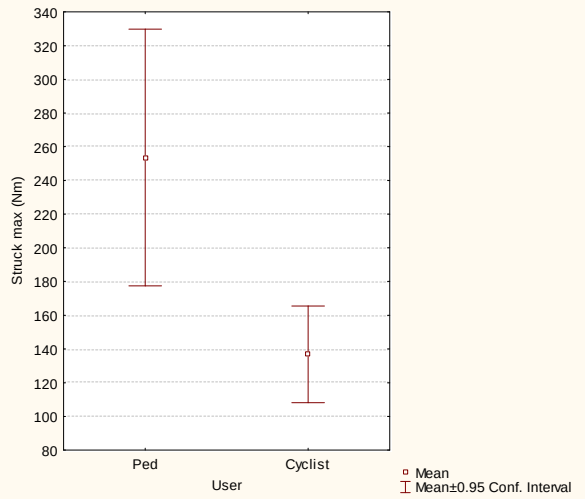

Figure 3-15: Means of Struck Bending Moment for Pedestrian and Cyclist Users

In Figure 3-15, the bars represent the 95% confidence levels and they span different regions for the two user groups. A conclusion was determined from the graph that the pedestrian bending moment results are significantly different and the number of data points between groups was not equal.

To understand the dispersion or spread of the data values within categories, such as the struck knee bending moment, the variance term is sometimes used. The larger the variance, the larger the spread, centred on the mean value of the data. The mean value is calculated from adding all data values together and dividing by the number of data values.

The Analysis of Variance technique, or more commonly used term ANOVA, is a special case of linear regression. Upon first inspection of the simulation results a large scatter of cyclist injuries was observed. In order to establish the significance of the scatter the ANOVA was used to examine the relationship between the simulations. It was used to identify significant trends which would not have been possible by examining only scatter-plots.

The simulation results were defined as independent variables, for example the knee shear force results. The dependent or categorical variables were defined as the input groups which defined the simulations, for example, the vehicle type or vehicle speed.

The groups that showed the most significance were selected for further analysis and are discussed in Chapter 6. All of the ANOVA results were derived from the results tables in Appendix I.

The ANOVA technique allowed multiple categorical variables to be assessed within the same study, for instance, which vehicle type, and whether the user was a pedestrian or cyclist. The statistical significance between vehicle types was quantified and plotted on graphs to aid the interpretation of the data. For further information about the technique, refer to Rutherford (2001).

If an ANOVA was performed on the pedestrian and cyclist bending moment data the confidence levels were now similar in spread, as the ANOVA calculation analysed the variances between the two user groups and a clear trend was established between the two groups (Figure 3-16). The columns represent the ANOVA value for each category and the 95% confidence levels are highlighted by the spreader bars at the top of the columns.

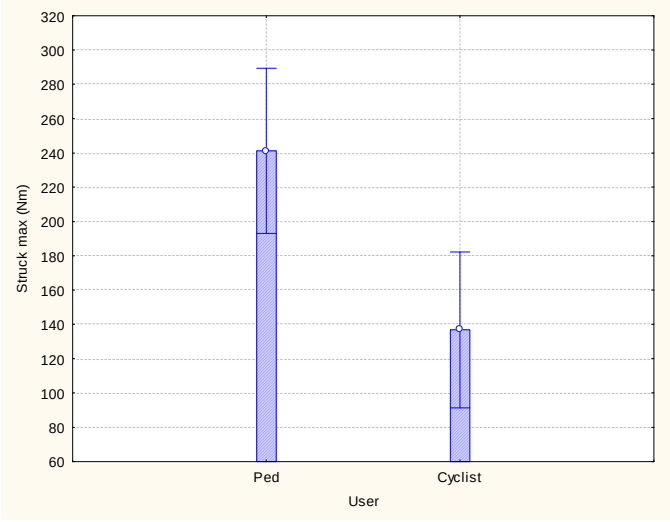

Figure 3-16: Means of Struck Bending Moment for Pedestrian and Cyclist Users using ANOVA technique

If three or more categorical variables are compared together, the application of the ANOVA technique could also be used. Trends can be more easily identified between variables which may have otherwise been missed and groups with different numbers

of data points can be considered. For these reasons the ANOVA was used to analyse the data from the simulations rather than the means of individual groups.

3.6.4 Principle Component Analysis

Principal Components Analysis (PCA) was a technique that was assessed for its suitability to be used for the modelling data generated. PCA is a statistical technique for identifying patterns in large datasets based on the underlying structure of the variables. Variables that are particularly correlated are grouped together and the resulting groups are ordered with respect to the amount of data variability they explain.

It was decided not to use the PCA approach as the ANOVA technique was capable of identifying the necessary trends from the modelling data.

3.7 STATISTICA

STATISTICA is a comprehensive, integrated data analysis, graphics, database management, and custom application development software. It features a wide selection of basic and advanced analytical procedures for business, data mining, science, and engineering applications (StatSoft, 2008). It was suited to the data generated during this research, as it provided the necessary techniques, such as least squares fit, the calculation of correlation coefficients and ANOVA within one software package.

To aid the statistical analysis of the data generated through this research a number of extra variables were added to the data set to enable quick referencing of categories. Different vehicle types, vehicle speed, pedestrian or cyclist and head impact angle relative to 65 degrees were added. In the discussion section these categories were used with reference to which cases were chosen to be analysed. Full results are provided in Appendix I.

Chapter 4 Cyclist and Pedestrian - Phase 1 Results

4.1 Validation of the FE Bicycle Model

The validity and robustness of the FE model was evaluated by comparing the simulation results with the physical test results. This validation process gave confidence in the use of the cyclist and vehicle model and enhanced the reliability of the results. The validation detailed in section 3.4.5 only referred to the Humanoid (cyclist) model, whereas it was also necessary to validate the bicycle model.

The bicycle was subjected to a dynamic rear loading impact from a rigid moving flat wall. Figure 4-1 shows the set-up of the bicycle with the moving wall at the instance just before impact. The bicycle is inverted and rigidly fixed at the seat and handlebar locations.

By analysing the deceleration versus time data of the moving wall with the corresponding data from the FE model a comparison was obtained. The FE model deceleration data was in agreement with the physical test data up to 155 ms, as shown in Figure 4-2, with the wheel buckling and the frame distorting in both the model and physical test, Figure 4-3. The shape of the highly deformed wheel in the model was similar to the real-world tests and the lack of frame deformation was also comparable between the model and physical test.

After the initial impact at time zero, the wheel collapsed up-to 150 ms at a constant rate of deceleration. At 150 ms the simulation model showed a large spike of deceleration, highlighting a stiffening of the structure. The test data did not show this aspect but continued at the constant level of deceleration. Although the model was in agreement with the test data to demonstrate the collapse of the wheel, once the moving wall contacted with the bicycle frame at 150 ms, the model was not in agreement. However, it was considered that during the impact sequence the frame would not be loaded to such a critical level and therefore the alignment between model and test was more important during the collapse mechanism of the wheel. It was later determined in the subsequent series of simulations that the failure characteristics of the bicycle frame had little influence on the injury values of the

cyclist. As the wheel was impacted from the end in this scenario the major failure mechanisms were not identical to the side-on collisions analysed in this study.

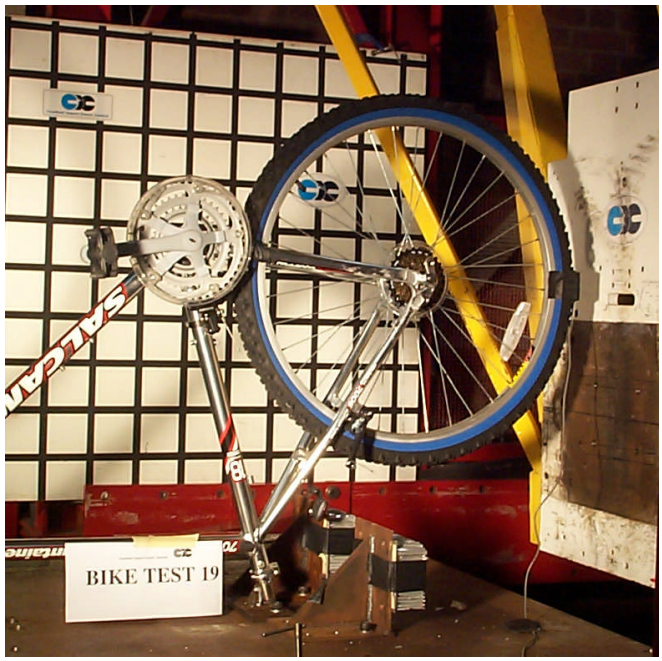

Figure 4-1: Dynamic Bicycle Set-Up for Test 19

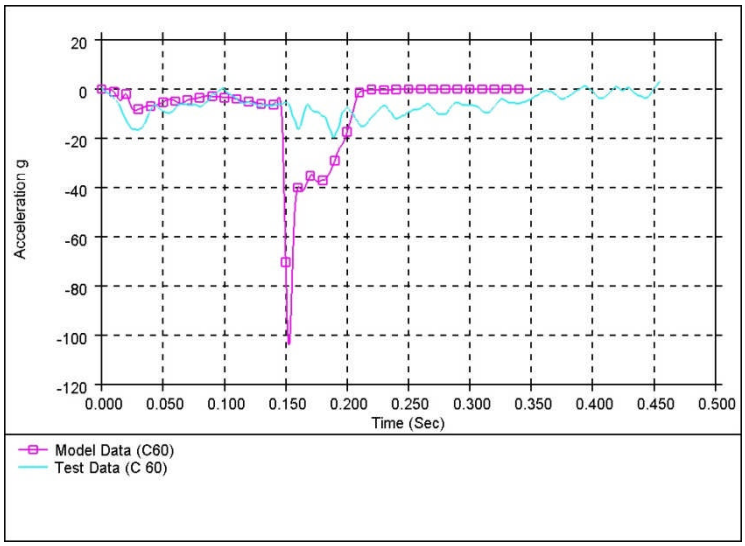

Figure 4-2: Test and Model Decelerations from Rear Wall Impact with Bicycle

Figure 4-3: Deformed Bicycle from Flat Wall Rear Impact Scenario – Model and Test

4.2 Phase 1 Cyclist Simulation Set-Up

The Phase 1 series of simulations, as explained in Chapter 3.2, were conducted to evaluate a cyclist interacting with a vehicle in a typical side impact collision. The simulations were chosen to reflect a wide range of different vehicle to cyclist accident scenarios and to identify the direction for the subsequent Phase 2 modelling and physical testing activities.

Figure 4-4: Cyclist in X=0 Side on Position

The 20 simulations conducted for the Phase 1 simulations are detailed in Table 4-1. The struck leg up case for scenarios 1, 2 and 3 is shown in Figure 4-4, with the leg nearest the vehicle in a raised orientation and with the pedal crank at its highest orientation. The non-struck leg was in a more straightened orientation and was the second leg to be contacted by the vehicle.

Scenario	Simulation Description	Vehicle Speed m/s	Cyclist Speed m/s	
1	Struck leg Up, Side on impact, vehicle 5 m/s	5	0	B
2	Struck leg Up, Side on impact, vehicle 10 m/s	10	0	B
3	Struck leg Up, Side on impact, vehicle 15 m/s	15	0	
4	Struck leg Up, +500mm offset, 10 m/s	10	0	
5	Struck leg Up, -500mm offset, 10 m/s	10	0	
6	Struck leg Up, -1000mm offset, 10 m/s	10	0	
7	Struck leg Up, +1000mm offset, 10 m/s	10	0	
8	Struck leg Up, side on, No Bike 5 m/s	5	0	
9	Struck leg Up, side on, No Bike 10 m/s	10	0	
10	Struck leg Up, side on, No Bike 15 m/s	15	0	
11	Struck leg Up, 10 deg bicycle impact 10 m/s	10	0	
12	Struck leg Up, 20 deg bicycle impact 10 m/s	10	0	
13	Struck leg Up, bicycle 5 m/s, vehicle 10 m/s	10	5	
14	Struck leg Down, Side on impact, vehicle 5 m/s	5	0	B
15	Struck leg Down, Side on impact, vehicle 10 m/s	10	0	B
16	Struck leg Down, Side on impact, vehicle 15 m/s	15	0	
17	Struck leg Down, No Bike, vehicle 10 m/s	10	0	
18	Struck leg Down, bicycle 5 m/s, vehicle 10 m/s	10	5	
19	Struck leg up, +500 mm offset, bicycle 5 m/s	10	5	
20	Struck leg up, -500 mm offset, bicycle 5 m/s	10	5	

Table 4-1: First Phase of Cyclist Simulations, highlighting the Baseline Simulations

The four cyclist simulations with the B label, refer to the Baseline simulations which were used for comparison purposes with pedestrian simulations at a later stage. The Baseline simulations consisted of the struck leg up and struck leg down simulations at two different vehicle speeds. For scenarios 4-8, the cyclist was offset from the longitudinal centreline of the vehicle by 500mm or 1000mm for both leg orientations. Figure 4-5 shows the Baseline simulation followed by the -500mm and -1000mm scenarios for the struck leg up case.

Figure 4-5: Cyclist Positioning for Struck Leg Up for Baseline (2), -500 mm (5) and -1000 mm (6)

The cyclist positioned at the centreline with 20 degrees rotation is shown in Figure 4-6 and the No Bike simulations consisted of the cyclist in the struck leg up orientation, but no contact interaction defined with the cyclist. The No Bike simulations were intended to show the influence of the bicycle structure on the kinematics of the cyclist, when compared with the Baseline simulations.

Figure 4-6: Cyclist Positioning at Centreline for 20 degrees Rotation

The velocity of bicycle for scenarios 13 and 18 was set to 5 m/s, which approximated the average velocity of an adult cyclist (11.2 mile/hr) and was the velocity used by Bellogi (2005).

The struck leg down scenario was the opposite of the struck leg up scenario and was used in simulations 14-18. The leg nearest the vehicle was in a straightened orientation and the leg furthest from the vehicle was in a raised (or bent) orientation. Scenarios 14 and 15 were designated as Baseline simulations.

4.2.1 Large Family Car Model

The large family car (LFC) model was the representation of the relevant vehicle components which would be involved in a cyclist or pedestrian front end impact. The bumper, bonnet and windscreen were represented, but unnecessary components such as the wheels, doors or rear-end structure were not included. The validity of the model to represent the geometry of a large family car, was tested by comparing the centreline profile of the model with the large family car geometry profile corridor developed by Carter (2005), see Figure 4-7.

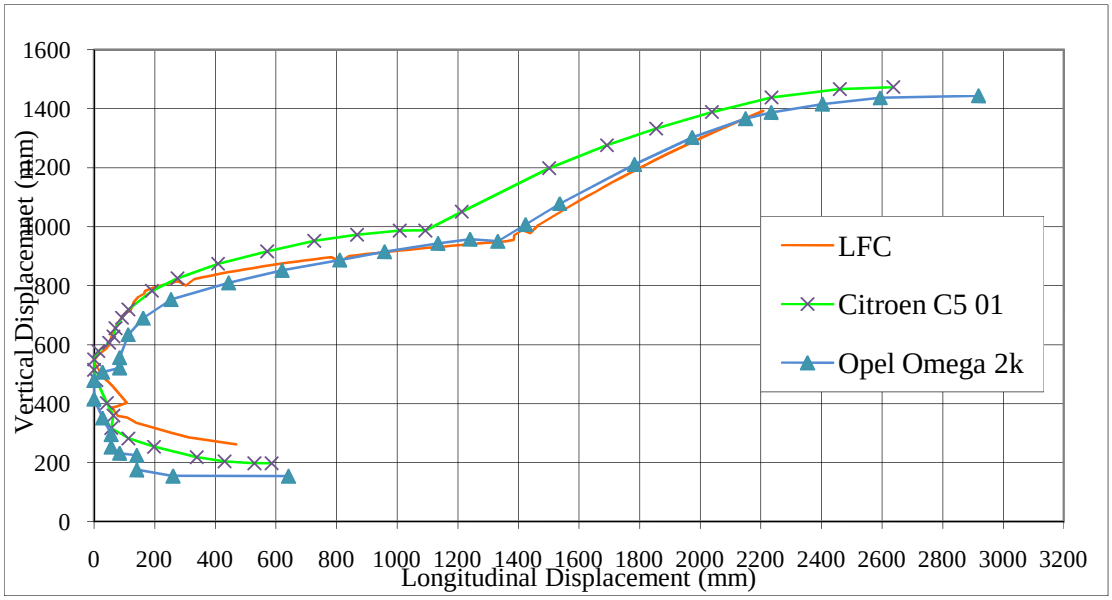

Figure 4-7: Comparison of Large Family Car Model Profile with LFC Geometry Corridor Limits

4.2.2 Pedestrian Wrap Around Distance (WAD)

In the current pedestrian legislative tests, the definition of the Wrap Around Distance (WAD) of a pedestrian with a certain vehicle has been defined by Directive 2003/102/EC (European Parliament and Council, 2003). The WAD of a pedestrian is used to determine the contact location for the impactors used in the tests. For the LFC and other vehicles used in this study, the WADs have been calculated and markers positioned on the vehicle shapes to indicate the ranges within which each impactor (lower legform, upper legform, child head or adult head) should be used. According to the legislation, the adult head impactor locations are between the 1500mm and the 2100mm lines and these distances are marked on the vehicle geometries by a line of single elements laterally across the vehicle, Figure 4-8.

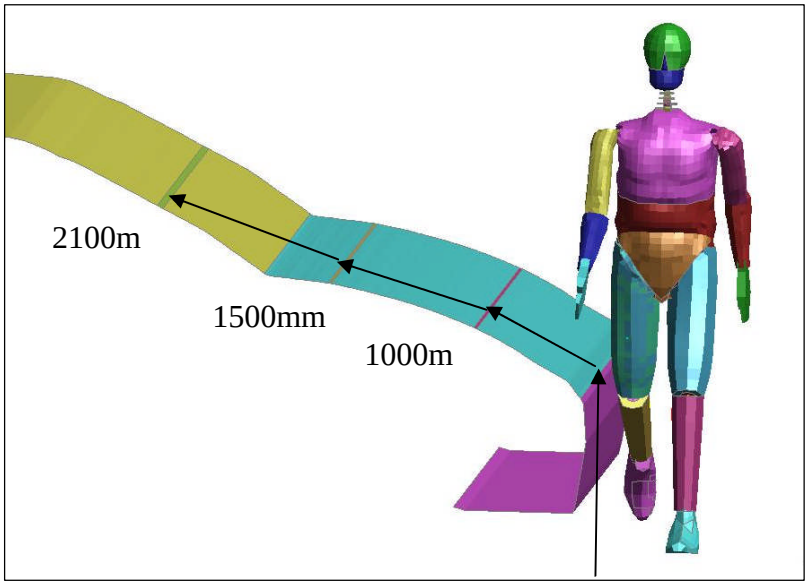

Figure 4-8: Wrap Around Distances, WAD for Large Family Car

4.3 Cyclist Simulation Results

4.3.1 Introduction

The cyclist trajectories, knee injuries, head velocities and tibia accelerations for the first phase of simulations are documented below. The four cyclist Baseline simulations included the two cycling leg orientations for two different vehicle impact velocities. A comparison was then made between the various cycling simulations.

Further analysis was then performed for the cyclist baseline simulation results with pedestrian simulation results.

4.3.2 Baseline Simulations Trajectory Results

A comparison of the cyclist kinematics for the struck leg up and struck leg down scenarios at a vehicle impact speed of 10 m/s is given in Figure 4-9 and Figure 4-10. The time interval between frames is 50 ms, but the final frame is individually labelled. In Figure 4-9, upon impact the raised struck leg of the cyclist moved away from the bicycle and onto the vehicle bonnet. The cyclist subsequently became detached from the bicycle, slid up the bonnet and the head impacted the vehicle on the windscreen beyond the 2100 mm WAD position on the vehicle. A full shoulder contact occurred just prior to the head impact. At the lower vehicle speed of 5 m/s the cyclist also wrapped around the front of the vehicle but did not slide and therefore the head impacted towards the rear edge of the bonnet. At the greater vehicle speed of 15 m/s, the cyclist traversed across the bonnet and struck the windscreen higher up in comparison to the 10 m/s.

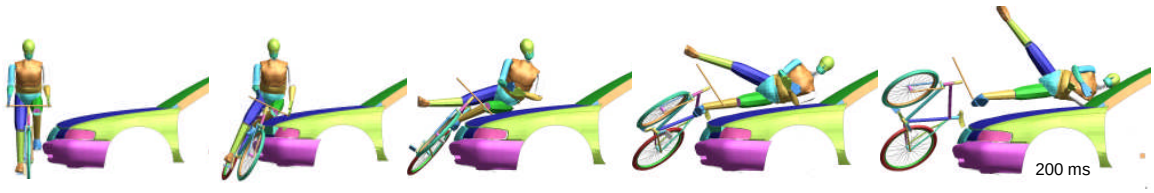

Figure 4-9: Cyclist Struck Leg-Up Kinematics from Impact by the Large Family Car Model

In Figure 4-10, the vehicle moves from left to right, all other kinematic plots show the vehicle moving from right to left. In the struck leg down scenario, the lower leg was trapped momentarily between the vehicle front and the bicycle, causing the cyclist to rotate around the bumper contact point and then the leading edge of the bonnet. The cyclist then had similar kinematics to the SLU, but the head contact was just beyond the 2100 mm WAD position on the vehicle.

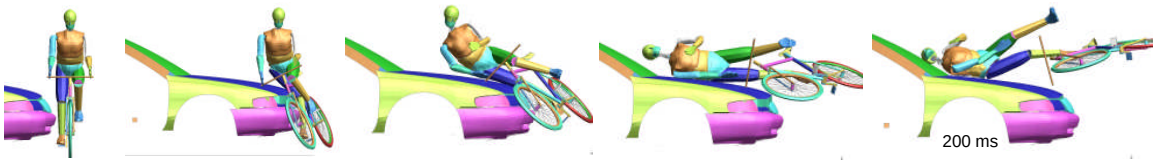

Figure 4-10: Cyclist struck leg-down kinematics from impact by the LFC

4.3.2.1 Offset Impact Orientations

For the offset scenarios 4-7, the cyclist did not fully engage with the front of the vehicle as seen in Figure 4-11 and as a consequence of its initial position, a twisting motion was imparted onto the cyclist. The head was projected towards the ground rather than the vehicle for the +1000mm scenario, as can be seen in the latter stages of the simulation.

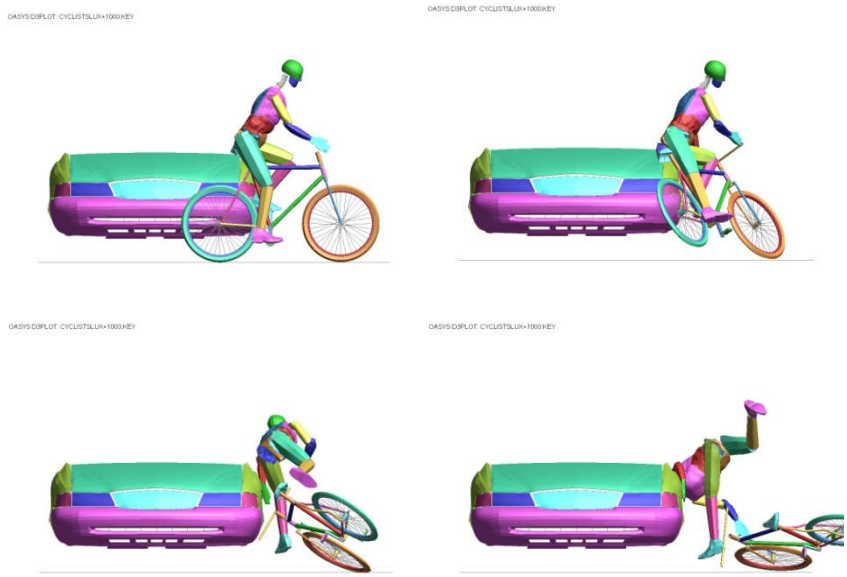

Figure 4-11: Kinematics of Struck Leg Up +1000mm Offset

For the simulation at +500 the cyclist's head struck the A-Pillar of the vehicle, rather than the windscreen for the baseline simulation, Figure 4-12.

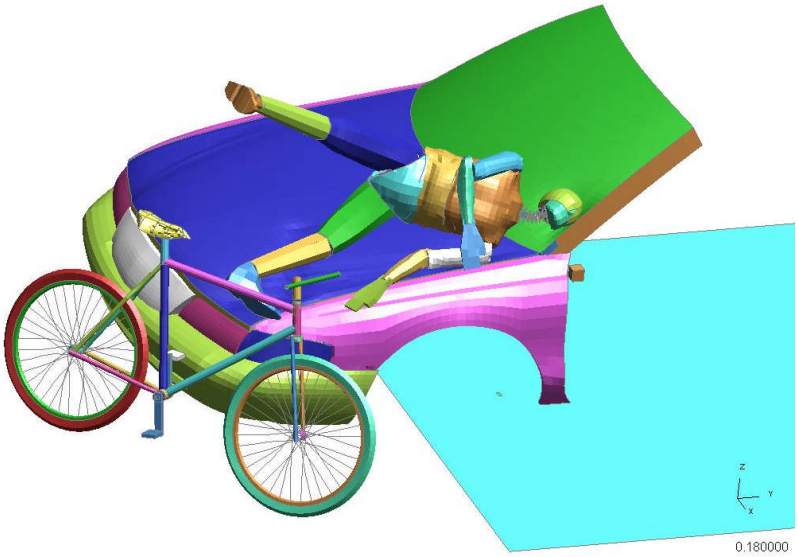

Figure 4-12: Head strike of the Struck Leg Up at X +500 (Simulation 4)

4.3.2.2 No Bike Scenarios

The struck leg up simulation with no bike (simulation 9), was compared with the simulation with the bicycle included in the scenario Baseline (simulation 2). Figure 4-13 shows the kinematics at various stages. After 100 ms, the Baseline scenario showed the upper torso leaning closer to the vehicle and the arms were positioned closer to the torso. At approximately 200 ms, the head struck the windscreen for both simulations, but the head struck further up the windscreen in the no bike simulation, left side of Figure 4-13. Therefore, the bicycle had the effect of holding back the cyclist and reducing the distance that it travelled up the bonnet.

In Figure 4-13 the bicycle has been included in the No Bike scenarios but no contact definitions were defined between bicycle and vehicle. The bicycle was therefore still included in the plots but played no role in the kinematics.

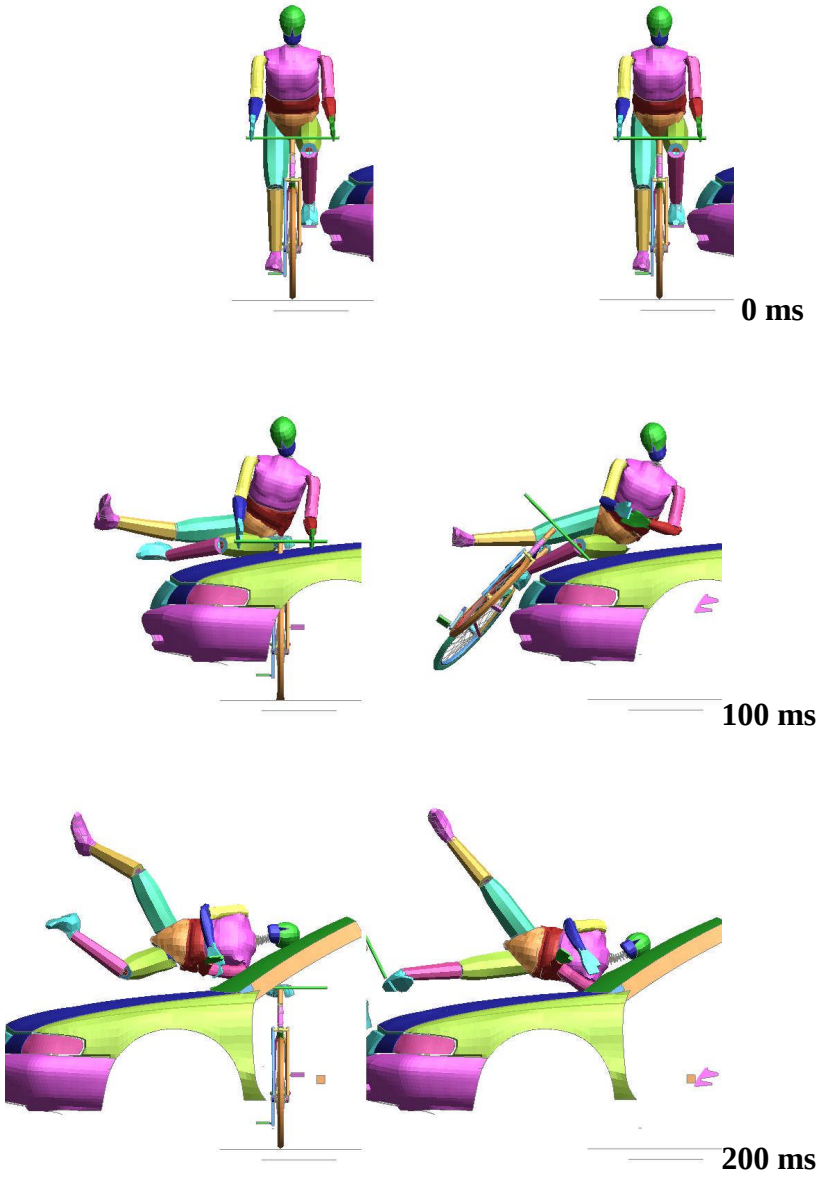

Figure 4-13: Comparison of No Bike and Baseline Scenarios. 0, 100 and 200 ms

4.3.2.3 Baseline Comparison of Struck Leg Up V Struck Leg Down

Figure 4-14 shows a typical comparison of the struck leg down (simulation 15), next to the struck leg up (simulation 2) simulations at the 10 m/s impact speed. The SLU scenario showed the cyclist projected onto the bonnet in a lateral orientation, whilst

the SLB case projected the cyclist onto its back. The head also struck higher up the bonnet in the SLU case.

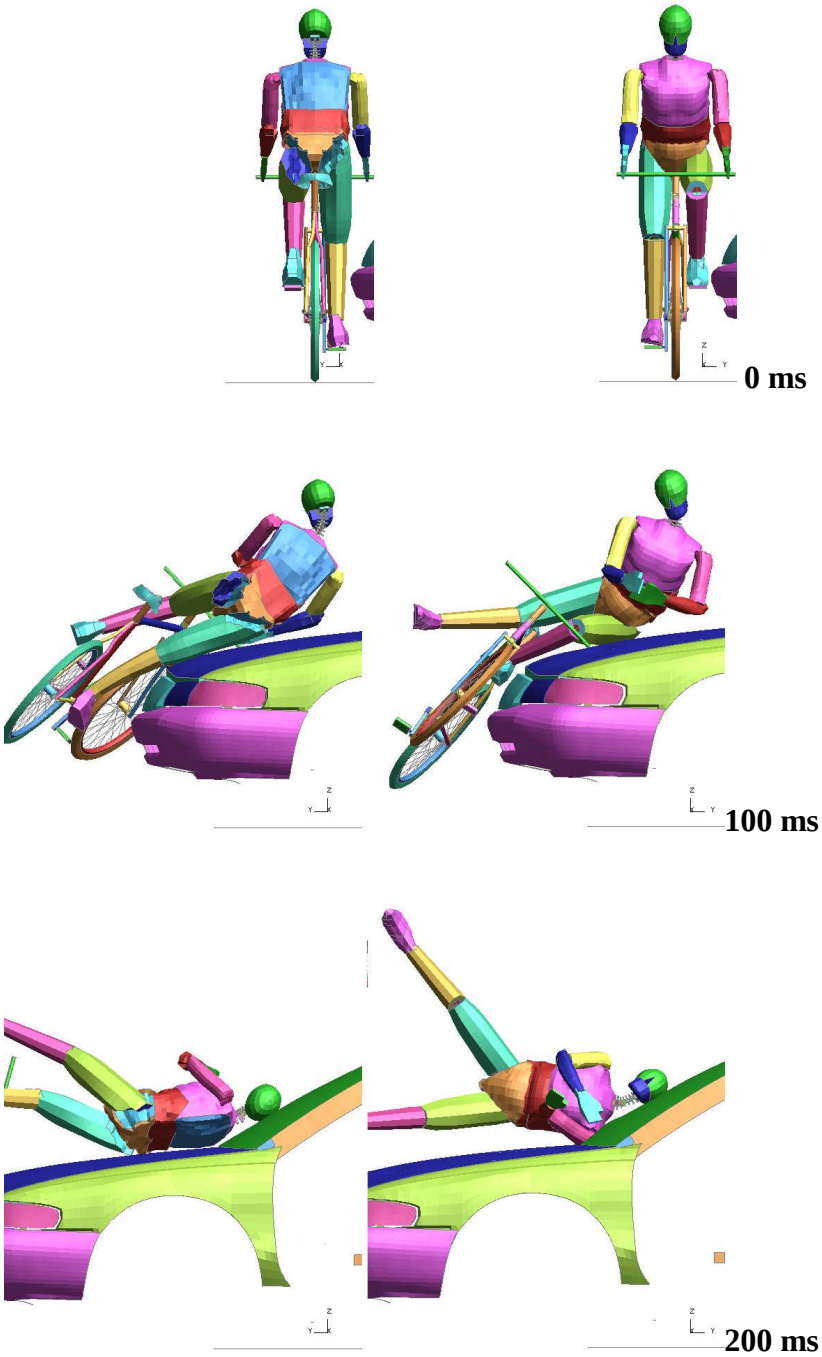

Figure 4-14: Comparison of SLD and SLU Scenarios at 10 m/s.

0, 100 and 200 ms.

4.3.2.4 Cyclist with Initial Velocity

When the cyclist was prescribed an initial velocity, as in simulations 13, 18, 19 and 20 the kinematics showed the cyclist develop a lateral component to the trajectory across the bonnet of the vehicle. Although the cyclist's legs were initially struck in the middle of the vehicle, the head struck the edge of the windscreen for the 10 m/s, +500mm simulation.

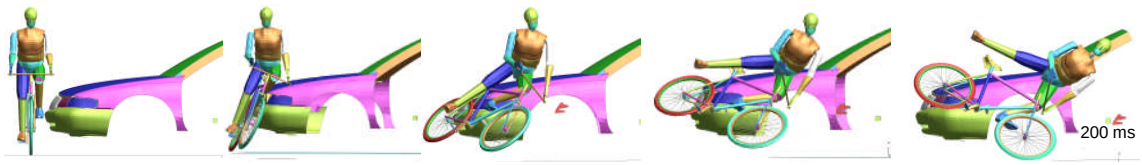

Figure 4-15: Cyclist Struck Leg-Up Kinematics from Impact by the Large Family Car Model with Cyclist Speed of 5 m/s and Offset +500 mm

4.3.2.5 Angled Impacts

For the angled impacts of 10 and 20 degrees the kinematics were very similar to the Baseline scenarios. The head impact timings were all within 10 ms and the head locations were within 100 mm of the Baseline windscreen locations.

4.3.2.6 Offset Scenarios

Two scenarios are shown in Figure 4-16 and Figure 4-17 for the cases where the cyclist was offset 500 mm to the left of the vehicle centreline and for the case where the cyclist was offset 500 mm to the right of the vehicle centreline and had a forward speed of 5 m/s, respectively.

Figure 4-16: Cyclist Struck Leg-Up Kinematics from Impact by the Large Family Car Model with Cyclist Offset +500 mm

Figure 4-17: Cyclist Struck Leg-Up Kinematics from Impact by the Large Family Car Model with Cyclist Speed of 5 m/s and Offset -500 mm

For an offset of +/- 500 mm the head struck the windscreen, but for three scenarios the cyclist's head did not strike the vehicle. These were when the cyclist was offset from the vehicle by + and – 1000 mm from the centreline and when the cyclist was moving with a velocity across the vehicle. In these cases the cyclist fell to the side of the vehicle with only the legs engaging with the vehicle. When the cyclist had an initial velocity the likelihood of the head avoiding the windscreen was increased.

4.3.3 Calculation of the Head Trajectory

The specific location of the head centre of gravity (CG) was identified and represented in the Humanoid Model by a single reference point. The accelerations, velocities and displacements were extracted for the cg and plotted against a time axis.

The trajectories for the cyclist and pedestrian cases were obtained by using the vertical and longitudinal displacements of the head. Initially, the individual displacement components were plotted against time and then the longitudinal displacement of the vehicle was subtracted from the longitudinal displacement of the head, to determine the relative longitudinal head displacement. The vertical and relative longitudinal displacements were combined to produce a single trajectory plot for the head CG. The lateral displacement of the head across the vehicle body was negligible compared to the other values and was not taken into consideration.

The struck leg up trajectory plots for the head chest and pelvis are shown in Figure 4-18. The trajectory plots are representations of the displacements of the vertical and longitudinal directions of the head, chest and pelvis CG's, in relation to the vehicle. The lateral component was not included. The starting positions for the trajectories

were referenced from the ground, i.e. the head was 1650 mm from the ground plane. The starting height for the first phase of simulations did not change and no normalising of results was needed. The displacement of the vehicle has been subtracted from the longitudinal component of the trajectory to aid the presentation of results.

The dark blue lines represent the 10 m/s simulation and the cyclist head, chest and pelvis centre of gravities travelled the furthest longitudinal distance. For the 5 m/s simulations, the head trajectories (light blue and pink) did not move further longitudinally after impact. This was due to the fact that after the head struck the vehicle bonnet and the cyclist did not have enough inertia to travel any further up the vehicle front. For the 10 m/s simulations, the cyclist had greater inertia and started to travel further up the vehicle front after first contact.

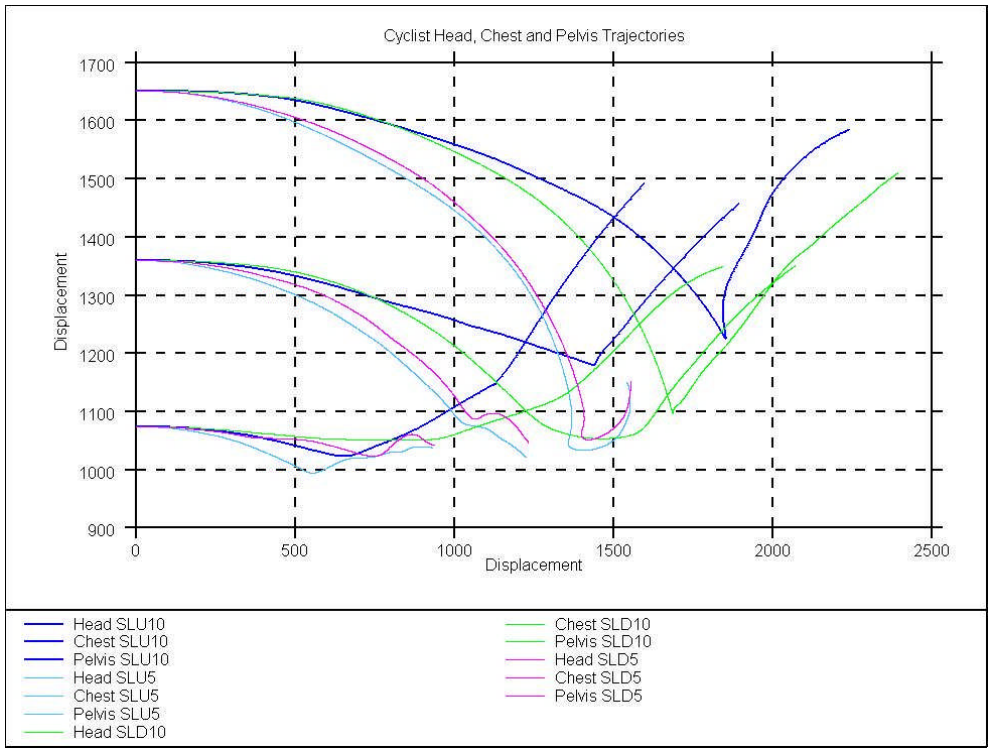

Figure 4-18: Cyclist SLU and SLD Head, Chest and Pelvis Trajectories for 5 and 10 m/s Impacts

The trajectories for the body parts started at the same location irrespective of the cyclist stance, as the lower limbs were the only changes to the overall stance. The green traces showed that the trajectories for the struck leg down at 10 m/s, produced the furthest longitudinal trajectories of the body parts. For the 5 m/s simulations, the struck leg up and down results at 5 m/s showed similar trajectory distances for the body parts and were less than the 10 m/s scenarios.

In the struck leg down simulation, the head did not come into contact with the windscreen due to the shoulder of the cyclist model engaging with the bonnet and preventing the head coming into contact. It was a recognised issue with the current Humanoid Model that the shoulder region needed to be more flexible, as it was too stiff to replicate an accurate bio-fidelic collapse mechanism. With a more bio-fidelic shoulder model, the head would be more likely to strike the bonnet for this scenario.

The struck leg up at 10 m/s simulation (dark blue), showed the influence of the windscreen position on the trajectory of the head which did not fall in height as much as the 5 m/s simulations. Also, the chest CG for the SLU 10 m/s scenario struck the vehicle at the intersection of bonnet and windscreen and did not fall in height as much as the SLD 10 m/s scenario. The pelvises for all of the simulations fell a short distance (less than 100mm) during their trajectories.

4.3.4 Definition of Knee Results

The simulations results have been analysed in four different categories. These have been chosen to highlight the main aspects from the simulation results. To aid the interpretation of the knee results, Figure 4-19 shows the interpretation of the positive and negative bending moments and shear forces in the knee. The right knee showed a positive bending moment as the lower leg was knocked away by the vehicle, whilst the left knee showed a positive shear force as the vehicle predominately struck the upper leg. Correspondingly, the negative bending moment was when the upper leg was struck by the vehicle and the knee rotated in the opposite direction.

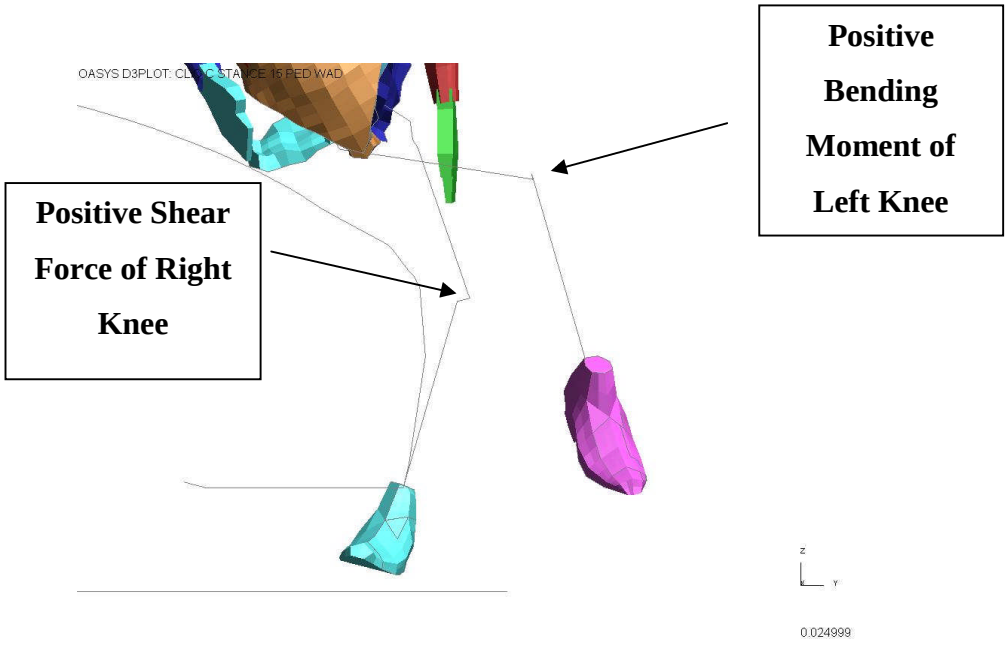

Figure 4-19: Knee Force and Moment Definitions

4.3.5 Cyclist Tibia Accelerations

The tibia acceleration results for the struck and non-struck legs did not show any significant differences between the different orientations and scenarios for the cyclist. In Figure 4-20, the accelerations for the majority of the simulations are around the 200g level. The increased acceleration result of 1400g for the SLD 10 m/s with the moving cyclist was caused by the leg becoming trapped between the vehicle and the bicycle. For the equivalent simulation with the bicycle stationary, the g level was 207g. Therefore, the 1400g value was deemed to be an unlikely result and highlighted the sensitive nature of the tibia acceleration. The non-struck tibia in the SLD 10 m/s scenario with and without moving bicycle had a similar g level.

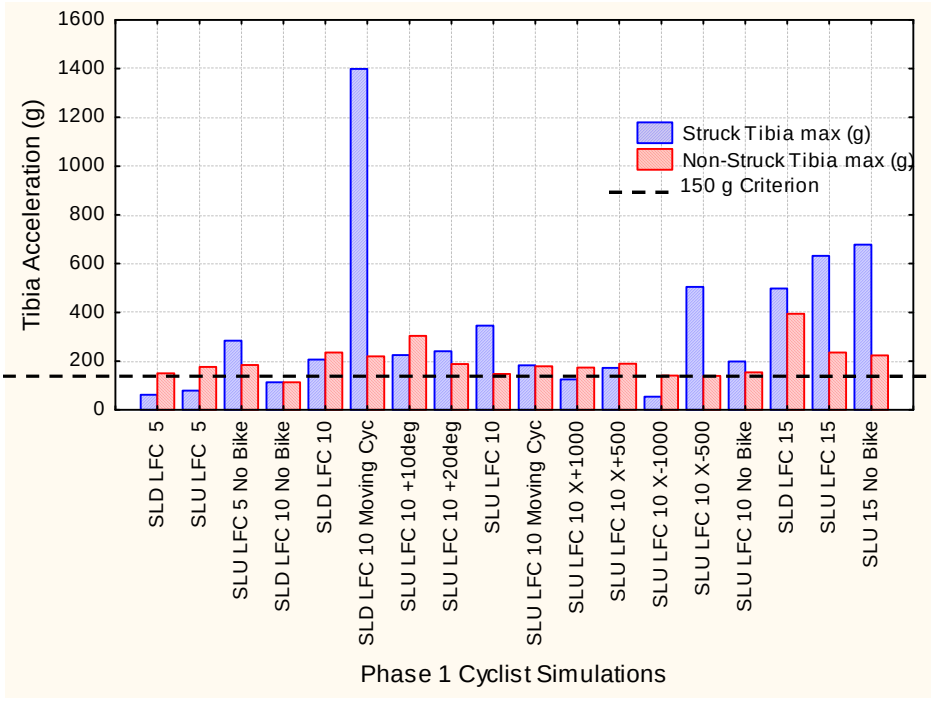

Figure 4-20: Cyclist Struck Leg and Non-Struck Leg Tibia Accelerations

The struck leg did not always have a greater acceleration level, even though it came into contact with the vehicle first, in comparison with the non-struck leg. The non-struck tibia could receive a loading at a similar time to the struck leg, especially in the struck leg up orientation, as the vehicle loaded the foot, seat tube and subsequently the non-struck leg, Figure 4-21. The EEVC WG17 150g criterion is shown on the graph, with a dashed line.

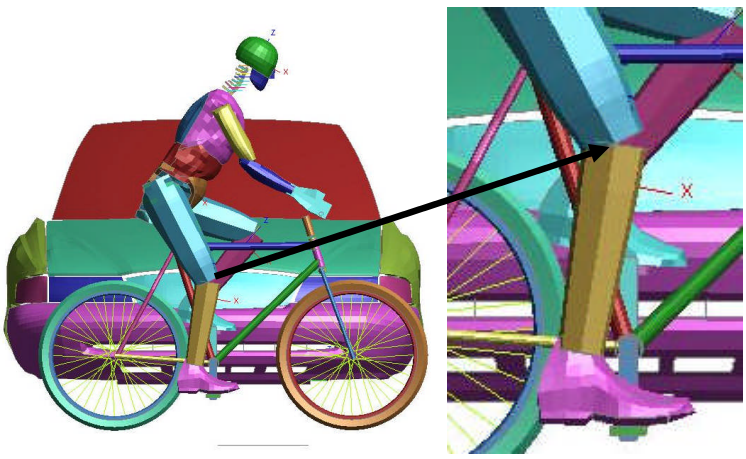

Figure 4-21: Loading of Non-Struck Tibia via Vehicle, Foot and Seat Tube

4.3.6 Cyclist Knee Shear Forces

The knee shear forces for the struck leg are given in, Figure 4-22 and non-struck in Figure 4-23. A maximum value (on the right of Figure 4-22) refers to the force that the knee received when the upper leg was displaced after being struck by the vehicle. A minimum value refers to the lower leg being displaced. The list of Phase 1 cyclist simulations are displayed on the y-axis with their names referenced from Table 4-1. For the majority of cases the struck leg produced higher force values and in particular the cyclist struck leg down simulations always had the highest values in comparison with the struck leg up cases. The highest force value for the struck leg was predominately positive, which meant that the vehicle impact was above the knee and pushed the upper leg away. For the non-struck leg the highest force value was in the negative direction for the majority of cases. This implied that the knee was experiencing a different loading mechanism between legs. The exception to this rule was the cyclist simulations without any bicycle included, when for the non-struck leg the positive force direction was the highest. These cases may be considered to be more pedestrian-like as the influence of the bicycle is not simulated.

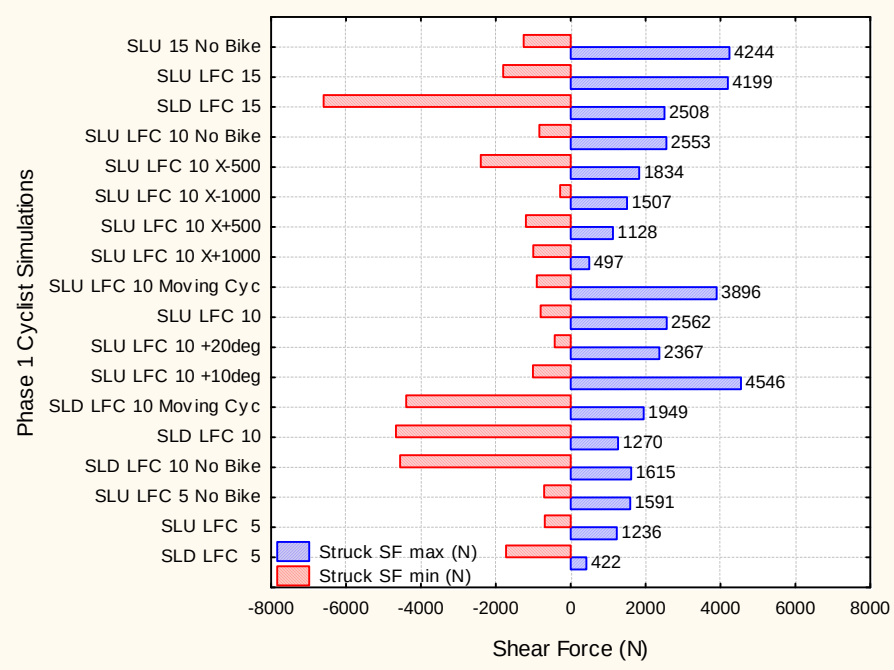

Figure 4-22: Phase 1 Cyclist Shear Forces for Struck Leg

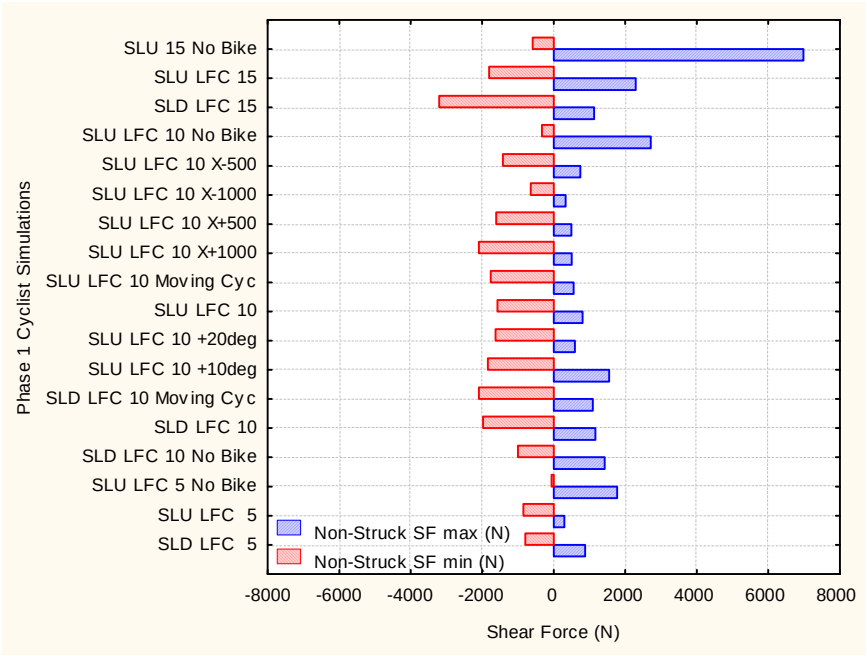

Figure 4-23: Phase1 Cyclist Shear Forces for Non-Struck Leg

The cyclist simulations at 10 m/s showed the variation in shear forces with impact position across the front of the vehicle – the highest was at the centreline and lowest away from the centreline. The knee shear forces from the additional cyclist impact scenarios at a vehicle speed of 10 m/s showed significant differences.

4.3.7 Cyclist Knee Bending Moments

The knee bending moments for the struck leg from all the simulations are given in Figure 4-24. These show that cyclists and pedestrians have similar knee bending moment values regardless of leg orientations. The lowest value was for a cyclist offset 1000 mm to the right of the vehicle (SLU LFC 10X-1000), where the cyclist was brushed aside by the vehicle. Otherwise the knee bending moments from all the cyclist scenarios at a vehicle speed of 10 m/s were very similar.

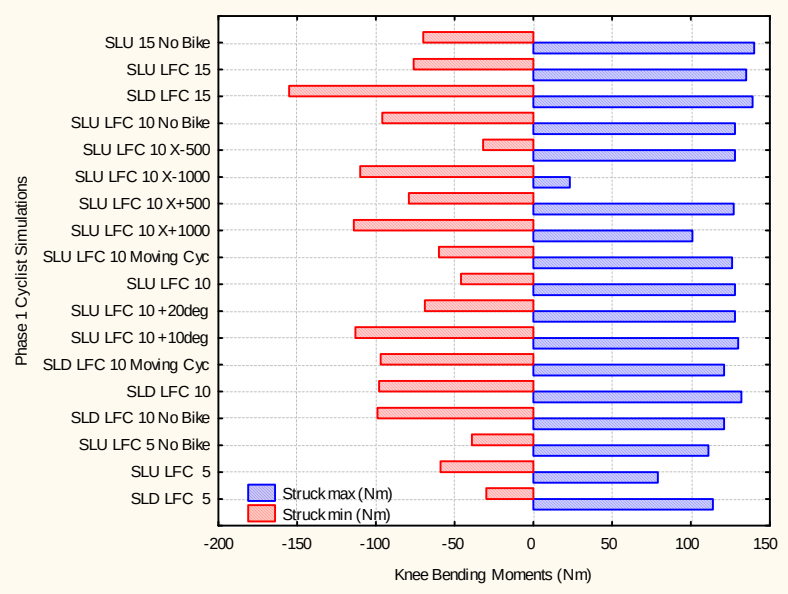

Figure 4-24: Struck Leg Knee Bending Moments

4.3.8 Cyclist Head Velocities

Another method of distinguishing the differences or similarities between the simulations was to analyse the head strike velocities. The following table shows the head strike speed onto the bonnet or windscreen at the moment just before impact, Table 4-2.

The windscreen part of the vehicle model had not been modelled for the purposes of external head impact and the impact characteristics were not considered appropriate for calculating reliable head accelerations or HIC values. All the cyclist head impacts occurred on the windscreen and in most cases shortly after a shoulder impact to either the bonnet or windscreen of the vehicle (as typified in Figure 4-9). Nevertheless, the velocity values from the cyclist simulations were generally higher than those for pedestrians, where the point of head contact was on the bonnet.

The head velocities were measured just prior to impact with the vehicle and were derived as a resultant velocity of the head centre of gravity. When the vehicle speed increased for the struck leg up and struck leg down simulations (5 to 15 m/s) the head velocity also increased, but the head velocity remained below the vehicle velocity for

the majority of scenarios. The exception to this rule were two scenarios, struck leg down at 10 m/s and struck leg up at 10 m/s with +500mm offset. In these cases, the velocity of the head was influenced by the head orientation just prior to impact which was caused by the lack of bio-fidelic capability in the shoulder mechanism. When the torso twisted onto its back, as was seen in the struck leg down simulation, the head was able to flex with less resistance from the neck and gain a higher velocity prior to impact. If the head struck the vehicle with the neck in a lateral orientation, the neck offered more resistance to bending and the head velocities were lower than the vehicle velocity, as was seen in the struck leg up simulations.

	Simulation Description	Vehicle Speed m/s	Head Strike Speed m/s	Time of Contact ms
1	Struck leg Up, Side on impact, vehicle 5 m/s	5	No Contact	-
2	Struck leg Up, Side on impact, vehicle 10 m/s	10	11.23	169
3	Struck leg Up, Side on impact, vehicle 15 m/s	15	17.27	120
4	Struck leg Up, +500mm offset, 10 m/s	10	12.98	169
5	Struck leg Up, -500mm offset, 10 m/s	10	7.17	184
6	Struck leg Up, -1000mm offset, 10 m/s	10	No Contact	-
7	Struck leg Up, +1000mm offset, 10 m/s	10	No Contact	-
8	Struck leg Up, side on, no bike 5 m/s	5	4.75	293
9	Struck leg Up, side on, no bike 10 m/s	10	7.42	183
10	Struck leg Up, side on, no bike 15 m/s	15	8.15	146
11	Struck leg Up, 10 deg, bicycle impact 10 m/s	10	7.40	181
12	Struck leg Up, 20 deg, bicycle impact 10 m/s	10	7.50	181
13	Struck leg Up, bicycle 5 m/s, vehicle 10 m/s	10	No Contact	-
14	Struck leg Down, vehicle 5 m/s	5	No Contact	-
15	Struck leg Down, vehicle 10 m/s	10	11.9	158
16	Struck leg Down, vehicle 15 m/s	15	17.6	116
17	Struck leg Down, No bike, vehicle 10 m/s	10	No Contact	-
18	Struck leg Down, bicycle 5 m/s, vehicle 10 m/s	10	No Contact	-

Table 4-2: Cyclist Head Velocities and Timings Prior to Impact

4.4 Comparison of Cyclists and Pedestrians

A comparison was made between four of the cyclist simulations performed in Phase 1 and four pedestrian simulations. The four cyclist simulations were the struck leg up and struck leg down at 5 and 10 m/s vehicle speeds. A table of the simulations is shown in Table 4-3.

The cycling simulations were conducted with the bicycle at X = 0 position and for all cases the cyclist and pedestrian were not moving at point of impact. The pedestrian model was positioned sideways-on, at the longitudinal centreline of the vehicle. This positioning with the struck leg back and struck leg forward cases is shown in Figure 4-25.

	Vehicle Speed (m/s)	Description
Cyclist		
SLU5front	5	Struck leg up
SLU10front	10	Struck leg up
SLD5front	5	Struck leg down
SLD10front	10	Struck leg down
Pedestrian		
Struck leg back stance5	5	Struck leg back stance
Struck leg forward stance10	10	Struck leg forward stance
Struck leg back stance10	10	Struck leg back stance
Struck leg forward stance5	5	Struck leg forward stance

Table 4-3: Comparison Phase 1 Simulations of Pedestrians and Cyclists

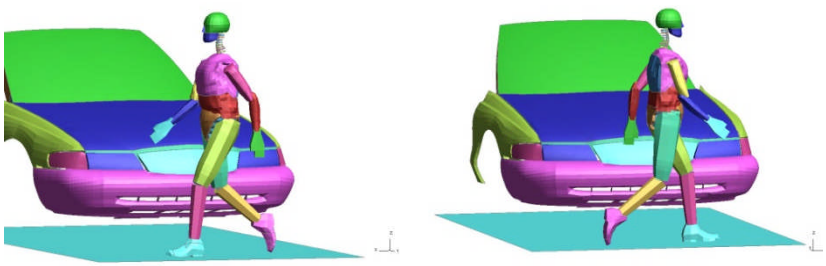

Figure 4-25: Pedestrian Positioning at Centreline for SLB and SLF

The struck leg back stance, as shown in the left-hand side of Figure 4-25, simulated a particular walking stance of a pedestrian. The arms and legs were orientated with the joints of the pedestrian adjusted to provide any initial joint forces at their starting position. The pedestrian had the struck leg in an elevated position, whilst the leg which was furthest away from the vehicle supported the entire pedestrian mass. The struck leg forward stance shown in the right of Figure 4-25 is the mirror image of the struck leg back stance, but in this stance the struck leg supported the entire pedestrian mass.

There was no direct similarity between the struck leg back and any particular cycling stance because the limb orientations were different. However, the pedestrian struck leg back stance was comparable to the cyclist struck leg down simulation, because the initial struck leg was in a vertical position.

A comparison of the pedestrian kinematics for a vehicle impact speed of 10 m/s is shown in Figure 4-26 and Figure 4-27. The general kinematics of the two scenarios were similar to the cyclists' kinematics, particularly up until 150 ms. More rotation of the body of the pedestrian about his own vertical axis was evident in the struck leg-forward scenario, but head impact was at 151 ms in each case and towards the rear edge of the bonnet, before the 2100 mm WAD position on the vehicle. After head contact the pedestrian then continued to slide up the bonnet.

Figure 4-26: Pedestrian Struck Leg-forward Kinematics from Impact by the Large Family Car

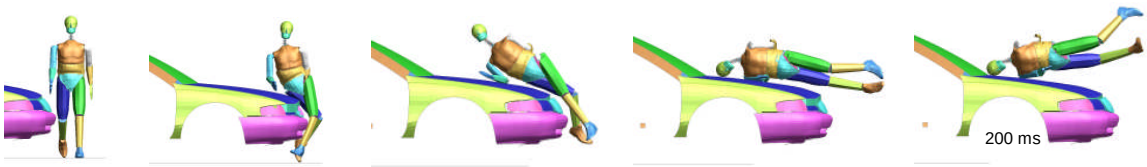

Figure 4-27: Pedestrian Struck Leg-back Kinematics from Impact by the Large Family Car

4.4.1 Pedestrian and Cyclist Head Impact Locations

An alternative way of analysing the trajectories of the pedestrian and cyclist was to look at the impact locations of the various body parts onto the vehicle. In the eight scenarios, the head impact locations were identified and marked on vehicle plot. The cyclist and pedestrian head impacts were grouped together and indicated within the circles, Figure 4-28. The cyclist head impacts occurred further up the vehicle front compared with the pedestrian impacts, which all occurred on the bonnet. If the simulation did not have a specific head contact the head contact point shown in Figure 4-28 and Figure 4-29, was derived from the nearest location of the head to the bonnet just before impact.

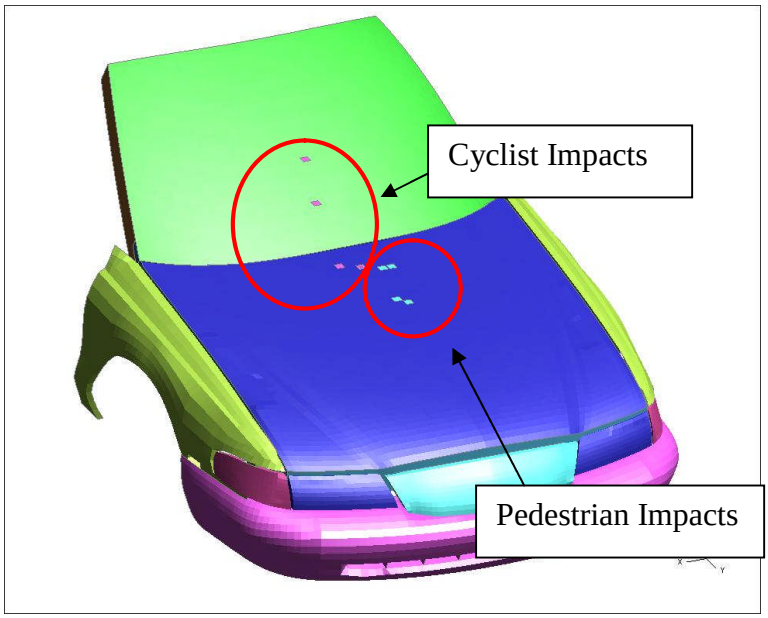

Figure 4-28: Head Impact Locations for Pedestrians and Cyclists

When comparing the 5 and 10 m/s impacts for both pedestrians and cyclists, the 5 m/s impacts all occurred on the bonnet whilst the 10 m/s occurred at the base of the bonnet and on the windscreen, Figure 4-29.

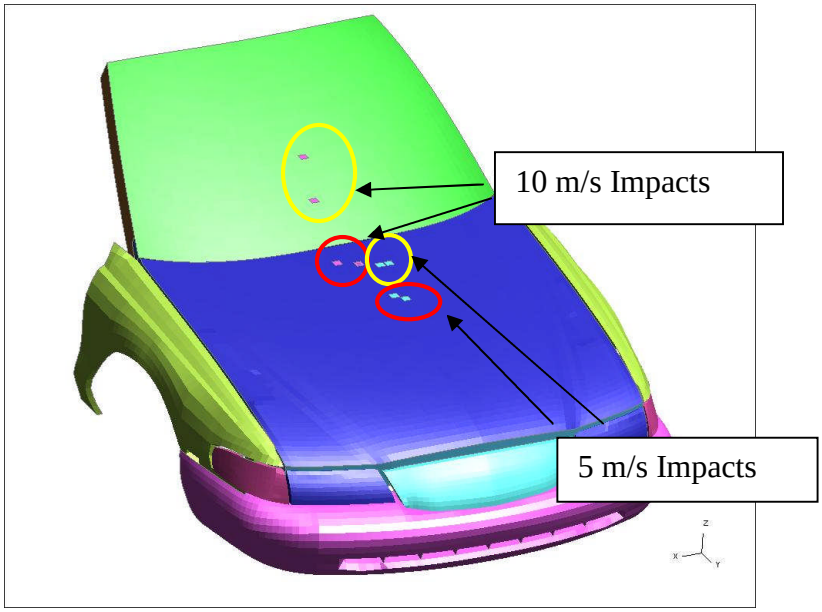

Figure 4-29: Head Impact Locations for 5 and 10 m/s Pedestrian and Cyclist Head Impacts

4.4.2 Pedestrian and Cyclist Tibia Results

The tibia results showed that the cyclist had lower injury levels in comparison with the pedestrian. The tibia g was lower for the cyclist at 5 and 10 m/s and it was below the EEVC WG17, 150g level used in the pedestrian impactors. Both sets of pedestrian results showed levels in excess of the legislative level, Figure 4-30.

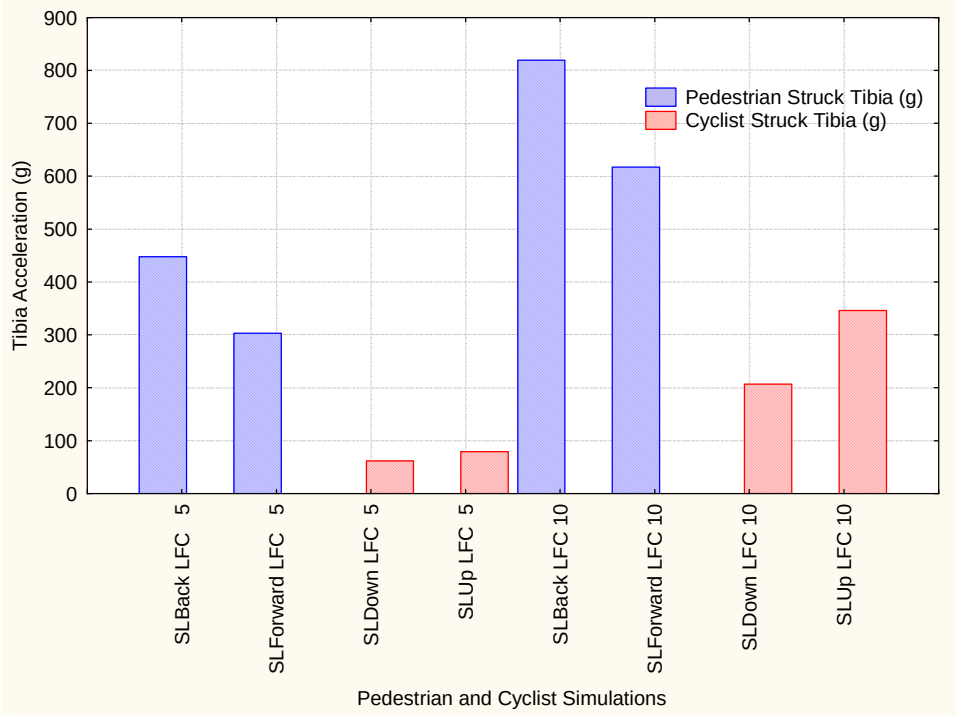

Figure 4-30: Pedestrian and Cyclist Tibia g Results

4.4.3 Pedestrian and Cyclist Pelvis Accelerations

The pelvis accelerations from the eight simulations are shown in Figure 4-31, where a similar trend to the tibia results was observed. These show that cyclist and pedestrian pelvis accelerations are significantly different, with the pedestrian values being generally double or greater than those for a cyclist. The greater height of the cyclist's pelvis removed the possibility of a direct impact to the pelvis or via the top of the struck leg from the bonnet leading edge of the vehicle. The peak pelvis accelerations for cyclists were all related to an impact on the top of the bonnet which reduced it severity as it was a glancing impact.

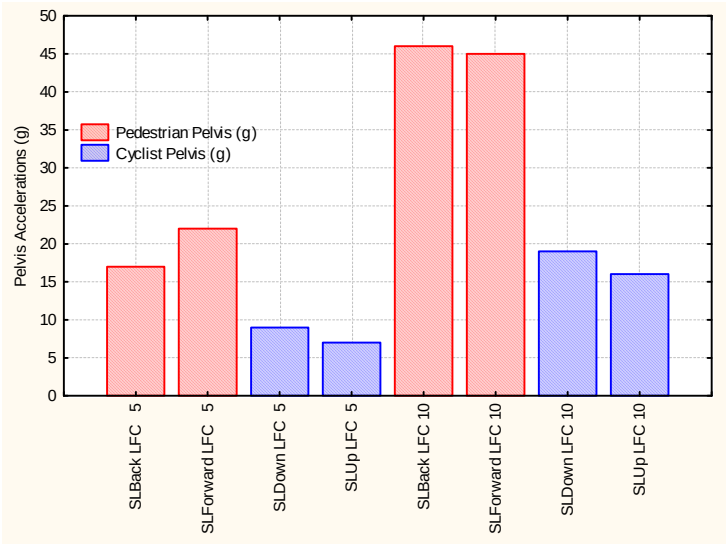

Figure 4-31: Cyclist and Pedestrian Pelvis Accelerations

4.4.4 Discussion on 1st Phase Cyclist and Pedestrian Simulations

Side impact stances were chosen to represent a range of scenarios because they represented the most common type of cyclist accidents as shown by Otte (1989). 73% of accidents were from the front of the vehicle into a cyclist.

The trajectory results highlighted that the nature of the fall and subsequent kinematics upto and after head impact varied between pedestrians and cyclists. The simulations were left to run after vehicle to head impact to observe their general orientation, although they were not left to run until ground contact, as this would have led to excessive run times, especially if the cyclist or pedestrian was projected over the vehicle which happened at the higher speeds. For the 5 m/s simulation, the cyclist actually started to slide off the front of the vehicle after impact without reaching the windscreen.

The speed of the cyclist was chosen to be 5 m/s (11.1 mile/hr), which was deemed to be an average speed for an adult cyclist. At higher cyclist speeds the head contact with the vehicle could be deemed further unlikely, no matter where the first point of contact between cyclist and vehicle. The relationship between the cyclist's speed to vehicle speed would determine if there was going to be contact between the head and

bonnet. If the cyclist speed was equal or even higher than the vehicle speed the cyclist was less likely to impact the vehicle, whereas if the cyclist speed was lower than the vehicle speed it was more likely to strike the front of the vehicle.

In general, the 18 simulations used in the first phase showed a number of interesting issues, including the influence of the moving cyclist and the different starting orientations of the legs. With the cyclist having a larger surface area than a pedestrian it would be more likely to be struck by the vehicle in a real world collision. Even if the wheel was clipped by the vehicle, the cyclist was capable of being spun around and projected towards the vehicle. For simulations when the cyclist was nearly clear of the vehicle at X+1000, the rear wheel of the cyclist was struck, causing the cyclist to disengage from the bicycle and to be projected onto the ground.

When the orientation of the pedals was changed between SLU and SLD the cyclist displayed different kinematics in each circumstance. When the struck leg was up, the cyclist projected further up the bonnet because the struck leg was able to be up lifted onto the bonnet in a shorter time. Alternatively, when the struck leg was down, the bicycle played more of a role in the simulations because the leg was momentarily trapped between the vehicle and the bicycle, preventing the cyclist from wrapping around the bonnet. There are obviously a myriad of pedal positions which could have been chosen which would have produced their own unique set of conditions and results. However, the two orientations were designed to replicate the extremes of leg positions.

The head struck further up the windscreen for the no bike simulation (simulation 9), in comparison to when the bicycle interactions were defined in simulation 2. The other body parts also showed different trajectories due to the inclusion of the bicycle, which in general, prevented the cyclist from projecting up the vehicle front. Therefore, the early contacts and interactions between the bicycle and the cyclist had an influence on the trajectories of the individual body parts even after the cyclist and the bicycle had lost contact. The stance of the cyclist for simulations 8-10 was not obtainable in reality, but the comparison provided an opportunity to assess the influence of the bicycle.

A fundamental result was that the head contact for the pedestrian impacts were on the bonnet, whereas the cyclist's were on the windscreen. This indicated that the pedestrian's head did not travel as far up the vehicle front due to its different initial orientation and the non-inclusion of the bicycle. In the initial set-up, the cyclist's head was in a similar position to the pedestrian's, therefore the difference in head contact location with the vehicle was due to the bicycle influence and the differing leg positions. When the simulations with no bicycle contacts defined were taken into consideration as well, the stance had a greater influence on the cyclist's trajectory rather than the bicycle. This can be summarised by looking at the head trajectories for the five simulations plotted in, Figure 4-32. The pedestrian trajectories (red and blue together) travelled the least in the longitudinal direction, compared to the two cyclist stances (blue and light orange lines). The green line, representing the no bike simulation, shows the head travelling the furthest longitudinally and not being influenced by the bicycle.

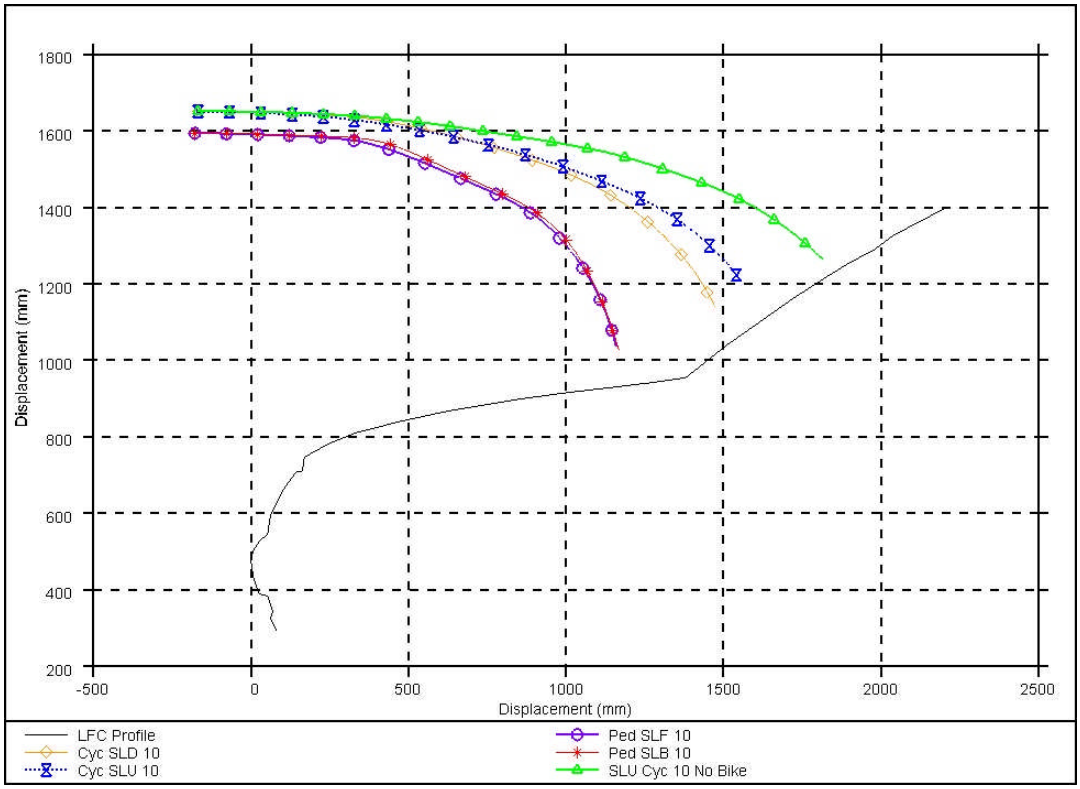

Figure 4-32: Head Trajectories for 10 m/s Phase 1 Simulations

Although at this stage there is not a legislative test procedure specific for cyclist head impacts onto the vehicle front, they are deemed to be covered by the pedestrian impactor test procedures. The simulations have shown that the cyclist's head is likely to strike in a different location to the pedestrian, indicating that the test procedures need updating to incorporate the unique cyclist impact conditions. The orientation of the head prior to impact greatly influenced the speed of impact due to the variations of neck properties; therefore the test procedure should take this into account. To incorporate the motion of the head moving up the bonnet towards the windscreen, in addition to moving across the bonnet may prove challenging. The single test speed currently used for legislative tests such as Euro NCAP and the European Directive, may also need to be expanded to cover a range of impact scenarios to take into account the needs of cyclists.

4.5 Summary of Phase 1 Simulation Results

The Phase 1 results have highlighted factors such as initial leg stance, speed of vehicle and the movement of the bicycle having a significant influence on the cyclist kinematics and injuries. Other factors that did not have such an effect included angled orientation of the cyclist and offset impacts from the centreline of the vehicle.

The impact location of the head varied between cyclists and pedestrians with the cyclist head impacts being more likely to occur on the windscreen for this particular vehicle geometry. The vehicle geometry was highlighted as being a significant factor and merited further investigation in Phase 2.

The struck leg up and down scenarios will be further analysed in Phase 2 to understand their influence with different vehicle geometries and speeds. The shear force and bending moments of the knee will also be analysed in greater depth.

4.6 Phase 1 Physical Testing Set-Ups

4.6.1 Types of Tests

Three types of physical tests were performed in this phase of the research. Static tests were performed on all three bicycle types to understand the failure mechanisms and loads that the bicycle could withstand. Secondly, dynamic pendulum tests were performed on bicycles to capture the dynamic response and to understand the interaction between the wheels and frame. Finally, full vehicle to cyclist and pedestrian reconstructions were performed, with different cyclist leg orientations.

4.6.2 Types of Bicycles

Three types of bicycles were used to represent the range of bicycle sizes used in normal road traffic conditions, Table 4-4.

Bicycle Type	Frame Material
Adult Mountain Bicycle	Aluminium Frame
Junior Mountain Bicycle	Steel Frame
Juvenile Bicycle	Steel Frame

Table 4-4: Bicycle Types.

4.7 Phase 1 Static Bicycle Tests

4.7.1 Static Set-Ups

A static test rig, as shown in Figure 4-33, was used to conduct 16 static tests on the three bicycle types. The hydraulic actuator moved an impactor in a horizontal plane and applied a static load at a rate of 1 mm/s. The resistance to motion of the actuator was captured by a load cell situated on the front face of the impactor and provided force versus displacement output. Two linear bearings were used to control the translational orientation and movement of the impact face and the bicycle was fixed to a rigid platform which was bolted to the ground.

Figure 4-33: Actuator and Platform used for Static Tests.

4.7.2 Static and Dynamic Bicycle Test Matrix

Table 4-5, shows the test matrix to cover the three different bicycles for the static and dynamic bicycle tests. In some cases repeat tests were conducted to ensure that the test results were reliable and that the data acquisition system was working consistently. The range of test scenarios provided detailed test data suitable for validation of the FE model and provided a better understanding of the collapse mechanisms.

Test Number	Direction of Impact	Type of Bicycle
Test #1	Rear	Junior
Test #2	Front	Junior
Test #3	Front	Junior
Test #4	Rear	Junior
Test #5	Front	Adult
Test #6	Rear	Adult
Test #7	Rear	Adult – Frame Only
Test #8	Rear	Junior – Frame Only
Test #9	Bending Test on Seat Tube	Junior
Test #10	Bending Test on Forks	Junior
Test #14	Rear	Juvenile
Test #15	Rear	Juvenile
Test #16	Front	Juvenile
Test #17	Front	Juvenile
Test #20	Front	Juvenile
Test #21	Rear	Juvenile

Table 4-5: Test Matrix for Phase 1 Static Bicycle Testing.

4.7.3 Static Test Results

The static test results on the junior bicycles highlighted that the angle of impact was important in determining the collapse properties. If the bicycle was loaded directly from the front as in test#2, the front forks deformed and the tyre engaged with the down tube of the bicycle. When the test was conducted with slightly turned handlebars (through 1-2 degrees) the wheel was allowed to move further and the forks deformed more, test #3.

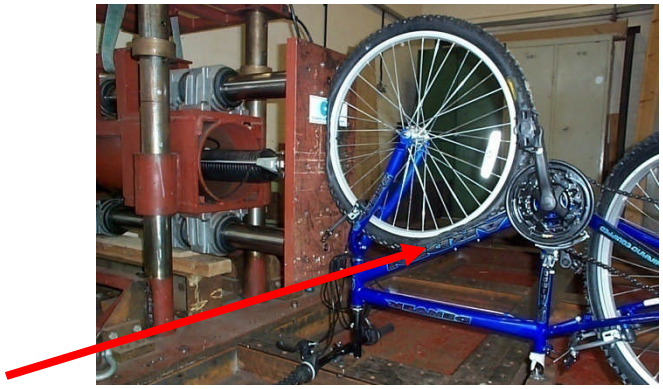

Figure 4-34: Test #2 Showing Wheel Engaging with Downtube.

Figure 4-35: Test #3 Showing Deformations of Forks and Wheel Collapse.

The wheel collapsed through a number of defined phases. Initially, the tyre was crushed which built up pressure within the inner tube. Subsequently, the rim of the wheel was then loaded through the crushed tyre and deformed permanently. The rim of the tested bicycle was made from one piece of metal joined together by welding. At this location the rim strength was weaker and the tests showed that the collapse mechanism for the wheel was highly influenced by the position of this joint on initial impact. Figure 4-36 shows a photograph of a wheel failing by this method.

Figure 4-36: Wheel Failure in Adult Bike at Rim Connection Location, Test #12

The spokes provided a limited initial amount of resistance to the loading and they failed by buckling. For the rear impact scenarios, tests #1, #4 and #6, the frame provided an improved resistance to the wheel deformation not observed for the front impact scenarios. The wheel became held by the rear stays of the frame and prevented the wheel from undergoing excessive damage. After the wheel had deformed the impactor contacted the frame directly and the load increased after approximately 270mm of actuator displacement, Figure 4-37 and Figure 4-38. The initial increase of the curve to 6kN represented the load generated by the tyre and wheel. In comparing the Test #4 junior bicycle and Test# 6 adult bicycle the load responses in the different sizes of bicycles were shown to be similar.

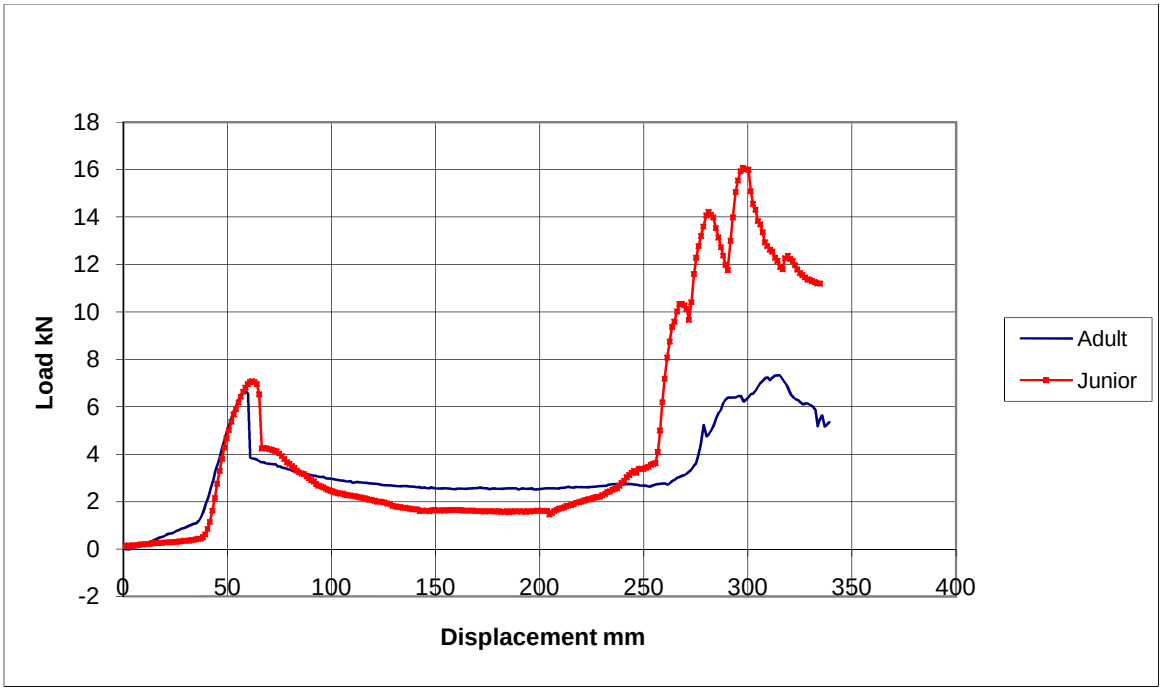

Figure 4-37: Test Data for Static Junior (Test #4) and Adult Bicycle (Test #6)

Figure 4-38: Wheel Supported by Rear Stays, Test #4

A number of tests, conducted without wheels, identified the properties of the bicycle frame in isolation. In these tests the frame was directly loaded onto the rear axles, in

test #8 for the junior bike and test #7 for the adult bicycle. In Figure 4-39, the initial slope of the test #8 curve was smoother than the test with the wheel, as previously seen in Figure 4-37.

After a peak load of 18.5kN occurred at 19mm of deflection, the curve dropped until there was 70 mm of deflection. The impactor had crushed the rear dropouts and there was a direct load path to the rear stays. The increase in load after 70mm was due to the rear dropouts being crushed and the rear stays being axially loaded.

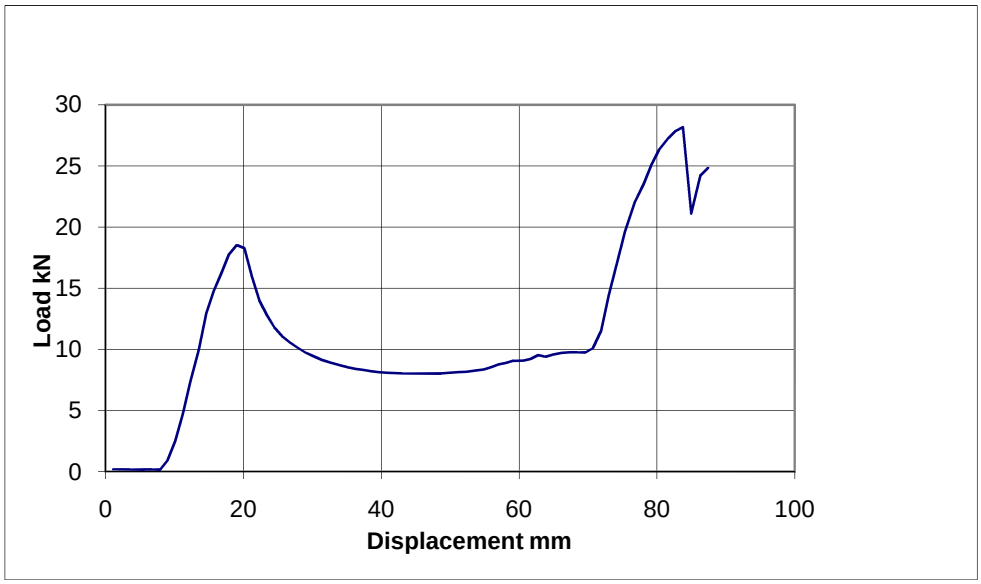

Figure 4-39: Static Test #8, Junior Bike –No Wheels

Bending moment tests were conducted on individual tubes to determine the bending moment properties to be used for initial validation of the FE model. The post test #9 bicycle is shown in Figure 4-40, with the seat tube being pulled towards the front of the bicycle by an attachment to the bottom bracket assembly. A solid steel tube was inserted into the seat tube, to initiate the bending failure above the seat joint.

Figure 4-40: Post Test of Test #9 Junior Bicycle.

4.8 Phase 1 Dynamic Bicycle Tests

4.8.1 Dynamic Test Set-Ups

Five dynamic tests of the bicycle frames were conducted on a pendulum rig, Figure 4-41. The bicycles were inverted and the handlebars and seat post were fixed to a rigid platform. The saddle was removed and the seat pin was also fixed to the platform. The brake and gear cables were removed and the tyres were inflated to a standard operating pressure of 50psi (0.34MPa). The chain was left on the bicycle. For these tests the adult bicycle was used for four of the tests and the junior bicycle once, Table 4-6.

	Impact Direction	Bicycle
Test #11	Rear	Adult
Test #12	Rear	Adult
Test #13	Rear	Adult
Test #18	Rear	Junior
Test #19	Rear	Adult

Table 4-6: Test Matrix for Dynamic Bicycle Testing

4.8.2 Impact Energy Calculation

From the static tests previously conducted, the energy required to deform the bicycle frames permanently was calculated by measuring the area under the Load V Displacement graph. For the junior bicycle the energy absorbed was calculated at 603J, but for the adult bicycle the energy was greater, hence the energy input was set at 1kJ. The dynamic tests were conducted on a pendulum rig, Figure 4-41, which was a swinging bob mechanism, which was allowed to rotate about two pivot points. The rig was 4 metres high with a swing arm of 3.5 metres length. As the bob was released its motion was kept in a vertical plane by the parallelogram motion, which was controlled by two pivot points and bearings. As the bob was released under gravity, the energy and subsequent velocity of the impact were determined. A schematic of the tests is shown in Figure 4-42. For the bicycle crash tests it was only necessary to lift the bob to less than 1m in height, as the energies being applied to the bicycle frame were low compared to other structures which had been tested on the rig such as bus and coach components.

Figure 4-41: Pendulum Used for Dynamic Tests

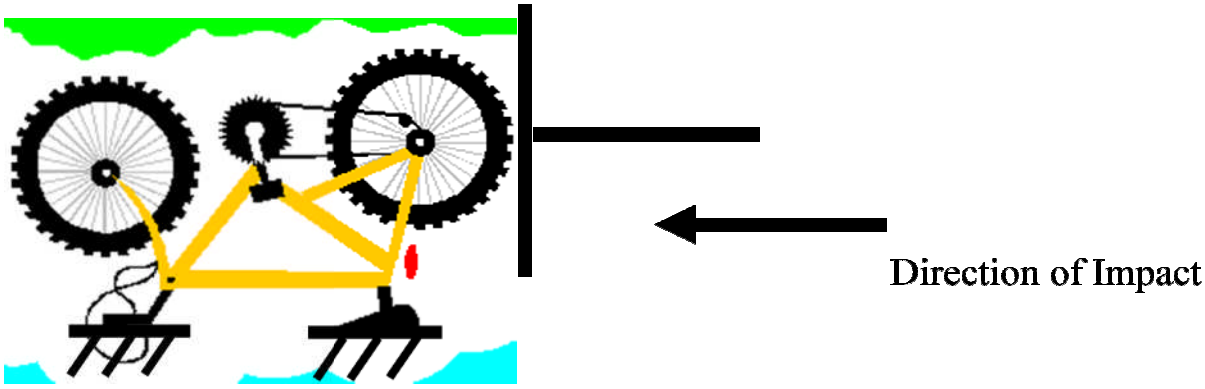

Figure 4-42: Schematic of Phase 1 Dynamic Testing

The dynamic tests were filmed using high-speed photography, which identified the finer details of the collapse method. The capture rate of the high-speed film was 1000 frames per second. This was more than adequate to provide enough images, to be able to review the results and provide reliable material for the finite element model validation procedure. Still images were also captured from the static and dynamic tests.

4.8.3 Phase 1 Dynamic Bicycle Test Results

An initial dynamic test on the rear of the adult bicycle was conducted at an impact velocity of 2 m/s, test#11. The bicycle seat and the handlebars were rigidly fixed to the ground. The test set-up is shown in Figure 4-43, with the bicycle inverted and the pendulum in its position prior to being released. A front plate was also positioned as a precaution to prevent the bicycle from becoming detached from the rig. The post test deformed bicycle is shown in Figure 4-44, with the wheel extensively buckled and broken at the wheel rim connection. However, the frame was not deformed from this first test; therefore it was decided to perform a second test at an increased energy level. By increasing the velocity to 2.5 m/s the energy input to the bicycle increased to 1.46 kJ. For Test#12 the frame deformed as shown in Figure 4-45, with the rear stays being rotated about the bottom bracket. Upon closer inspection, the aluminium tubing was split just below the seat post tube, Figure 4-46. This type of failure at a location in the vicinity of the frame joint, but not on the weld was typical of an aluminium bicycle tube failure.

Figure 4-43: Pre Test Photograph of Test #11

Figure 4-44: Post Test Photograph of Test #11

Figure 4-45: Post Test photograph of Test #12.

Figure 4-46: Post Test Photograph Showing Split in Aluminium Frame Near Seat Post.

4.9 Phase 1 Dynamic Cyclist Tests

Four tests were conducted using the vehicle mock-up, bicycle and dummy as described in section 3.3.3 Dynamic Sled Testing. The dummy and the bicycle were able to be re-used for each test and the vehicle bumper foam suffered minor indentations and was not replaced between tests. The high speed film captured the impact event and a series of still photographs pre and post impacts were taken. Four tests were conducted in the first phase and are shown in Table 4-7.

The cyclist struck leg back orientation, referred to the leg being struck first by the vehicle positioned towards the rear of the bicycle, Figure 4-47. The non-struck leg was in a forward position, due to the 180 deg alignment of the bicycle cranks and pedals.

Test	Dummy Orientation	Impact Speed (m/s)
1	Cyclist Struck leg Back	4.86
2	Cyclist Struck leg Back	4.71
3	Cyclist Struck leg Forward	4.79
4	Pedestrian Walking Stance	4.78

Table 4-7: Physical Test Set-Ups

Figure 4-47: Struck Leg Backwards Orientation – Pre Test

To decelerate the trolley and to simulate a level of vehicle braking the wire break system was used as described in section 3.3.8 Wire Break System. The deceleration pulses are shown in Figure 4-48, with a constant breaking of 1g followed by the trolley stopping at 0.2 sec.

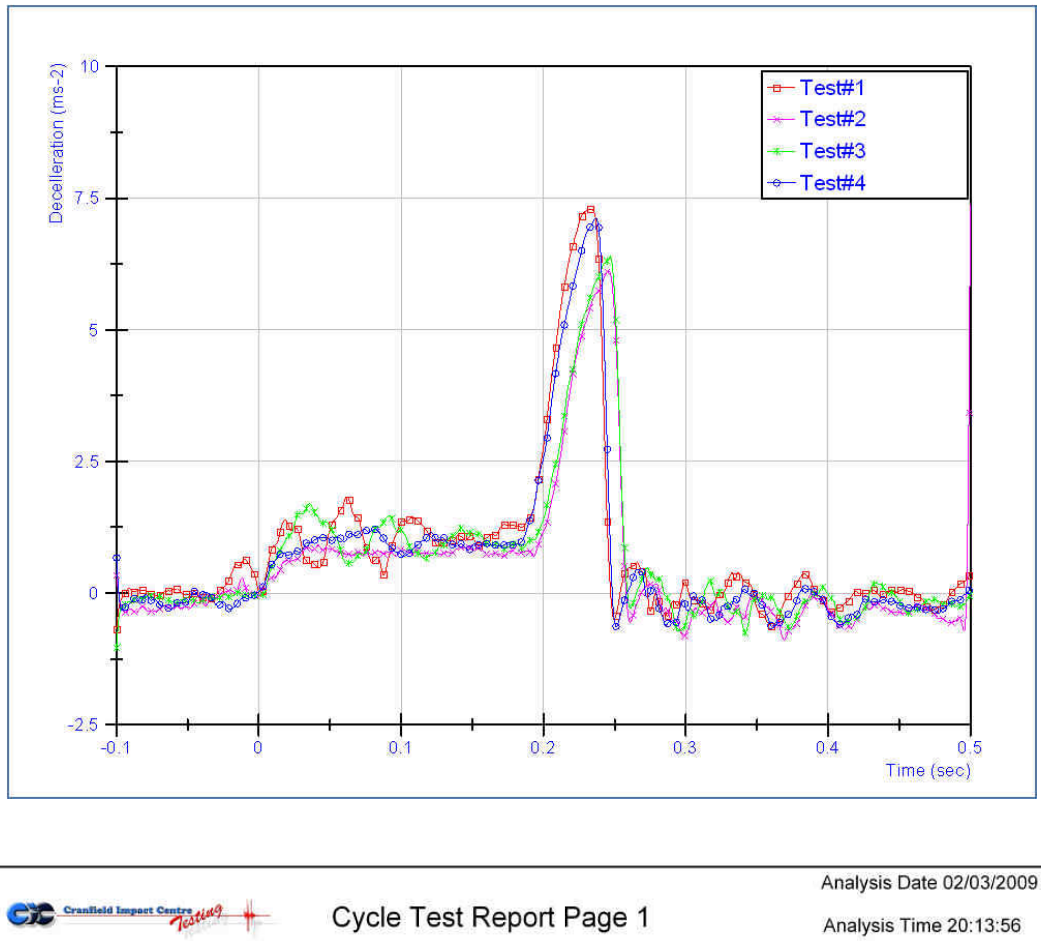

Figure 4-48: Phase 1 Sled Deceleration Pulses

4.9.1 Head Impacts

The pedestrian's head was in a lower vertical position than the cyclist's before impact, because the bicycle provided a greater elevation for the cyclist. In fact, the torso and legs of the cyclist were all higher for this particular bicycle, where the stance of the cyclist was considered to be upright. A racing cyclist would infact adopt a lower rider profile position and this was physically tested in Phase 2.

In a trial test, the release mechanism for the dummy was not released at the correct time and as a result the dummy was suspended during the first 100 ms of the impact. The results were considered un-realistic, but it highlighted that it was important to release the dummy before impact.

In Test 1 the non-struck foot fell off the pedal accidently prior to impact with the vehicle, because the tape holding the foot in place became detached during the last few minutes before the test and went unnoticed. As a result the cyclist was effectively sitting astride the saddle with both feet at a similar height. When the vehicle struck the cyclist, the non-struck foot was not resting on the pedal and therefore affected the cyclist kinematics and prevented the cyclist from easily mounting the vehicle. The head impact location for test 1 was on the bonnet in a similar location to the pedestrian test. The initial leg orientation of the cyclist was influential in affecting the kinematics of the cyclist and as subsequent test results showed when the feet where placed onto the pedals correctly, the head struck a different location.

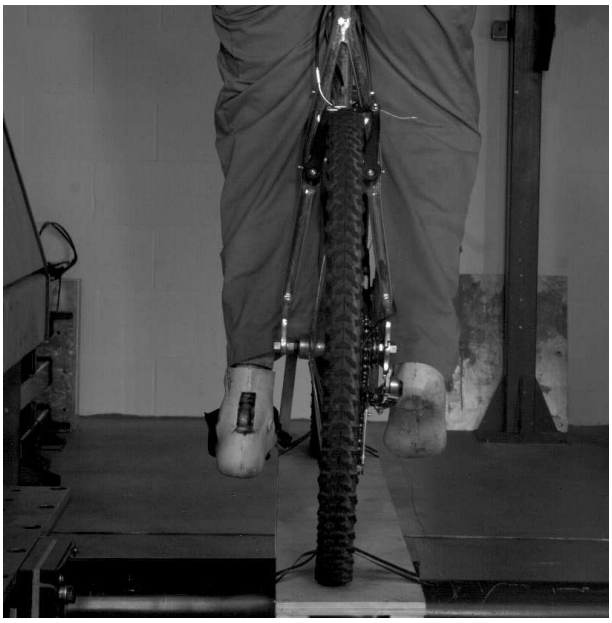

Figure 4-49: Cyclist Test 1 Showing Non-Struck Foot Off Pedal

For test 3 the cyclist's feet remained on the pedals and the cyclist struck the vehicle, slid up the bonnet and the head struck the base of the windscreen. The kinematics are shown in Figure 4-50. During the test the wooden panels that represented the vehicle panels deformed to replicate the metallic structures of a vehicle, but no permanent deformation was observed.

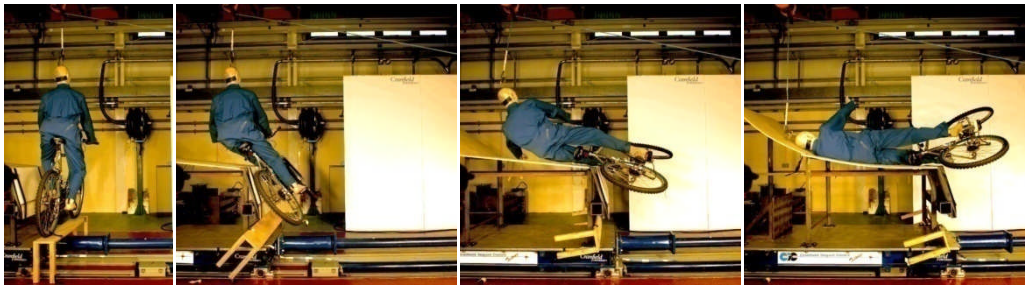

Figure 4-50: Cyclist Test 3 Kinematics

For the pedestrian tests the same dummy was used but with a walking stance adopted. With the lower height of the head and the lack of a bicycle, the dummy in this case wrapped around the vehicle and pivoted about the leading edge of the bonnet. The dummy slightly twisted during the impact, with the head leaning towards the bonnet on impact. The initial walking stance caused this twisting motion to be induced into the dummy.

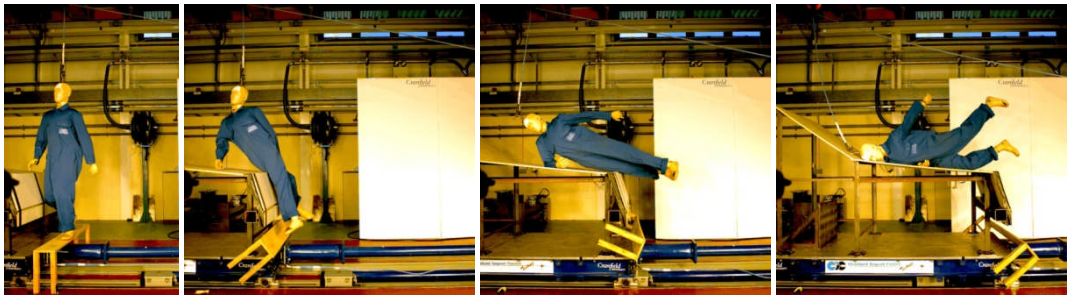

Figure 4-51: Pedestrian Test 4 Kinematics

Both the kinematics of the cyclist and pedestrian showed a similar tendency to wrap around the bumper, mount the bonnet and subsequently strike the vehicle bonnet or windscreen. The trajectories of the head are shown in Figure 4-52, up to the time of head strike onto the vehicle. An outline shape of the vehicle has also been included. The values have been obtained by tracking the head using the TEMA software, with the high speed film captured for each test.

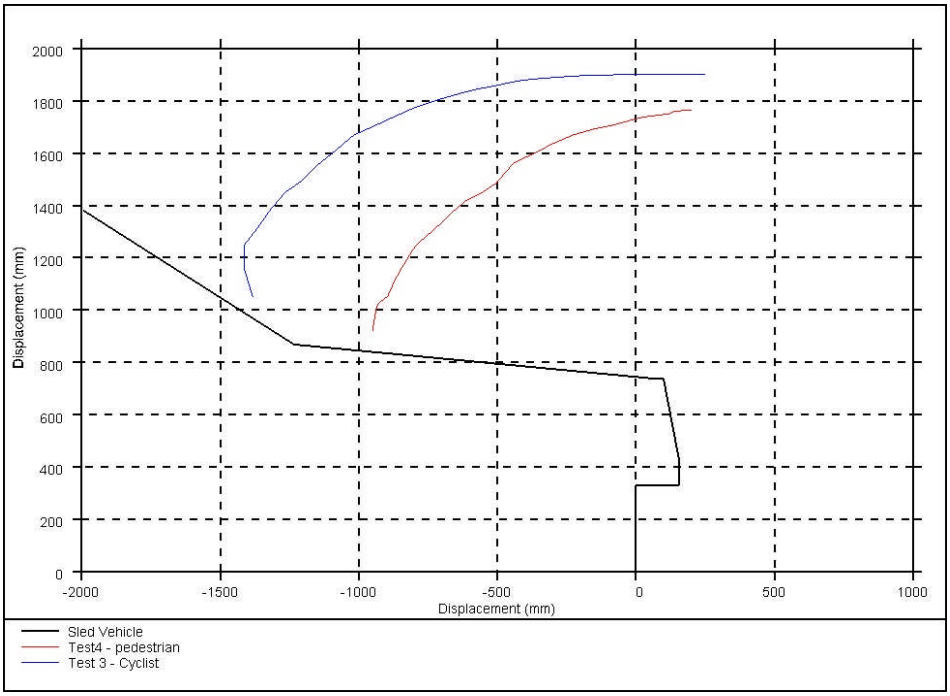

Figure 4-52: Head Trajectories of Pedestrian and Cyclist Sled Tests

An important finding from the tests was that the pedestrian struck the vehicle on the bonnet, whereas the cyclist struck further up on the windscreen. This difference between pedestrian and cyclist head strike location is significant in determining their head injuries. From the simulation results the velocity on impact was affected by the geometry of the vehicle, but unfortunately in these physical tests the head injury levels cannot be compared, as the dummy is not adequately instrumented and the vehicle stiffness is not accurate. However, the initial stance, height of the bonnet leading edge and length of bonnet played a defining role in the kinematics of the pedestrian or cyclist.

4.10 Validation between Phase 1 Modelling and Testing

The Phase 1 physical testing reinforced the different head impact locations of the pedestrian and cyclist, which had been observed in the modelling exercise. The physical tests did not exactly replicate the simulations as there was not a dummy model of the Sierra Stan available and the wooden panels of the vehicle did not strictly match the stiffness of the modelled vehicle. Even though the physical testing

was limited to a few cases, the difference was still evident and the high speed photography was able to show the head impacts and orientations prior to vehicle impact. The modelling exercise, which was more comprehensive, again demonstrated the cyclist accident scenario as having characteristics different from pedestrians. The difference was enough to consider a more detailed investigation in Phase 2 to categorise and quantify the distinction and to propose future changes to current pedestrian legislation.

Chapter 5 Cyclist and Pedestrian - Phase 2 Results

5.1 Simulations Set-Up

5.1.1 Introduction

The Phase 1 simulations were conducted with a large family car model (LFC) to examine a range of parameters including the vehicle speed, the cyclist's speed, the initial positioning and orientation of the cyclist and the leg positions. Pedestrian simulations were also considered for comparison purposes with a subset of the cyclist scenarios.

For the Phase 2 simulations three new vehicles were introduced to represent a wider range of vehicle profiles as the Phase 1 simulations had highlighted the importance of vehicle shape. A set of parametric studies with a Supermini model (SM), a Multi-purpose vehicle (MPV) model and a sports utility vehicle (SUV) model were conducted. Wrap around distances (WAD) (as previously explained in 4.2.2), were determined for the three vehicles and these distances have also been shown on the vehicle geometries by a line of single elements laterally across the vehicle. The knee, pelvis, chest and head results were analysed for the vehicle types and in particular comparisons were made between the cyclist and pedestrian simulations.

5.1.2 Vehicle Stiffness

The contact stiffness between the vehicle and cyclist can be modelled in a variety of ways with the LS-DYNA finite element code. If material properties of the vehicle and the cyclist are fully known and understood, the contact can be defined as two independent bodies and the software code can determine which body deforms the most on impact. In such cases, a friction component is also defined by the user, but the material properties determine the deformation and absorption capabilities.

In the Phase 2 simulations, the vehicle geometry was known, but the stiffness of the vehicle and details of the components under the exterior panels were not known. Therefore, the LS-DYNA keyword CONTACT_RIGID_TO_RIGID definition was used, with the bonnet and windscreen elements not able to demonstrate deformation

as they were modelled rigidly. Instead, a force versus deflection curve was used to determine the contact stiffness between the vehicle and individual body parts. The force deflection curves were obtained from EuroNCAP data, where legislative pedestrian impactors had been used against vehicle structures which corresponded to the SM, MPV and SUV vehicle groups. For the cyclist in Phase 1, the properties of the soft tissue (such as muscles and skin) and the bones were modelled with the capability to predict the likelihood of bone fracture. These properties were negated when using the RIGID_TO_RIGID contact as the absorption capabilities of the impactors (or skin) were taken into account in the stiffness curves.

5.1.2.1 Supermini Model SM

The Supermini model represented the profile of a Renault Clio. As was previously used in Phase 1, the current legislative WAD point locations were calculated and added onto the vehicle profile, as shown in Figure 5-1.

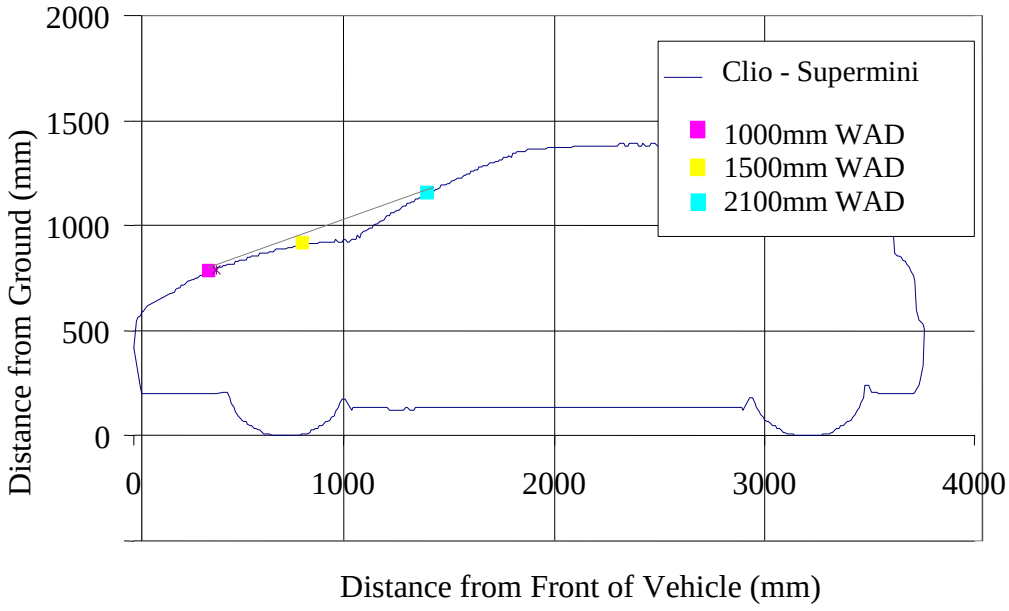

Figure 5-1: Supermini Vehicle Profile, Clio

The vehicle stiffness characteristics, as measured during the EuroNCAP tests were utilised for the simulations and are given in Figure 5-2, Figure 5-3 and Figure 5-4,

along with test locations for the head, upper and lower legform. For the bumper characteristic the R1 and R3 curves were used, showing a deformation of 0.06m, with a corresponding force of 25-30kN. The bonnet and windscreen had a lower impact force, in the range of 2-6kN due to the lower stiffness of those regions, (R7-R17).

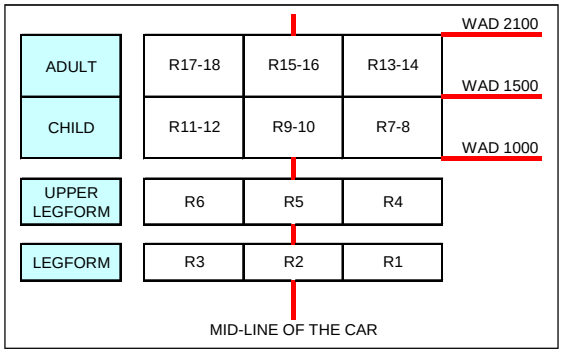

Figure 5-2: Supermini EuroNCAP Test Locations

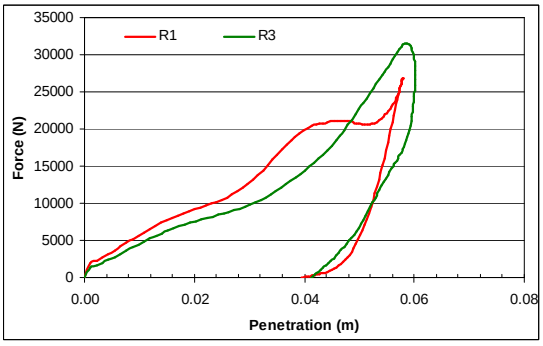

Figure 5-3: Supermini Vehicle Stiffnesses for the Bumper

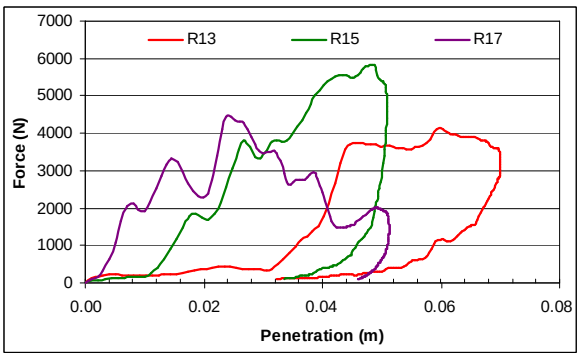

Figure 5-4: Supermini Vehicle Stiffnesses for the Bonnet

5.1.2.2 Multi-Purpose Vehicle Model - MPV

The MPV represented the vehicle profile of a VW Sharan, but utilised the EuroNCAP impact test data from a VW Touran when formulating the LS-DYNA contact definitions. The Sharan profile fitted more within the MPV corridor. The WAD point locations were marked on the vehicle profile, to identify the regions where the EuroNCAP impactors would contact the vehicle as shown in Figure 5-5.

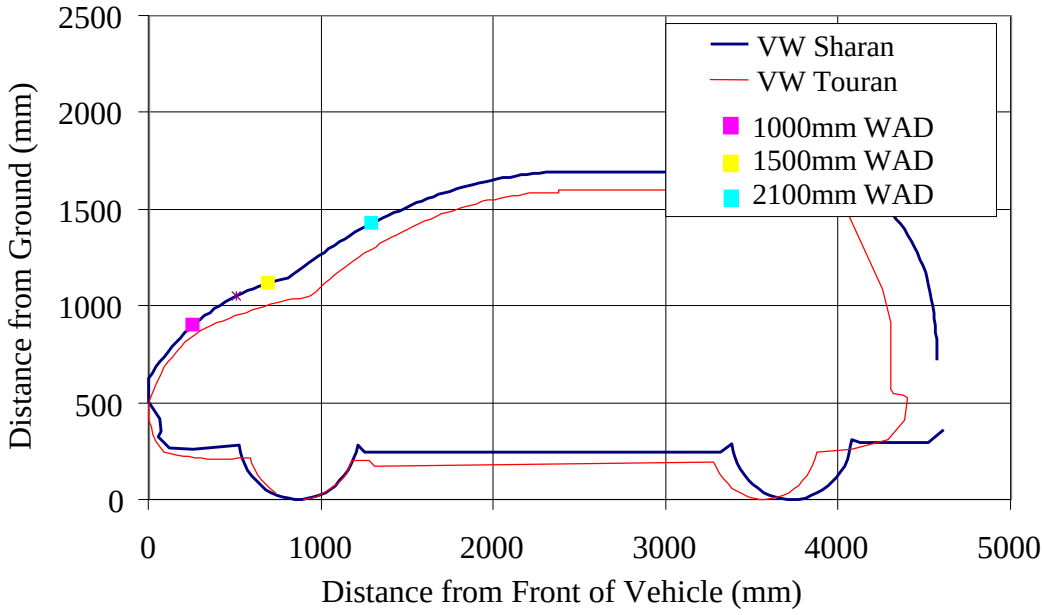

Figure 5-5: MPV Vehicle Profile, Sharan and Touran

5.1.2.3 Sports Utility Vehicle - SUV

A Jeep Grand Cherokee profile was used to represent the vehicle profile of a SUV model. As no EuroNCAP impact test data was available for the Jeep, a Hyundai Sante Fe was used for the model.

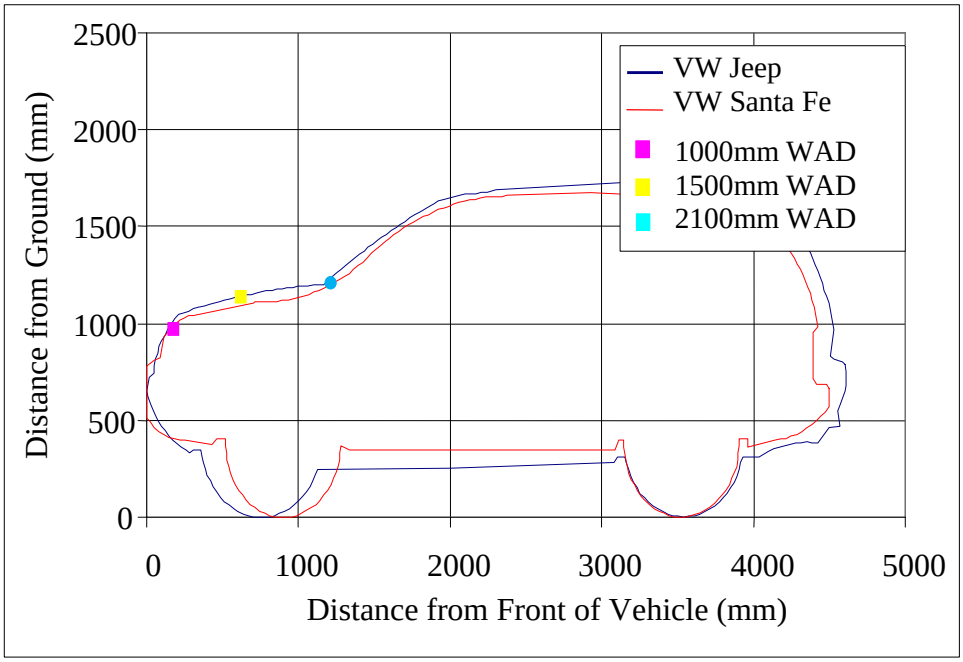

Figure 5-6: SUV Vehicle Profile, VW Jeep and VW Santa Fe

Both vehicles have similar profiles and belong in the same group. As previously conducted for the Large Family Car, Supermini and Multi-Purpose Vehicle models, the WAD point locations were added to the vehicle profile, as shown in Figure 5-6.

5.1.3 Cyclist and Pedestrian Stances

For the three different vehicle shapes, two different cyclist stances were chosen. The struck leg up and the struck leg down are shown in Figure 5-7, and they were similar to the Phase 1 stances.

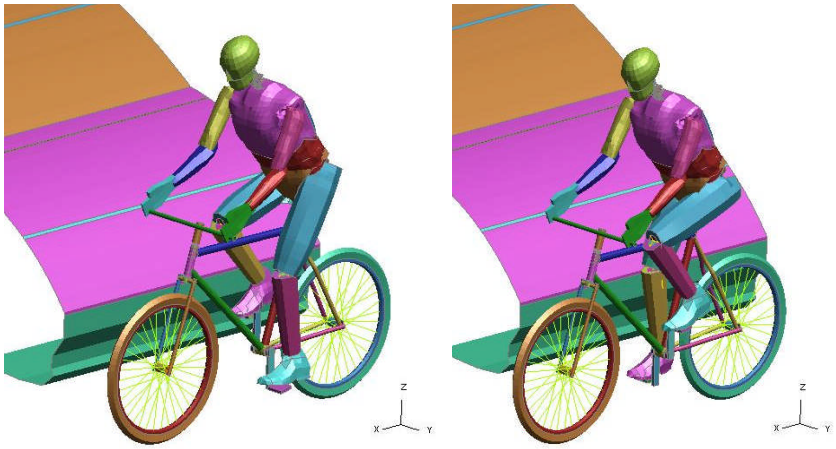

Figure 5-7: Struck Leg Up and Struck Leg Down Cycling Stance

For the pedestrian simulations the struck leg back stance as shown in Figure 5-8, simulated a particular walking stance for a pedestrian. The struck leg forward (SLF) stance was the mirror image of the struck leg back (SLB) stance, but in this stance the struck leg supported the entire pedestrian mass.

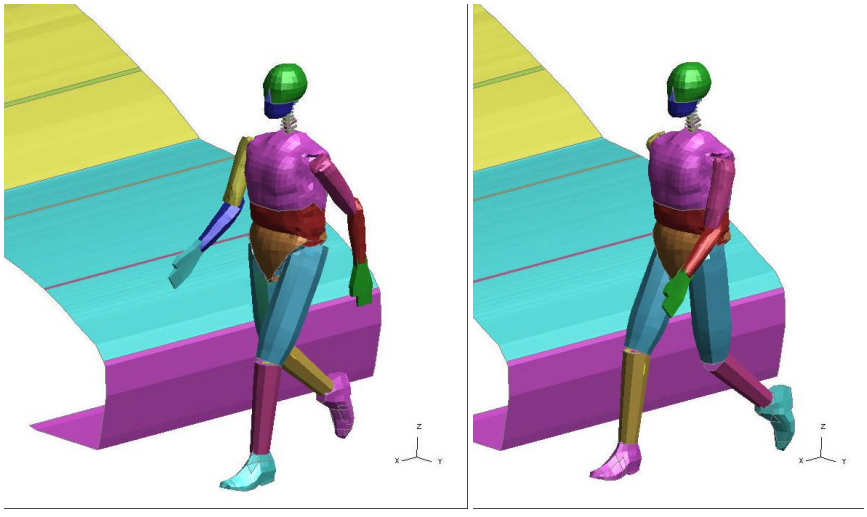

Figure 5-8: Struck Leg Back and Struck Leg Forward Pedestrian Stances

The details of the simulations performed in Phase 2 are shown in Table 5-1 and Table 5-2. In total, 18 cyclists and 18 pedestrian LS-DYNA simulations were conducted.

Test	Dummy Orientation	Vehicle	Velocity (m/s)
1	Struck leg Up	SM	5
2	Struck leg Up	SM	10
3	Struck leg Up	SM	15
4	Struck leg Up	SUV	5
5	Struck leg Up	SUV	10
6	Struck leg Up	SUV	15
7	Struck leg Up	MPV	5
8	Struck leg Up	MPV	10
9	Struck leg Up	MPV	15
10	Struck leg Down	SM	5
11	Struck leg Down	SM	10
12	Struck leg Down	SM	15
13	Struck leg Down	SUV	5
14	Struck leg Down	SUV	10
15	Struck leg Down	SUV	15
16	Struck leg Down	MPV	5
17	Struck leg Down	MPV	10
18	Struck leg Down	MPV	15

Table 5-1: Cyclist Simulations – 2nd Phase

Test	Dummy Orientation	Vehicle	Velocity (m/s)
1	Struck leg back stance	SM	5
2	Struck leg back stance	SM	10
3	Struck leg back stance	SM	15
4	Struck leg back stance	SUV	5
5	Struck leg back stance	SUV	10
6	Struck leg back stance	SUV	15
7	Struck leg back stance	MPV	5
8	Struck leg back stance	MPV	10
9	Struck leg back stance	MPV	15
10	Struck leg forward stance	SM	5
11	Struck leg forward stance	SM	10
12	Struck leg forward stance	SM	15
13	Struck leg forward stance	SUV	5
14	Struck leg forward stance	SUV	10
15	Struck leg forward stance	SUV	15
16	Struck leg forward stance	MPV	5
17	Struck leg forward stance	MPV	10
18	Struck leg forward stance	MPV	15

Table 5-2: Pedestrian Simulations – 2nd Phase

5.2 Kinematic Results

5.2.1 Introduction

The kinematics from the cyclist and pedestrian simulations relate to the motion or movements of the cyclist during the impact phase, without reference to the injuries sustained. Although kinematics were not definitive in showing the different injuries received by the cyclist, they were indicative of potential injuries and their mechanisms. In this sub-section of the results, the key characteristics of the pedestrian and cyclist kinematics are highlighted with particular reference to the Supermini (SM) case as this showed a number of characteristics that were evident in all of the analysed vehicles.

5.2.2 Sliding of the Cyclist and Pedestrian

The SM cyclist struck leg up (SLU) kinematics, are shown in Figure 5-9. This example shows a number of the key elements between vehicle and pedestrian or cyclist. The first (elevated) leg is struck by the bumper or leading edge of the vehicle and the other leg (non-struck) is subsequently either struck by the vehicle or bicycle. The pelvis and torso regions wrap around the vehicle and the arms and shoulder region strike the bonnet or windscreen followed by the head. In terms of kinematics, the difference in initial leg stance between SLU and SLD did not significantly alter the motion of the cyclist or the wrapping around the vehicle. Figure 5-10 shows the SLD kinematics for the SM at 10 m/s, with the head impacting the windscreen, only slightly higher up than the SLU case. The SUV and MPV vehicle types also produced similar kinematics, but not necessarily the same injury levels.

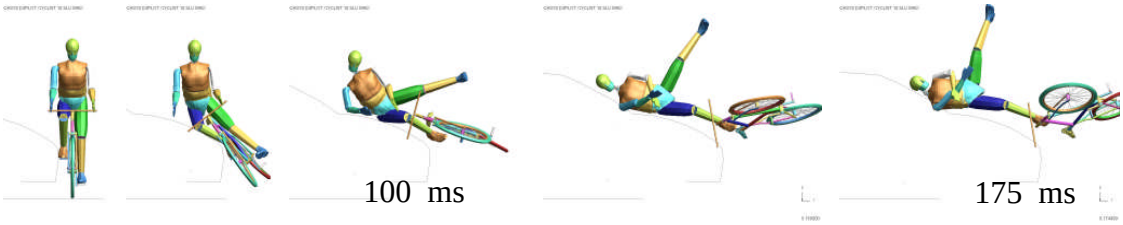

Figure 5-9: Cyclist Struck Leg-up Kinematics from Impact by the Supermini Vehicle Model

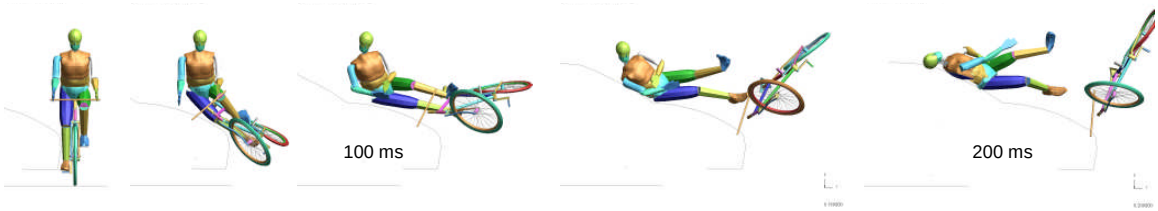

Figure 5-10: Cyclist Struck Leg-down Kinematics from Impact by the Supermini Vehicle Model

In the SM and MPV cases, the pedestrian was struck just above the knee which resulted in a significant lateral rotation of the struck knee joint. For the SUV the contact was closer to the pelvic region which resulted in less rotation of the legs, and more force applied directly to the pelvis. The rotation around the pelvic and abdominal region did not increase the risk of injury in itself but the subsequent torso/neck and head kinematics were influenced by the pelvis rotation. The cyclist and pedestrian in the SUV case were prevented from sliding onto the bonnet as it wrapped around the vehicle and at the slower speeds the cyclist and pedestrian started to actually move away from the vehicle. After the head contact with the SUV, the pedestrian or cyclist did not continue its motion over the vehicle as was seen for the higher speed impacts for other vehicles. This pushing of the cyclist or pedestrian away from the vehicle was also witnessed in the 5 m/s Phase 2 physical tests conducted and described later in this chapter.

5.2.3 Non Struck Leg

The non-struck leg was pushed into an elevated position as a result of contact with the bicycle and actually never came into contact with the vehicle for all types. The injuries sustained by the non-struck leg were due to the impact load being applied through the struck leg and the bicycle. As the load was applied over a larger surface area it was more distributed and the knee injuries for the non-struck leg were less influenced by vehicle shape. This was a fundamental difference between the pedestrian and the cyclist in the manner of force transfer from the vehicle.

5.2.4 Pedestrian Struck Leg Forward and Struck Leg Back Kinematics

For the pedestrian impacts at a vehicle impact speed of 10 m/s, the kinematics of the SM were generally similar for the struck leg forward (SLF), Figure 5-11 and struck leg back (SLB) cases. The legs interacted more with each other compared to the cyclist and showed differences between the SLF and SLB stances, with the struck leg shifting in front of the non-struck leg and the struck leg moving behind for the SLB case. These differences slightly affected the rotation of the pedestrian about its own axis, with the SLF case rotating onto its back rather than staying in a side on orientation. All of the vehicles for the SLF cases showed this rotating of the whole body which in turn affected the head orientation prior to impact. Depending on the orientation of the neck and head, its velocity was affected just before impact, because of the neck's different lateral and fore/aft properties. The head also struck earlier at 139 ms in the SLF SM case, as a consequence of the pedestrian whole body rotation, as against 149 ms in the SLB case. The arms and shoulders contacted the vehicle before the head, although the arms were pushed away and did not influence the kinematics of the torso and head. The shoulder did have an influence on the head impact velocity by restraining the torso movement and allowing the head and neck to rotate prior to impact with the vehicle.

Figure 5-11: Pedestrian Struck Leg-forward Kinematics from Impact by the Supermini Vehicle Model

5.2.5 Position of Cyclist/Pedestrian Relative to Vehicle

A geometric feature of the initial cyclist stance which affected the kinematics was that the lower legs were at a higher vertical position than the pedestrian, but also the position of the lower legs in relation to the leading edge of the vehicle was also significant. The struck and non-struck knee joints of the cyclist were positioned above the vehicle leading edge for the SM, below for the SUV, but straddled the MPV leading edge depending on stance. While, the pedestrian's knee joints were all below or aligned with the vehicle leading edge for all the vehicle types. The position (or posture) of the cyclist in relation to the bicycle remained constant for all cases. The SUV frontal geometry prevented both cyclists and pedestrians from sliding onto the bonnet due to the greater height of the bonnet leading edge which was at approximately pelvis height and well above the knee joint, Figure 5-12. Therefore, the vehicle geometry and its alignment with the cyclist and pedestrian greatly influenced the kinematics.

Figure 5-12: Cyclist Struck Leg-up Kinematics from Impact by the SUV Model

5.2.6 Effect of Bicycle

The absence of the bicycle in the pedestrian cases had an effect on the kinematics of the legs. In particular, for the SLB cases and the 5 m/s cases they stayed together and

did not separate. For the pedestrian SLF, MPV and SUV cases the legs became separated during the simulation as it was easier for the forward leg to move laterally combining with the rotation of the whole body, Figure 5-13. In the cyclist case, the lower legs were moved out of contact when struck by the vehicle, but for the pedestrian they wrapped around all the vehicles more closely and reduced the sliding motion of the pedestrian.

For all the pedestrian SM, MPV cases and the cyclist SLU case, the legs split and in particular the struck leg was pushed away from the vehicle. A scenario that would not always be possible for the cyclist as the bicycle would prevent such movement.

Figure 5-13: Pedestrian Struck Leg-back Kinematics from Impact by the SUV Model

5.2.7 Calculation of the Head Trajectory and WADs

The trajectories for the cyclist and pedestrian cases were obtained by using the vertical and longitudinal displacements of the head cg during the simulations. Initially, the individual displacement components (longitudinal and vertical) were plotted against time. Then the longitudinal displacement of the vehicle was subtracted from the longitudinal displacement of the head, to determine the relative longitudinal head displacement. The vertical and relative longitudinal displacements were combined to produce a single trajectory plot for the head CG. The lateral displacement of the head across the vehicle body was negligible compared to the other values, and was not taken into consideration.

The vehicle profiles were obtained from the FE models used in the simulations and converted into the curve file format suitable for viewing in T/HIS. Markers were also positioned on the vehicle to show the WAD for each vehicle type as specified in the

current pedestrian legislation. Vertical lines showing the 1000, 1500 and 2100mm vertical lines can be seen in Figure 5-14 and Figure 5-15.

For the LFC and SUV, the 2100mm marker was just at the base of the windscreen, but for the SM and MPV the 2100mm marker was near the mid-position of the windscreen. The 2100mm marker is the highest position up the vehicle front that the head impactor can be used in the current pedestrian legislative test procedure and in most cases the impactor is not tested on the windscreen.

5.2.8 Comparison of Head Trajectories for the Different Vehicles

The four different vehicle shapes gave contrasting cyclist and pedestrian head kinematics. The trajectories for the SM vehicle and the range of impact locations are shown in Figure 5-14. For the SM, the cyclist head impacts were solely on the windscreen and for one simulation, (struck leg down at a vehicle speed of 15 m/s) the head struck the roof of the vehicle. This was the only simulation across all vehicle types when this occurred. The pedestrian results straddled the base of the windscreen and the back edge of the bonnet and were defined over a smaller range in comparison with the cyclist results.

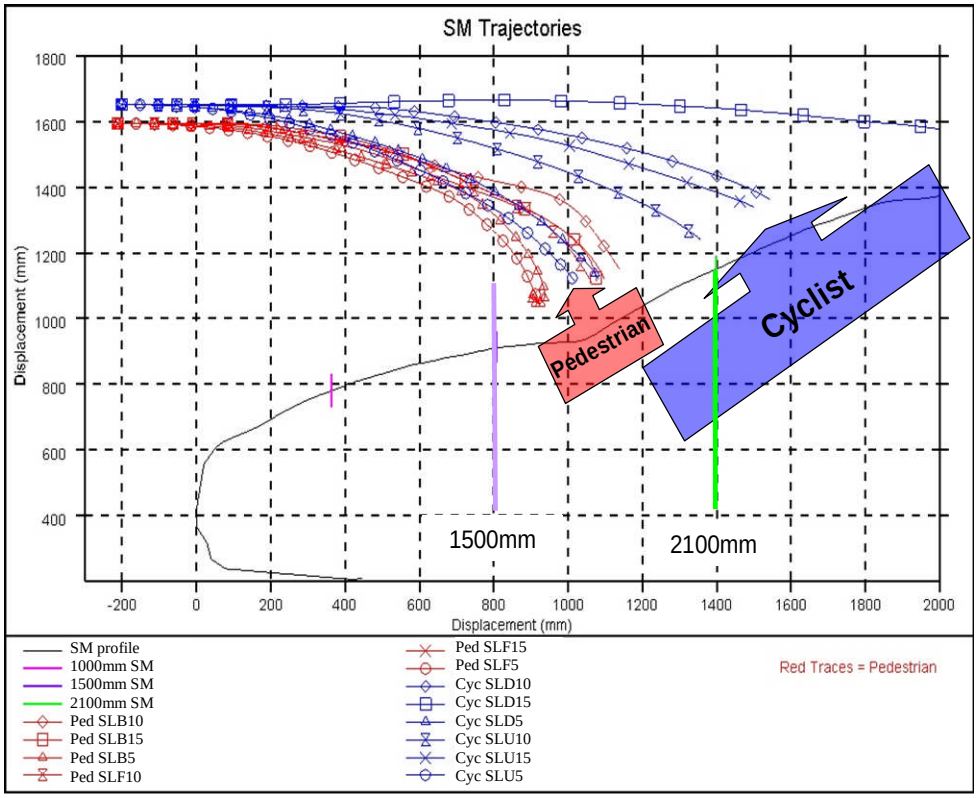

Figure 5-14: Supermini Head Trajectories

For the SUV simulations, the pedestrian and cyclist head only struck the bonnet region of the vehicle. The wrapping motion of the cyclist and pedestrian prevented any sliding occurring and therefore the windscreen was not impacted. For the SUV vehicle type, the current legislation would appear to define impact zones that were very similar to the simulation results.

Another feature of the head at 5 m/s was that for the SUV vehicle the head tended to turn towards the bonnet before impact whereas for the other two vehicles the head remained nearly side-on. For the faster speed at 15 m/s as well, this difference between vehicles was observed with the SUV producing head impacts onto the bonnet only. The exact position of the head impact and its position in relation to the WAD of the vehicle are considered in Chapter 6.

For the MPV, there was a distinct grouping of pedestrian head impacts in the region of the base of the windscreen (some locations on the bonnet and some on the

windscreen), but cyclist impacts occurred solely on the windscreen. Although two of the pedestrian contacts struck below the 2100 mm marker, these were at a vehicle speed of 5 m/s and considerably below the legislative speed of 11 m/s.

For the SM and MPV vehicle types the cyclist showed a greater tendency than the pedestrian to slide along the bonnet, which subsequently influenced the head contact position with the vehicle.

In the Phase 1 LFC case, the pedestrian head strikes were all within the legislative region on the bonnet, but the cyclists straddled the bonnet and the base of the windscreen. A number of the simulations did not actually record a head strike as the shoulder interacted with the bonnet in a side on position and the orientation of the head was kept above the bonnet. These simulations can be seen in Figure 5-15, as the trajectories do not finish at the normal distance from the vehicle, instead they locally re-coil. For impacts with the windscreen, the head was more likely to strike because the head did not have to rotate as much to make contact with the angled orientation of the windscreen.

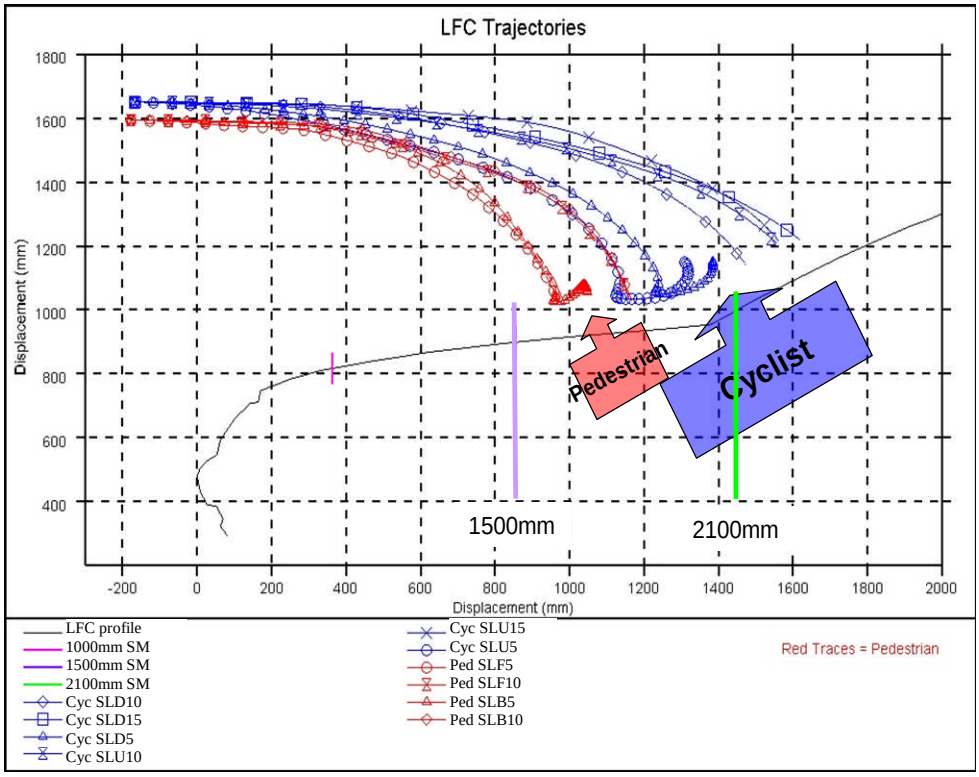

Figure 5-15: LFC Head Trajectories

In all vehicle types, the cyclist struck leg down scenario at 15 m/s, produced the greatest longitudinal trajectory and the struck leg up scenario at 5 m/s produced the shortest trajectory path. The spread over which the head impacted the vehicle for certain types of scenarios was calculated in the longitudinal direction only. The MPV head trajectories were grouped with less than 300 mm spread, compared with the LFC head trajectories that were grouped with a spread of 600 mm. This result indicated that the MPV vehicle produced a smaller range of scatter and the change in impact conditions did not influence the head impact location as much as the LFC.

For the SM pedestrian kinematics there was very little sliding, instead a wrapping around the vehicle front occurred. Although in comparison with the SM, both pedestrian and cyclist MPV head impact locations were on the windscreen due to the shorter bonnet length.

The cyclist to vehicle head impact locations in general, were further up the bonnet, in comparison with the pedestrian, even with similar vehicle impact speeds for all

vehicle types. The cyclist simulations for all four vehicles also had a wider spread of impact locations compared to the pedestrian.

5.3 Modelling Injury Results

5.3.1 Explanation of Knee Results

The accelerations, forces and moments from the Phase 2 simulations were analysed for each of the vehicle types. For the struck leg bending moment and shear force, a sign convention was used to identify in which directions the struck knee was bending and shearing. It changed according to the vehicle geometry, between cyclists and pedestrians and between initial leg orientations. In the Phase 2 simulations the vehicle moved from left to right, according to the view point shown in the kinematic results and the sign convention is defined in Figure 5-16. Therefore, by reference to the pedestrian kinematics given in the second image from the left in Figure 5-13 – SUV kinematics, the pedestrian's struck leg initially experiences positive bending while the other (or non-struck leg) experiences negative bending. Later on in the impact both legs experience positive bending. Positive shear represents movement of the upper leg to the right relative to the lower leg (or the movement of the lower leg to the left relative to the upper leg). Negative shear is the inverse case.

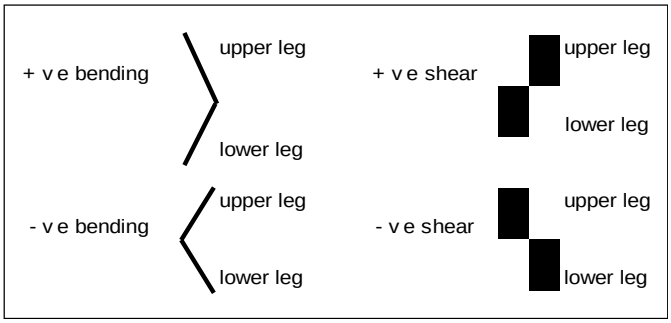

Figure 5-16: Sign Convention for Knee Bending and Shear

5.3.2 Tibia Accelerometer Results

The tibia accelerometer was positioned on the upper third of the lower leg beam elements which represented the tibia and fibula bones and underneath the solids that represented the soft tissue. The 150g level was used for comparison purposes, as it is

the EEVC WG17 lower leg pedestrian impactor legal test requirement. For the majority of cyclist and pedestrian simulations at 10 and 15 m/s the accelerometer level was above the 150g level and at lower vehicle speeds the struck tibia was greater than the non-struck tibia; Figure 5-17 shows results with the 150g level indicated for the SUV vehicle.

At higher speeds the non-struck tibia tended to be of a higher magnitude due to the increase in energy, apart from in the SM case. The difference between the levels of the non-struck and struck legs was greater for the cyclist with a wider range of scatter, probably due to the vehicle being prevented from striking the non-struck leg directly and a more complex series of interactions between vehicle, bicycle and cyclist occurring. For the SM and LFC vehicles the pedestrian levels were generally higher than the cyclist, but for the MPV and SUV vehicles there was a mixed set of results, as shown by the pedestrian SLD results in Figure 5-17.

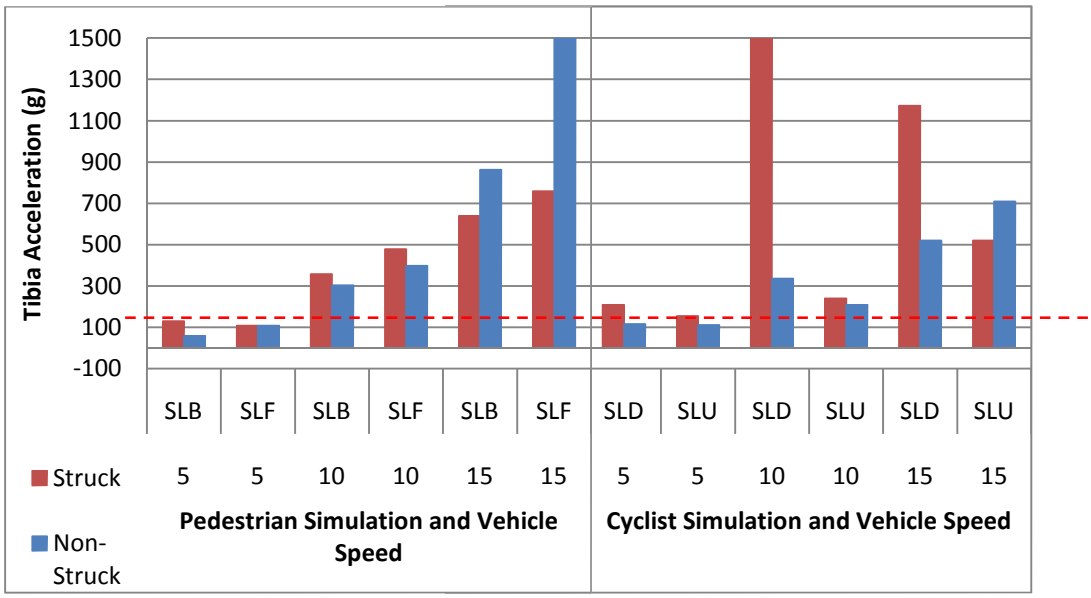

Figure 5-17: SUV Tibia Accelerations

Focusing on the cyclist simulations only, the struck leg-down scenario was significantly worse than the non-struck leg for three of the vehicles other than the LFC. The higher values for the SLD was most likely due to the leading edge of the vehicle bonnet striking the leg just below the knee (almost directly in line with the

accelerometer location) and the leg being caught between the vehicle and the bicycle, Figure 5-18. Whereas, for the cyclist struck leg-up scenario the impact was at the ankle and for pedestrian cases was well above the knee.

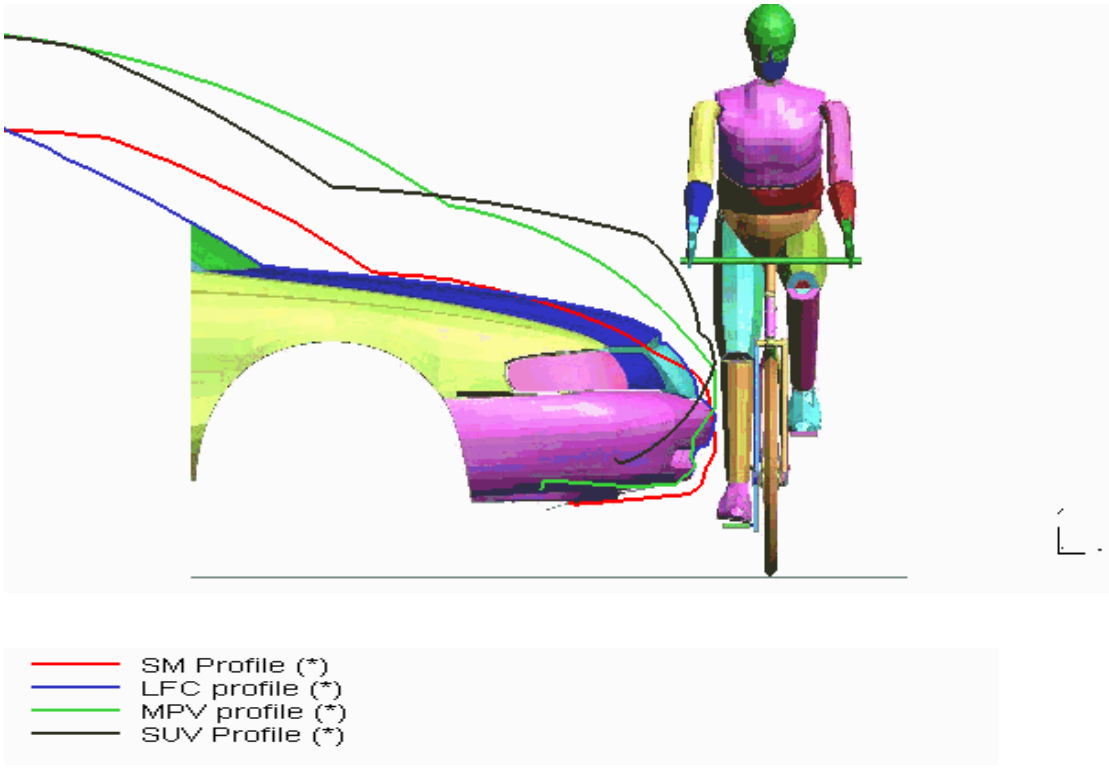

Figure 5-18: Different Vehicle Sizes Compared with a Cyclist

5.3.3 Bending Moment Results

The maximum struck leg knee bending moments are shown in, Figure 5-19 , for the SM. The pedestrian scenarios (on the left hand side of the figure) have a greater magnitude in the positive direction than the minimum (or negative) values, but for the cyclist the minimum values are of a higher magnitude. In the pedestrian case, the positive bending of the knee is more likely to place the medial ligament into tension, but for the cyclist, the lateral ligament on the other side of the knee is more likely to be placed in tension. The cyclists have shown a different injury mechanism when compared with the pedestrians and the trend occurred again for the MPV with the pedestrian showing the highest magnitude of bending moment in the positive direction and negative for the cyclist cases. The significance of this difference is that

the current legislation does not recognise the varying properties of the medial and lateral ligaments and the simulations have shown that they are both involved in pedestrian and cyclist impacts. In a similar manner to the Phase 1 results, the LFC results did not show any difference in the maximum bending moment direction and the SUV also did not highlight the difference. For these two vehicles the bonnet leading edge struck below the knee for the pedestrian and at or above for the cyclist, which affected the loading characteristic from the vehicle.

Ignoring the direction of bending moment, the pedestrian bending moments for all vehicle types other than the LFC, were of a higher value than those for cyclists. The value used to assess the severity of the bending moment was 114 N m. In the SM example of results in Figure 5-19, the pedestrian moments consistently exceeded this level, whereas the cyclist only exceeded it at the higher vehicle speeds. The SUV produced the highest injury levels for all the vehicles, especially for the pedestrian SLF cases where moments in excess of 600 N m were obtained.

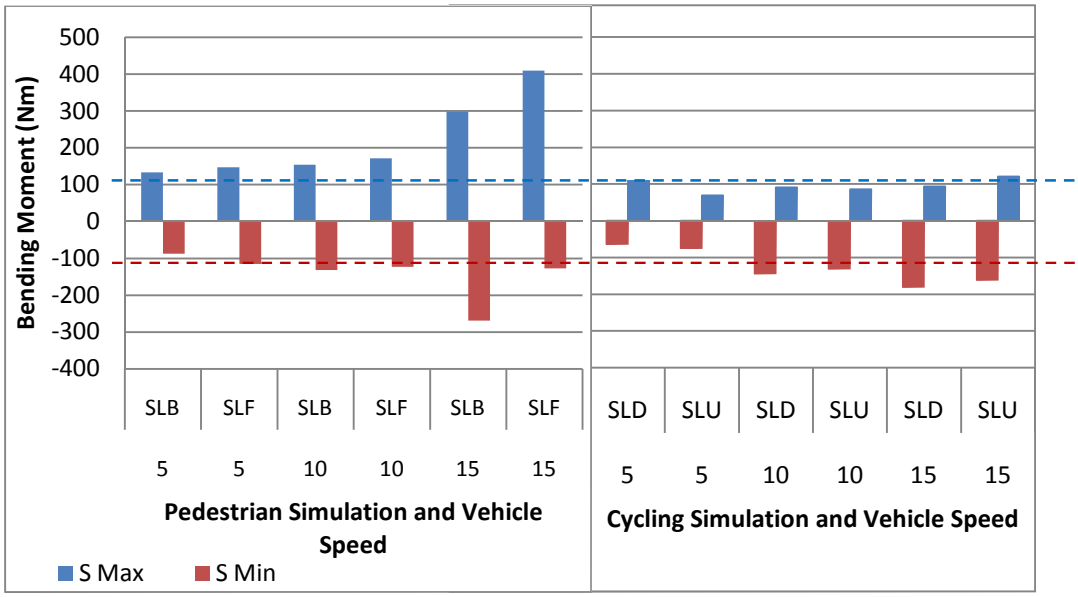

Figure 5-19: Supermini Knee Maximum and Minimum Bending Moments

5.3.4 Knee Shear Forces

In a similar outcome as was observed for the cyclist knee bending moments, the SM and MPV minimum shear force was of a higher magnitude than the maximum value. As the knee shear and bending elements of the model are both located at the centre of the knee it was not surprising to see similar patterns emerge in their outputs. Figure 5-20 shows the trend for the MPV, apart from one cyclist simulation at 15 m/s.

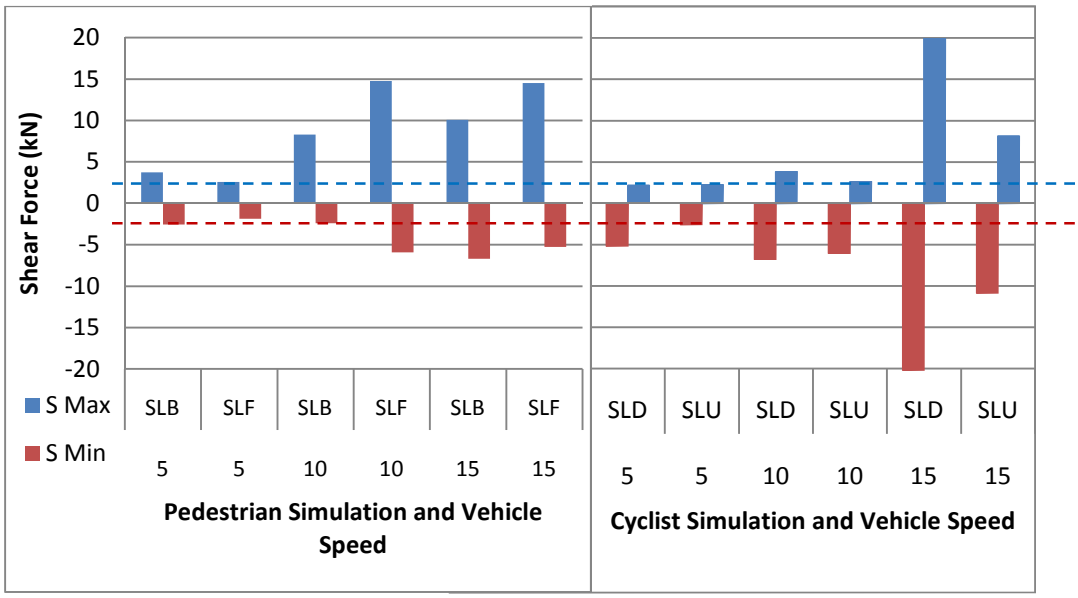

Figure 5-20: MPV Struck Knee Maximum and Minimum Shear Forces

For the SUV the trend was also evident in the knee shear forces but not in the bending moments. Perhaps this was due to the greater bending of the knee experienced in the other vehicles, whereas the flatter front of the SUV did not allow the bending moment to fully develop. The shear force peak always occurred before the bending moment peak; hence the SUV was able to identify the new injury mechanism only through the shear force results.

For the SM and SUV cases the pedestrian and cyclist knee shear forces were of a similar magnitude at the 5 m/s and 10 m/s cases, but at 15 m/s the pedestrian shear forces increased significantly to a maximum of 16 kN. The increase in vehicle speed generally corresponded to an increase in shear force, except for the cyclist SLU cases.

Overall, the pedestrian knee shear forces were greater than those for cyclists and the SUV vehicle showed the highest set of results across the three impact speeds.

5.3.5 Pelvis Accelerations

The pelvis accelerations were generally lower for all the cyclists cases as the greater height of the cyclists' pelvises ensured that the contact between the vehicle and upper leg/pelvis region occurred after the leg contact. By the time that the pelvis of the cyclist came into contact with the vehicle, it had rotated and skimmed the vehicle, as the body began to wrap around the vehicle. In the pedestrian case the upper leg was struck first and the pelvis received more of a perpendicular impact from the vehicle.

The SUV pelvis accelerations were greater than the other vehicle types, but were very similar for both categories of road user, Figure 5-21, which is in contrast with the other two vehicle types where the cyclist levels were nominally lower than the pedestrian's. This may be caused by the high sided nature of the SUV and the direct vehicle contact to the pelvis as shown in Figure 5-22. The other vehicles did not have such high vehicle profile geometry and the pelvis rotated and translated before contact with the bonnet.

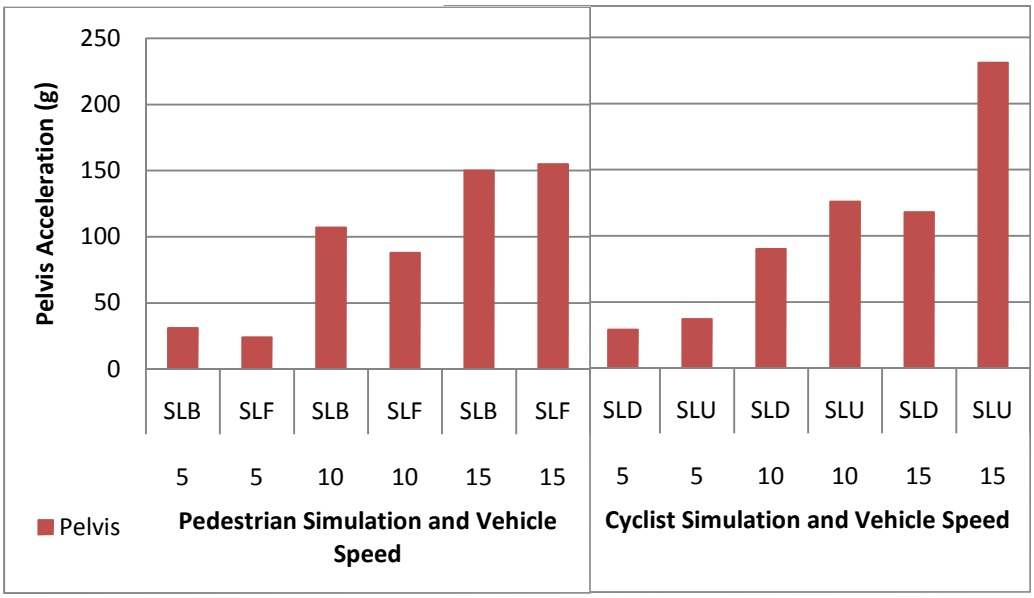

Figure 5-21: SUV Pelvis Accelerations

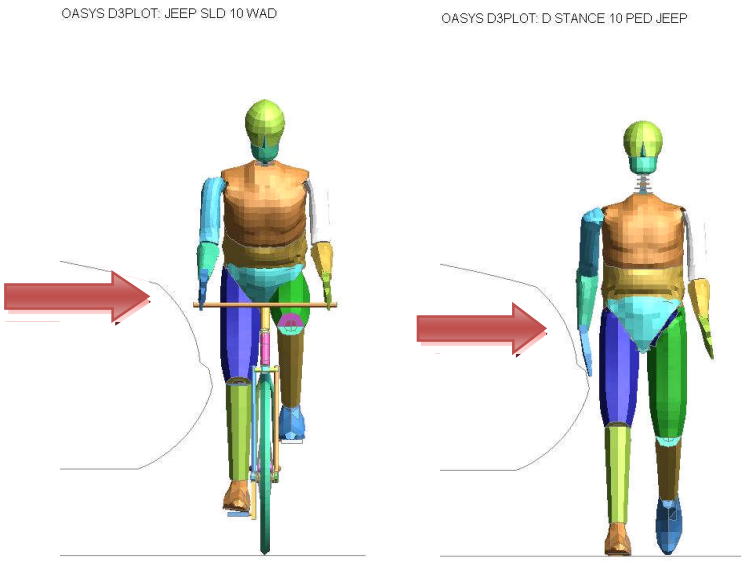

Figure 5-22: Direct Loading of Cyclist and Pedestrian Pelvis by SUV

5.3.6 Chest Accelerations

In contrast, the cyclists' and pedestrians' chest accelerations were lower than the pelvis accelerations. This was probably caused by the glancing impact that the chest had with the bonnet or windscreen. The SUV vehicle produced the highest levels, especially for the pedestrian SLB cases where levels over 100g were obtained. In the SM case the levels were at or below 50g for all vehicle speeds and were similar for pedestrians and cyclists alike. They were not influenced by the fact that the cyclist chest/shoulder impacts were on the windscreen of the vehicle, whereas for the pedestrian the chest/shoulder impacts were on the bonnet of the vehicle. Figure 5-23 shows the gradual increase of the MPV chest levels as the vehicle speed increases and also the similarities between cyclist and pedestrian levels.

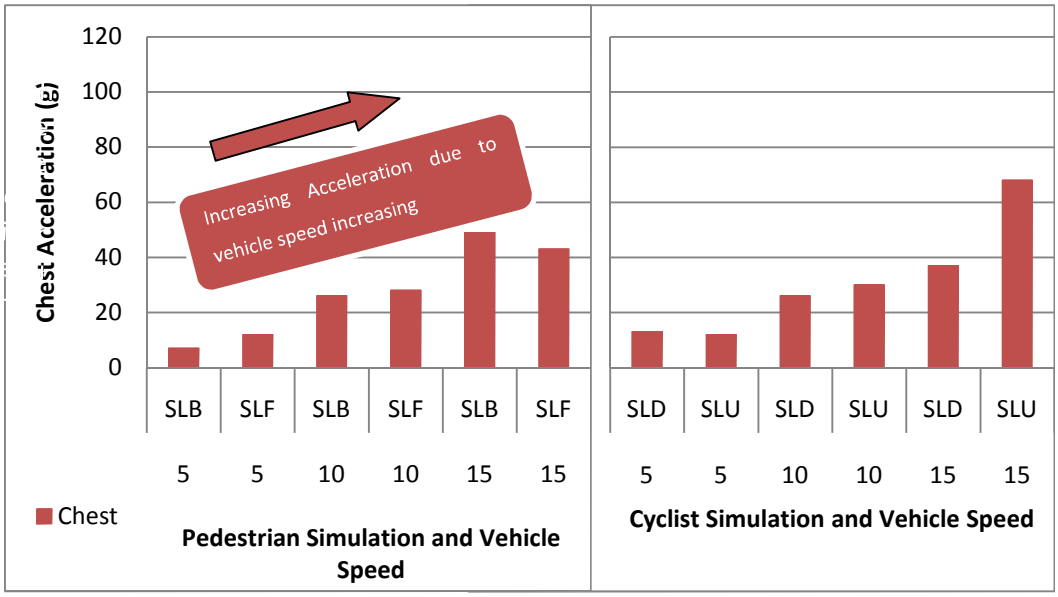

Figure 5-23: MPV Chest Accelerations

5.4 Cyclist and Pedestrian Head Injuries

5.4.1 Introduction

In addition to the cyclist and pedestrian injuries described in the previous section, the head was analysed in greater detail, as it is a major injury mechanism that occurs in cyclist road traffic accidents. The trajectory of the head was obtained from the simulation results and they offered a visual interpretation of the differences between the paths of the cyclists and pedestrians, beyond just identifying the location of the head strike onto the vehicle. The location of the head prior to contact with the vehicle also offered the opportunity to obtain the angle of contact and speed of impact. No detailed data was obtained of the head impact event with the bonnet.

5.4.2 Calculation of Head Impact Angle

To compare the impact angle of the head with the bonnet or windscreen, a reference point was recorded at first contact between the head and vehicle. The time value was obtained by analysing graphical outputs of the trajectory paths at every plotted time

state and recording the point at which the head struck the vehicle. The point prior to contact was determined to be the previous point in time. A graphical output of the head contact was plotted using D3-PLOT (post-processor software) and to aid the process, the head was plotted in a transparent mode in order to visualise the centre of the head. Two lines were then constructed to calculate the angle. The first one started at the head CG and extended along the longitudinal axis. The second was a tangent to the head CG trajectory curve, along the last few points of the path before vehicle contact. Finally, the angle between the two lines was determined; Figure 5-24 illustrates how the angle was calculated for an impact on the MPV shape, in the cyclist struck leg down simulation at 10 m/s.

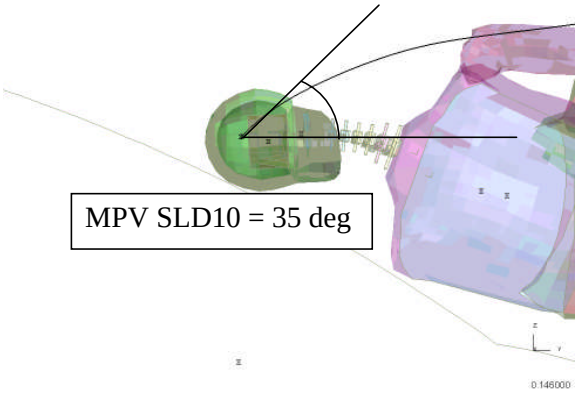

Figure 5-24: Calculation of Head Impact Angle with Vehicle Contact

5.4.3 Head Impact Angle Results

In a number of cases such as the LFC pedestrian simulation at 5 m/s, the head did not strike the bonnet because the trajectory path continued beyond the moment when it came within closest proximity to the vehicle. Non-contact with the vehicle was due to firstly the horizontal alignment of the torso on impact with the vehicle preventing the head from reaching the bonnet. A second reason was the velocity of the vehicle not being fast enough to generate the whole body rotation in the cyclist or pedestrian. Table 5-3 shows the head impact angles for all simulations. The gaps in the table are due to no head contact and the shaded area is where no simulations were conducted.

Simulation	SUV	MPV	LFC	SM
SLB 5		71		
SLF 5	64	100	67	75
SLB 10	124	85	64	63
SLF 10	128	77	61	66
SLB 15	99	114		89
SLF 15	103	71		67
SLD 5				50
SLU 5	71	33		
SLD 10	123	35	58	45
SLU 10	129	55	43	41
SLD 15	94	30	42	
SLU 15	125	44	45	33

Table 5-3: Head Impact Angles (degrees)

(highlighted figures are those less than 65 degrees)

Although the vertical head displacement was very similar for the MPV and SUV, the angle of head contact varied, with the SUV producing impact angles greater than the other three vehicle types. The impacts occurred on the generally horizontal SUV bonnet, compared with the inclined angle of the windscreen for the other three vehicles. When the upper torso of the pedestrian or cyclist struck the rear of the bonnet for all simulations, there was no opportunity for the head to fully rotate and achieve a similar vertical displacement as the torso. Therefore, the head struck the windscreen rather than the bonnet. However for the SUV, the head contacts were all sufficiently towards the front of the bonnet so that the windscreen did not play a role in the head trajectory. The SM and LFC produced the smallest angles that were similar to the legislation angle of 65 degrees and the cyclist angles were all below the 65 degree level.

Further discussion on the head impact angle is provided in Chapter 6.

5.4.4 Calculation of Relative Head Impact Velocity

To calculate the velocity of the head just prior to impact, the time value immediately before head contact was used which had been calculated previously for the trajectory path results. At this time reference, the head cg velocity component results were extracted and a resultant velocity was calculated by the following equation:

$$(V_{Resultant}\,Head)^2 = (V_x\,Head)^2 + (V_y\,Vehicle - V_y\,Head)^2 + (V_z\,Head)^2$$

The individual head acceleration components were able to be extracted from the Humanoid Model and processed. The vehicle velocity was in the y (longitudinal) direction and was subtracted from the y component of the head velocity, to calculate the head impact y velocity, relative to the vehicle velocity. The z and x-axis velocity components were squared and then added to the y velocity relative to the vehicle. Finally the square root of this summation produced the head resultant velocity relative to the vehicle. The x-axis was in the lateral direction of the vehicle and therefore was not dominant in the simulations other than those when the bicycle had an initial velocity applied. The z and y axis were more critical with initially the y component and then subsequently the z component becoming more dominant in the resultant calculation.

Estimates of the relative head impact velocity could also be obtained from the high speed camera film (Appendix J), but they are not as accurate due to the output frequency, tracking software and the estimation of the centre of the head. The simulations produced output at the rate of 10,000 Hz whereas the camera delivered 1,000 Hz. The camera output also required the head cg to be tracked continuously during the simulations by the attachment of target markers. As the head rotated about all three axes before head impact it was not possible to provide accurate data.

5.4.5 Head Impact Velocity Results

After initial contact between the vehicle and the cyclist/pedestrian there was an increase in the relative head velocity for all simulations. The kinematics showed how, as the torso and lower limbs were struck, the head momentarily stayed in the same

position. As the lower limbs and, subsequently, the lower torso, began to wrap around the front end of the vehicle, the head and neck began to translate and rotate. With the neck offering a degree of flexibility, the head was initially oriented away from the vehicle, but subsequently whipped back towards the vehicle front. It was during this stage of the kinematics, that the highest relative velocity of the head was recorded; see Table 5-4 for all vehicle head impact velocities. As the head began to slow down, for most scenarios it dropped below the initial vehicle velocity by a considerable margin before the head struck the bonnet. Although in this study the head impact injuries with the vehicle have not been analysed they would represent the most serious injury that the pedestrian's or cyclist's head would experience.

Simulation	SUV	MPV	LFC	SM
SLB 5		0.9		
SLF 5	1.3	3.5	4.5	5.8
SLB 10	5.3	7.3	6.5	7.8
SLF 10	2.6	6.7	7.6	11.6
SLB 15	15.6	12.1		11.4
SLF 15	10.8	12.5		14.9
SLD 5				5.2
SLU 5	3.4	3.1		
SLD 10	6.4	6.4	11.9	8.3
SLU 10	6.2	6.9	11.2	10.2
SLD 15	10.8	9.4	17.6	
SLU 15	12.6	13.6	17.7	14.1

Table 5-4: Head Velocity Just Prior to Vehicle Impact (m/s)

(Highlighted Cells indicate Head Velocity greater than vehicle velocity)

The LFC produced the highest head impact velocities for the cyclist with all the values being greater than the vehicle velocity, making it the vehicle most likely to produce more potentially damaging head impact conditions. Whereas the MPV was the only vehicle that did not produce any head impacts higher than the vehicle velocity. In only 3 out of a possible 22 cases did the head velocity get above vehicle

velocity for the pedestrian scenarios, but the cyclist had 6 out of a possible 24, making the cyclist more likely to receive higher levels of injury.

The difference in head impact velocity to vehicle velocity is relevant when future cyclist legislation is considered. Choosing a velocity of 11 m/s (40 km/hr) for the test velocity of the head impactor does not necessarily relate to a vehicle impacting the cyclist at 11 m/s.

By analysing the time of head contact, the highest relative head impact velocities for the pedestrian cases were earlier than for the cyclist cases – at each vehicle speed. This was probably accounted for by the different kinematics in the pedestrian and cyclist simulations. As in the case of the SUV, in both cyclist SLU and SLD simulations at 10 m/s, the head struck the vehicle at a velocity significantly lower than the initial vehicle velocity, in these cases below 7 m/s,

Figure 5-25, and for the SM case much later than the pedestrian head impacts – a consequence of the further rearward impact locations.

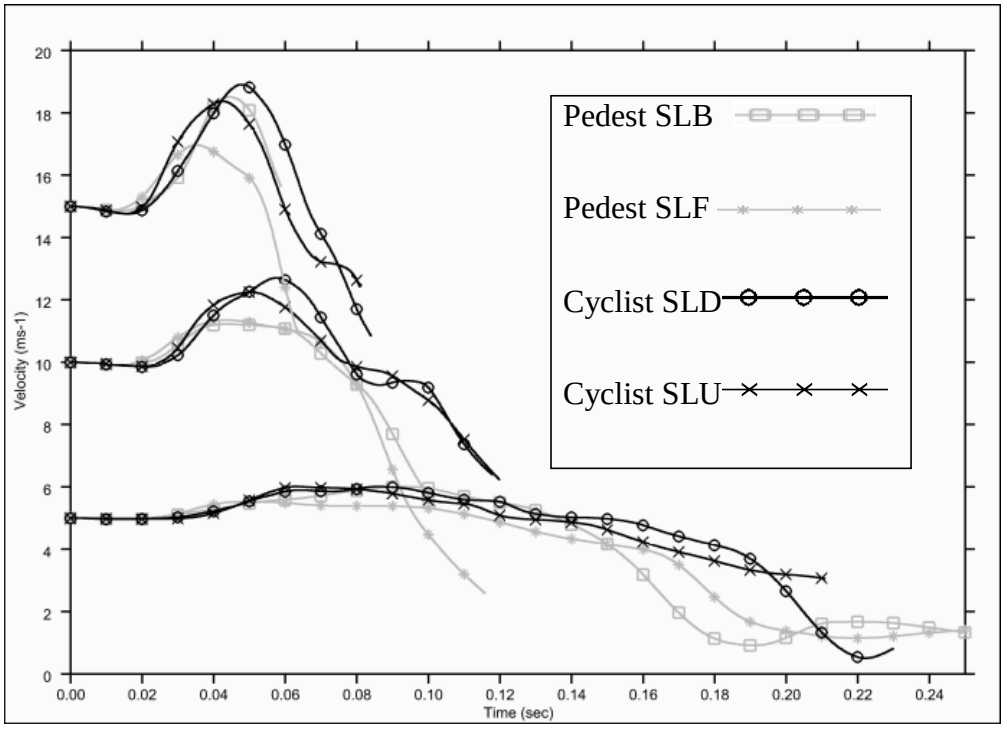

Figure 5-25: SUV Head Velocities

5.5 Phase 2 Physical Test Set-Ups

To complement the modelling activities in Phase 2 a series of physical tests were conducted using the apparatus described in Chapter 3. The aim of the Phase 2 tests was to investigate cyclist impacts with a racing style position,

Figure 5-26, in comparison with the Phase 1 orientation and to investigate an alternative vehicle shape. The flat handlebars used in Phase 1 were replaced with dropped or racing style ones with the intention being to judge, if the racing position would have an effect on the impact location of the head. The same vehicle shape used in Phase 1 was used for four of the tests, and then the vehicle was raised by 250mm to represent a SUV type vehicle, (

Figure 5-26). The dummy was held by a manually operated bomb release mechanism which made the timing of the release critical. Several practice attempts were made to ensure that the dummy did not fall from its intended initial riding position before vehicle contact. A number of trial tests were conducted and deemed invalid as the dummy was held in the air for too long a period and became suspended before being struck. Nine tests were conducted in Phase 2, Table 5-5.

Test Code	Dummy Orientation	Vehicle
2	Cyclist Struck leg Back	SFC
3	Cyclist Struck leg Down	SFC
4	Cyclist Struck leg Up	SFC
5	Cyclist Struck leg Forward	SFC
6	Cyclist Struck leg Back	SUV
7	Cyclist Struck leg Up	SUV
8	Cyclist Struck leg Back	SUV
9	Cyclist Struck leg Down	SUV

Table 5-5: Second Phase Test Set-Ups

Figure 5-26: Racing Cyclist Orientation Set-Up

5.6 Phase 2 Physical Test Results

5.6.1 LFC Vehicle

For each of the four physical tests conducted a different leg orientation was positioned prior to impact. These were the struck leg up and down which were similar to the modelling activities conducted in Phase 2. The dummy's legs were struck by the vehicle and the whole dummy subsequently rotated around the leading edge of the bonnet. There was a small amount of dummy sliding before head contact and during the impact the dummy marginally orientated itself onto its back, accounting for the head impact on the rear of the head. The head location point was recorded by analysing the high speed films and was then plotted onto a vehicle profile. The struck leg back and up head contacts were in similar positions at the base of the windscreen and rear edge of the bonnet.

In the struck leg down test the head contact was on the bonnet and not as far back as the other three tests. The entrapment of the leg between bicycle and vehicle as it was fully extended prevented the sliding and rotating of the dummy towards the windscreen. This trend was also witnessed in the Phase 2 modelling activities for the struck leg down cases.

The struck end of the bicycle handlebars evaded contact with the bumper and grill regions of the vehicle, but struck the bonnet just above the grill and the bicycle stayed between the dummy's legs during the tests.

5.6.2 SUV Vehicle

For these tests three of the four SUV tests produced a head contact on the bonnet in a similar position (within 250mm). The kinematics indentified that the dummy wrapped around the leading edge of the vehicle and stayed side-on during the whole event and very little sliding occurred. The increase in vertical height of 250mm from the LFC had a significant effect on the results, with the dummy pivoting about the pelvis instead of the legs as was the case for the LFC, Figure 5-27 and Figure 5-28.

The handlebars and bicycle were pushed away from the vehicle during the impact event, as the handlebars and saddle were below the leading edge of the vehicle. The bicycle became disengaged from the cyclist and did not influence the kinematics or possible leg injuries of the dummy after this event.

In test 6 (SLB), there was no head contact with the vehicle as the dummy was effectively pushed away from the vehicle in the direction of travel. No rotation of the dummy occurred and no part of the dummy contacted the bonnet. On closer inspection of the high speed film, the dummy was released too soon before vehicle impact and the head/torso of the dummy fell too far and rested on the bicycle before impact. Figure 5-29 shows the lowered position of the head and the twisted orientation of the torso in the first frame. Therefore, this test was not compared with the other three SUV vehicle tests, although it did highlight the importance of correct release of the dummy and more importantly how the initial stance of the dummy with respect to the vehicle was critical in determining the kinematics.

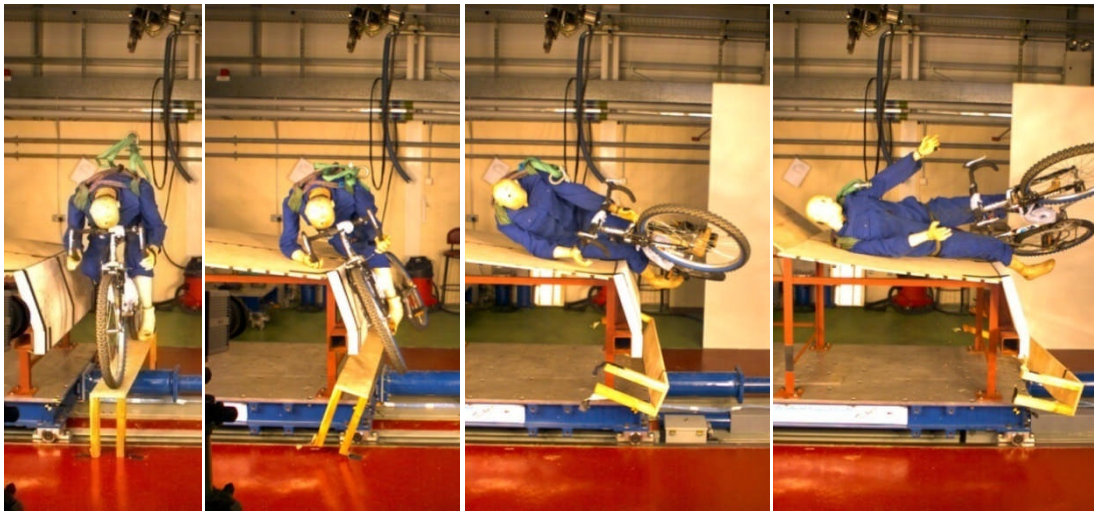

Figure 5-27: Test 2 Kinematics LFC, 0-300 ms

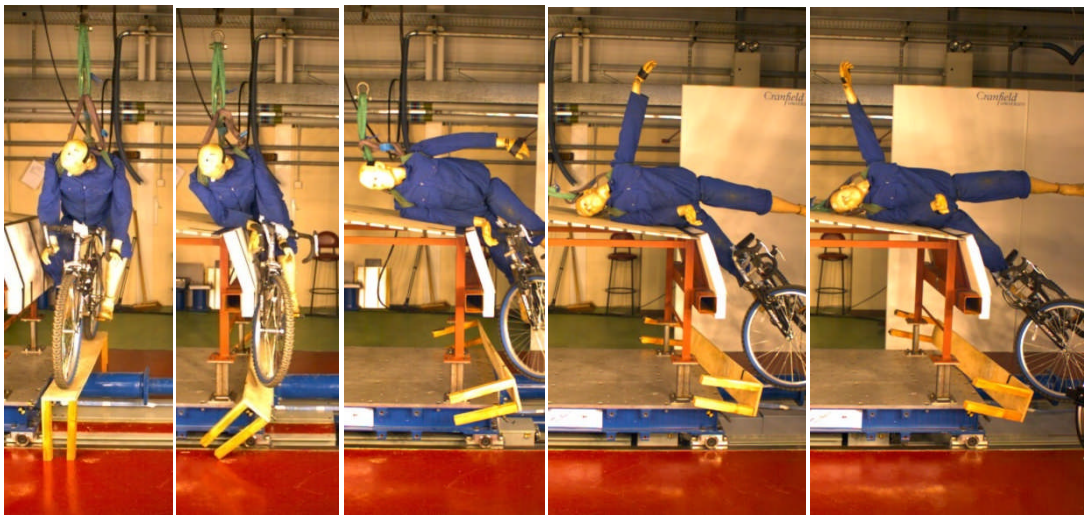

Figure 5-28: Test 8 Kinematics SUV, 0-300 ms

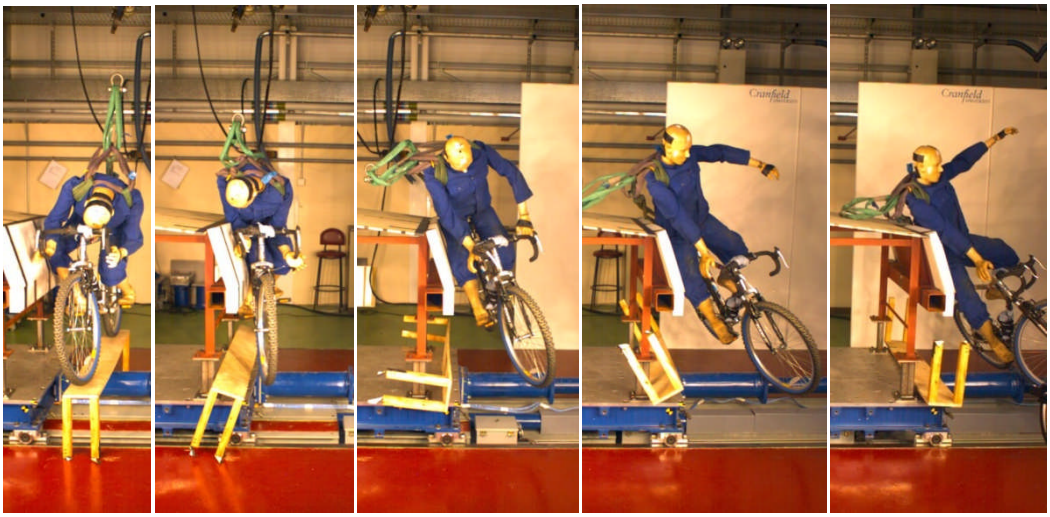

Figure 5-29: Test 6 Kinematics SUV, 0-300 ms

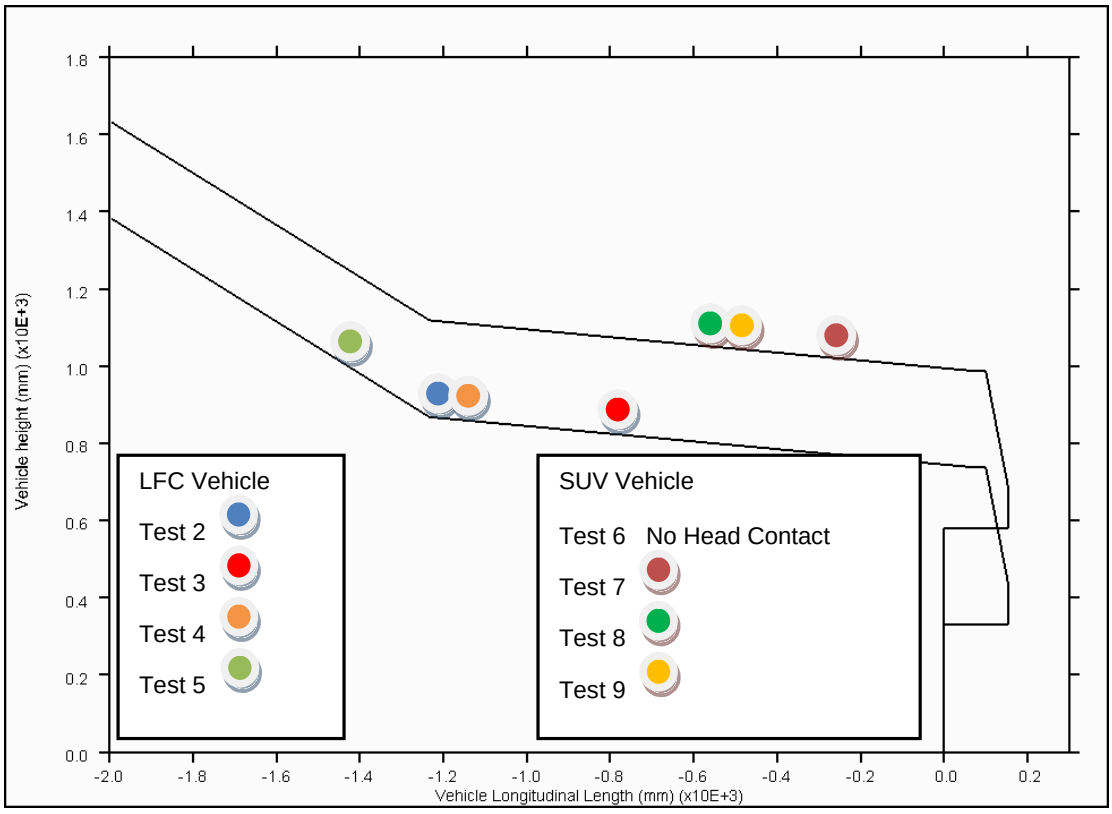

Figure 5-30: Phase 2 Physical Tests - Head Impact Locations

5.7 Conclusions from Physical Tests

The physical tests showed similar head impact locations as was seen in the modelling activities of Phase 2. The SUV vehicle produced head impacts on the bonnet only, Figure 5-30 and the increase in vehicle height for the SUV produced different kinematics, including the reduction of dummy slide as was also witnessed in the LFC cases. Even though no leg injuries could be assessed from the dummy during the tests, the bicycle became detached much earlier for the SUV case and therefore would have had less influence on kinematics. The variations in head contact locations for the LFC were more influenced by the initial leg orientations of the cyclist.

Chapter 6 Discussion

6.1 Introduction

The injuries sustained by a cyclist have been shown, through simulations and physical tests, to be different from those sustained by a pedestrian when struck by a vehicle. The cyclist should not be simply grouped with the pedestrian as a vulnerable road user, but as a unique user with different injuries and kinematics. The bulk of previous research has concentrated on pedestrian injuries and ignored the cyclist as being a unique vulnerable road user. Maki et al. (2003) is one of the few publications to date that has actually compared cyclist and pedestrian collisions with vehicles. This discussion chapter brings together the findings which have been reported in the two phases of modelling and physical testing activities and discusses the implication for future cyclist and pedestrian fatalities.

In Phase 1 a range of side-ways aligned cyclist and pedestrian scenarios were performed with the intention of highlighting those that were high risk in terms of user injuries. A more focused approach in Phase 2 eliminated the use of angled bicycle impacts and those impacts which were offset from the centreline of the vehicle and focused on different vehicle geometry. The vehicle geometries have been selected from modern vehicles and have not been previously addressed. The cyclist modelling work by Janssen and Wismans (1988; 1985) used vehicles which were only relevant at the time of the research.

Instead of analysing individual vehicle results or specific leg orientations, comparisons were made across all of the vehicle types to identify which situations produced the most damaging consequences for cyclists' injuries. The use of the ANOVA statistical technique enabled trends and differences to be highlighted for the large range of data recorded. These trends could not be identified by solely viewing data through scatter plots, as different categories of vehicles were needed to be considered.

6.2 Sources of Scatter

6.2.1 Sample Set of Cyclist Accident Scenarios

The simulations chosen to be analysed in this research were a sample of the total number of different types of real world cyclist accidents. They were selected to represent a wide range of impact conditions, which would mimic the entire real world accident scenarios which have occurred to date. A task to capture every scenario that has occurred to date, and will subsequently occur in the future, would be an impossible undertaking. In 2007, there were over 16,000 cyclist accidents in the UK that resulted in serious injuries and each accident had different impact conditions which cannot be feasibly modelled in 16,000 FE models. However, Otte (1989) showed that 73% of cyclist impacts are with the front of the vehicle, so the model and tests undertaken were considered to capture a high proportion of real world accidents.

6.2.2 Modelling Results Scatter

In 8 out of the 70 simulations, the head was very close (within 10-20 mm) to impacting the vehicle but no head impact angle was recorded. The reason for no head strike in these cases was probably due to the lack of cyclist/pedestrian momentum to fully wrap around the vehicle, which was particularly evident at slow speeds. An alternative view was that the non bio-fidelic nature of the shoulder mechanism prevented the neck from flexing sufficiently. The Humanoid shoulder model could be adapted in a further study, to represent a more bio-fidelic mechanism of the upper torso/shoulder and offer the capability to analyse injuries.

The initial side-ways alignment of the cyclist/pedestrian with the vehicle also played a role in the subsequent head and shoulder interaction with the vehicle. If there had been an initial rotation during the early stages of the impact kinematics, the shoulder would not have necessarily come into contact before the head and hence play a less significant role.

The Humanoid Model was capable of replicating knee injuries but not bone fracture due to the rigid construction of the femur and tibia/fibula leg bones. This modelling

may have constrained the loading from the vehicle into the knee joint, rather than allowing the bones to fracture and offsetting the loading. However, during physical tests long bone fracture was not observed by Cardot et al. (2006), but failures at the knee joint were found. A more detailed model of the knee joint including the malleolus and the condyles would allow these types of fractures to be recorded.

No soft tissue injuries such as muscle tears or bruising were modelled as the approach was only capable of detecting knee or explicit ligament damage as a combination of medial, lateral and cruciate ligaments. The properties of the ligaments were represented by discrete spring elements and it was not possible to model any changes in physical shape during their extension or compression. The absence of detailed bone modelling such as Arnoux et al. (2002a) may have affected the knee ligament results and it is recommended that a detailed bone model is used for future studies.

The technique of using FE to model cyclist accidents has been shown in other research to be a valid assessment method and capable of capturing high impact events (Bermond et al., 1993; Arnoux et al., 2002a; Kikuchi et al., 2008). LS-DYNA was chosen as the most suitable FE code, as the Humanoid Model had been developed in LS-DYNA and had been used in previous pedestrian research, (Howard, 2002; Hardy et al., 2007). Using an alternative software code would have implemented different material models and FE algorithms. It was essential that the model was validated at a component and cyclist/pedestrian interaction with vehicle level, for a wide range of impact conditions. The validation of the cyclist and vehicle models has been previously addressed in sections 3.4.5, 3.5.1 and 4.1. By comparing the simulations to cadaver tests the simulation models have been shown to be accurate within the range of vehicle speeds used in this research.

Obviously, an increased number of simulations would have improved the predictability of the model, but the side-on collision was deemed to be the most high risk scenario. There are a myriad number of accidents which were not capable of being analysed due to time constraints, but accident data highlighted which scenarios to investigate and is the most reliable method to select the most high risk scenarios. It

should also be considered that the accuracy of the accident data when determining the chosen modelling scenarios is of paramount importance.

6.2.3 Relationship to Real World Injuries

The Humanoid Model used in the simulations did not have the capability to react or change its position prior to impact. In a similar manner, the dummy used in the physical tests did not react to the impending impact so they were effectively lumped masses with articulations defined at joint locations. In a real world cyclist accident, depending on the scenario, the cyclist may well have time to change direction if he can see the vehicle approaching. The muscles can tense and the head is likely to look towards the oncoming vehicle. However, at the time of first impact and during the accident the cyclist has very little time to react or change his position as the momentum of the vehicle would easily overcome any cyclist momentum. The cyclist will effectively become a series of lumped masses and the behaviour would be very similar to the simulations and physical tests. Therefore, the lack of muscle tension is not seen as an important aspect for influencing the kinematics of the cyclist.

6.2.4 Head Rotational Acceleration

Another finding of the parametric study was that there were a number of SUV impact cases where the (linear) head accelerations were at their highest prior to head impact on the vehicle. This occurred during the period when the head was rapidly rotating from a near upright orientation to a position below the horizontal to strike the vehicle – all head impacts were on the bonnet for the SUV. The rotational motion in these cases needs further examination to understand the levels of the rotational and linear accelerations and the potential for injury before and during contact with the vehicle.

6.2.5 Test Result Scatter

The static tests performed on the bicycle tubes showed very little scatter in results as shown in Figure 6-1. Both curves are closely matched and the displacement of the wheel at failure is within 5mm. These results are typical of steel structures due to the material properties and the manufacturing tolerances of the bicycle tubes.

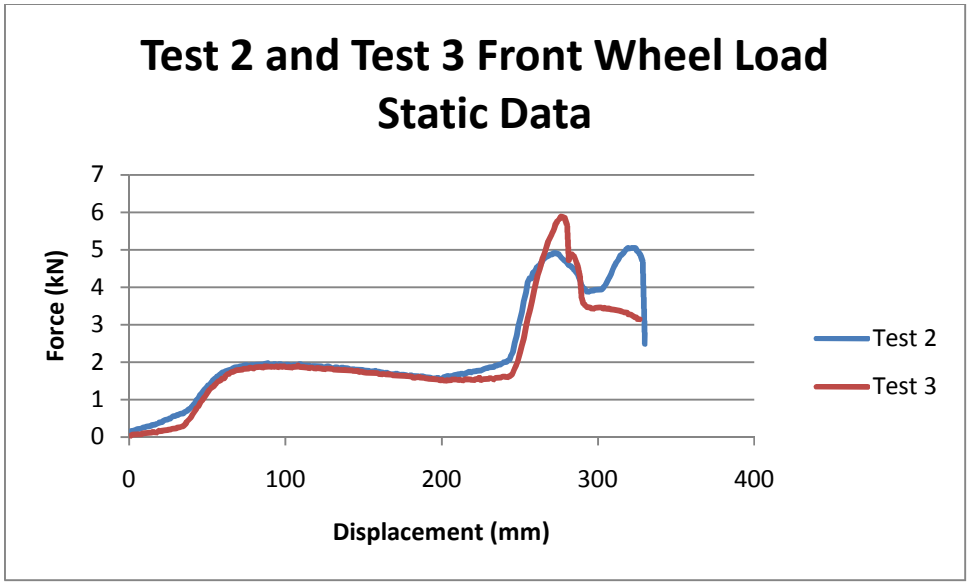

Figure 6-1: Test 2 and Test 3 – Repeat Static Tests on Bikes

In the case of the dynamic impacts, the tests highlighted a number of issues with sled testing that made it difficult to reproduce the same test speed, due to the mechanism of the sled relying on compressed air. There was a margin of error of 3% for the sled velocity measurement, which was calculated by a pair of light sensors just prior to impact.

The positioning of the cyclist prior to impact also varied, especially the feet position on the pedals and their orientation. The feet were strapped to the pedals, but as a dummy does not have the same muscle control that a human has, the legs and feet moved during the period of being set-up and struck. In fact, on a number of occasions the dummy had to be re-adjusted just before firing the sled after a foot had fallen off the pedal. This aspect of lack of ability to control a dummy's motions in a complex position, is one of the reasons that a full-sized dummy is not used for pedestrian (or future cyclist) legislation. The other reason is the scatter obtained by using a full dummy and the sensitivity due to minor changes in stance. During this research more emphasis was placed on the modelling activity due to the repeatability of the simulations and the ability to show specific injuries. The physical testing of the dummy was used for validation of the cyclist kinematics, but no injury data could be compared between the two methods.

6.3 Limits of Knowledge

The physical location of a cyclist, in particular height from the ground prior to impact is an important consideration for meaningful evaluation of the injury risk potential. Any changes to the set-up can affect the kinematics as was shown in the Phase 1 results. With all the physical tests and simulations conducted only a selection of scenarios were evaluated, but they were enough to show the differences between cyclists and pedestrians as well as the effect of the moving cyclist. The relationship and similarities of the scenarios to real world accidents has been confirmed with the accident investigations of Otte (1989) and Maki and Kajzer (2001) .

The current legislative testing regimes assume that a pedestrian is in a straight legged 'gait' on impact. This is not wholly accurate for a pedestrian but for a cyclist it is even more unrealistic, given the range of leg orientations during the rotation of the crank in the cycling motion. The recognition of the important physical orientation differences between cyclists and pedestrians immediately prior to an accident is fundamental to understanding their influence. The sideways orientation of the cyclist was deemed to be the most severe and the worst case scenario. As the vehicle struck the cyclist first, before any contact with the bicycle, it was not able to impart any rotation and the cyclist received a direct impact from the vehicle. Any movement of the cyclist going across the vehicle would have reduced the opportunities for the head to strike the vehicle, as was shown in the Phase 1 simulations. It may be considered that the simulations do not represent real world conditions with the lack of bicycle velocity in the Phase 2 simulations, but they are very similar to a slow speed bicycle impact (less than 5 m/s) and identical to a cyclist impact whilst stationary at a road traffic junction.

Although the cyclists analysed in this study have been of adult stature, there are a significant number of child cyclist casualties across European countries. The difference in initial head position for child cyclist and pedestrian stances is less than the differences shown for the adult cases. Therefore, head trajectories onto vehicles for child cyclists may show different trends to adult cyclists.

The throw distance has not been calculated in this research as the focus was on the injuries associated with the vehicle and not the secondary injuries when the cyclist struck the ground or road furniture, for example lampposts or railings. In some specific instances the secondary injury can be more injurious, but research performed in the APROSYS project has shown that not to be the case in the majority of accidents, (Grünert, 2009). The throw distance calculation method used by Otte and Mukherjee is more useful when reconstructing vehicle accidents for litigation purposes.

6.4 Use of ANOVA to Highlight Significant Trends Among Simulation Results

The ANOVA (analysis of variance) technique was used to highlight trends not shown by inspecting individual simulation results. The technique was described in Chapter 3.6.3. The technique is particularly suitable when bar charts are not sufficient to identify trends due to the quantity and scatter of data. The ANOVA technique was used for all the data values generated from the simulations Appendix I, but only those that showed significant differences for cyclists and pedestrians injuries are shown in this discussion.

For the graphs used in this discussion section, the head impact angle or relative velocity were known as independent variables and were positioned on the y-axis. The categorical variables, such as vehicle type and user, were positioned on the x-axis. The plots consisted of a solid bar highlighting the ANOVA value with a 95% confidence band associated with it. If two vertical confidence bands did not overlap, they were concluded to have a significant statistical difference. For example, in Figure 6-2, the head impact angles for the SUV with cyclist and pedestrian simulations, were significantly higher than the other vehicle types. It can be concluded that there was no significant difference between the other three vehicle types, as their confidence bars were very similarly aligned.

6.4.1 Head Impact Angle

The greater height of the cyclist's pelvis, compared to a pedestrian, had an important effect on the head impact position of the cyclist on the vehicle. When the cyclist's pelvis was higher than the bonnet edge the cyclist was more likely to wrap around the vehicle and then, in a secondary motion, slide up the bonnet. In the SUV case, the cyclist's pelvis was below the leading edge and subsequently the cyclist kinematics only showed the capability to rotate rather than slide.

Some of the angles were unable to be calculated from the results due to the head not striking the vehicle and subsequently the impact velocity was not calculated. The ANOVA method was performed as it was able to accommodate for these absent results in the data set. For the lower vehicle speed, there was not always enough momentum of the cyclist or pedestrian to rotate to the extent that the head wrapped around and struck the vehicle. The lower legs and torso engaged with the vehicle and then the velocity of both entities reached an equal value and then subsequently started to move together before head impact.

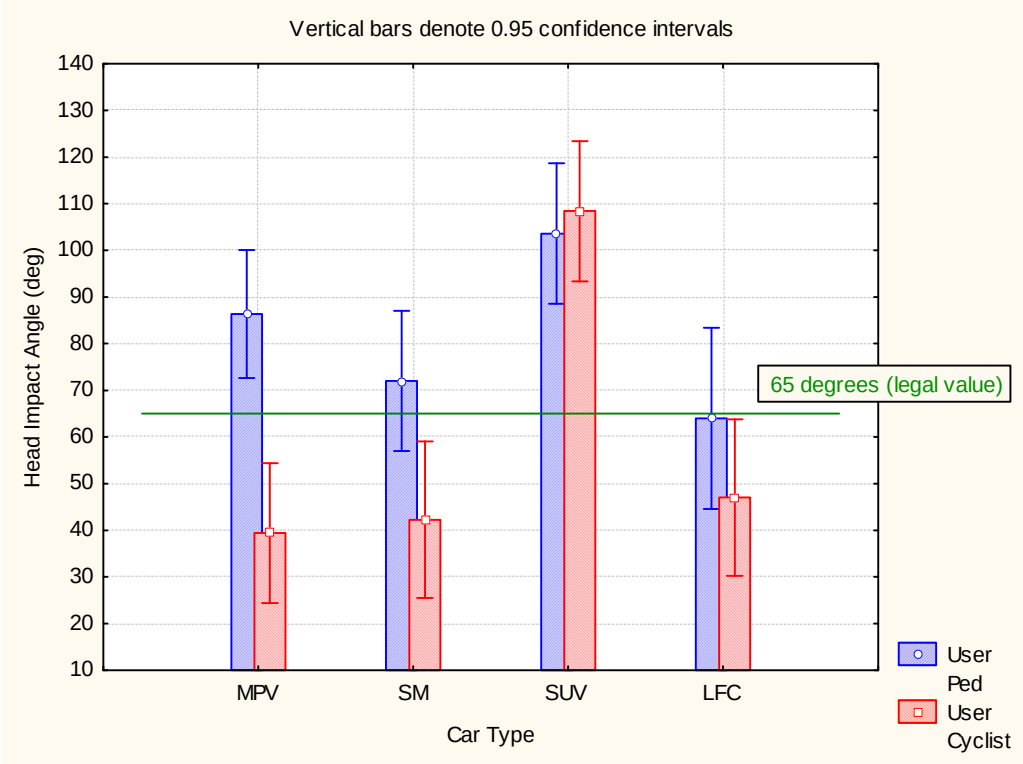

Figure 6-2: Comparison of Mean Head Impact Angles for Vehicle Types calculated by the ANOVA technique

The SUV produced the highest impact angles for the pedestrian and cyclist, but in particular the cyclist head impact angles were significantly less than the pedestrian angles for the SM, MPV and LFC vehicles. A summary of Figure 6-2 is shown in Figure 6-3, with only the User identified on the x-axis and the difference between the pedestrian and cyclist more clearly shown with all head impact angles analysed.

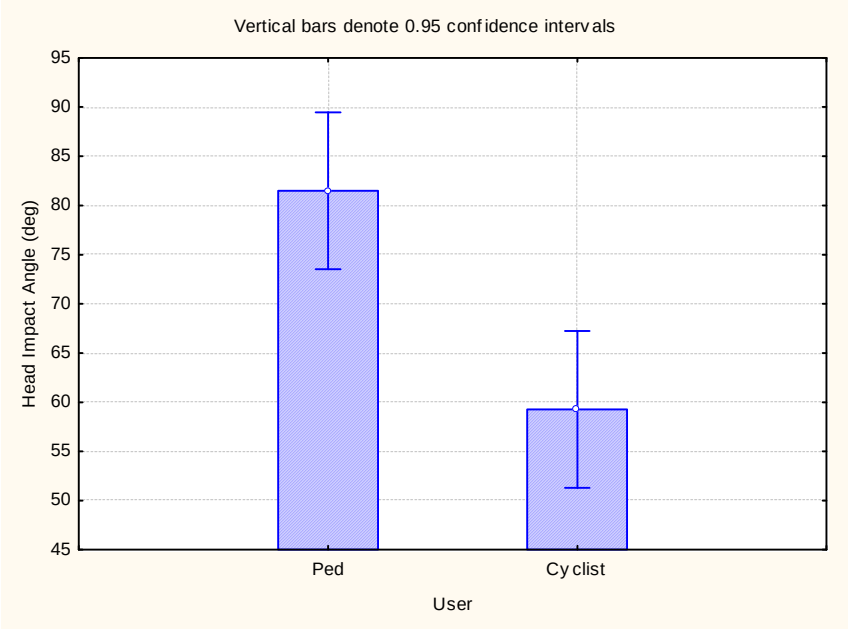

Figure 6-3: Comparison of Mean Head Impact Angles for Pedestrian and Cyclist calculated by the ANOVA technique – All Vehicles

In Figure 6-4 the SUV vehicle has been removed from the analysis and the difference between the two user groups was more pronounced. The values obtained from this ANOVA analysis were used to generate the proposed new cyclist impactor regulations detailed in Chapter 7.

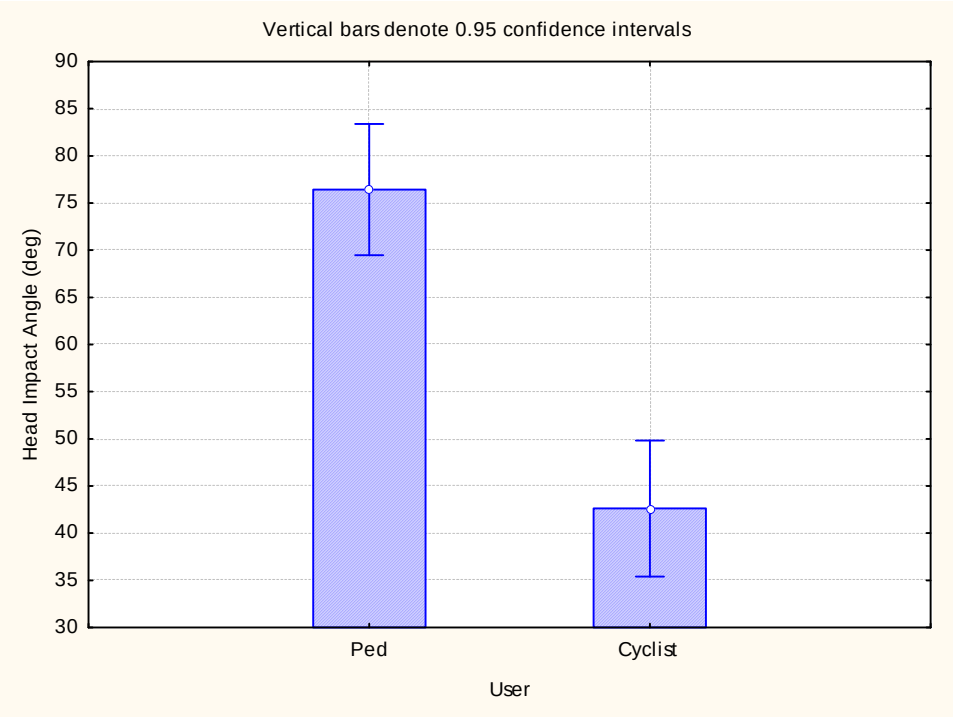

Figure 6-4: Comparison of Mean Head Impact Angles for Pedestrian and Cyclist calculated by the ANOVA technique – LFC, SM, MPV only

6.4.2 Head Relative Velocity Results

The head velocities did not show any significant differences between the pedestrian and cyclist simulations for three of the vehicle types (SM, MPV and SUV), whereas the LFC showed an increase, as shown in Figure 6-5. This was due to the lack of simulations performed at 5 m/s vehicle velocity. The ANOVA value of the LFC consisted of simulation data from 10 and 15 m/s only which skewed the data towards a higher value. For the other vehicles the ANOVA value was calculated from the complete range of 5 m/s up-to 15 m/s vehicle velocities.

Huijbers and Janssen (1988) predicted that there was a 'great variety' between vehicle head impact velocity for different vehicle types, but only an Opel Kadett vehicle showed impact velocities below the vehicle speed. An impact of 40 km/hr (or 8 m/s) between an Opel Kadett and a cyclist produced a head velocity of 7 m/s, the other four vehicles produced head velocities higher than vehicle speed. The Opel was a large fronted vehicle but not as high as the SUV vehicle used in this research.

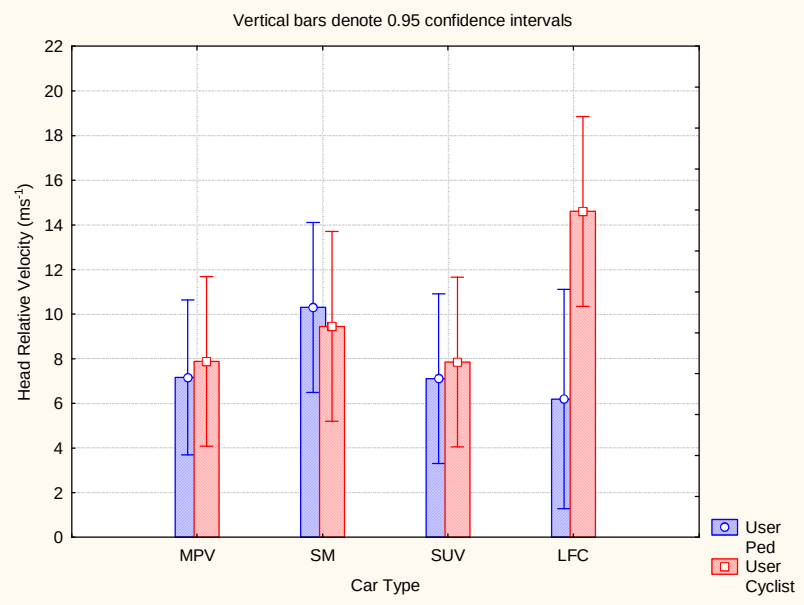

Figure 6-5: Comparison of Mean Head Relative Velocities for Vehicle Types calculated by the ANOVA technique

In general, all the head relative velocities were below the impact speed of the vehicle with some exceptions. This contradicts with Huijbers (1988) simulation model results for the vehicles that he used, but direct comparisons are difficult as the vehicle shapes are not identical and in Huijbers models the number of cases was limited. Between both approaches it can be determined that there is a range of relative head impact velocities and a definitive value is not easily obtainable. However, from the simulation models performed in this research the impact velocity was considerably more likely to be below vehicle impact speed.

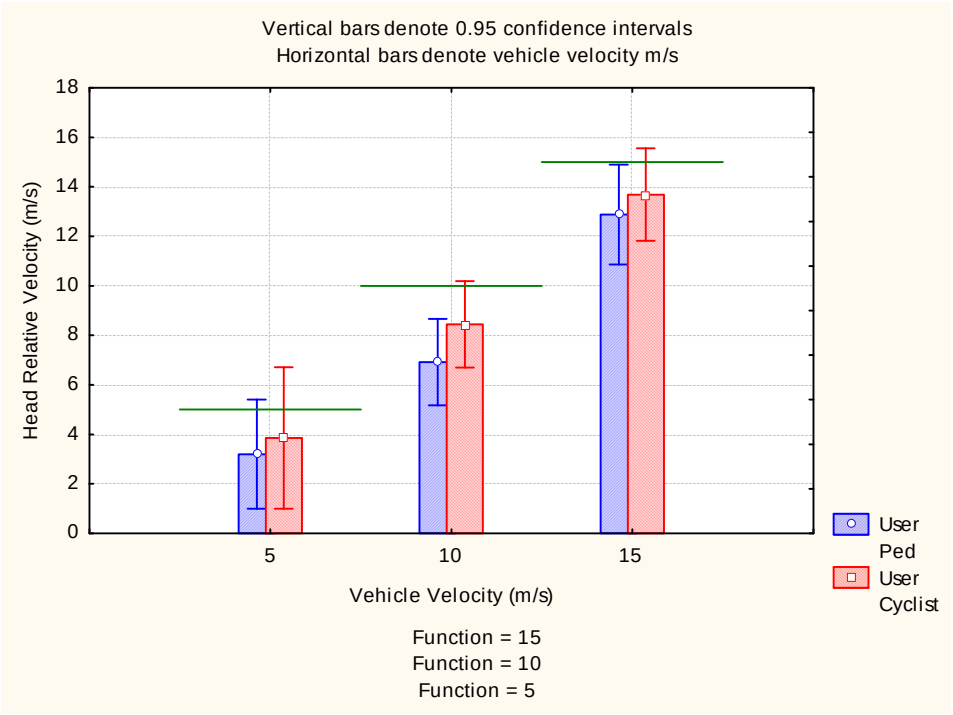

Figure 6-6: Comparison of Mean Head Relative Velocities for different Vehicle Velocities calculated by the ANOVA technique

The solid lines in Figure 6-6 at 5, 10 and 15 m/s represent the vehicle speeds used in the simulations.

The pedestrian head results (velocities and impact angles) were generally grouped together whereas the cyclists' results showed more scatter and variability. An increase in vehicle speed was associated with a cyclist head impact location towards the windscreen or roof region. With the pedestrian head impact locations being grouped together, this suggested that the current legislative test may be protecting pedestrians over a wider range of impact conditions than just those specified in the legislation. A proposal to adapt the current legislation to include cyclist, as well as pedestrian head impacts, may well need to cover a considerably greater area of the vehicle front.

The significant difference in maximum bending moment between the cyclists and pedestrians, for the SUV vehicle type are shown in Figure 6-7. For the other vehicle types there are differences in values between pedestrians and cyclists, but they are not significant as the 95% confidence bars overlap.

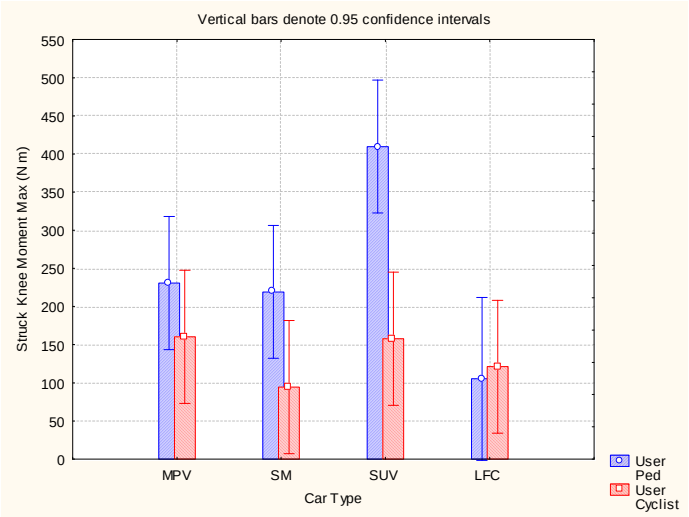

Figure 6-7: Comparison of Mean Struck Knee Bending Moments for different Vehicle Types Calculated by the ANOVA Technique

As was mentioned the bar charts of the results chapters showed the potential different knee injury mechanism for cyclists when the minimum bending moment is greater in magnitude than the maximum direction. However, the ANOVA technique for both struck and non-struck cyclist knees does not highlight any difference, Figure 6-8. The pedestrian results are higher in the positive direction in the left-hand graph, but for the cyclists on the right they are similar for positive and negative magnitude. Therefore, when using bar charts to analyse data, (as was performed in the results section) there was a perceived difference, but when using ANOVA the difference was not observed. The ANOVA technique analysed the results taking into account the variance of all the vehicle results and perhaps the SUV and LFC results diminished the effect. Therefore, a second ANOVA was performed solely on the MPV and SM knee bending moments, but the results were still inconclusive, with no significant difference being observed between maximum and minimum bending moments.

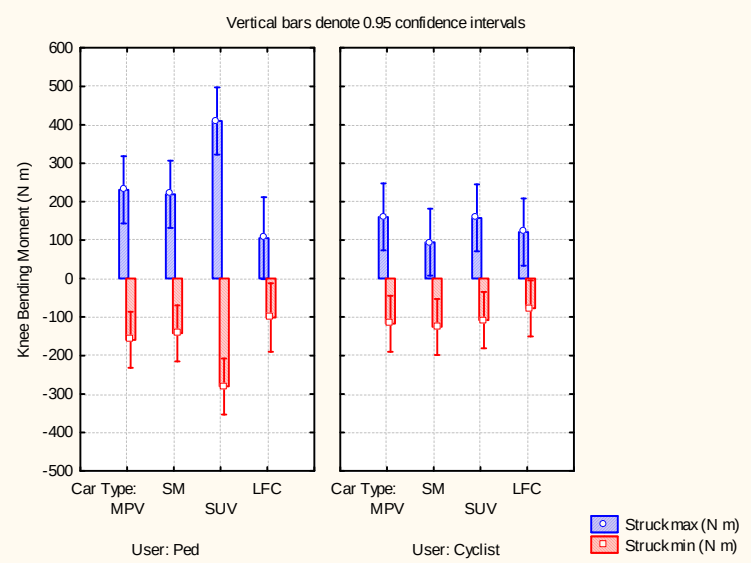

Figure 6-8: Comparison of Mean Knee Bending Moments for Pedestrian and Cyclists and for different Vehicle Types and Calculated by the ANOVA Technique

Plotting the same data with the vehicle velocity on the x-axis, Figure 6-9, the pedestrian knee bending moments are only significantly worse above 15 m/s. For the slower velocities at 5 and 10 m/s there was no major significant difference between the pedestrian and cyclist simulation results. At the higher vehicle velocity of 15 m/s, the kinematics differ markedly between the pedestrians and cyclists. Perhaps at the higher vehicle speed more scatter is introduced into the results and the pedestrian is more exposed to the impact of the vehicle and the cyclist is protected by the bicycle.

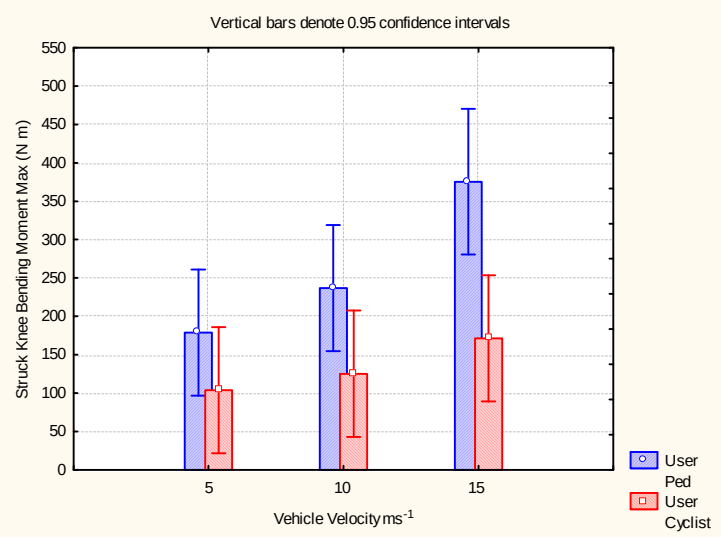

Figure 6-9: Comparison of Mean Struck Knee Bending Moments for different Vehicle Velocities Calculated by the ANOVA Technique

6.4.3 Struck Leg Knee Shear Values

An ANOVA analysis of the knee shear forces for the pedestrian and cyclists did not reveal any major significant differences between the two user groups, but when the data were included from the minimum (or negative) shear force values a different view emerges, Figure 6-10.

The struck and non-struck knee shear forces show a significant difference between pedestrians and cyclists. The pedestrian maximum knee shear force, as shown in the left hand graph of Figure 6-10, has a higher range of force levels compared to the minimum values. However for the cyclist the minimum values are all of a higher magnitude than the maximum values. Therefore, the new injury mechanism which was previously observed in the bending moment bar chart results, but not seen in the ANOVA, has now been identified in both the bar charts and the ANOVA for the shear forces. Although a difference has been observed in the peaks for the shear forces, a limitation of the model is that the same characteristics have been used for the medial, lateral and cruciate ligaments of the knee. To fully utilise the model it would be advantageous to obtain material data for both sets of loading paths and to repeat

the simulations with the more representative properties inserted. It could then be established if the opposite shear direction was significant for knee injuries.

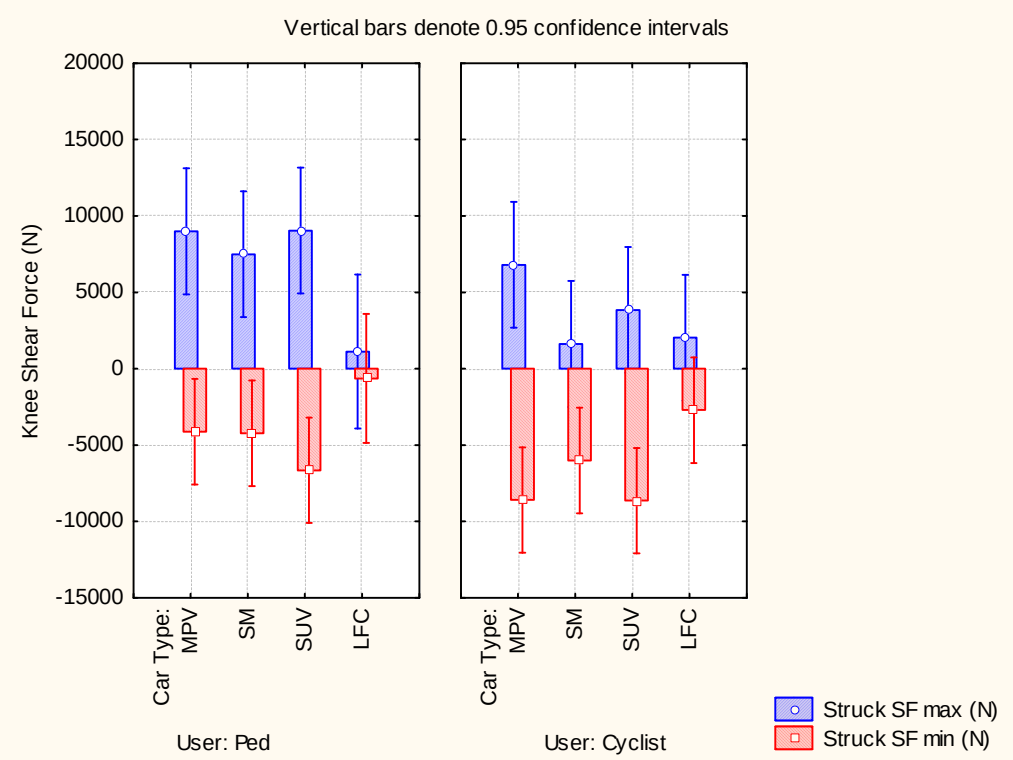

Figure 6-10: Comparison of Mean Knee Shear Forces for Pedestrian and Cyclists and different Vehicle Types Calculated by the ANOVA Technique

As was observed for the knee bending moment the pedestrian knee shear increased considerably at 15 m/s vehicle impacts, Figure 6-11. Again this could be due to the increase in scatter of results at the higher speeds, but the pedestrian may be also being further exposed to direct contact with the vehicle. As the cyclist is struck its torso begins to wrap around the vehicle quicker than the pedestrian and climb the bonnet and windscreen. Therefore, the cyclists' legs were removed from the direct impacts from the vehicle front end and instead experienced glancing impacts from the bonnet and windscreen.

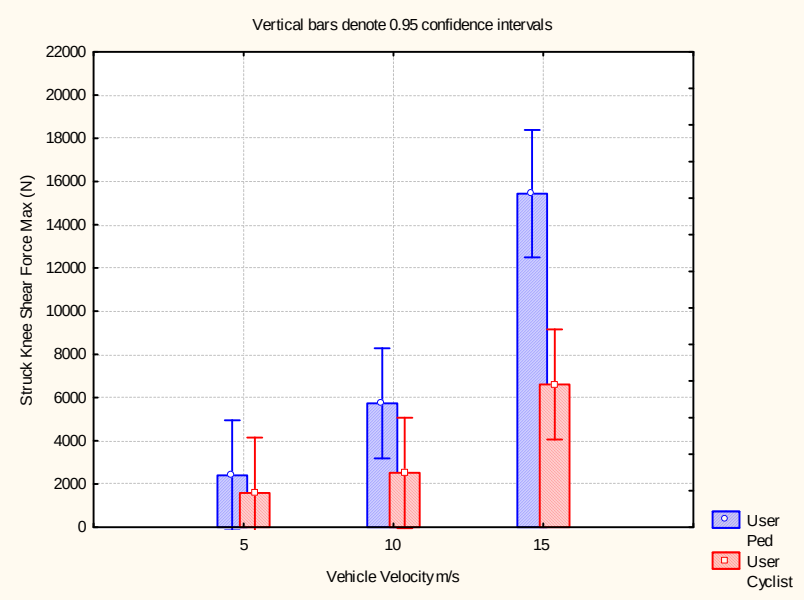

Figure 6-11: Comparison of Mean Struck Knee Shear Forces for different Vehicle Velocities Calculated by the ANOVA Technique

An observation of (Otte, 1989) was that no serious cyclist injuries occur 'below a speed of 30 km/hr'. This speed equates to 8.3 m/s, which was in between the 5 and 10 m/s, but interpolating the ANOVA prediction gives a knee shear value of 2kN for cyclists. A value of 2kN is below the critical value of 2.6kN specified by Kajzer (1997) and was not of a significant value to cause serious ligament injury. Therefore, the model was predicting similar levels of injury from previous published data.

6.5 Consequences for Cyclist Accidents with Vehicles

6.5.1 Influence of Different Vehicle Size and Shape

The result chapters were extensively focused on the head impact location and its conditions on impact with the bonnet. Four vehicles were used to represent a wide range of current vehicles used on the road and they had a range of bonnet lengths and windscreen angles. A feature of them which had a significant influence on the cyclist and pedestrian injuries was the bonnet leading edge. This is sometimes referred to as the top height of the grill, and is the transition point between the bumper/grill area and the bonnet. In some cases the transition point is defined by a clearly defined angle

(as in the SUV case) but in others the two areas merge without a significant change in profile (MPV).

Whatever the bonnet leading edge height was, the pedestrian and cyclist were clearly affected in the majority of simulations by the relative position. The wrap around kinematics observed in both types of vulnerable road user, when the human body pivots about the torso or pelvis also affected the eventual head impact location.

The pelvis acceleration was plotted against the bonnet leading edge, Figure 6-12. The x axis of Figure 6-12 shows the variation in height for the SUV (1056mm) vehicle which was significantly higher than the other vehicles. Any regression analysis of all three vehicles would be significantly influenced by the SUV results; therefore instead the scatterplot was chosen to show that there was no effect identified with the leading edge height and pelvis accelerations, or any other Humanoid injuries, for the four vehicle types.

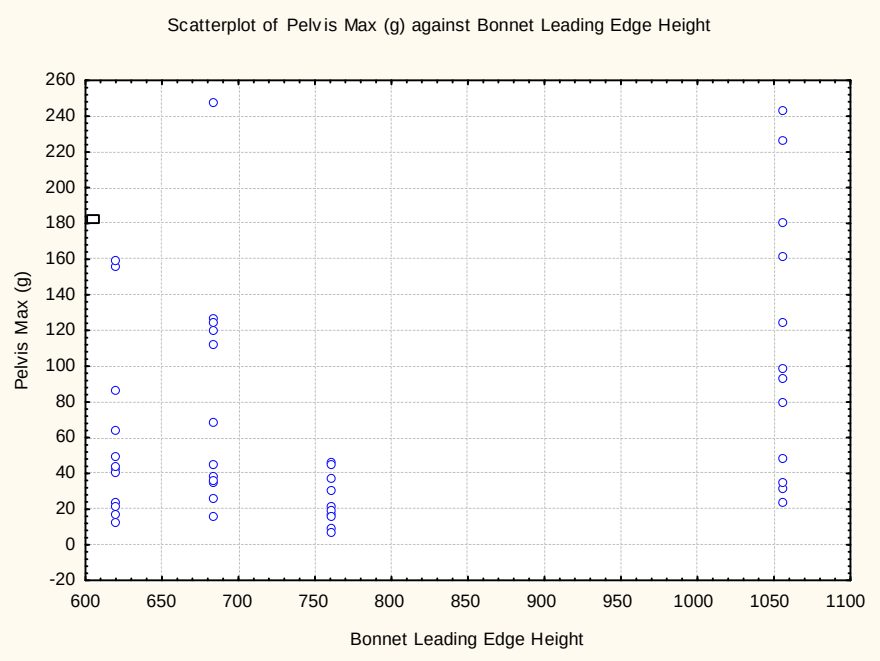

Figure 6-12: Regression Analysis of Pelvis g and Bonnet Leading Edge Height

In contrast the difference in kinematics was influenced by the height of the vehicle front end and the initial height of the user relative to the vehicle. This phenomenon

has also previously been noted by Janssen (1985) and Ishikawa (1994). In the Janssen paper the approach used vehicles which were over 25 years old which do not reflect the current vehicle fleet. Vehicle shapes and stiffness have changed and therefore this current research is more relevant with the increased use of SUV and MPV's.

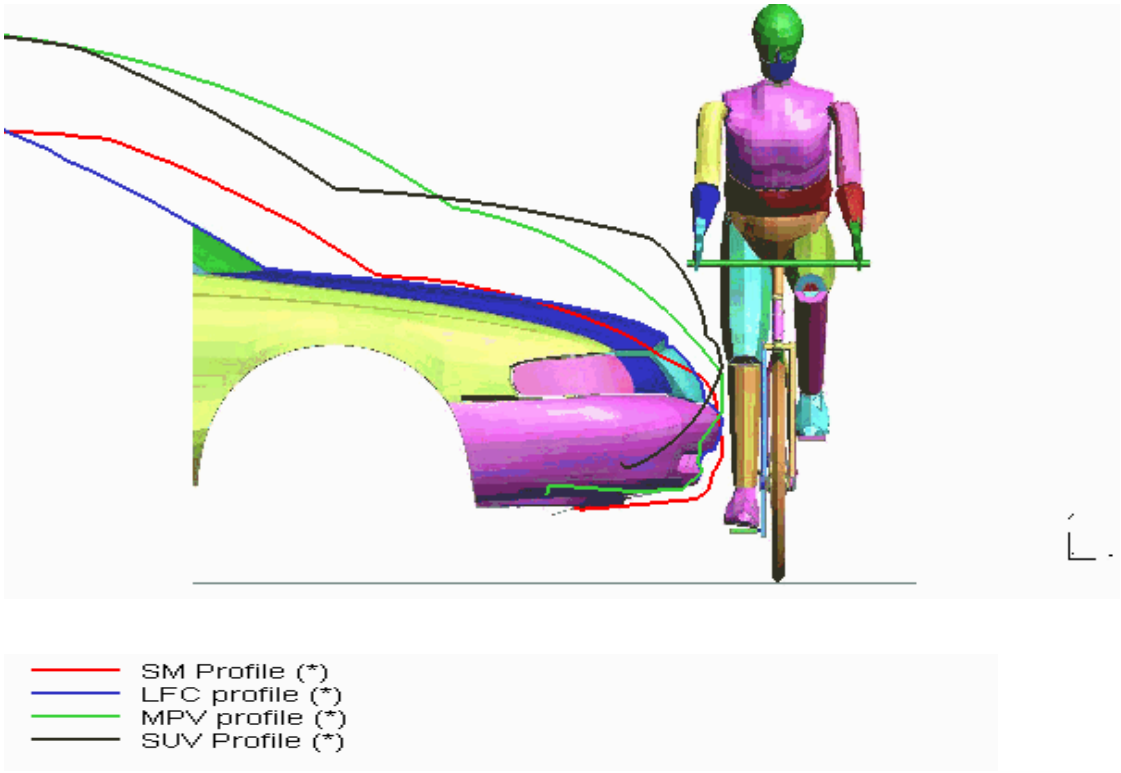

Figure 6-13: Different Vehicle Sizes Compared with a Cyclist

In order to highlight the effect of different vehicle shapes, Figure 6-13, the 10 m/s simulations have been compared as they produced three contrasting head impact locations. In Figure 6-14, the simulations have been frozen at the time of head impact as the head struck the SUV vehicle, followed by the MPV and SM. The time needed for the head to impact the vehicle varied and was a consequence of the shape of the vehicle front and this inducing a partially rotational and sliding motion in the cyclist torso. In the SUV simulation, the torso rotated with the head striking the bonnet half way up, but with very little sliding. The MPV simulation showed the cyclist sliding up the bonnet but due to the shape of the angled windscreen the head and neck did not

rotate as was observed for the SUV. Head impact location does not fully characterise the influence of different vehicle shapes on head injury, as shown here by the SUV and MPV, but other aspects should also be considered such as, the stiffness of the vehicle and the velocity of impact. As the vehicle geometry and stiffness properties have not been defined for every region of the windscreen and bonnet, the full extent of head injuries was not able to be obtained from the simulations. For example, no HIC's or linear head accelerations were calculated.

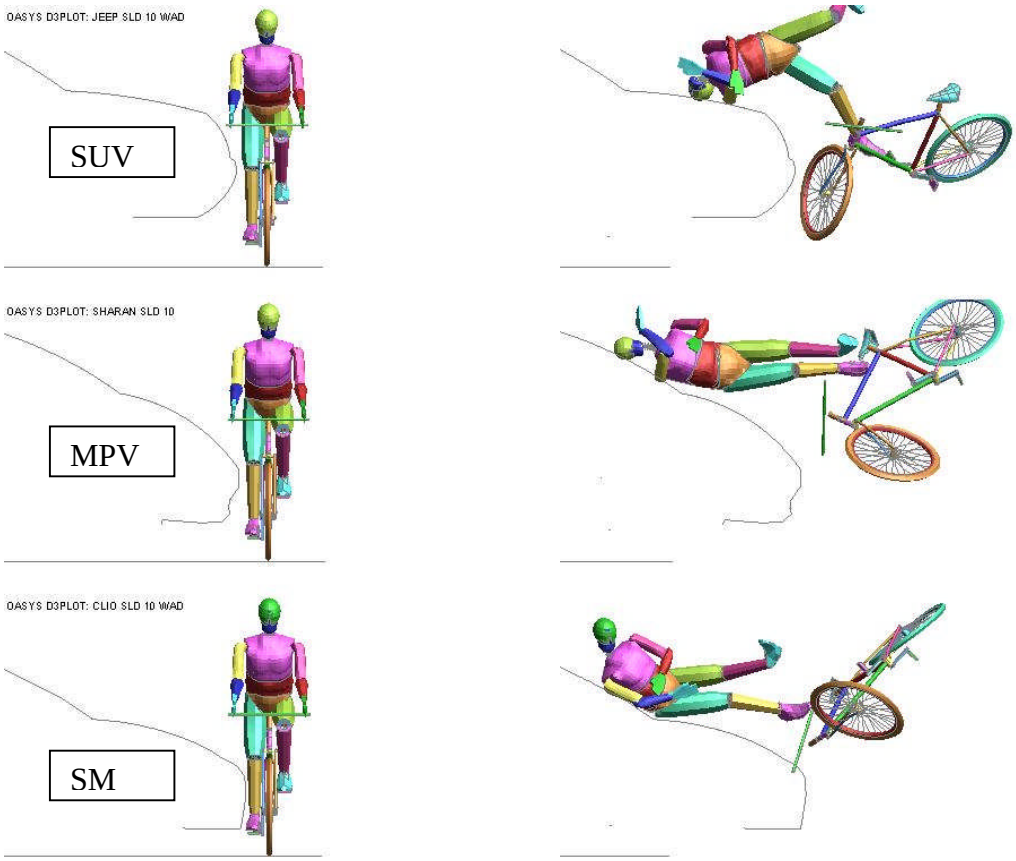

Figure 6-14: Variance of Head Impact Locations with Different Vehicle Shapes

The simulation results confirm that the initial stance and gait differences in cyclist and pedestrians have effects on injury risks. The cyclist head starts in a higher position, (103mm higher) and can vary due to riding position and bicycle. The research has not addressed child cyclists and their differences with their pedestrian counterparts, but this needs to be investigated to fully understand all of the cyclist

injuries. In particular, the 12-16 age range may be more pertinent for cyclists whereas for pedestrians the child range most at risk is younger, (Carter, 2005).

Maki et al. (2003) also showed that SUV vehicles produced head impacts that landed on the bonnet of the vehicle. In addition, Maki also showed that the head impacts were in very similar positions for cyclists and pedestrians, Figure 6-15, a similar result was observed in the simulations. For the sedan car the cyclist had a head location further up the bonnet than the pedestrian, a result which was also very similar to the results produced in the simulations for the SM and LFC. As the vehicle shapes were different a direct comparison was not possible. Although the physical sled tests also agreed with this grouping of trajectories for the SUV and further longitudinal trajectory of the cyclist for the LFC.

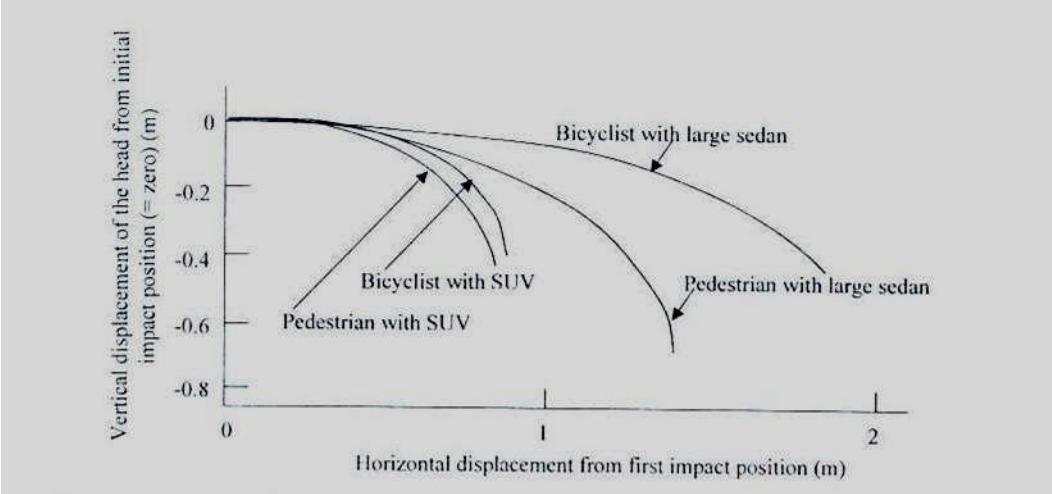

Figure 6-15: Pedestrian and Bicycle Head Trajectories, (Maki et al., 2003)

6.5.2 Influence of Cyclist and Pedestrian Stances

In the pedestrian simulations the struck knee bending moment results provided an indication of the likelihood of knee injury for the different cyclist and pedestrian stances. The SLF stances showed the greatest level of knee bending moment when compared with the other stances, Figure: 6-16. The SLF stance was when the struck leg was supporting the entire body mass just prior to vehicle impact and therefore a contact force was generated between the foot and ground. This contact force reduced

the ability of the knee to be pushed away by the vehicle impact and induced higher loads into the knee joint. In the SLB stance, the foot was off the ground and therefore there was less resistance from the struck leg.

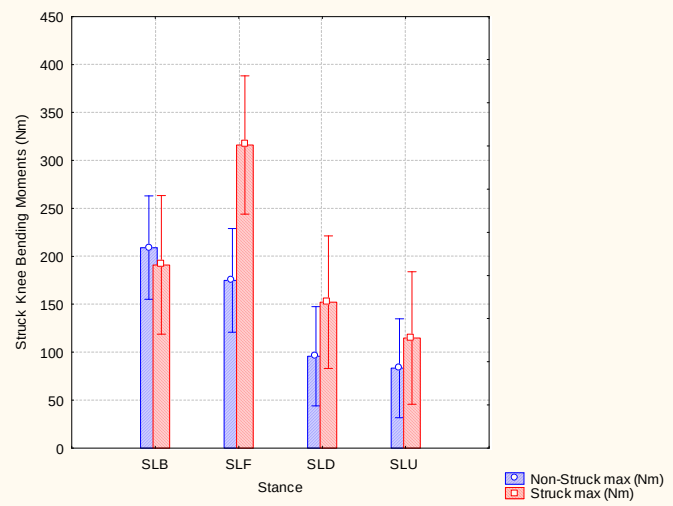

Figure: 6-16: Struck Leg Max and Min Bending Moments – Different Pedestrian and Cyclist Stances

The four different stances used for pedestrian and cyclist simulations showed that the two pedestrian stances produced higher bending moments. The difference can be accounted for by observing the interaction between the legs, bicycle and vehicle. As the cyclist SLU simulation had an elevated struck leg its motion onto the bonnet occurred earlier and allowed the cyclist to slide along the bonnet towards the windscreen. However, in the early stages of impact for the SLD case, the struck leg is trapped by the vehicle and bicycle and has the effect of holding the cyclist against the vehicle for 10-20 ms. It is only after this period that the cyclist wraps around the vehicle, but the maximum bending moment has already occurred. The struck knee results showed a greater bending moment of 144 N m in the SLD simulation, compared to 85 N m for the SLU. The difference between SLU and SLD simulations was also observed in the tibia accelerometer results.

6.5.3 The Influence of Bicycle Mass

To determine the influence of the bicycle in the cyclists' kinematics, simulations were conducted without the bicycle, but with the cyclist remaining in its initial stance, Figure 6-17, shows the set up used of the SM and LFC vehicles and the results from these simulations were compared to those from the equivalent simulations but with the bicycle. Although these simulations are fictitious, they did identify the effect of the bicycle.

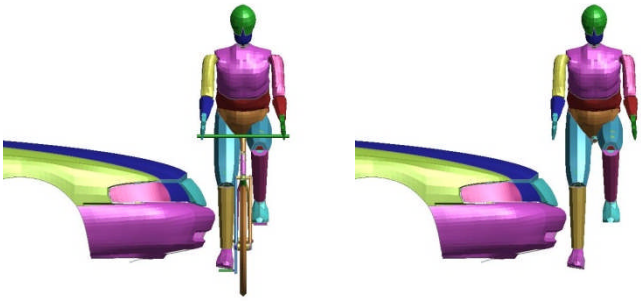

Figure 6-17: LFC Set-Up With and Without Bicycle

A number of the knee injury levels were of a lower magnitude for the non-struck leg than those for the struck leg, which was similar to the scenarios with the bicycle. Although for the SUV and SM the knee bending moments were higher without the bike and the shear forces were also higher without the bicycle for the SUV, SM and MPV. As the bicycle was missing the model more resembled a pedestrian in nature, but not in stance.

As was previously shown in Figure 4-13, the lack of bicycle interaction had the effect of increasing the longitudinal trajectory of the head and in general, the simulation results were either of a similar or a higher magnitude without the bicycle.

6.5.4 The Influence of Vehicle Stiffness

The stiffness of the vehicle varied for the three vehicle types used in Phase 2, but the effect of changing the vehicle stiffness had a negligible effect on cyclist's kinematics. A number of additional simulations were performed where the stiffness of the vehicle

bumper and bonnet was doubled, by allowing the same amount of deflection, but doubling the load. Two vehicle shapes were used, the SM and the SUV, as they represented two contrasting vehicle shapes. The 10 m/s vehicle speed was chosen as a mid range speed and only cyclist impacts were considered. The results for the knee and head impact locations did not change significantly which is a conclusion that concurs with Janssen (1985).

6.6 Legislative Leg Impact Test Parameters

6.6.1 Introduction

The link between the original cadaver tests and the legislative impactors is not always transparent as various researchers have addressed the topic and interpreted test data using different analysis techniques. As a result there needs to be a link, or transfer function, between any test criteria derived from cadaver or accident reconstruction and the implementation of a legislative impactor. In most cases a risk function is derived from the data, but the basis of creating the function can be subjective. An injury risk curve of 20-50% is sometimes chosen, (20% in the case of WG 17) but it is also worth considering that a vehicle manufacturer would design below the legislation to ensure compliance and therefore vehicles may well have lower injury risks associated with them.

6.6.2 Leg Impactor Orientation

The magnitude of most knee parameters in the cyclist simulation results were higher in the cases where the struck leg or non-struck leg were down and therefore close to being straight with marginal flexion of the knee. As the knee bends the lateral and medial ligaments are not held in tension prior to impact and therefore their effect on the knee joint in a lateral impact are limited. Instead, the cruciate knee ligaments (anterior and posterior) are more active in absorbing loads from the vehicle or bicycle. In the modelling simulations, this drop in lateral and medial ligament representation was not introduced and therefore the cyclist knee joint was effectively stiffened when held in the SLU stance. In the pedestrian stances the struck knee was

only flexed by 20 degrees in the SLF and the SLB stances and therefore these were considered to be in a nominally straightened stance.

The pedestrian simulations indicated that the current lower leg impactor with its straight orientation should remain unchanged as the straightened leg produced the highest levels of injury. Properties of a bent knee have been identified by Viano (2004) and Banglmaier (2003), but not in a lateral impact orientation. However, as the properties of a bent knee have not been fully identified, it would be beneficial to investigate the knee properties at various stages of the cyclist leg orientations. To look at straight and flexed (90 degrees) only captures a percentage of possible leg impact orientations prior to impact.

It was mainly in the scenarios with the struck leg up (when the knee was bent to a maximum angle of over 90 degrees) that the lateral ligament was identified as being the most damaged. Consideration should therefore be given to the development of a lower leg impactor specifically for cyclists with a flexed rather than straight knee joint. The identification of the appropriate injury criteria for knee bending and knee shear should be based on results from future human tissue testing.

6.6.3 Leg Impact Height

Due to its position on the bicycle the cyclist's limbs are higher from the ground than the equivalent pedestrian. In the SLD scenario the knee joint of a cyclist is further from the ground by on average of 100 mm to 150 mm compared to a pedestrian. In the struck leg-up scenario the knee is still higher by between 300 mm and 340 mm.

Currently the straight leg impactor is positioned 25mm from the ground, but to represent a cyclist the impactor should be raised to 125mm from the ground. This increase in height would have an effect on the alignment of the impactor to the bumper of the vehicle and therefore affect which ligament experienced tension. For certain vehicles such as the SUV, the knee may then align directly or below the bumper where previously the impact was above the knee.

6.6.4 Leg Injury Criteria

In the parametric study the struck leg knee bending moments for the SM and MPV cyclist struck leg-up scenarios showed a different injury mechanism to all the pedestrian scenarios. Therefore, this may question the validity of the current knee bending criteria for cyclists in these scenarios. Although as identified in the simulations the numerical value of the knee bending moments in the cyclist impacts were generally lower than those for pedestrians, the current pedestrian test criteria are likely to be appropriate to provide adequate levels of safety for cyclists in these cases. The current pedestrian criteria could be viewed as a worst case cycling scenario, Table 7-1.

The different injury mechanism showed that the medial ligaments, along with other ligaments in a cyclist's knee may experience tensile forces which may cause ligament damage. There are also different interactions between the leg bones as they are aligned differently when in the flexed position. A number of researchers including, (Levine, 1986), (Kajzer et al., 1993) and (Arnoux et al., 2002b) have investigated the knee collapse under cycling and pedestrian stances. Although the number of physical tests has been limited, only Cardot (2006) has showed data from a flexed cadaver knee test. The injury criterion used for knee bending in the current sub-system impactor leg does not represent the capabilities of the knee in this opposite model of bending and shear.

To address the safety requirements of cyclists where this reverse mode of bending occurs, research to identify the capabilities of the lateral collateral ligaments (or others) of the knee will be needed. There is no particular evidence to suggest that a cyclist's knee is different, in terms of stiffness, from a pedestrian's knee, but the failure mechanism may be different depending on the orientation. In addition, the procedure of introducing a physical impactor device for the other knee ligaments will need to be considered.

The level of bending moment failure in the Humanoid Model was set at 110 N m which was derived from Kajzer's tests in 1993 and 1997. The 110 N m corresponded

to 11.4 degrees of knee rotation. Ramet et al. (1995) reported from tests that a 20% risk of ligament damage was obtained at 16 degrees and Matsui (2003) gave the 20% injury risk at 19.2 degrees. Therefore, the value used in the model may be viewed as being conservative, but even at the lower levels of rotation the ligaments would be strained and injured. There is also variability in human ligament strengths which is not always accounted for in the data. Further work is needed to perhaps to define a range of failure angles for the four knee ligaments or to model the ligaments as separate entities and obtain more accurate data relating to them.

The capability of the bones to fracture is also significant in determining ligament injury, a capability that the current TRL legform does not possess. The Flex Pedestrian Legform Impactor or Flex-PLI has been developed by the Japan Automobile Research Institute (JARI) to create a more bio-fidelic impactor. It has the four main ligaments represented and the ability to show bone fracture at several positions. It has not been implemented into any legislation yet as the design is still to be finalised, but it is likely to be used by the future GTR legislation. The Flex-PLI may also be used to replicate cyclist impacts if it can be flexed enough from its initial straight orientation prior to impact. A different set of risk curves are needed for the Flex-PLI as it is more bio-fidelic than the TRL legform.

6.6.5 Tibia Acceleration

On average the tibia accelerations from pedestrian impacts were slightly higher than those for cyclists and therefore the current pedestrian criteria are likely to be appropriate to provide adequate levels of safety for cyclists. The EEVC WG17 value of 150 g was reached by the majority of 10 and 15 m/s simulations but this level has been determined as a level ‘that limits the contact force to control tibia injuries’ (European Parliament and Council, 2003). This statement is not very conclusive and that is because the 150 g level has not been determined by any definitive study. One of the studies used to obtain the original EEVC WG10 values were cadaver tests performed by (Cesari et al., 1991). The EEVC WG 17 stated that a 50% risk of tibia fracture related to 200-220 g level. Therefore, at the lower level of 150 g level the risk

of fracture is 20%. It was the aim of EEVC WG17 to obtain 20% injury risk criteria for the pedestrian legform.

6.6.6 Pelvis

At vehicle impact speeds up to 10 m/s most of the cyclist and pedestrian pelvis acceleration results from the parametric study were less than 80 g. At a vehicle impact speed of 15 m/s some on the pelvis accelerations reached as high as 250g (MPV and SUV cyclist impact cases) but on average the level was near 130g. Most of the levels were therefore at or below 130g, which is a criteria used in side impact facing automotive dummies. The 130g level represents a 50% chance of pelvis fracture when registered with a WorldSID dummy, (Edwards, 2007).

There are no consumer or legislative test procedures for pedestrian pelvis impacts, although some pelvis injuries are recorded in accident data. The results for cyclists are no more detrimental than for pedestrians and therefore no definitive recommendation for a cyclist pelvis impact test was made.

6.6.7 Chest

Even at a vehicle impact speed of 15 m/s, the chest accelerations from all but one of the cyclist impact scenarios were below 55 g, while two-thirds of the chest accelerations from the pedestrian scenarios were significantly above this level. At vehicle impact speeds below 15 m/s all cyclists' and pedestrians' chest accelerations were lower than this value and all but two were below 36 g. The current American FMVSS 208 automotive criteria uses a chest acceleration value of 60 g, (Carhs Training, 2008) which is higher than all the levels recorded and therefore it was not deemed necessary to recommend any chest specific cyclist test.

6.6.8 Virtual Testing

To objectively assess the new regions of the vehicle defined in these proposed changes to adult head impact test locations, the chosen sites of the impacts need to be distributed over the full region of the vehicle. Virtual Testing (or mathematical

modelling) allows that, by its ability to test at an infinite number of places and to perform those tests in a cost effective time frame. For the current legislation, the bonnet region is divided into segments and tests are performed at locations which have been designated by the legislator or vehicle manufacturer. The grid formation avoids the need to negotiate the exact head impactor locations and delivers a significant increase in the number of test sites evaluated.

6.7 Achievement of Objectives

In order to judge the success of this work the objectives have been re-assessed for their level of completion.

6.7.1 Establish the significant differences in terms of input variables and outcomes between cyclist and pedestrian accidents involving vehicles.

The differences between cyclists and pedestrians have been established by analysing the specific input variables of typical vehicle to bicycle accidents. The modelling activity has allowed those variables to be controlled in order to identify which factors are of most importance. The outcomes of the models were also examined, in particular, the levels of human injury with a reference to their tolerance levels. Many different accident scenarios were considered to encompass real world accidents and add validity to the research. A back to back comparison between pedestrians and cyclists has also not been researched to such depths.

6.7.2 Use simulation models and physical testing to replicate real world cyclist accident scenarios.

The unique combination of using the reconstruction of bicycle accidents and the use of mathematical modelling enabled a number of significant conclusions to be drawn. The two methods have been used in numerous other research activities, but in tandem cyclist accidents have not been modelled previously using four different vehicle geometries.

6.7.3 To analyse the injury data from a human mathematical model of a cyclist.

The use of a human body model instead of using a dummy model enabled real cyclist injury mechanisms to be analysed, instead of dummy injury indices. Real cyclist injuries, such as knee ligament failures in shear and bending are beyond the capability of a normal crash test dummy due to their physical construction. That was a limitation of the physical testing as only dummies could be used which did not have the ability to measure real world knee injuries, but the modelling was able to identify these injuries.

6.7.4 Recommend future legislative testing techniques for cyclists, based on existing pedestrian legislation.

Future legislation pertaining to cyclists was recommended based on the modelling and physical tests results. These new test specifications were derived from the current pedestrian legislation, maintaining the use of body part impactors, but striking different parts of the vehicle.

Chapter 7 Proposal for New Cyclist Legislation

7.1 Background

The results obtained from the simulations have suggested that the current European Phase 1 pedestrian legislative test criteria are appropriate to provide adequate levels of safety for pedestrians. The head impact locations and the knee injuries sustained at 40 km/hr have shown to be similar. Nevertheless, there is an opportunity in the current testing procedures to enhance the levels of safety for cyclists by modifications to the pedestrian test criteria. The original WG 17 values were reduced in severity when introduced into the Phase 1 legislation and in Phase 2 (due to be introduced in 2010) the figures have also changed. The GTR proposal from Japan is identical in severity to the Phase 2 legislation but the use of the Flex-PLI leg is introduced.

The current EEVC WG17 test methodologies were used, Table 7-1, and then adapted to include the different requirements of cyclists. The emphasis was on formulating new cycling criteria, but in some instances recommendations have also been included for pedestrians where there were differences between the modelling results and the current legislation. Recommendations were not made to change the HIC value used for pedestrian head impacts as that was beyond the scope of this research. The Upper Leg impactor should also not be changed.

		EEVC WG17	European Directive Phase 1	GTR
Lower Legform Impactor	Velocity (km/hr)	40	40	40
	Acceleration (g)	150	200	170
	Bending (deg)	15	21	19
	Shearing (mm)	6	6	6
Adult Head impactor	Velocity (km/hr)	40	35	35
	Impact Angle (deg)	65	65	65
	WAD (mm)	1500-2100	1700-2100	1700-2100

Table 7-1: Summary of Current Pedestrian Legislation

7.2 Pedestrian Simulation Head Impact Location Results

All the pedestrian head trajectories showed that the head struck the bonnet within the 1000 mm to 2100 mm WAD markers. This underlined that the current legislation for pedestrian head impact testing was in the appropriate region for those vehicles. The increase in vehicle velocity from 5 to 15 m/s did not considerably change the impact position of the head, which indicates that the current legislative test is protecting pedestrians over a wide range of impact conditions.

7.3 Cyclist Simulation Head Impact Location Results

The cyclist to vehicle head impacts were further up the bonnet in comparison with the pedestrian for all vehicle types. The majority of the SM, MPV and LFC cyclist head strikes occurred on the windscreen apart from one SM simulation, struck leg down at 15 m/s, when the head struck the roof of the vehicle. This was the only simulation across all vehicle types when this occurred.

The EEVC WG17 test states that the adult head impactor should strike the vehicle between a wrap around distance of 1500 and the 2100 mm. In the cyclist scenarios with the SUV, all the head impact locations lay on the bonnet, at a similar WAD to the pedestrian locations and therefore in the case of the SUV it is proposed to keep the same region for cyclists as for pedestrians, 1500 mm to 2100 mm, Table 7-2. However, for the other cyclist cases there is a need to change the WAD contact regions to reflect the different kinematics of cyclists. With the MPV and LFC vehicles, the head impact locations were further towards the windscreen and beyond the 2100 mm WAD location. Therefore, for these vehicles, it is proposed to shift the region for adult head impactor testing from 1500 – 2100 mm to 1700 – 2300 mm. This shift of 200 mm is justified on the basis that the head impacts were consistently in this region for a wide range of cycling stances and vehicle impact velocities. It is interesting that the proposed European Directive Phase 2 have also proposed a WAD of 1700 – 2100 mm, eliminating the 1500 – 1700 mm band. Instead, a child head impactor has been proposed, but to reiterate this is intended for pedestrians only.

The SM category of vehicle produced head impact locations starting from the 1700 mm WAD location, the same as the MPV and LFC vehicles, but in some instances the head trajectory was predicted to be close to or above the top edge of the windscreen. Therefore, it is proposed to define a region from the 1700 mm WAD to the top of the windscreen for SM vehicles.

	Vehicle Type			
User	SM	LFC	MPV	SUV
Cyclist	1700-top of windscreen	1700-2300	1700-2300	1500-2100
Pedestrian	1500-2100	1500-2100	1500-2100	1500-2100

Table 7-2: Proposed WADs (mm) for adult head impact location regions

7.4 Head Impact Angle

The EEVC WG17 and European Directive Phase 1 and 2 test head impactor is set at 65 degrees, which is an angle that seems to be justified based on the values obtained from the pedestrian and cyclist simulations. According to the ANOVA analysis and reported in Section 6.4, the pedestrian and cyclist SUV angles were similar (100 degrees) but for the SM, LFC and MPV there were a range of angles with the pedestrian head impacts higher than 65 degrees and the cyclist head impact angles were lower. Therefore, a unique test should be used for cyclists and pedestrians by lowering the proposed 65 degrees to 40 degrees for cyclists and increasing the angle to 80 degrees for pedestrians, Table 7-3. As the angle of impact is designated by a horizontal datum line irrespective of vehicle geometry, an impact to the windscreen will have different consequences from an impact with the bonnet. This issue has not been fully addressed yet as the majority of physical tests are only performed on the nominally flat bonnet of the vehicle. Future windscreen tests will need to re-address this issue.

User	Vehicle Type			
	SM	LFC	MPV	SUV
EEVC WG17 Head Impact Angle	65	65	65	65
Proposed Cyclist	40	40	40	100
Proposed Pedestrian	80	80	80	100

Table 7-3: Proposed Head Impact Angles for Head Impactor

7.5 Head Impact Relative Velocity

It was not considered necessary to change the head impact velocity for cyclists. Currently the head and leg impactor velocities are the same, 40 km/hr. In the Phase 2 proposal the head impactor velocity is to be reduced by 87.5% to 35 km/hr, the leg impactor velocity remains at 40 km/hr. Analysing the head impact velocities from the simulation models identified that they also occurred below the vehicle impact velocity, but by a factor of 80% instead. Assuming the leg impactor velocity is the same as vehicle velocity and the same factor derived from the simulations (80%) is applied to the head impactor velocity, the corresponding vehicle velocity would be increased to 43.75 km/hr (or 12.15 m/s), Table 7-4.

The proposed new test method uses the 80% factor applied to the current WG17 test methodology. The head impactor velocity is reduced to 32 km/hr (8.8 m/s) and keeps the leg impactor velocity of 40 km/hr.

	Leg Impactor Velocity	Head Impactor Velocity	Calculated Equivalent Vehicle Velocity from Head velocity (80%)
EEVC WG17 Head Impact Velocity (km/hr)	40	40	-
Phase 2 Proposal (km/hr)	40	35	43.75
Proposed Test Method (km/hr)	40	32	40

Table 7-4: Proposed Head Impact Velocity for Head Impactor

7.6 Feasability of the New Proposed Cyclist Legislation

With these recommendations for changes to the current and proposed impactor test parameters, it is realised that an increase in physical testing scenarios will result in an increase in test costs. Therefore, mathematical modeling (virtual testing) may be more appropriate to capture the complete safety assessment of a vehicle. Or a combination of the two techniques could be realised ensuring that the VT has an element of validity about its process.

This research has highlighted a number of key issues to address when formalizing new cyclist criteria, but significantly the current pedestrian impactors do not fully represent cyclist impactors and the above recommendations address those shortcomings.

Chapter 8 Conclusions

- The hypothesis of this research that there are differences between cyclists and pedestrians have been proved by using the FE modelling and physical testing.
- The simulation models have predicted that when cyclists and pedestrians were struck by a motor vehicle there are differences between the two vulnerable user groups. Their whole body kinematics can be distinguished in two phases, initially a rotation followed by a sliding action. The SUV vehicle produced more of a rotation action, whereas the SM, LFC and MPV produced a combination of the two.
- In the modelling and physical tests the cyclists' heads struck further up the vehicle fronts when compared to pedestrians. For the SM vehicle, the cyclist's head struck the windscreen region and the pedestrian's head struck the bonnet region, regardless of what the impact speed of the vehicle. For other vehicle types such as the SUV the head only struck the bonnet and for the MPV the cyclist's head struck further up the vehicle front, but across both the windscreen and bonnet region.
- The FE modelling predicted that pedestrians had greater knee injuries in terms of shear forces, bending moments of the knee and tibia accelerations of the legs.
- For the higher vehicle impacts the knee injuries reached the defined levels set in the model for the shear forces and bending moments. At this level it was determined that the knees had reached a 20% risk of injury and any further rotation or displacement would have increased this risk.
- Both cyclist physical tests and simulation kinematics showed similarities. In particular the head impact locations were identified as being in similar vehicle locations. The scatter of physical test results was not observed in the simulations due to the explicit capability of the model to define one scenario.
- The ANOVA analysis of the simulation results have shown the head impact conditions to be similar, in terms of impact speed for pedestrians and cyclists, but the impact location and angles were different.

- As the vehicle speed increased from 10 m/s to 15 m/s the difference between cyclists and pedestrians knee injuries in particular the knee shear was more exaggerated. In comparison at the lower speeds of 5 m/s, the cyclists and pedestrians showed similar injury levels.
- The cyclist and pedestrian initially had different orientations prior to impact with the vehicle. The pelvis and feet were higher for the cyclist and the struck knee was more flexed in the SLU case. As a consequence of the positioning, the cyclist struck knee showed a tensioning of the lateral ligament, whereas the pedestrian showed a tensioning of the medial ligament.
- The vehicle stiffness had a negligible effect on cyclist injuries, but the vehicle geometry had a greater effect for the kinematics.
- The inclusion of the bicycle influenced the kinematics of the cyclist by preventing further motion up onto the windscreen and possibly over the roof.

New injury criteria and adjusted impact test procedures are needed to align the needs of cyclists along with pedestrians. These new criteria are summarised in the following conclusions;

- The current legislation does not cover all head impact locations for cyclists and therefore needs to extend the scope to the windscreen and A-Pillar of the vehicle. For certain vehicles such as the SUV, the current legislation is adequate in protecting cyclists and pedestrians and does not need to change.
- The current EEVC WG17 leg impactor is capable of representing cyclists as well as pedestrians in current legform tests, but is not capable of identifying all the injury mechanisms such as lateral ligament tensioning.
- The proposed head impactor angle for cyclists is 40 degrees which is lower than the current legislative value of 65 degrees and the proposed pedestrian head impact angle is higher at a value of 80 degrees for the MPV, SM and LFC. For the SUV the proposed impactor angle is 100 degrees for cyclists and pedestrians.
- The head impact velocity for cyclists and pedestrians was very similar and below the vehicle impact velocity by 80%. Therefore, it was proposed that the

head impactor velocity be set at 32 km/hr instead of the current value of 40 km/hr.

- The modelling results have shown that the location of the WAD for the head impactor should remain at 1500-2100 mm. For the cyclist case, different vehicles require their own regions. The SM should be from the 1700 mm to the top of the windscreen. The LFC and the MPV should be from the 1700 mm to the 2300 mm mark and the SUV should be the same as the pedestrian.
- As an alternative to using a WAD calculation the head impact location for the impactor may be determined by performing a series of physical dummy tests into vehicle fronts. By using a dummy the vehicle alignment, in particular the height of the leading bonnet edge would be considered for every vehicle type.

Chapter 9 Further Work

- More bio-mechanical tests are needed to determine the strength of knees when they are flexed, as during the cycling action. The strength and performance of the lateral ligament also needs to be addressed as they are more common in cyclists' impacts with vehicles.
- More detailed accident cases for cyclists need to be collected in order to better understand cyclist accidents and their consequences for injury causation. They can no longer be grouped with pedestrians as a vulnerable road user, but as a category on their own.
- Further investigations should focus on other cyclist accident scenarios which were beyond the scope of this study. These should be based on accident data which represents the most recent vehicle fleet and current cycling behaviour.
- Different vehicle types should be investigated to analyse the varied geometry and stiffness associated with the bonnet, bumper A-Pillar and windscreen components. This would enable an analysis of head injuries instead of only head impact conditions conducted in this research.
- Different bicycle types and orientations of cyclists should be analysed to understand the nature of racing and leisure cyclists. Child cyclists should also be analysed as they represent a significant majority of total fatalities and injuries.
- The FE stochastic modelling approach would provide a more comprehensive assessment of cyclist kinematics and identify the key parameters which affect pedestrian/cyclist injuries.
- A more detailed brain model could examine the injuries sustained by the head when impacting the windscreen and the surrounding structure of the vehicle. To ensure accurate head impact conditions the shoulder mechanism should be further developed to initiate a more improved bio-fidelic response from the Humanoid Model.

- Additional impact testing may be required to provide improved safety for cyclists by increasing the test locations or the number of tests performed with the current impactors. The use of Virtual Testing could be used to provide a more comprehensive assessment of a vehicle.

Appendix A <u>Adult Bike Dimensions</u>

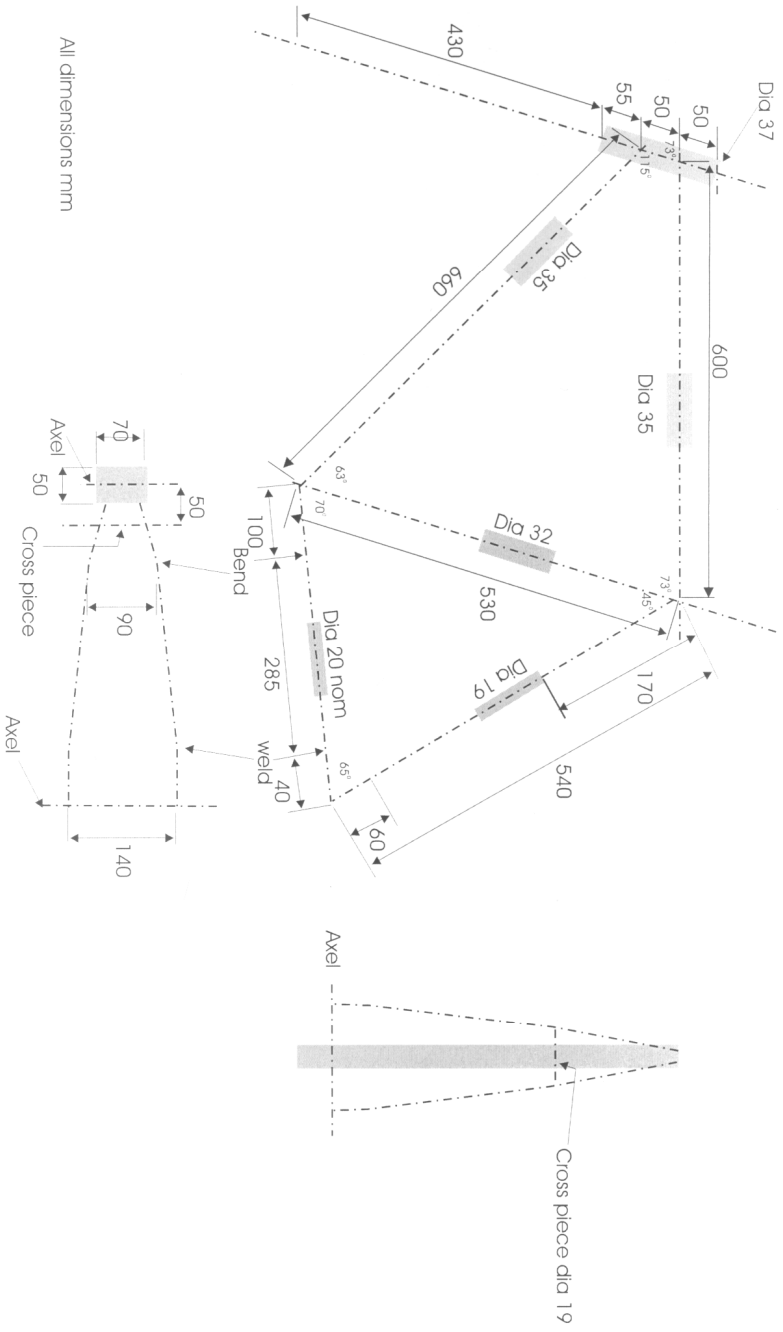

Appendix B Examples of Statistical Techniques

Least Squares Fit

The least squares fit methodology is demonstrated by the following example. Four points were obtained of the head impact velocity (y) against vehicle velocity (x).

(1,6) (2,5)(3,7) (4,10)

To provide a line that best fits these four points it is necessary to solve the equation;

$y = B_1x+B_2$

Four equations can be determined which have the two unknowns B_1 and B_2

$1B_1 + 1B_2 = 6$

$1B_1 + 2B_2 = 5$

$1B_1 + 3B_2 = 7$

$1B_1 + 4B_2 = 10$

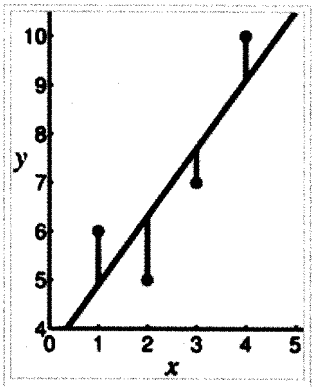

A plot of the data points (in red), the least squares line of best fit (in blue), and the residuals (in green).

Figure B-1: Linear Least Squares Fit Example (ref. Wikipedia)

The vertical lines in Figure B-1 refer to the residuals of the data set and it is these which the methodology is trying to minimise for all points. A partial derivative equation is

solved for B1 and B2 by squaring the four equations and values for B1 and B2 can be calculated to give the equation;

$y = 3.5 + 1.4x$

The residuals of the four points are 1.1, -1.3,-0.7 and 0.9

This straight line equation has two significant uses. It can be used to identify trends in data sets which would not necessarily be seen by plotting the data in a scatter plot. Furthermore the line can be used to predict the values of variables from scenarios which had not been performed or simulated.

To understand how good an approximation the line is to the data a measure of how the two variables co-relate. Or by increasing one of the variables how does the other variable relate to it. The correlation coefficient was calculated by using the mean and standard deviation of the variable.

If two sets of variables have a coefficient of close to 1 there is a near perfect positive correlation. That means that as one set of variable values increase, the other one increases as well. The coefficient can also be a negative number (-1), which shows that the values can also be correlated but one set of variable values increase whilst the second one decreases. Table B-2 shows the correlation coefficients for the struck knee for the first phase of simulation results.

This procedure was repeated for all the variables in the model to generate a correlation coefficients matrix. This table of coefficients showed the relationship between variables and identified what were the levels of correlation.

Variable	Correlations (041208) Marked correlations are significant at p < .05000 N=20 (Casewise deletion of missing data) Include cases: 51:70			
	Struck max (Nm)	Struck min (Nm)	Struck SF max (N)	Struck SF min (N)
Struck max (Nm)	1.00	-0.76	0.41	-0.32
Struck min (Nm)	-0.76	1.00	-0.16	0.46
Struck SF max (N)	0.41	-0.16	1.00	0.07
Struck SF min (N)	-0.32	0.46	0.07	1.00

Table B-1: Correlation Matrix for Right Knee - Phase 1 Simulations with case 63

The values highlighted in red are significant as they showed two sets of data that are above 0.4 in value and therefore tended towards correlation. The two variables considered were the maximum shear forces and bending moments for the struck knee. As these two indicators of loading to the knee were in close proximity, if the knee was struck severely from the vehicle, both injury variables tended to record high values. The cases for the first phase of simulations were numbers 51 to 70 and there were 20 in total.

One of the data points in Figure 3-13 appeared to be an outlier which affected the results as the bending moment value was significantly lower than other data points (23 N m). On closer inspection of the data point the value referred to a simulation where the cyclist was positioned offset from the centre line of the vehicle by 1m. As the vehicle struck, the cyclist's trajectory was towards the side of the vehicle and did not strike the bonnet or windscreen. Subsequently the knee injuries were of a lower magnitude to other simulations when the whole of the cyclist engaged with the vehicle front.

If this one result is excluded from the cases selected, the correlation coefficient factor increased from 0.41 to 0.57 (Table B-2 and Figure B-2). Therefore, the lower bending moment result had severely influenced the correlation coefficient and had led to a misleading initial conclusion.

	Correlations (041208) Marked correlations are significant at p < .05000 N=19 (Casewise deletion of missing data) Include cases: 51:70 Exclude cases: 63			
Variable	Struck max (Nm)	Struck min (Nm)	Struck SF max (N)	Struck SF min (N)
Struck max (Nm)	1.00	-0.24	0.57	-0.29
Struck min (Nm)	-0.24	1.00	-0.10	0.51
Struck SF max (N)	0.57	-0.10	1.00	0.10
Struck SF min (N)	-0.29	0.51	0.10	1.00

Table B-2: Correlation Matrix for Right Knee - Phase 1 Simulations without case 63

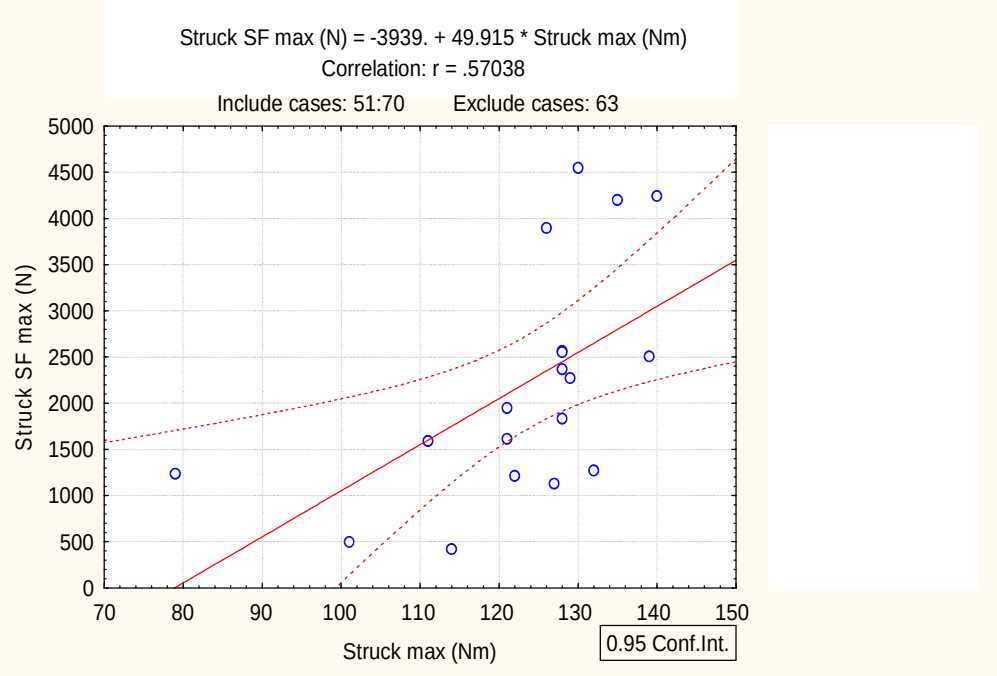

Figure B-2: Scatter Plot of Struck Knee Max Bending Moment Versus Struck Knee Max Shear Force – Phase 1 Simulations without Case 63

When using the correlation coefficient tables and graphs to highlight influences between injury values for the phase 1 and 2 simulations the outline results were checked to see if the cases were suitable to be included in the correlation table. The least squares method enabled a further check to be made of the data to identify if the residuals were not too far from the straight line.

ANOVA V Scatter Plot Example

Figure B-3 shows a scatter plot of the Head Impact Angle versus User group. The scatter of the data makes it difficult to identify a trend between the two user groups or to actually quantify a difference. It may be deduced that the pedestrian angles are generally higher but there are also some cyclist angles which are just as high as the pedestrians. Figure B-4 shows an ANOVA analysis with a clear distinction between the two user groups with a single value (with confidence bands) to define each user group.

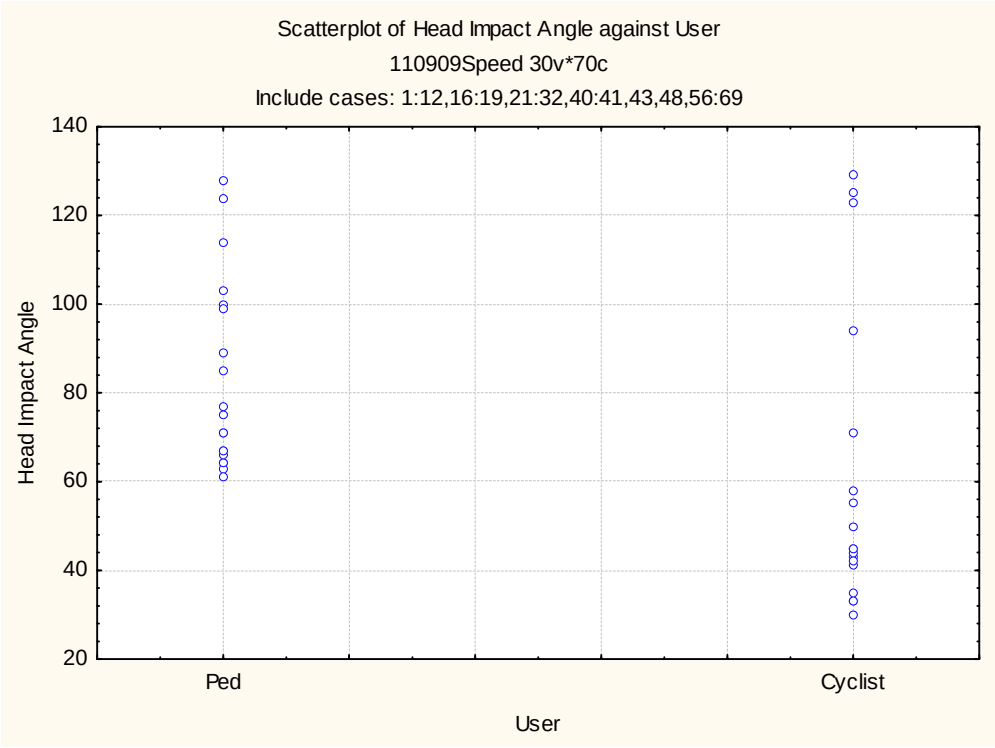

Figure B-3: Scatter Plot of Head Impact Angle versus User

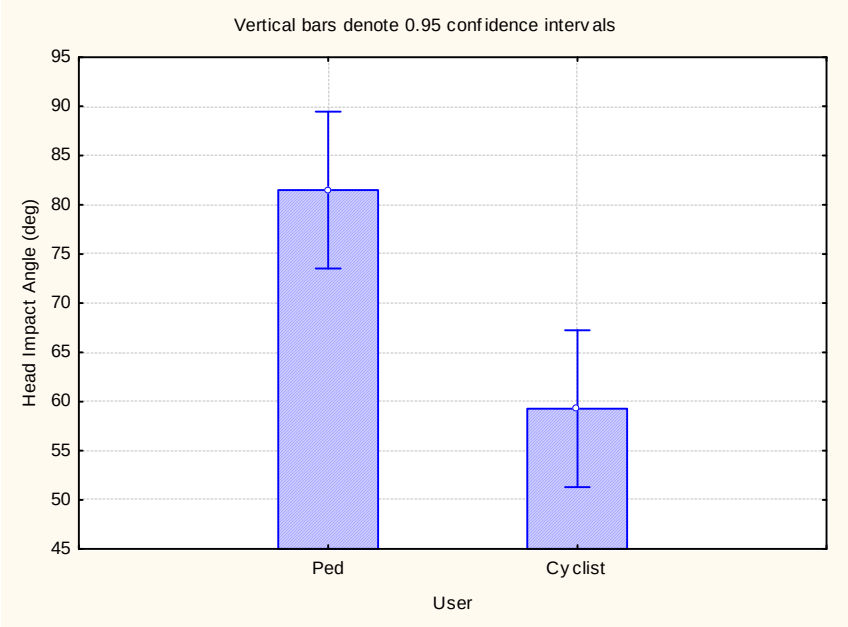

Figure B-4: Comparison of Head Impact Angles for Pedestrians and Cyclists Calculated by the ANOVA Technique

Appendix C Phase 1 Simulations

Job Name	
Ped10StanceC	Pedestrian stationary, vehicle at 10 m/s, C Stance
Ped10StanceD	Pedestrian stationary, vehicle at 10 m/s, D Stance
Ped5StanceC	Pedestrian stationary, vehicle at 5 m/s, C Stance
Ped5StanceD	Pedestrian stationary, vehicle at 5 m/s, C Stance
SLD10frontnobike2	Cyclist stationary, Struck leg down, vehicle 10 m/s, No bike
SLD5frontx	Cyclist stationary, Struck leg down, vehicle 5 m/s
SLDfront10x	Cyclist stationary, Struck leg down, vehicle 10 m/s
SLDfront15x	Cyclist stationary, Struck leg down, vehicle 15 m/s
SLDhum5	Cyclist 5 m/s, Struck leg down, vehicle 10 m/s
slu+10deg	Cyclist stationary, Struck leg up, vehicle 10 m/s and 10 deg
slu+500hum5	Cyclist 5 m/s, Struck leg up, vehicle 10 m/s and offset +500mm
slu10+20deg	Cyclist stationary, Struck leg up, vehicle 10 m/s and 20 deg
SLU10front#3foam#3	Cyclist stationary, Struck leg up, vehicle 10 m/s
slu10fronthum5#3	Cyclist 5 m/s, Struck leg up, vehicle 10 m/s
SLU10x+1000	Cyclist stationary, Struck leg up, vehicle 10 m/s and offset +1000mm
slu10x+500	Cyclist stationary, Struck leg up, vehicle 10 m/s and offset +500mm
slu10x-1000	Cyclist stationary, Struck leg up, vehicle 10 m/s and offset -1000mm
slu10x-500	Cyclist stationary, Struck leg up, vehicle 10 m/s and offset -500mm
slu15front	Cyclist stationary, Struck leg up, vehicle 15 m/s
slu-500hum5	Cyclist 5 m/s, Struck leg up, vehicle 10 m/s and offset -500mm
slu5front	Cyclist stationary, Struck leg up, vehicle 5 m/s
slufront10nobike	Cyclist stationary, Struck leg up, vehicle 10 m/s, No bike
slufront15nobike	Cyclist stationary, Struck leg up, vehicle 15 m/s, No Bike
slufront5nobike	Cyclist stationary, Struck leg up, vehicle 5 m/s, No Bike

Appendix D Phase 1 and 2 Cyclist Simulation Head Results

Model description	Vehicle type	Vehicle velocity (m/s)	Head impact angle (deg)	Head impact velocity (m/s)
Struck leg up	SM	5	++	++
		10	41	10.2
		15	33	14.1
Struck leg down	SM	5	50	5.2
		10	45	8.3
		15	#	#
Struck leg up	LFC	5	++	++
		10	43	11.2
		15	45	17.7
Struck leg down	LFC	5	++	++
		10	58	11.9
		15	42	17.6
Struck leg up	MPV	5	33	3.1
		10	55	6.9
		15	44	13.6
Struck leg down	MPV	5	++	++
		10	35	6.4
		15	30	9.4
Struck leg up	SUV	5	71	3.1
		10	129	6.2
		15	125	12.6
Struck leg down	SUV	5	++	++
		10	123	6.4
		15	94	10.8

++ Head did not strike the vehicle

Head struck the roof

Table D-3: Cyclist Head Impact Angle and Relative Velocity Results

Appendix E Vehicle Stiffnesses

The vehicle stiffness characteristics and their locations on the vehicle, as measured during the EuroNCAP tests and utilised for the simulations are given in Figure E-5 and Figure E-8.

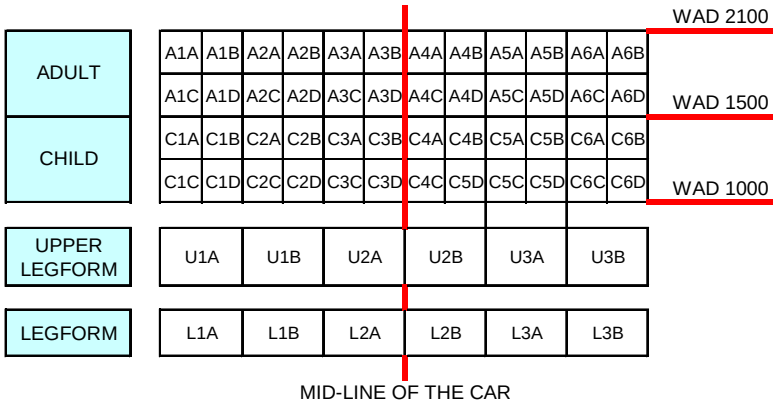

Figure E-5: EuroNCAP test locations

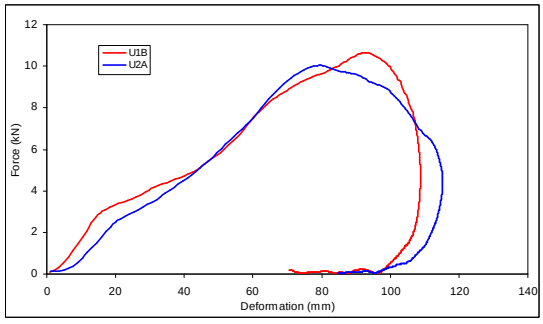

Figure E-6: MPV Vehicle Stiffnesses for the Bonnet Leading Edge

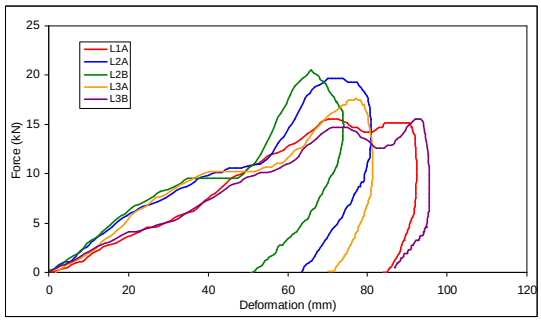

Figure E-7: MPV Vehicle Stiffnesses for the Bumper

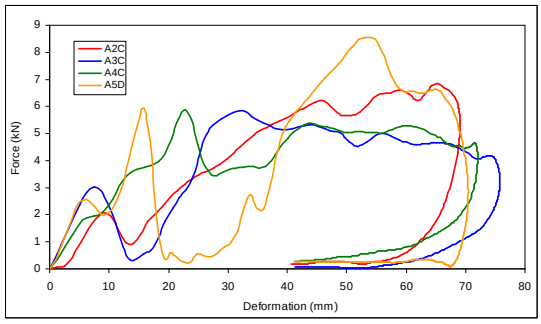

Figure E-8: MPV Vehicle Stiffnesses for the Bonnet

The vehicle stiffness characteristics and their locations on the vehicle, as measured during the EuroNCAP tests and utilised for the simulations are given in Figure E-9 and Figure E-11.

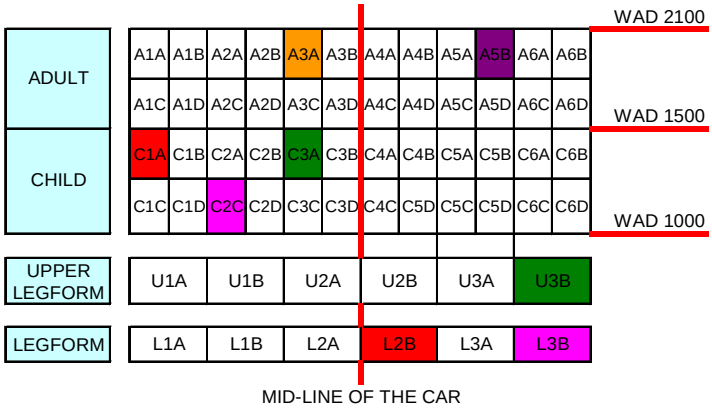

Figure E-9: SUV EuroNCAP test locations,(coloured sections highlight tests conducted)

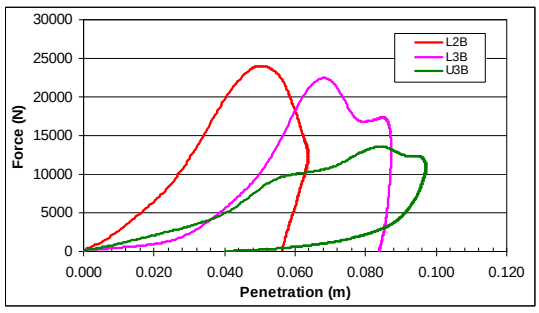

Figure E-10: SUV Vehicle Stiffnesses for the Bumper

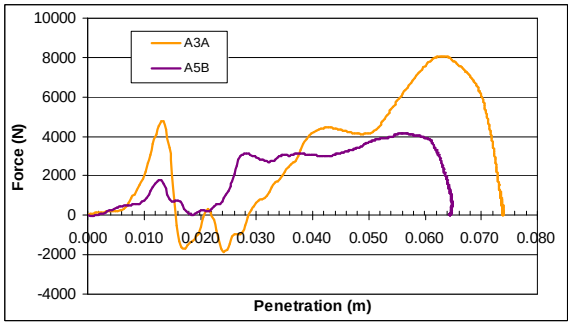

Figure E-11: SUV Vehicle Stiffnesses for the Bonnet

Appendix F Pedestrian Simulation Head Impact Results

Model description	Vehicle type	Vehicle velocity (m/s)	Head impact angle (deg)	Head impact velocity (m/s)
Struck leg back	SM	5	++	++
		10	63	7.8
		15	89	11.4
Struck leg forward	SM	5	75	5.8
		10	66	11.6
		15	67	14.9
Struck leg back	LFC	5	++	++
		10	64	6.5
Struck leg forward	LFC	5	67	4.5
		10	61	7.6
Struck leg back	MPV	5	71	0.9
		10	85	7.3
		15	114	12.1
Struck leg forward	MPV	5	100	3.5
		10	77	6.7
		15	71	12.5
Struck leg back	SUV	5	++	++
		10	124	5.3
		15	99	15.6
Struck leg forward	SUV	5	64	1.3
		10	128	2.6
		15	103	10.8

++ Head did not strike the vehicle

Table F-4: Pedestrian Head Impact Angle and Relative Velocity Results

Appendix G Kinematics

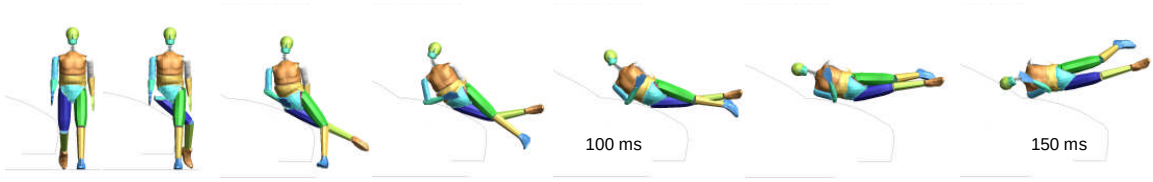

Figure G-12: Pedestrian Struck Leg-back Kinematics from Impact by the Supermini Model

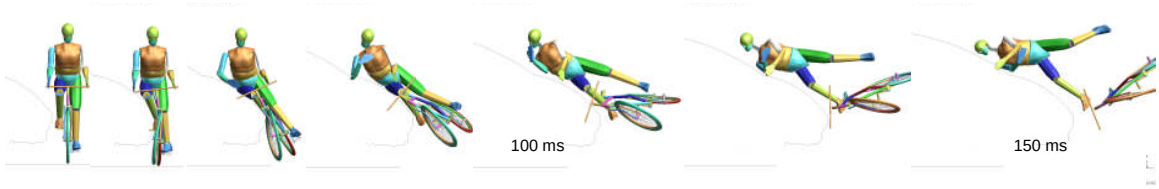

Figure G-13: Cyclist Struck Leg-up Kinematics from Impact by the MPV Model

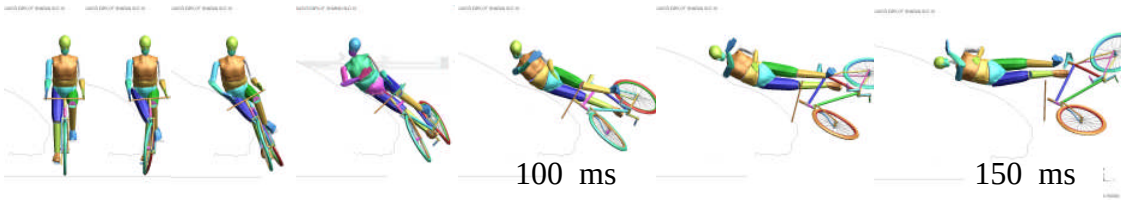

Figure G-14: Cyclist Struck Leg-down Kinematics from Impact by the MPV Model

Figure G-15: Pedestrian Struck Leg-forward Kinematics from Impact by the MPV Model

Figure G-16: Pedestrian Struck Leg-back Kinematics from Impact by the MPV Model

Figure G-17: Cyclist Struck Leg-down Kinematics from Impact by the SUV Model

Figure G-18: Pedestrian Struck Leg-forward Kinematics from Impact by the SUV Model

Appendix H Head Trajectory Results

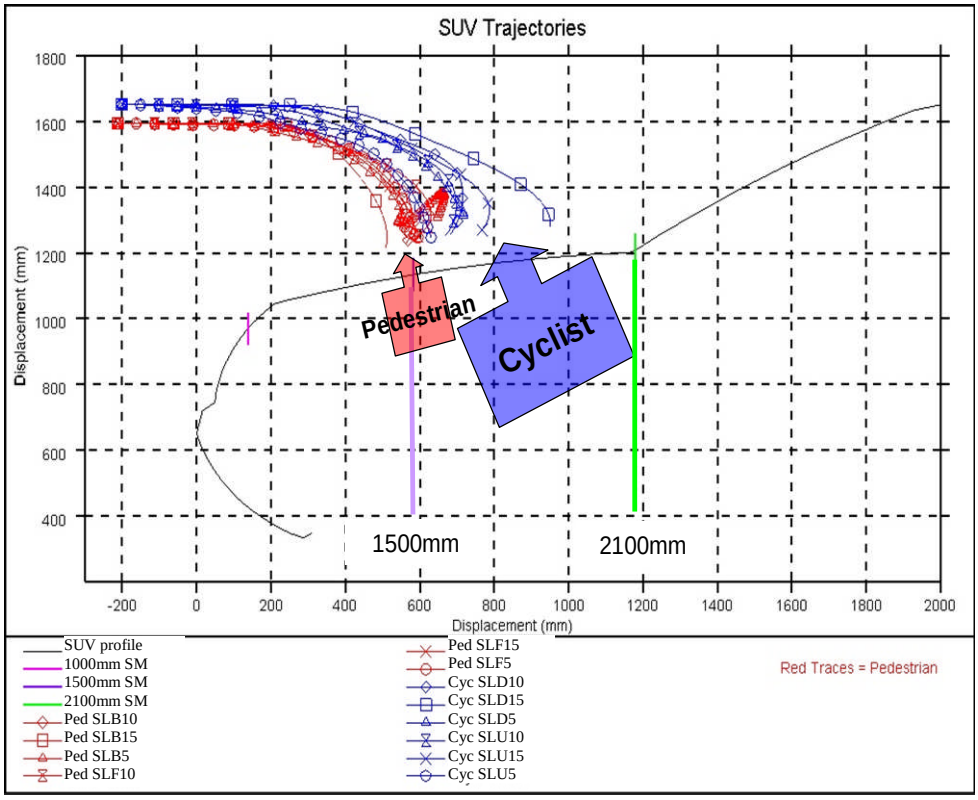

Figure H-19: SUV Head Trajectories

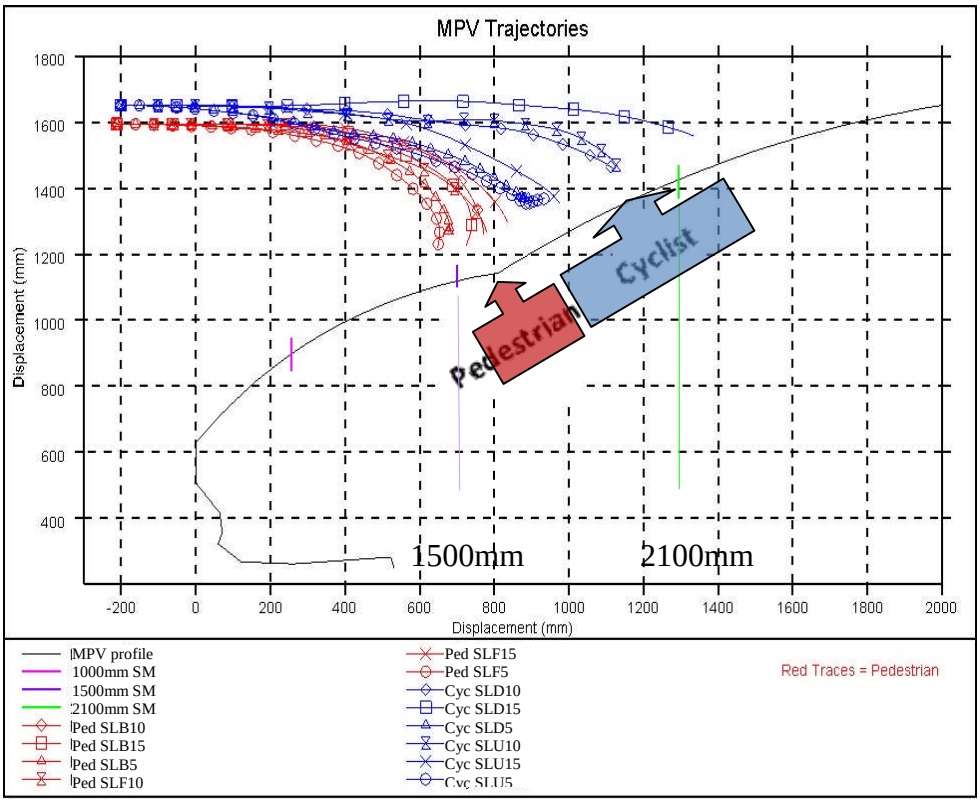

Figure H-20: MPV Head Trajectories

Appendix I Simulation Results Phase 1 and Phase 2

User	Vehicle Speed (m/s)	Simulation Features	Non-Struck max (N m)	Non-Struck min (N m)	Struck max (N m)	Struck min (N m)	Struck SF max (N)	Struck SF min (N)	Non-Struck SF max (N)	Non-Struck SF min (N)	Pelvis Max (g)	Chest Max (g)	Struck Tibia max (g)	Non-Struck Tibia max (g)
Cyclist	5		78	-88	79	-59	1236	-687	300	-847	7	12	79	176
Cyclist	10		101	-98	128	-46	2562	-806	810	-1575	16	48	346	148
Cyclist	15		118	-126	135	-76	4199	-1803	2289	-1808	37	35	632	236
Cyclist	10	+500 Offset	107	-119	127	-79	1128	-1192	491	-1609	17	23	173	189
Cyclist	10	-500 Offset	117	-96	128	-32	1834	-2400	750	-1419	17	20	505	140
Cyclist	10	-1000 Offset	110	-25	23	-110	1507	-280	333	-648	10	11	54	141
Cyclist	10	+1000 Offset	58	-86	101	-114	497	-1001	506	-2093	16	23	125	174
Cyclist	5	No Bike	42	-23	111	-39	1591	-707	1777	-59	12	14	284	184
Cyclist	10	No Bike	80	-71	128	-96	2553	-833	2711	-333	15	35	199	154
Cyclist	15	No Bike	132	-124	140	-70	4244	-1253	6989	-587	24	33	678	224
Cyclist	10	10 deg	117	-82	130	-113	4546	-1003	1553	-1845	24	59	225	304
Cyclist	10	20 deg	113	-118	128	-69	2367	-425	591	-1629	15	39	240	188
Cyclist	10	Bike 5m/s	110	-116	126	-60	3896	-907	553	-1765	12	11	182	179
Cyclist	5		30	-20	114	-30	422	-1720	878	-799	9	12	62	150
Cyclist	10		86	-17	132	-98	1270	-4667	1164	-1977	19	18	207	235
Cyclist	15		119	-26	139	-155	2508	-6590	1129	-3207	31	37	498	394
Cyclist	10	No Bike	42	-118	121	-99	1615	-4553	1428	-1002	13	22	113	113
Cyclist	10	Bike 5m/s	41	-62	121	-97	1949	-4388	1097	-2099	21	80	267	220
Cyclist	10	Bike 5m/s, '+500	117	-116	129	-85	2274	-539	409	-1126	16	25	158	147
Cyclist	10	Bike 5m/s, '-500	90	-68	122	-101	1212	-595	596	-1271	6	4	144	176
Ped	5		126	-75	130	-63	515	-111	430	-1202	17	11	448	96
Ped	10		130	-83	139	-49	1336	-452	501	-1756	46	18	819	326
Ped	10		20	-109	77	-136	961	-486	700	-560	22	12	303	141
Ped	5		18	-115	75	-157	1702	-1503	1230	-518	45	13	617	338

Figure I-21: Phase 1 Simulation Results (Part 1)

User	Vehicle Speed (m/s)	Simulation Features	No Bike	Head Contact Time	Head Impact Angle (deg)	Head Angle Relative to 65 deg	Longitudinal Head Displacement	Vertical Head Displacement	Head Relative Velocity	Head/Vehicle Velocity Ratio	Stance	Bonnet Leading Edge Height	WAD to Windscreen Base
Cyclist	**5**		Bike								SLU	761	2071
Cyclist	**10**		Bike	171	43	0.66			11.23	1.1	SLU	761	2071
Cyclist	**15**		Bike	121	45	0.69			17.7	1.2	SLU	761	2071
Cyclist	**10**	**+500 Offset**	Bike		42						SLU	761	2071
Cyclist	**10**	**-500 Offset**	Bike		36						SLU	761	2071
Cyclist	**10**	**-1000 Offset**	Bike								SLU	761	2071
Cyclist	**10**	**+1000 Offset**	Bike								SLU	761	2071
Cyclist	**5**	**No Bike**	Bike		54						SLU	761	2071
Cyclist	**10**	**No Bike**	Bike		33						SLU	761	2071
Cyclist	**15**	**No Bike**	Bike		18						SLU	761	2071
Cyclist	**10**	**10 deg**	Bike		71						SLU	761	2071
Cyclist	**10**	**20 deg**	Bike		32						SLU	761	2071
Cyclist	**10**	**Bike 5m/s**	Bike								SLU	761	2071
Cyclist	**5**		Bike								SLD	761	2071
Cyclist	**10**		Bike	156	58	0.89			11.9	1.2	SLD	761	2071
Cyclist	**15**		Bike	114	42	0.65			17.6	1.2	SLD	761	2071
Cyclist	**10**	**No Bike**	Bike								SLD	761	2071
Cyclist	**10**	**Bike 5m/s**	Bike								SLD	761	2071
Cyclist	**10**	**Bike 5 m/s,+500**	Bike		37						SLU	761	2071
Cyclist	**10**	**Bike 5 m/s,-500**	Bike								SLU	761	2071
Ped	**5**		No Bike								SLB	761	2071
Ped	**10**		No Bike	150	64	0.98			6.5	0.7	SLB	761	2071
Ped	**10**		No Bike	257	67	1.03			4.5	0.9	SLF	761	2071
Ped	**5**		No Bike	150	61	0.94			7.6	0.8	SLF	761	2071

Figure I-22: Phase 1 Simulation Results (Part 2)

(Gaps in Table refer to when calculations where not possible due to no head contact)

User	Vehicle Speed (m/s)	Car Type	Non-Struck max (N m)	Non-Struck min (N m)	Struck max (N m)	Struck min (N m)	Struck SF max (N)	Struck SF min (N)	Non-Struck SF max (N)	Non-Struck SF min (N)	Pelvis Max (g)	Chest Max (g)	Struck Tibia max (g)	Non-Struck Tibia max (g)
Ped	**5**	**MPV**	123	-104	173	-134	3723	-2575	1597	-1262	38	9	150	132
Ped	**5**	**SM**	129	-97	134	-87	2560	-2233	1003	-2800	17	14	154	177
Ped	**5**	**SUV**	145	-129	162	-125	2851	-1641	829	-154	48	16	59	130
Ped	**5**	**MPV**	98	-67	174	-74	2592	-1875	735	-478	35	18	115	130
Ped	**5**	**SM**	115	-49	147	-115	3766	-2314	602	-1106	24	90	140	220
Ped	**5**	**SUV**	123	-82	436	-128	2221	-1434	1041	-868	32	12	108	108
Cyclist	**5**	**MPV**	101	-71	137	-63	2147	-5157	1214	-965	26	22	67	218
Cyclist	**5**	**SM**	46	-53	109	-64	1686	-5082	1292	-1226	22	11	93	218
Cyclist	**5**	**SUV**	131	-94	144	-78	2594	-4866	1195	-1610	24	23	116	209
Cyclist	**5**	**MPV**	59	-88	87	-84	2220	-2562	1096	-1742	16	18	119	279
Cyclist	**5**	**SM**	37	-92	69	-75	936	-1465	745	-1134	12	45	97	149
Cyclist	**5**	**SUV**	60	-33	90	-67	1545	-4958	1015	-1086	35	17	110	154
Ped	**10**	**MPV**	181	-130	191	-141	8286	-2409	9408	-6503	68	61	331	279
Ped	**10**	**SM**	161	-120	154	-132	1903	-3689	3977	-3410	43	43	278	365
Ped	**10**	**SUV**	159	-127	193	-154	6327	-2653	5100	-2326	181	132	303	357
Ped	**10**	**MPV**	156	-137	293	-178	14777	-5915	8668	-6916	120	45	1270	409
Ped	**10**	**SM**	145	-107	172	-123	4551	-3775	2735	-2196	50	29	294	305
Ped	**10**	**SUV**	274	-154	677	-413	7033	-6431	6928	-6833	93	52	397	478
Cyclist	**10**	**MPV**	116	-45	156	-67	3828	-6795	2304	-4824	45	29	270	629
Cyclist	**10**	**SM**	42	-115	91	-144	1144	-6993	1781	-1500	64	65	103	491
Cyclist	**10**	**SUV**	137	-118	150	-46	3392	-8982	2202	-6995	80	26	336	1807
Cyclist	**10**	**MPV**	97	-114	125	-123	2610	-6037	735	-4501	36	54	302	317
Cyclist	**10**	**SM**	16	-73	85	-130	1750	-4312	585	-7043	40	61	304	335
Cyclist	**10**	**SUV**	105	-117	135	-128	3582	-5392	1754	-3782	124	27	208	239
Ped	**15**	**MPV**	478	-200	254	-241	10082	-6678	27912	-22337	127	82	1251	382
Ped	**15**	**SM**	406	-209	299	-269	16059	-9601	14641	-9339	156	77	747	998
Ped	**15**	**SUV**	262	-198	273	-239	16980	-12173	14011	-13872	226	236	862	640
Ped	**15**	**MPV**	328	-137	300	-188	14513	-5267	15711	-8298	112	250	1482	442
Ped	**15**	**SM**	256	-137	410	-128	16116	-3763	11842	-5174	159	90	888	1435
Ped	**15**	**SUV**	388	-187	717	-622	18879	-15610	16582	-16357	162	99	2008	758
Cyclist	**15**	**MPV**	82	-44	300	-163	21912	-20193	4818	-9028	124	45	388	3536
Cyclist	**15**	**SM**	119	-124	93	-180	2092	-13898	5843	-4878	86	61	191	3234
Cyclist	**15**	**SUV**	138	-120	260	-140	6707	-16608	1823	-11738	99	43	519	1172
Cyclist	**15**	**MPV**	141	-180	156	-204	8125	-10867	7633	-12388	248	92	695	460
Cyclist	**15**	**SM**	55	-121	120	-161	2110	-4276	804	-11985	44	65	682	303
Cyclist	**15**	**SUV**	132	-139	168	-188	5239	-11019	3326	-14753	243	49	709	520

Table I-5: Phase 2 Simulation Results (Part 1)

User	Vehicle Speed (m/s)	Car Type	Head Contact Time (ms)	Head Impact Angle (deg)	Head Angle Relative to 65 deg	Longitudinal Head Displacement (mm)	Vertical Head Displacement (mm)	Head Relative Velocity (m/s)	Head/Vehicle Velocity Ratio	Stance	Bonnet Leading Edge Height (mm)	WAD to Windscreen Base (mm)
Ped	**5**	**MPV**	225	71	1.09	885	238.73	0.9	0.1	SLB	684	1614
Ped	**5**	**SM**				1117	531.73			SLB	619	1808
Ped	**5**	**SUV**								SLB	1056	2088
Ped	**5**	**MPV**	202	100	1.54	850	299.73	3.5	0.7	SLF	684	1614
Ped	**5**	**SM**	231	75	1.15	1161	595.73	5.8	1.0	SLF	619	1808
Ped	**5**	**SUV**	274	64	0.98	847	349.73	1.3	0.3	SLF	1056	2088
Cyclist	**5**	**MPV**								SLD	684	1614
Cyclist	**5**	**SM**	237	50	0.77	1351	585.46	5.2	0.8	SLD	619	1808
Cyclist	**5**	**SUV**								SLD	1056	2088
Cyclist	**5**	**MPV**	281	33	0.51	1131	226.46	3.1	0.6	SLU	684	1614
Cyclist	**5**	**SM**	236			1311	580.46			SLU	619	1808
Cyclist	**5**	**SUV**	223	71	1.09	934	456.46	3.26	0.7	SLU	1056	2088
Ped	**10**	**MPV**	113	85	1.31	971	280.73	7.3	0.7	SLB	684	1614
Ped	**10**	**SM**	141	63	0.97	1358	441.73	7.8	0.7	SLB	619	1808
Ped	**10**	**SUV**	106	124	1.91	815	364.73	5.3	0.5	SLB	1056	2088
Ped	**10**	**MPV**	113	77	1.18	973	264.73	6.7	0.7	SLF	684	1614
Ped	**10**	**SM**	128	66	1.02	1296	488.73	11.6	0.9	SLF	619	1808
Ped	**10**	**SUV**	120	128	1.97	841	353.73	2.57	0.3	SLF	1056	2088
Cyclist	**10**	**MPV**	146	35	0.54	1315	144.46	6.4	0.8	SLD	684	1614
Cyclist	**10**	**SM**	167	45	0.69	1933	262.46	8.3	0.4	SLD	619	1808
Cyclist	**10**	**SUV**	123	123	1.89	954	454.46	6.4	0.8	SLD	1056	2088
Cyclist	**10**	**MPV**	156	55	0.85	1320	150.46	6.9	0.8	SLU	684	1614
Cyclist	**10**	**SM**	155	41	0.63	1602	432.46	10.2	0.9	SLU	619	1808
Cyclist	**10**	**SUV**	126	129	1.98	966	457.46	6.2	0.8	SLU	1056	2088
Ped	**15**	**MPV**	78	114	1.75	905	316.73	12.1	0.4	SLB	684	1614
Ped	**15**	**SM**	93	89	1.37	1294	496.73	11.4	0.5	SLB	619	1808
Ped	**15**	**SUV**	62	99	1.52	765	381.73	15.6	1.0	SLB	1056	2088
Ped	**15**	**MPV**	78	71	1.09	1028	245.73	12.5	0.8	SLF	684	1614
Ped	**15**	**SM**	89	67	1.03	1312	475.73	14.9	0.8	SLF	619	1808
Ped	**15**	**SUV**	67	103	1.58	841	358.73	10.8	0.7	SLF	1056	2088
Cyclist	**15**	**MPV**	111	30	0.46	1534	45.46	9.4	0.8	SLD	684	1614
Cyclist	**15**	**SM**				2474	160.46			SLD	619	1808
Cyclist	**15**	**SUV**	87	94	1.45	1232	420.46	10.8	0.9	SLD	1056	2088
Cyclist	**15**	**MPV**	83	44	0.68	1155	230.46	13.6	1.1	SLU	684	1614
Cyclist	**15**	**SM**	116	33	0.51	1773	343.46	14.1	0.7	SLU	619	1808
Cyclist	**15**	**SUV**	85	125	1.92	1067	437.46	12.6	1.0	SLU	1056	2088

Table I-6: Phase 2 Simulation Results (Part 2) (Gaps in Table refer to when calculations where not possible due to no head contact)

Appendix J Phase 2 Test Animations

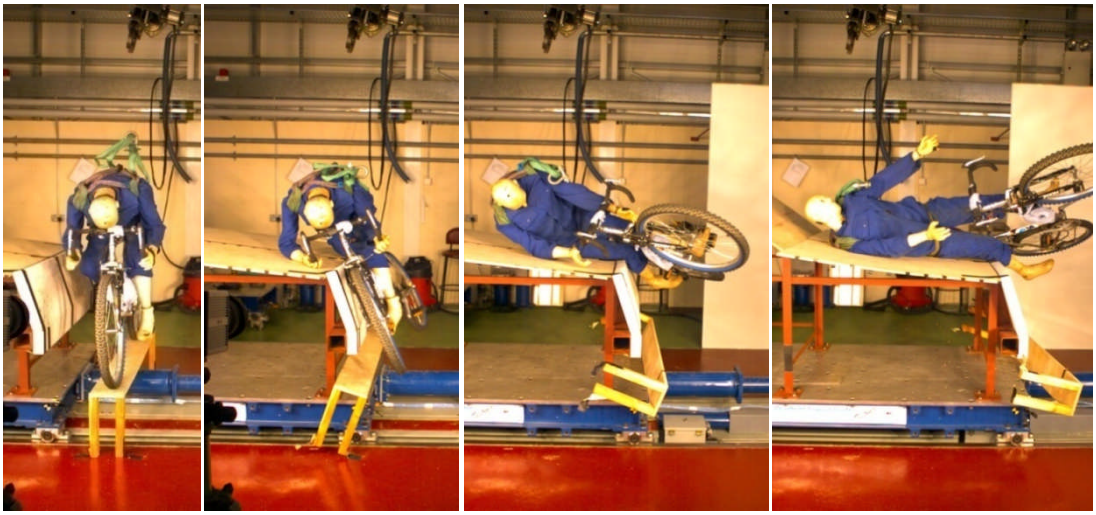

0 s **0.1 s** **0.2 s** **0.3 s**

Test 2

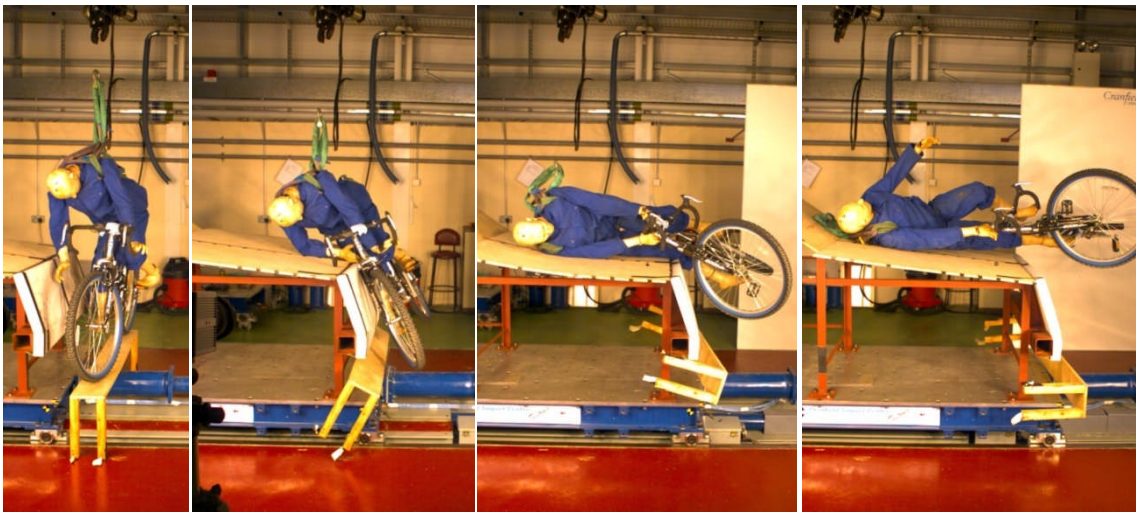

0 s **0.1 s** **0.2 s** **0.3 s**

Test 3

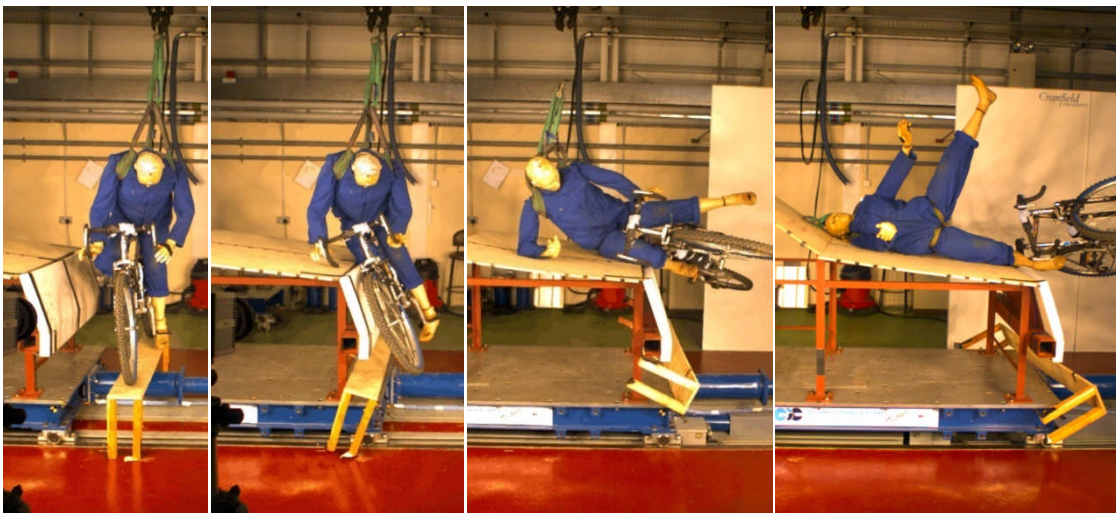

0 s **0.1 s** **0.2 s** **0.3 s**

Test 4

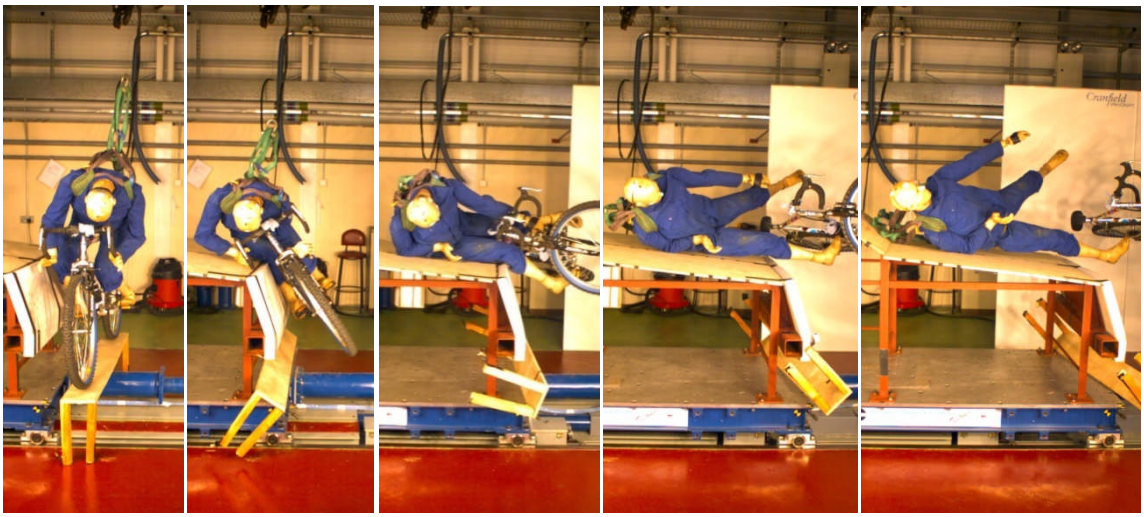

0 s **0.1 s** **0.2 s** **0.3 s** **0.4 s**

Test 5

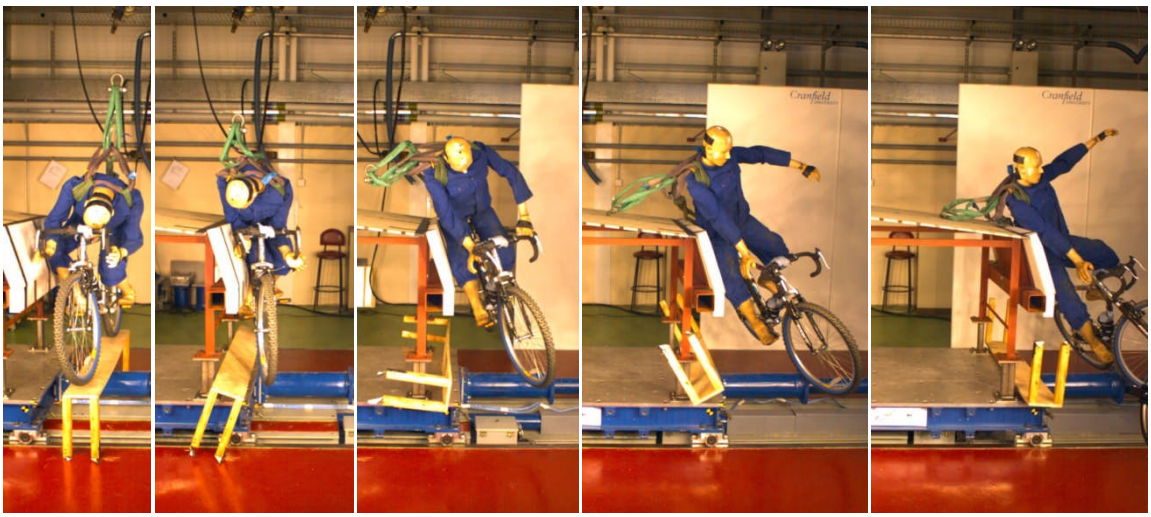

0 s **0.1 s** **0.2 s** **0.3 s** **0.4 s**

Test 6

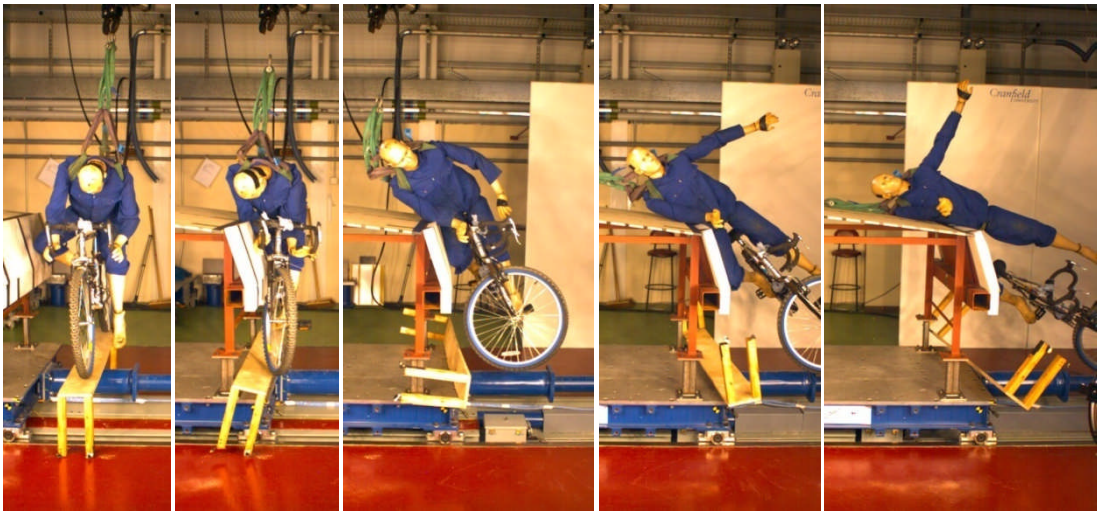

0 s **0.1 s** **0.2 s** **0.3 s** **0.4 s**

Test 7

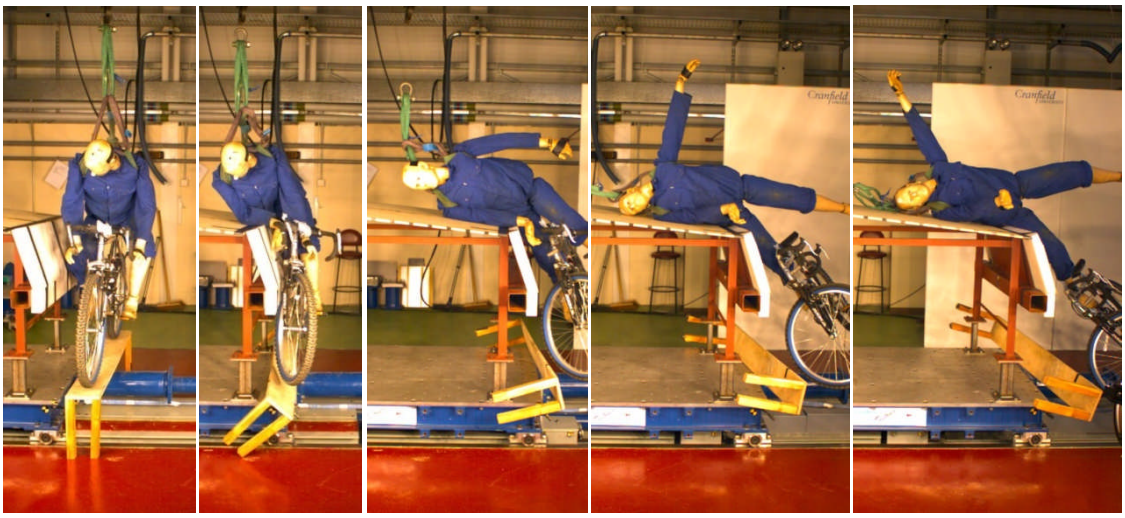

0 s **0.1 s** **0.2 s** **0.3 s** **0.4 s**

Test 8

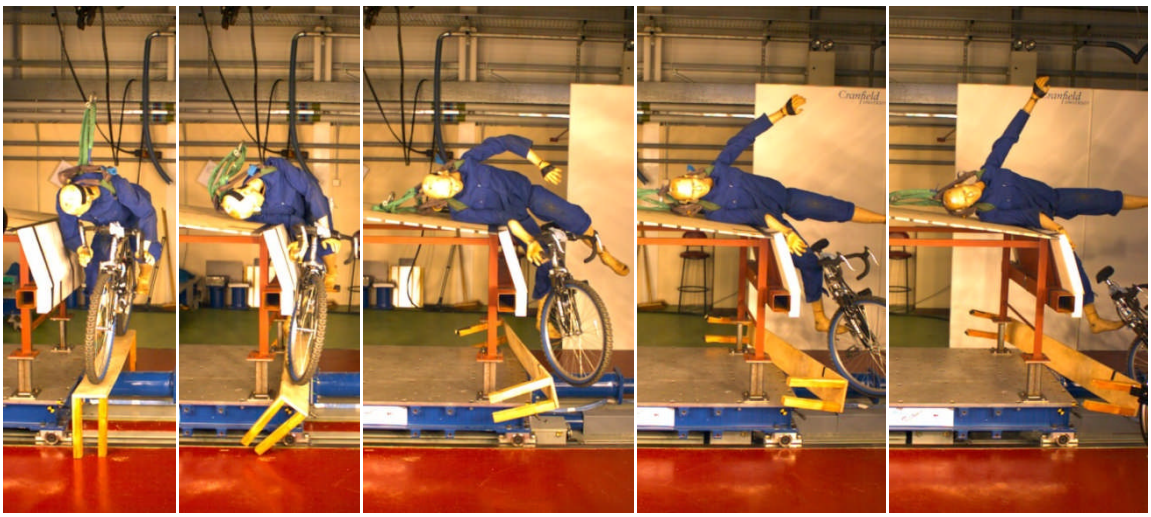

0 s **0.1 s** **0.2 s** **0.3 s** **0.4 s**

Test 9

Appendix K References

Arnoux, P. J., Cesari, D., Behr, M., Thollon, L. and Brunet, C. (2005), "Pedestrian lower limb injury criteria evaluation: A finite element approach", *Traffic Injury Prevention,* vol. 6, no. 3, pp. 288-297.

Arnoux, P. J., Thollon, L., Kayvantash, K., Cavallero, C. and Brunet, C. (2002a), "Advanced Lower Limbs Model with Radioss Application to Frontal and Lateral Impacts ", *International IRCOBI Conference on The Biomechanics of Impact* Munich, Germany, INRETS, France, pp. 373-375.

Arnoux, P. J., Cavallero, C., Chabrand, P. and Brunet, C. (2002b), "Knee ligament failure under dynamic loadings", *International Journal of Crashworthiness,* vol. 7, no. 3, pp. 255-268.

Backaitis, S. H. and Mertz, H. J. (eds.) (1994), *Hybrid III: The First Human-Like Crash Test Dummy,* 1st ed, Society of Automotive Engineers, USA.

Bandak, F. A. and Eppinger, R. H. (1994), *A Three-Dimensional Finite Element Analysis of the Human Brain Under Combined Rotational and Translational Accelerations,* 942215, SAE, USA.

Banglmaier, R. F., Rouhana, S. W., Beillas, P. and Yang, K. H. (2003), "Lower extremity injuries in lateral impact: a retrospective study", *Annual proceedings / Association for the Advancement of Automotive Medicine,* vol. 47, pp. 425-444.

Bellogi, P., Lee, I. and Ahmesd, N. (2005), *Car to Bicycle Side Crash Simulation,* No 109-05, 2005-08-0523, SAE, Japan.

Bermond, F., Ramet, M., Bouquet, R. and Cesari, D. (1993), "A finite element model of the pedestrian knee-joint in lateral impact", *1993 International IRCOBI Conference on the Biomechanics of Impacts,* 8-10 September 1993, Eindhoven, International Research Council on Biomechanics of Injury, pp. 117-129.

Bolourchi, F. (1986), *Bicycle Frame Stress by means of Finite Element Analysis*, 1, American Society of Mechanical Engineers, Design Engineering Division (Publication) DE, USA.

Cardot, J., Masson, C., Arnoux, P. J. and Brunet, C. (2006), "Finite element analysis of cyclist lower limb response in car-bicycle accident", *International Journal of Crashworthiness*, vol. 11, no. 2, pp. 115-129.

Carhs Training (2008), *Safety Companion 2008*, Carhs.Training gmbh, Alzenau, Germany.

Carter, E. (2005), *Definition of vehicle and pedestrian/cyclist impact conditions*, available at: http://www.aprosys.com/Documents/deliverables/sp31_005R.pdf (accessed 14/12/08).

Cesari, D., Alonzo, F. and Matyjewski, M. (1991), "Subsystem test for pedestrian lower leg and knee protection", US Department of Transportation, National Highway Traffic Safety Administration. (ed.), in: November 1991, pp. 310-317.

China Automotive Information Net (2008), *China Accident Statistics*, available at: http://english.autoinfo.gov.cn/autoinfo_eng/Transportation/Traffic/jtsgtj/webinfo/2008/10/1223511595211948.htm (accessed 07/11/08).

Courant, R. (1943), "Variational methods for the solution of problems of equilibrium and vibrations", *Bulletin of the American Mathematical Society*, vol. 49, pp. 2165-2186.

Department for Transport (2007), *Car UsageDfT*, available at: http://www.dft.gov.uk/162259/162469/221412/217792/2214291/TSGB2007Final_linksV12.pdf (accessed 16/11/2008).

Depreitere, B., Van Lierde, C., Maene, S., Plets, C., Sloten, J. V., Van Audekercke, R., Van der Perre, G. and Goffin, J. (2004), "Bicycle-related head injury: A study of 86 cases", *Accident Analysis and Prevention*, vol. 36, no. 4, pp. 561-567.

Edwards, M. J. (2007), *Evaluation of the use of the WorldSID dummy in the AE-MDB test and further AE-MDB development*, APROSYS SP1 - D1.1.1C-Part1 AP_SP11-0132.

Eilert-Petersson, E. and Schelp, L. (1997), "An epidemiological study of bicycle-related injuries", *Accident Analysis and Prevention*, vol. 29, no. 3, pp. 363-372.

Eppinger, R., Sun, E., Bandak, F., Haffner, M., Khaewpong, N., Maltese, M., Kuppa, S., Nguyen, T., Takhounts, E., Tannous, R., Zhang, A. and Saul, R. (1999), *Development of Improved Injury Criteria for the Assessment of Advanced Automotive Restraint Systems - II* , NHTSA.

European Commission, Directorate-General for Energy and Transport (ed.) (2008), *EU Energy and Transport in Figures*, European Communities, Belgium.

European New Car Assessment Programme (2009), *EuroNCAP*, available at: http://www.euroncap.com/home.aspx (accessed 01/09).

European Parliament and Council, (2003), *Directive 2003/102/EC of the European Parliament and of the Council of 17th November 2003 relating to the protection of pedestrians and other vulnerable road users before and in the event of a collision with a motor vehicle and amending Council Directive 70/156/EEC*, Directive ed., EU, Brussels, Belgium.

FunnyPictures.net.au (2009), *That moment before pain*, available at: http://www.funnypictures.net.au/before-the-pain/ (accessed 27/01/09).

Green Car Congress (2010), *Per-Capita Car Ownership in China to Climb 67% by 2010*, available at: http://www.greencarcongress.com/2006/05/percapita_car_o.html (accessed 07/05).

Grünert, J. (2009), *Assessment of the relevance of the secondary (ground) impact and its influence on injuries*, available at: http://www.aprosys.com/Documents/deliverables/FinalDeliverables/AP%20SP32%20010R%20D324%20-%20April 02007.pdf (accessed 06/30).

Haight, W. R. and Eubanks, J. J. (1990), "Trajectory analysis for collisions involving bicycles and automobiles", *SAE Trans*, vol. 99, no. Sect 6, pp. 528-546.

Hallquist, J. (1976), *Preliminary User's Mannuals for DYNA 3D and DYNAP*, UCID-17268, University of California, Lawrence Livermore National Laboratory.

Hardy, R., Watson, J. and Howard, M. (2000), "Developments in the simulation of real world car to pedestrian accidents using a pedestrian humanoid finite element model", *International Journal of Crashworthiness*, vol. 5, no. 1, pp. 103-116.

Hardy, R. N., Watson, J. W., Carter, E., Neal-Sturgess, C. E., Joonekindt, S., Yang, J., Hermann, K., Baumgartner, D., Guerra, L. J. and Martinez, L. (2007), *Impact conditions for pedestrians and cyclists*, available at: http://www.aprosys.com/Documents/deliverables/FinalDeliverables/AP%20SP32%20009R%20D323%20-%20Jan%202008.pdf (accessed 6/30).

Hardy, R. N., Watson, J. W. and Kayvantash, K. (2009), "Safety Requirements for Cyclists During Car Impacts to the Legs", *21st ESV Conference 2009*, 17th – 18th June 2009, Stuttgart, Germany, Enhanced Safety Vehicle, pp. 09 –0462.

Horgan, T. J. and Gilchrist, M. D. (2003), "The creation of three-dimensional finite element models for simulating head impact biomechanics", *International Journal of Crashworthiness*, vol. 8, no. 4, pp. 353-366.

Howard, M., Thomas, A., Koch, W., Watson, J. and Hardy, R. (2000), "Validation and application of a finite element pedestrian humanoid model for use in pedestrian accident simulation", *Proceedings of the International IRCOBI Conference Biomechanics of Impact*, pp. 101.

Howard, M., Watson, J. and Hardy, R. (1998), "The simulation of real world car to pedestrian accidents using a pedestrian humanoid finite element model", *International Journal of Crashworthiness*, vol. 3, no. 4, pp. 347-357.

Howard, M. S. (2002), *Pedestrian Accident Simulation and Protection Technology Evaluation* (PhD thesis), Cranfield University, UK.

Huijbers, J. J. W. and Janssen, E. G. (1988), "Experimental and Mathematical Car-Bicycle Collision Simulations", Institute for Road Safety Research SWOV Leidschendam (ed.), in: *32nd Stapp car Crash Conference,* Vol. 881726, Atlanta, Georgia.

Incel, N. A., Ceceli, E., Durukan, P. B., Erdem, H. R. and Yorgancioglu, Z. R. (2002), "Grip strength: Effect of Hand Dominance", *Singapore medical Journal,* vol. 43(5), pp. 234-237.

Ishikawa, H., Kajzer, J., Ono, K. and Sakurai, M. (1994), "Simulation of car impact to pedestrian lower extremity: Influence of different car-front shapes and dummy parameters on test results", *Accident, Analysis and Prevention,* vol. 26, no. 2, pp. 231-242.

Ishikawa, H., Kajzer, J. and Schroeder, G. (1993), "Computer Simulation of Impact Response of the Human Body in Car-Pedestrian Accidents", SAE (ed.), in: *Stapp Car Crash Conference, November 1993,* Vol. 933129, 1993, San Antonio, CA, USA, pp. 235.

Jacobsen, P. L. (2003), "Safety in numbers: more walkers and bicyclists, safer walking and bicycling", *Injury prevention : Journal of the International Society for Child and Adolescent Injury Prevention,* vol. 9, pp. 205-209.

Janssen, E. G. and Wismans, J. (1985), "Experimental and mathematical simulation of pedestrian-vehicle and cyclist-vehicle accidents", *Proceedings of 10th International Technical Conference on Experimental Safety Vehicle,* Oxford, UK, pp. 977.

Janssen, E. G. and Wismans, J. (1987), "Evaluation of Vehicle-cyclist Impacts through Dummy and Human Cadaver Tests", *11th ESV,* 12th-15th May 1987, Washington DC, USA, TNO, Delft, The Netherlands.

Jiroušek, O. and Jíra, J. (2005), "Comparison of finite element and experimental simulation of human head response to impact", *VDI Berichte,* vol. 1899, pp. 463-472.

Kajzer, J., Cavallero, C., Bonnoit, J., Morjane, A. and Ghamouchi, S. (1993), "Response of the knee joint in lateral impact: Effect of bending moment", *Proceedings of the International IRCOBI Conference,* 8th-10th Sept, Eindhoven, The Netherlands.

Kajzer, J., Schroeder, G., Ishikawa, H., Matsui, Y. and Bosch, U. (1997), "Shearing and bending effects at the knee joint at high speed lateral loading", *41st Stapp Car Crash Conference,* November, Lake Buena Vista, Florida, US.

Kerrigan, J., Bhalla, K., Madeley, N., Funk, J., Bose, D. and Crandall, J. (2003), "Experiments for establishing pedestrian-impact lower limb injury criteria", *SAE International Congress & Exposition,* Vol. 2003-01-0895, March 2003, Detroit, US.

Kerrigan, J., Murphy, D., Drinkwater, D., Kam, C., Bose, D. and Crandall, J. (2005), "Kinematic corridors for PMHS tested in full-scale pedestrian impact tests", *19th International Technical Conference on the Enhanced Safety of Vehicles,* Vol. 05-0394, June, Washington DC, US.

Kikuchi, Y., Takahashi, Y. and Mori, F. (2008), "Full-Scale Validation of a Human FE Model for the Pelvis and Lower Limb of a Pedestrian", *Pedestrian Safety, Vehicle Aggressivity & Compatability in Automotive Crashes,* Vol. 2008-01-1243, April 14-17, Detroit, Michigan, SAE International, Warrendale, PA15096-0001,USA.

Levine, R. S. (1986), "A review of the long-term effects of selected lower limb injuries", *Symposium on the Biomechanics and Medical Aspects of Lower Limb Injuries,* October, San Diego, California, US, pp. 143–159.

Livermore Software Technology Corporation (2007), *LS-DYNA Keyword User's Manual,* Version 971 Volume 1, Livermore Software Technology Corporation (LSTC), California, US.

Maki, T., Asai, T. and Kajzer, J. (2000), "Behavior of bicyclists in accidents with cars", *JSAE review*, vol. 21, no. 3, pp. 21.

Maki, T. and Kajzer, J. (2001), "The behavior of bicyclists in frontal and rear crash accidents with cars", *JSAE Review*, vol. 22, no. 3, pp. 357-363.

Maki, T., Kajzer, J., Mizuno, K. and Sekine, Y. (2003), "Comparative analysis of vehicle-bicyclist and vehicle-pedestrian accidents in Japan", *Accident Analysis and Prevention*, vol. 35, no. 6, pp. 927-940.

Manoli, A. (1986), "Adult Pedestrian Injuries - Medical Aspects", SAE (ed.), in: *Symposium on Biomechanics and Medical Aspects of Lower Limb Injuries*, Vol. paper 861928, 29-30 October 1986, San Diego, USA, SAE, pp. 186.

Masson, C., Arnoux, P. J., Brunet, C. and Cesari, D. (2005), "Pedestrian injury mechanisms & criteria. A coupled experimental and finite element approach,", *19th International Technical Conference on the Enhanced Safety of Vehicles*, Vol. 05-0335, June, Washington DC, USA.

Matsui, Y. (2003), "New injury reference values determined for TRL legform impactor from accident reconstruction test", *International Journal of Crashworthiness*, vol. 8, no. 2, pp. 179-188.

MatWeb (2009), *Aluminum 7005-T6, 7005-T63 and 7005-T6351*, available at: http://www.matweb.com/search/DataSheet.aspx?MatGUID=34c308934f7a4be589a80ecbee94406e&ckck=1 (accessed 04/09).

McLundie, W. M. (2007), *Investigation of two-wheeled road traffic accidents using explicit FE techniques* (PhD thesis), Cranfield University, UK.

Mills, N. J. (2006), "Oblique Impacts on Bicycle Helmets", *2006 International IRCOBI Conference on the Biomechanics of Impact*, September 2006, Madrid, Spain, IRCOBI, INRETS, France, pp. 425.

Mills, N. J. (2008), "Comments on Depreitere et al. Lateral head impacts and protection of the temporal area by bicycle safety helmets", *The Journal of Trauma*, vol. 65, no. 2, pp. 479-481.

Mukherjee, S., Chawla, A., Mohan, D., Chandrawat, S. and Agrawal, V. (2006), "Throw Distance Variations in Bicycle Crashes", *IRCOBI Conference Proceedings*, September 2006, Madrid, Spain, pp. 341.

Nader, R. (1965), *Unsafe at any Speed: the designed-in dangers of the American automobile*, Grossman, New York.

Nagasaka, K., Mizuno, K., Tanaka, E., Yamamoto, S., Iwamoto, M., Miki, K. and Kajzer, J. (2003), "Finite Element Analysis of Knee Injury Risks in Car-to-Pedestrian Impacts", *Traffic Injury Prevention*, vol. 4, no. 4, pp. 345-354.

Nahum, A. and Melvin, J. (1993), *Accidental Injury - Biomechanics and Prevention*, First ed, Springer-Verlag, Edwards Brothers INC., Ann Arbor, MI, USA.

Neilson, I. (1999), *Pedestrian and Cyclist Protection on Road Vehicles with High or Flat Fronts*, ID#183, Parliamentary Advisory Council for Transport Safety - PACTS, UK.

Otte, D. (1989), "Injury mechanism and crash kinematic of cyclists in accidents - An analysis of real accidents", *33rd Stapp Car Crash Conference*, Vol. SAE, Washington DC, USA, pp. 892425.

Peters, G. and Peters, B. (2002), *Automotive Vehicle Safety*, First ed, Taylor and Francis, USA.

Ramet, M., Bouquet, R., Bermond, F. and Carire, Y. (1995), "Shearing and bending human knee joint tests in quasi-static lateral load", *International IRCOBI Conference Proceedings*, Brunnen, Switzerland, pp. 93-105.

Räsänen, M. and Summala, H. (1998), "Attention and expectation problems in bicycle-car collisions: An in-depth study", *Accident Analysis and Prevention,* vol. 30, no. 5, pp. 657-666.

Richter, M., Otte, D., Haasper, C., Knobloch, K., Probst, C., Westhoff, J., Sommer, K. and Krettek, C. (2007), "The current injury situation of bicyclists - A medical and technical crash analysis", *J.Trauma Inj.Infect.Crit.Care,* vol. 62, no. 5, pp. 1118-1122.

Rodgers, G. B. (1995), "Bicyclist deaths and fatality risk patterns", *Accident Analysis and Prevention,* vol. 27, no. 2, pp. 215-223.

Rose, D. and Sullivan, O. (1996), *Introducing Data Analysis for Social Scientists,* 2nd Edition ed, Open University Press, UK.

Roudsari, B., Mock, C., Kaufman, R., Grossman, D., Henary, B. and Crandall, J. (2004), "Pedestrian crashes: higher injury severity and mortality rate for light truck vehicles compared with passenger vehicles", *Injury prevention : journal of the International Society for Child and Adolescent Injury Prevention,* vol. 10;154-158.

Roy, R., Baguley, P. and Watson, J. (2009), "Understanding the Cost Design Evaluation using Virtual Crash Testing", *International Conference on Research into Design, ICoRD'09,* 7th-9th January 2009, Indian Institute of Science, Bangalore, India, pp. 1.

Rutherford, A. (2001), *Introducing ANOVA and ANCOVA, a GLM approach,* 1st Edition ed, Sage Publications Ltd, Gateshead, UK.

SAE (March 1995), *Instrumentation for Impact Tests*, J211/1, SAE, USA.

Schuster, P. J., Chou, C. C., Prasad, P. and Jayaraman, G. (2000), "Development and validation of a pedestrian lower limb non linear 3D finite element model", *Stapp Car Crash Journal,* vol. 44, pp. 315-334.

Serre, T., Masson, C., Perrin, C., Chalandon, S., Llari, M., Py, M., Cavallero, C. and Cesari, D. (2007), "Real accidents involving vulnerable road users: In-depth investigation, numerical simulation and experimental reconstitution with PMHS", *International Journal of Crashworthiness*, vol. 12, no. 3, pp. 227-234.

Shanghai Star (2004), *Road accidents kill 300 a day in China* , available at: http://www.chinadaily.com.cn/english/doc/2004-04/12/content_322695.htm (accessed 13th July 2010).

Singh, M., Dey, R., Mukherjee, S., Mohan, D. and Chawla (2007), "Effect of Vehicle Design in Bicycle Frontal Crashes ", IRCOBI (ed.), in: *IRCOBI Conference* September 2007, Maastricht, The Netherlands, pp. 409.

Soden, P. D., Millar, M. A., Adeyefa, B. A. and Wong, Y. S. (1986), "Loads, Stresses, and Deflections in Bicycle Frames", *Journal of Strain Analysis*, vol. 21, no. 4, pp. 185-195.

StatSoft, I., (2008), *STATISTICA (data analysis software system)*, version 8.0 ed., Tulsa, OK, 74104, USA.

Tortora, G. and Grabowski, S. (2000), *Principles of Anatomy and Physiology*, 9th ed, John Wiley and Sons, Inc., New York.

UK Department for Transport (2008), *UK Road Casualties Great Britain : 2007*, available at: http://www.dft.gov.uk/pgr/statistics/datatablespublications/accidents/casualtiesgbar/roadcasualtiesgreatbritain20071 (accessed 16/11/2008).

van der Horst, M. J., Thunnissen, J. G. M., Happee, R., van Haaster, R. M. H. P. and Wismans, J. S. H. M. (1997), "Influence of muscle activity on head-neck response during impact ", *41st Stapp Car Crash Conference Proceedings*, November, Lake Buena Vista, FL, USA, pp. 487.

van Hassel, E., Bosma, F., Vendrig, R. and Happee, R. (2007), "Method of leg protection of Pedestrians and Cyclists by Vehicle Front Adaptation", *SAE Paper*, vol. 2007-26-009, pp. 91.

Verschueren, P., Delye, H., Depreitere, B., Van Lierde, C., Haex, B., Berckmans, D., Verpoest, I., Goffin, J., Vander Sloten, J. and Van der Perre, G. (2007), "A new test set-up for skull fracture characterisation", *Journal of Biomechanics*, vol. 40, no. 15, pp. 3389-3396.

Viano, D. (2004), "Bolster impacts to the knee and tibia of human cadavers and an anthropometric dummy", *Proceedings of 22nd Stapp Car Crash Conference*, October, 1978, Ann Arbor, US, pp. 780896.

Watson, J. W., Hardy, R. N. and Kayvantash, K. (2009), "Understanding the Nature of Cyclists' Head Impacts ", *International Research Council on the Biomechanics of Injury*, 9th-11th September 2009, York, UK, IRCOBI, Zurich, pp. 301.

Webster, B. (2008), *Olympic success provokes a chain reaction as millions turn to bikes*, November 22, The Times, available at: http://www.timesonline.co.uk/tol/news/uk/article5209077.ece, (accessed 7 July 2010).

Werner, S., Newberry, W., Fijan, R. and Winter, M. (2001), *Modeling of Bicycle Rider Collision Kinematics*, 2001-01-0765, SAE 2001 World Congress, Detroit, MI, USA.

Willinger, R., Ryan, G. A., McLean, A. J. and Kopp, C. M. (1994), "Mechanisms of Brain Injury Related to Mathematical Modelling and Epidemiological Data", *Accident Analysis & Prevention*, vol. 26, no. 6, pp. 767-779.

Yang, J. K. and Lovsund, P. (1997), *Development and validation of a human-body mathematical model for simulation of car-pedestrian collisions*, 1320, Chalmers Tekniska Hogskola, Goteborg, Sweden.

Yasuki, T. (2006), "Using THUMS for pedestrian safety simulations", *AutoTechnology*, vol. 6, pp. 44-47.